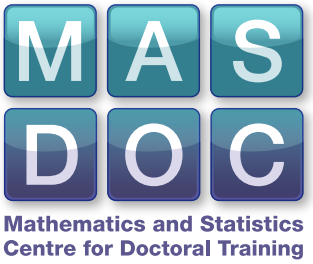

Optimisation of the PFC Functional

by

Simon Matthew Bignold

Thesis

Submitted for the degree of

Doctor of Philosophy

Mathematics Institute

The University of Warwick

June 2016

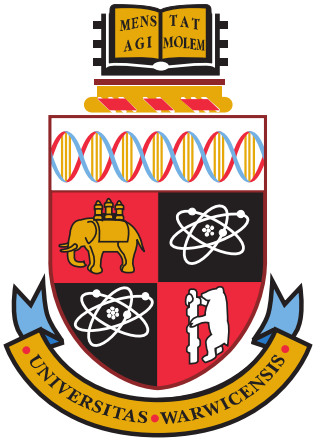

Contents

List of Figures

Acknowledgements

The work of this thesis was funded by the MASDOC DTC grant number EP/H023364/1.

First I would like to acknowledge the help of my two supervisors Christoph Ortner and Charlie Elliott. In particular I would like to thank Christoph, my first supervisor, for his constant help, support and advice.

I would like to thank Dave Packwood for his help and advice on developing algorithms to address the 'divergence' problem of Subsection 8.2.5. I would also like to thank Antoine Levitt for introducing me to the Łojasiewicz inequality which I have used extensively in Chapters 5-7.

I have really enjoyed my time in Warwick and would like to thank all the members of the Warwick Mathematics Institute and especially my fellow co-MASDOCs for providing a stimulating and friendly environment. Particular thanks go to Colin Sparrow for running a really inspiring and sociable department.

A PhD is a long process and numerous people have contributed their advice and support, both academically and socially, throughout the last four years. The following list is therefore probably incomplete and I apologise to anyone I may have inadvertently forgotten. Firstly I would like to thank the members of my MASDOC year for their support in the three years that we shared an office. I would also like to thank the residents of B3.04 for letting me borrow a desk in their office for the last year. Thanks also to the people who shared a house with me through the first three years of my PhD (Matt, Mike, Kirsty and Andrew). As well as the above I would also like to thank the many people who provided advice and entertainment throughout my PhD especially Owen, Steve, Chin, Amal, Abhishek, Alex, Matt, Yuchen, Felipe, Ben, Huan, Faz, Adam, John, Ollie, Jack, Jamie, Matt, Neil and Karina.

Last of all a special thanks go to my parents for their unflagging advice and support.

Declarations

I, Simon Bignold, declare that to the best of my knowledge this work is original and my own work except when otherwise specified by the references.

The material in this thesis has not to my knowledge been submitted for any other degree either at this university (the University of Warwick) or any other university. At the time of submission none of the work within this thesis has appeared or been submitted to any other publication.

Abstract

In this thesis we develop and analyse gradient-flow type algorithms for minimising the Phase Field Crystal (PFC) functional. The PFC model was introduced by Elder et al [EKHG02] as a simple method for crystal simulation over long time-scales. The PFC model has been used to simulate many physical phenomena including liquid-solid transitions, grain boundaries, dislocations and stacking faults and is an area of active physics and numerical analysis research.

We consider three continuous gradient flows for the PFC functional, the L^2-, H^{-1}- and H^2-gradient flows. The H^{-1}-gradient flow, known as the PFC equation, is the typical flow used for the PFC model. The L^2-gradient flow is known as the Swift-Hohenberg equation. The H^2-gradient flow appears to be a novel feature of this thesis and will motivate our development of a line search algorithm.

We analyse two methods of time discretisation for our gradient flows. Firstly, we develop a steepest descent algorithm based on the H^2-gradient flow. We further develop a convex-concave splitting of the PFC functional, recently proposed by Elsey and Wirth [EW13], to discretise the L^2- and H^{-1}-gradient flows.

We are able to prove energy stability of both our steepest descent algorithm and the convex-concave splitting scheme of [EW13]. We then use the Łojasiewicz gradient inequality (first developed in [Łoj62]) to prove that all three schemes converge to equilibrium.

For numerical simulations we undertake spatial discretisation of our schemes using Fourier spectral methods. We consider a number of implementation issues for our fully discrete algorithms including a striking issue that occurs when the number of spatial grid points is *low*. We then perform several numerical tests which indicate that our new steepest descent algorithm performs well compared with the schemes of [EW13] and even compared with a Newton type scheme (the trust region method).

Chapter 1

Introduction

The Phase Field Crystal (PFC) model was introduced in [EKHG02] as a basic model for crystal simulation. The idea of the PFC model is that we describe the free energy of a particle system by the PFC functional, that is

$$\mathcal{F}[u] = \frac{1}{2}\|\Delta u + u\|^2_{L^2(\Omega)} - \frac{\delta}{2}\|u\|^2_{L^2(\Omega)} + \frac{1}{4}\|u\|^4_{L^4(\Omega)} \tag{1.1}$$

where $\delta > 0$. We then obtain the equilibrium configuration of the system by minimising the PFC functional under the condition that the mean of the variable u is conserved, that is $⨍ u\mathrm{d}x = \bar{u}$. This constraint is equivalent to mass conservation. [EKHG02] also introduces a basic gradient flow equation to obtain this minimum. This equation, the PFC equation, is written as

$$u_t = \Delta[(\Delta + I)^2 u - \delta u + u^3].$$

The form of the PFC functional can be justified as a combination of a double-well potential, which is minimised by one of two phases, and a functional that is minimised by a periodic density (see [EG04]).

The advantage of the PFC model is that it favours cases where the minimiser is a periodic function and it can be shown that by an appropriate choice of the constants $\bar{u}$ and δ we can transition between a state of constant u (a fluid) and a state where u forms a lattice structure (see [EKHG02, Figure 1a)] or Figure 1.1). In the lattice state the areas of high density (u) can be taken to represent atoms and therefore the PFC model can be used to simulate the behaviour of crystalline structures. In particular, liquid-solid interfaces can be simulated by varying the values of $\bar{u}$ and δ. Compared to typical phase field models, the PFC model has the advantage that we are able to simulate the interactions of individual atoms. However, compared to true microscopic models the PFC model is coarse-grained in time and therefore acts on a diffusive time scale. In particular, Molecular Dynamics simulations (MD) must incorporate fast phonon interactions which means that an infeasible computational effort is required to reach the time scales needed for the relaxation of large scale domains ([Mel01] identifies a similar issue in the simulation of biological phenomena).

By contrast the PFC model has the advantage that it averages out these fast interactions and thus is more suited to addressing large time scales. We discuss this interpretation of the PFC model as a mesoscopic model in Subsection 1.1.1.

In this thesis we analyse and develop various gradient-flow type algorithms to minimise the PFC functional whilst conserving the average of u. In contrast to some of the literature, e.g. [WWL09] and [EW13], we do not necessarily seek to approximate the trajectory of the PFC equation, but instead concentrate on obtaining an algorithm that converges to an equilibrium point.

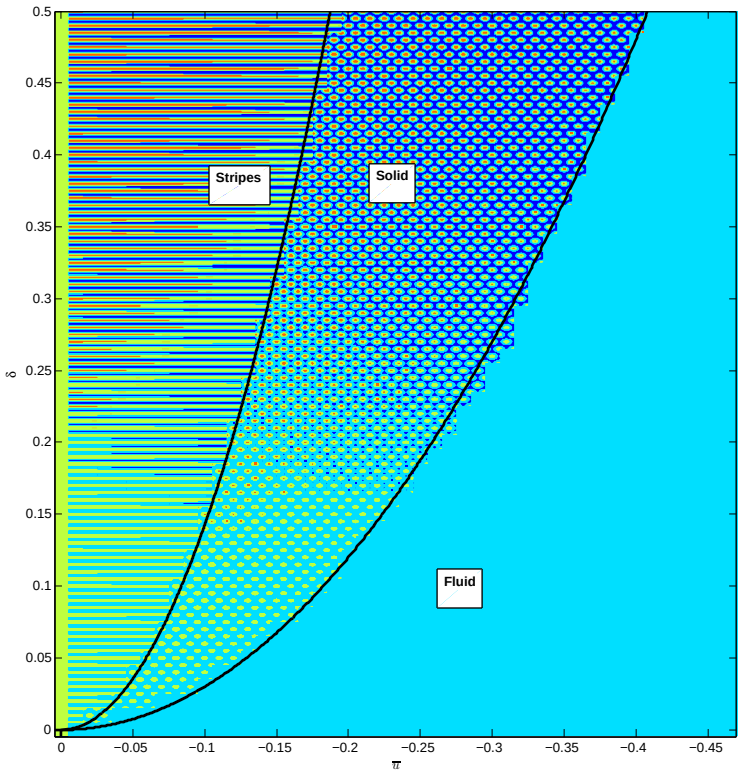

Figure 1.1: Phase diagram for the PFC model (see [EKHG02, Figure 1a)]). This figure is generated by using the trust region algorithm, Algorithm E.1.1, on the unit cell (see (8.1)) for different values of δ and $\bar{u}$. We start from $\bar{u} = \delta = 0$, we then succesively increment $\bar{u}$ by -0.01 and then increment δ by 0.01. For each new value of δ and $\bar{u}$ we obtain the equilibrium solution. The figure is then generated by placing the unit cells next to each other. We note the three phases: liquid, solid and striped.

1.1 Invitation to the Field

We have already suggested that following [EG04] the PFC functional can be justified as a combination of a double well potential and a potential that is minimised by a periodic

density. However, a broader and possibly more instructive justification for the PFC model is as an intermediate method between the microscopic method of molecular dynamics (MD, see e.g. [Mel01]) and the macroscopic phase field methods.

1.1.1 PFC as a Mesoscopic Model

The basic hierarchy of models is shown in [WGT$^+$12, Figure 2]. Consider a system of interacting particles, a MD simulation is obtained by assuming that all particles interact via Newtonian mechanics. The number of coupled equations to be solved increases with the number of particles. This means that MD simulations quickly become impractical.

Density Functional Theory (DFT) is a model of an interacting particle system that is simpler than MD but is still formulated on a microscopic scale. DFT is an equilibrium theory so we can use it to obtain efficient paths from given initial conditions to equilibrium, this is effectively equivalent to coarse-graining the time scale. An introduction to DFT is given in [AM00]. The principle of DFT is that one can describe a particle system by its free energy and that the free energy can be shown to be a functional of the one-particle density (this is the Hohenberg-Kohn Theorem, see Section 2.3). Although in principle the free energy is described by a functional of the one-particle density, in practice this functional is rarely known and is almost always approximated.

The PFC model is obtained by a simple and general method of approximating the free energy functional. We effectively use a curtailed density expansion in both real and Fourier space. More detail on this method is given in Chapter 2. The PFC model is particularly attractive as it has only two parameters, $\bar{u}$ and δ; c.f. (1.1).

The PFC model creates areas of high density that can be considered as atoms. From PFC simulations (e.g. the vacancy simulation of [EG04, Figure 7]) we can see that the PFC model is coarse-grained in time, that is the fast phonon vibrations are ignored and we act only on a diffusive time scale. Therefore "The PFC method operates on atomic length and diffusive time scales" [WGT$^+$12, page 1].

Two fundamental properties of this model should be highlighted. First, the derivation of the PFC model requires translational and rotational invariance and therefore the minimising density is also translationally invariant along both axes. Translational invariance along both axes is a necessary property required for a density that describes a crystalline system. Secondly, by altering the two parameters of the model, the solution obtained transitions between a constant density state (a fluid), and a 2D lattice state (one can see a phase diagram in [EKHG02, Figure 1a)] or Figure 1.1). This means that this model is well suited to solid liquid transition; however, we will not consider this situation in the present work.

Finally, one can coarse-grain the PFC model to obtain a phase-field model. We will briefly address this issue in Subsection 10.2.1. The PFC model is presented in the context of general phase field models in [EP10].

1.1.2 PFC Simulations

In the previous subsection we remarked that an advantage of the PFC model is that we can view it as a mesoscopic method of particle simulation. A more pragmatic motivation for studying the PFC model is that one can produce simulations that agree with observed phenomena.

We will give references to some PFC simulations that demonstrate physical phenomena in Subsection 1.2.2. Of particular interest is the study of [WK07] which shows quantitative agreement between PFC simulations and MD simulations in iron. We note that papers demonstrating such quantitative agreement seem to be rare. However, there is extensive literature on qualitative PFC simulations. These include, but are not limited to, stacking faults (see [BPRS12]), grain boundaries (see [PDA$^+$07]), dislocations (see [EKHG02]), liquid-solid boundaries and colloidal crystal growth (see [GTTP11] for both). We also note that PFC models can be undertaken in both two and three space dimensions without major theoretical changes.

We illustrate a phenomenon that is accessible using the PFC methodology in Figure 1.2. Specifically, we use the PFC equation coming from Algorithm 7.1.1 on a domain size $L = 32$. Using this simulation we see that locally a hexagonal lattice is formed and that grain boundaries are formed at the intersection of these lattice like regions.

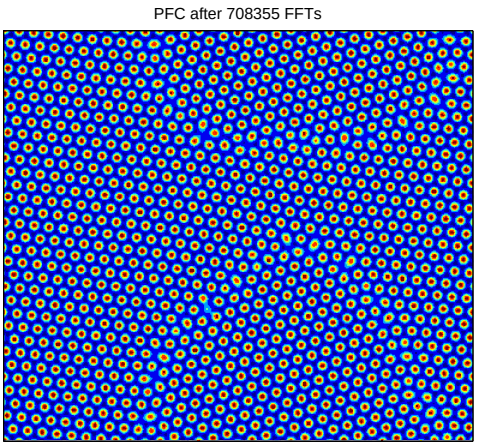

Figure 1.2: Solution for the PFC algorithm (Algorithm 7.1.1) after 708355 FFTs starting from random initial conditions given by (9.1) where $L = 32$. We note the formation of grains.

We also note that several extensions to the PFC model have been developed, see [WGT$^+$12]. Many phenomena have been simulated using these extensions (see [WGT$^+$12, Table 1]). Since the PFC model we study is generally simpler than these extensions, it is hoped that one may be able to better investigate these extensions through a thorough

understanding of the basic PFC model.

1.2 Literature Review

1.2.1 Modelling

We give a brief overview of some of the (many) papers that describe variants of the PFC model and their derivation. We place emphasis on the papers that develop features of the PFC model that we will need in this work. We also outline several review papers that survey the literature surrounding the PFC model. Finally, we mention two theses from the last five years that consider PFC simulations and which provide a good introduction to the topic.

The PFC approach was introduced in the paper [EKHG02]. This paper introduces the PFC functional which describes the energy of the model system. The authors then introduce a basic method for minimising this functional, that is the PFC equation. This paper provides a justification for using the PFC model by showing qualitative agreement between the model and the predictions of Read and Shockley for a grain boundary energy (see [RS50]). Finally, [EKHG02] introduces a binary PFC model which we will not consider in this thesis.

Another important contribution in the development of the PFC model is [EPB$^+$07], which introduces the idea of deriving the PFC model from DFT. This idea is developed in more detail in Chapter 2.

For the sake of clarity we briefly summarise the modified PFC (MPFC) model. The reason for highlighting this extension to the PFC model is that it seems to be very popular, in particular it is addressed in several of the numerical analysis papers we reference, e.g. [GW14], [GP15] and [WW10]. The MPFC equation was introduced in [SHP06]. The idea of this method is to minimise the PFC functional using a partial differential equation that attempts to incorporate elastic interactions. To obtain the MPFC equation the PFC equation is modified by adding a second-order time derivative, i.e. the MPFC equation is (see [SHP06, Equation (3)])

$$\partial_t^2 u + \beta \partial_t u = \alpha^2 \Delta \delta \mathcal{F}[u]$$

where $\alpha, \beta > 0$.

We now summarise several reviews of the PFC model that outline the key features of the model and collate references to some of the major areas of interest.

An extensive review of work on the PFC model is found in [WGT$^+$12]. This paper reviews the justification for and derivation of the PFC model see [WGT$^+$12, Chapter 1 and Sections 2.1, 2.3 and 3.1]. This paper also highlights several extensions to the basic PFC model including the MPFC model, the VPFC model and the binary PFC model. Although these models are not explicitly considered within this thesis, they suggest potential extensions to the work of this thesis. This paper also surveys physical phenomena that have been simulated using PFC-based techniques, see [WGT$^+$12, Table 1].

[EP10] presents the PFC model as a phase field model. This emphasises the link between the PFC methodology and this well developed field. [EP10] also considers the equilibrium properties of the one-mode approximation to the solution of the PFC equation in [EP10, Section 8.4] and the elastic constants of the PFC model in [EP10, Section 8.5].

A recent review of the PFC model is found in [AZ15]. Again, in this paper there is significant focus on the extensions to the original PFC model. However, this paper also outlines work on quantitative applications of PFC-based techniques.

We now outline two theses that focus on the PFC model. Both theses share similarities with this work although the specific focus is different in each.

The PhD thesis [Ban11] develops a numerical scheme to solve the PFC equation. The approach used in this thesis is based on a semi-implicit operator splitting (see [Ban11, Subsection 3.1.2]) and also addresses the binary PFC model. This thesis has an extensive literature review in [Ban11, Chapter 2].

The MSc thesis [Lar14] considers the PFC model in both one and two space dimensions.

1.2.2 Simulations and Applications

There is extensive literature on qualitative simulations undertaken using the PFC model. References to these can be seen in the reviews detailed above, particularly [WGT$^+$12]. However, we first give a review of work that compares the PFC model and experimental results quantitatively. It should be noted that there appear to be very few papers specifically on quantitative simulations using the original PFC model.

The first paper where a PFC model is compared quantitatively to experimental data is [WK07]. This is also the most well-known quantitative PFC model. The PFC model is compared quantitatively to MD simulations in iron (Fe). The results are shown in [WK07, Table II], we see that there is good agreement in the interfacial free-energy. However, [WK07, Page 8] claims that higher order anisotropies are needed to represent the whole free energy plot and [WK07, Table II] demonstrates that the quantitative agreement with these anisotropies is poor. This issue is also highlighted in [JAEAN09] which suggests that a modification of the PFC model, the eighth-order fitting version of the PFC model (the EOF-PFC), might lead to better quantitative simulations.

A more recent look at quantitative PFC simulations is [AZB14]. Again this paper compares PFC simulations with results from iron (Fe). In this paper the authors compare the PFC results to both MD simulations and experimental results. This paper obtains good quantitative agreement for the surface free energy and the latent heat, see [AZB14, Table V]. This paper notes that there is poor simulation of certain quantities such as the melting expansions (again [AZB14, Table V]) and that since the model is developed for Fe near a melting point it cannot be used for temperatures far from the melting point.

We now survey some of the work on qualitative PFC simulations. As noted above qualitative simulations have been undertaken using the PFC model since its inception in

[EKHG02].

A brief overview of several simulations from a variety of PFC models is given in [PDA$^+$07]. [PDA$^+$07, Figure 2] plots grain boundary energy against grain boundary mismatch and shows agreement between the PFC model, the Read-Shockley prediction and experiments in several materials (tin, lead and copper). [PDA$^+$07, Figure 9] shows a 3D simulation with prominent grain boundaries. Grain boundaries are also simulated using a coarse-grained version of the PFC model in [PDA$^+$07, Figure 8]. Finally, this overview discusses the MPFC equation and the binary PFC model. The MPFC equation is used to simulate dislocation glide in [PDA$^+$07, Figure 6] and the binary PFC model is used for a variety of simulations, see e.g. [PDA$^+$07, Figure 10].

We now outline several papers that consider PFC simulations of specific phenomena. The first paper we mention considers a situation which is similar to the large simulation we undertake in Section 9.1.

The paper [WV12] simulates grain growth in 2 dimensions using the PFC model in several different situations. [WV12, Section 3] considers a grain embedded within a larger grain where the first grain is misorientated with respect to the larger grain. The evolution of the grain is shown in [WV12, Figure 6]. These simulations are broadly similar to the situation we consider in Section 9.1; however, in our simulations the misorientated grain is much smaller relative to the background grain. This paper also considers a 3-grain simulation in [WV12, Section 4]. 3-grain simulations similar to those of [WV12, Section 4] could be undertaken using the methods described in this thesis; however, for the sake of brevity we do not pursue this option.

We briefly mention some papers that simulate interesting physical phenomena using the PFC model. Although we do not specifically address these phenomena within this thesis, these papers give a brief indication of the scope of the PFC model.

[BPRS12] uses the PFC model to simulate stacking faults. Illustrations of the qualitative results obtained by this paper are seen in [BPRS12, Figures 1 and 6]. This paper also compares the results obtained for several modifications of the PFC model (see [BPRS12, pages 5-7]).

The letter [HE08] shows that one can simulate the formation of epitaxial islands using the PFC model with an additional cubic term. 2D and 3D simulations of these islands are shown in [HE08, Figure 1]. This paper also uses a coarse-grained model to consider this island formation.

Finally, we briefly mention an extension of the PFC model as an example of how many phenomena can be simulated using simple modifications of the original PFC model. In [GTTP11] the PFC model is extended by adding an appropriate potential energy term (see [GTTP11, Section 2.3]) to the system. The paper shows that using this model one can obtain qualitatively correct simulations of several interesting phenomena. [GTTP11, Figure 8] shows a simulation of the liquid ordering around fixed particles. In this case the authors seem to obtain good qualitative agreement between experimental results and a PFC model supplemented by an appropriate external potential and a noise term. [GTTP11, Figure 12]

shows heterogeneous nucleation from a square lattice using the same model. This adaptation of the PFC model is also used to simulate colloid patterning and the creation of particle chains, the results of these simulations are compared to experimental results in [GTTP11, Figures 14] and [GTTP11, Figure 16] respectively.

1.2.3 Numerical Analysis and Scientific Computing

In this section we survey some of the papers that undertake numerical analysis of algorithms based on the PFC model. In general these papers focus on discretisations of the PFC equation.

We first highlight two papers that use the Łojasiewicz inequality to prove convergence of the MPFC equation. If φ is an equilibrium point, the Łojasiewicz inequality is satisfied if there exist constants $c \geq 0$, $\sigma > 0$ and $\theta \in \left(0, \frac{1}{2}\right]$ such that for all $\eta \in \bar{u} + H^2_{\#}(\Omega)$ (see Definition C.1.2 for the definition of $H^2_{\#}(\Omega)$) with $\|\eta - \varphi\|_{H^2(\Omega)} \leq \sigma$

$$\|\delta\mathcal{F}[\eta]\|_{H^{-2}(\Omega)} \geq c|\mathcal{F}[\eta] - \mathcal{F}[\varphi]|^{1-\theta}.$$

We will use the Łojasiewicz inequality extensively in Chapters 5-7. The paper [GW14] uses the Łojasiewicz inequality to prove that the solution of the MPFC equation converges to an equilibrium point of the PFC functional. We use similar methods to those used in this paper in Chapter 5 and use discrete analogues of these methods in Chapters 6 and 7.

The paper [GP15] uses the Łojasiewicz inequality to prove that the solution of a discretisation of the MPFC converges to an equilibrium solution. Although we do not specifically consider the MPFC equation we use the Łojasiewicz inequality to prove convergence of our schemes (which include a discretisation of the PFC equation) in Chapters 6 and 7.

We now survey several papers on the discretisation of the PFC equation. We conclude with the two papers ([WWL09] and [EW13]) that will be of most use for our thesis.

The recent paper [LSL15] introduces an operator splitting method for simulating the PFC equation. The authors introduce first and second order splittings to treat the non-linear term in [LSL15, Equations (10)] and [LSL15, Equation (18)] respectively. Basic numerical tests are undertaken using this method in [LSL15, Section 3]. The approach used by this paper is to split the scheme into linear and nonlinear subequations (see [LSL15, Section 2]). The authors claim that the linear subequation has a closed form in Fourier space. The operator splitting approach of this paper is compared favourably to the first and second order energy stable methods of [HWWL09] in [LSL15, Section 3] (the first order energy stable scheme is based on the method introduced in [WWL09]).

A semi-implicit method for both the SH and PFC equation is considered in [ZMQ13]. First order schemes for the SH and PFC equations are given in [ZMQ13, Equations (2.4)] and [ZMQ13, Equations (2.5)] respectively. Additionally [ZMQ13, Equations (2.8)] and [ZMQ13, Equations (2.9)] give second order finite difference schemes. Energy stability of the 1st order schemes for both equations is given in [ZMQ13, Theorem 2.1] and is given for the second order scheme in [ZMQ13, Theorem 2.2]. This paper also uses an adaptive

time-step method where the time-step is updated using [ZMQ13, Equation (3.1)]. Finally basic numerical tests are undertaken in [ZMQ13, Section 4].

Another semi-implicit approach to the PFC equation and the associated Swift-Hohenberg (SH) equation is given in [CW08]. The scheme is outlined in [CW08, Equations (4) and (5)]. [CW08, Section 2.2] shows the unconditional stability of the scheme and demonstrates that the Crank-Nicholson approach for the PFC equation is unstable. This paper (see [CW08, Section 2.3]) also considers updates taken in Fourier space, which we also use for our spatial discretisation in Chapter 8.

In [WWL09] the authors develop a time discretisation of the PFC equation using a convex-concave splitting. In [WWL09, Theorem 1.1] it is proved that such a scheme is energy stable. [WWL09] also introduces a space discretisation in Section 2. Finally, in [WWL09, Theorem 3.11] the authors prove an error estimate that shows that the approximation converges to a solution of the PFC equation when the time-step and grid spacing go to zero. We analyse a different convex-concave splitting in Chapter 7.

A finite element method for the scheme of [WWL09] is developed in [HWWL09]. In this paper they also develop a second order scheme for the PFC equation, [HWWL09, Equations (8)-(10)]. A multigrid numerical method for this second order scheme is developed in [HWWL09, Section 5.2]. This scheme is used to simulate heterogeneous nucleation in [HWWL09, Figures 7(a)-(c)].

The most significant reference for our thesis is [EW13]. This paper introduces a new convex-concave splitting to discretise the PFC equation and the SH equation. The existence of a similar scheme is proposed at the end of [HWWL09, Section 2]. The energy splitting used in this paper is

$$\mathcal{F}[u] = \mathcal{F}_{\mathrm{C},C_{\mathrm{stab}}}[u] - \mathcal{F}_{\mathrm{E},C_{\mathrm{stab}}}[u],$$

where, for $C_{\mathrm{stab}} > 0$,

$$\begin{aligned}
\mathcal{F}_{\mathrm{C},C_{\mathrm{stab}}}[u] &= \frac{1}{2}\|\Delta u + u\|^2_{L^2(\Omega)} - \frac{\delta}{2}\|u\|^2_{L^2(\Omega)} + \frac{C_{\mathrm{stab}}}{2}\|u\|^2_{L^2(\Omega)}, \\
\mathcal{F}_{\mathrm{E},C_{\mathrm{stab}}}[u] &= \frac{C_{\mathrm{stab}}}{2}\|u\|^2_{L^2(\Omega)} - \frac{1}{4}\|u\|^4_{L^4(\Omega)}.
\end{aligned}$$

We note that this splitting is only locally convex-concave. In particular $\mathcal{F}_{\mathrm{E},C_{\mathrm{stab}}}$ is only locally convex. The authors of [EW13] prove that a scheme for the SH and PFC equation based on this splitting is stable ([EW13, Theorem 2.1]) and that the solution of the scheme converges to the solution of the continuous flow (the SH or PFC equation depending on which equation is being discretised) as the time step goes to zero ([EW13, Theorem 2.3]). We carry out extensive analysis of this scheme in Chapter 7. The authors of [EW13] also use pseudo-spectral methods for their spatial discretisation (see [EW13, Sections 3.2 and 4.1]). This is the method we use for spatial discretisation in Chapter 8. The implementation is described at the end of [EW13, Section 4.1].

1.3 Outline and Summary of Results

The aim of this thesis is to develop and analyse various gradient-flow type algorithms to minimise the PFC functional whilst conserving the mass. In particular we focus on obtaining an efficient time discrete algorithm that converges to an equilibrium point of the PFC functional.

1.3.1 Outline

We begin with a basic introduction to the PFC model. In Chapter 2 we outline the method for deriving the PFC model from DFT. The link between DFT and the PFC model was first shown in [EPB+07] and can be used to justify the wide range of potential applications for the PFC model.

In Chapter 3 we introduce the basic machinery needed to formulate our PFC problem. We introduce the domain Ω and the space $H^2_{\bar{u}}(\Omega)$ from which we will choose our solution. We also formulate the PFC functional (3.1) and its first and second variations (Lemma 3.1.4). Finally, we show that critical points of the PFC functional satisfy the Euler-Lagrange equations (Lemma 3.3.1) and that the solution to the Euler-Lagrange equations is smooth (Lemma 3.3.3).

In Chapter 4 we introduce a method of reaching critical points of the PFC functional. Specifically, we use the technique of gradient flow (4.1). We introduce three gradient flows namely the H^{-1}-, L^2- and H^2-gradient flows (Definitions 4.2.1, 4.2.2 and 4.2.4), that is

$$\begin{aligned} \langle u_t, v\rangle_{L^2(\Omega)} &= -\delta\mathcal{F}[u, v] \qquad && \forall v \in H^2_{\#}(\Omega) \\ \langle u_t, v\rangle_{H^{-1}(\Omega)} &= -\delta\mathcal{F}[u, v] \qquad && \forall v \in H^2_{\#}(\Omega) \end{aligned}$$

and

$$\langle [(\Delta + I)^2 + \gamma I]u_t, v\rangle_{L^2(\Omega)} = -\delta\mathcal{F}[u, v] \qquad \forall v \in H^2_{\#}(\Omega)$$

where $\gamma > 0$. We then prove the existence of a solution to all three of these gradient flows (Lemmas 4.3.2 and 4.4.1) as well as uniqueness (Lemma 4.3.4) and regularity results (Lemma 4.3.3). The H^2-gradient flow is compared with and motivated by Newton's method.

After introducing the gradient flow methodology in Chapter 4 we then prove that the solutions of these gradient flows converge to equilibria. In a similar way to [GW14] we use a Łojasiewicz inequality to prove the convergence results and an estimate on their associated convergence rates. We first prove that the Łojasiewicz inequality holds for the PFC functional in the correct space, i.e. $H^2_{\#}(\Omega)$ (Theorem 5.0.1). We then use this result and a theorem of [HJ15] to prove convergence of the solution (Theorem 5.0.2).

The next two chapters are dedicated to the spatial discretisation of the gradient flow. This is the main focus of this thesis and also contains the majority of the novel results. We first consider a discretisation of our H^2-gradient flow in Chapter 6. In this chapter we

introduce a variable metric approach ((6.3)), that is

$$\left\langle [(\Delta + I) + \gamma_n I] \left(\frac{u_{n+1} - u_n}{\tau_n} \right), v \right\rangle = -\delta \mathcal{F}[u_n, v] \qquad \forall v \in H^2_{\#}(\Omega)$$

where

$$\gamma_n = \max\left(\gamma_{\min}, 3\overline{u_n^2} - \delta\right).$$

In our simulations of Chapter 9 we show that the variable metric scheme reaches equilibrium faster than the fixed metric scheme. Based on the variable metric approach we formulate an algorithm to reach equilibrium (Algorithm 6.1.1) and show that such an algorithm is energy stable (Proposition 6.2.3). Finally, we use the Łojasiewicz inequality to prove a general theorem that guarantees convergence of our scheme and the associated convergence rates (Lemma 6.3.2).

Chapter 7 extends the results of [EW13]. We first justify and formulate the convex-concave splitting schemes and then show that they are qualitatively similar to our H^2-gradient flow. Using similar techniques to Chapter 6 we can now prove energy stability of the schemes of [EW13] (Lemma 7.2.1) and convergence to equilibrium (Theorem 7.1.3).

In order to demonstrate the validity of our method we numerically test our algorithms. To do this we first introduce space discretisation via spectral methods in Chapter 8. We review several methods of choosing a time-step and pick the most efficient ones (Section 8.2). We then perform some basic numerical tests. We first test the effect of the number of spatial grid points on our methods and discuss an issue that arises when the number of spatial grid points is low (Subsection 8.2.5). Finally, we show the effect of the domain size on the convergence time of our algorithms (Subsection 8.2.6).

In Chapter 9 we undertake some larger simulations. We wish to show the potential applications of our method especially on problems that might be interesting to practitioners. In particular, we review simulations based on a lattice with a rotated crystal (Section 9.1) and also based on a random environment (Section 9.2). The rotated crystal environment has already been a focus of some PFC research in [Lar14].

Chapter 10 reviews the results of our thesis and outlines areas of future research.

1.3.2 Summary of Results

Having given a brief overview, we now highlight the novel features of this thesis. First we note that the vast majority of the PFC literature has been developed by the physics community. Therefore, although not unique in its numerical analysis focus, this thesis may provide a useful introduction to researchers more interested in a mathematical approach to the model.

The main novel aspect of this thesis is the introduction of a new H^2-gradient flow (Definition 4.2.4). We also introduce a variable metric version of the discrete form of this gradient flow in Subsection 6.1.2.

In Chapter 4 the existence theory for the H^2-gradient flow is based on well known

techniques. The existence theory for the other two gradient flows is also new although it is also based on well known techniques and similar existence results have been derived before for the PFC equation in different ways, e.g. in [WWL09]. We also prove that the solutions to the SH and PFC equations are continuously differentiable in $H^2(\Omega)$ given appropriate initial conditions (i.e. Lemma 4.3.3).

The Łojasiewicz inequality technique of Chapter 5 has been used for the MPFC equation, which is very similar to the PFC equation, in [GW14]. However the application of this method to the H^2- and L^2-gradient flows seems to be novel.

Since the H^2-gradient flow is a new feature of this thesis, Chapter 6, which focuses on developing an algorithm based on this method, is largely new. We note that the Łojasiewicz inequality has previously been applied to a discrete algorithm for minimising the PFC functional in [GP15]. A particularly interesting aspect of this chapter is the general convergence lemma, Lemma 6.3.2.

Although Chapter 7 focuses on a method developed in [EW13], we derive a new energy stability theorem for this scheme. We also use the Łojasiewicz inequality to prove convergence to equilibrium of this scheme, this convergence result appears to be new. Finally we develop a qualitative link between the scheme of [EW13] and our H^2-gradient flow.

The main aim of Chapter 8 is to develop and test a spatial discretisation of our schemes. However, we also highlight an issue when the number of spatial grid points is low which seems to be hitherto unknown and potentially could be very important to address in developing efficient simulations.

Chapter 2

Derivation Of the PFC Model

To provide a justification for the study of the phase-field crystal (PFC) model, we derive it via a series of approximations from density functional theory (DFT), which is a well-established method in statistical mechanics. The derivation that we give in this chapter will be purely formal.

We start from the statistical mechanics set-up of the canonical ensemble. That is, we have a fixed number of particles with the N-particle density given by $\hat{\rho}_N(X_N) = \exp[-\beta H_N(X_N, U_1)](N! Z_N(U_1, \Omega))^{-1}$. We choose to focus on a static system with a pair-wise interaction potential and an external potential that acts equally on all particles.

It is then possible to derive the equilibrium one-particle density $\rho_N(x)$ in three different ways. We also introduce the free energy, $\mathcal{F}_N[U_1, \Omega] = -\beta^{-1} \ln [Z_N(U_1, \Omega)]$, as an important quantity that describes the system. The density is the quantity we will focus on deriving as it will allow us to find the free energy.

We introduce the Hohenberg-Kohn functional and show the free energy can be obtained from the minimisation of the Hohenberg-Kohn functional over all possible one-particle densities, $\mathcal{F}_N[U_1, \Omega] = \min_{\tilde{\rho}} \left[\mathcal{F}_{\mathrm{HK}}[\tilde{\rho}] + \int_\Omega U_1(x)\tilde{\rho}(x)\mathrm{d}x \right]$. It is also shown that the minimising density corresponds to the equilibrium density. The Hohenberg-Kohn functional is split into an ideal gas part and the excess energy contribution $\mathcal{F}_{\mathrm{HK}}[\rho_N(x)] = \mathcal{F}_{\mathrm{HK,id}}[\rho_N(x)] + \mathcal{F}_{\mathrm{HK,exc}}[\rho_N(x)]$.

We can then formulate the PFC model by using a sequence of formal approximation steps. The excess energy and ideal gas contribution are both approximated individually and then re-combined to give the PFC functional as an approximation of the Hohenberg-Kohn functional.

2.1 Set-Up

We consider the formulation of DFT in the canonical ensemble. This assumes a constant number of particles which for the PFC model is physically reasonable. Indeed, most current

works on the PFC model conserve particle density through their choice of evolution equation (principally using the H^{-1}-gradient flow), see for example [WGT+12] and [EW13].

In general we consider a system of $N \in \mathbb{N}$ particles where d is the dimension of the system and positions are confined to a finite domain $\Omega \subset \mathbb{R}^d$. The Hamiltonian of the system is given by

$$H_N(X_N, U_1) = \sum_{i=1}^{N} U_1(x_i) + \sum_{1 \le i < j \le N} U_2(|x_i - x_j|)$$

where $X_N = (x_1, \ldots, x_N) \in \Omega^N$, $U_1 : \mathbb{R}^d \to \mathbb{R}$ is the external potential and $U_2 : \mathbb{R}^d \to \mathbb{R}$ is the interaction potential between particles. For simplicity, we consider U_2 as a pair-wise potential which depends only on the distance between two particles, hence it is rotationally and translationally invariant. We consider a static system; this means the Hamiltonian does not depend on momentum. If we also take particle momentum into account we have no additional difficulties. In fact we would only change the free energy computed below by an additive constant multiplied by N.

2.1.1 The Canonical Ensemble

To describe the statistical mechanics approach to DFT we introduce the canonical Gibbs measure. We define the Canonical Gibbs Ensemble following [Ada06, p.20], where we also introduce a $N!$ factor to account for indistinguishability of particles (this is to resolve the Gibbs paradox, see [Ada06, Section 4.1]).

Definition 2.1.1 (Canonical Gibbs Ensemble)**.** *Equip Ω^N with the Borel σ-algebra $\mathcal{B}_\Omega$. Then the probability measure $\gamma_\Omega^\beta \in \mathcal{P}(\Omega^N, \mathcal{B}_\Omega)$ with density*

$$\begin{aligned} \hat{\rho}_N(X_N) &= \hat{\rho}_N(X_N; U_1, \Omega) \\ &= \frac{\exp\left[-\beta H_N(X_N, U_1)\right]}{N! Z_N(U_1, \Omega)} \end{aligned} \tag{2.1}$$

is called the canonical ensemble.

The normalisation constant $Z_N(U_1, \Omega)$ is called the partition function, and can therefore be written as

$$Z_N(U_1, \Omega) = \frac{1}{N!} \int_{\Omega^N} \exp\left[-\beta H_N(X_N, U_1)\right] \mathrm{d}X_N \tag{2.2}$$

where the constant

$$\beta = \frac{1}{k_B T},$$

is the inverse temperature, scaled by Boltzmann's constant k_B.[1]

[1] (2.1) can be thought of as a probability measure weighting the various possible micro-states of the system.

2.1.2 The Helmholtz Free Energy

A quantity of great interest to us is the Helmholtz free energy hereafter referred to as the free energy. The free energy is an important quantity as it can be used to find fundamental quantities of the system including pressure and entropy see [Ada06, page 24]. Following [Ada06, page 23] we know the free energy is given by

$$\mathcal{F}_N[U_1, \Omega] = -\beta^{-1} \ln \left[Z_N(U_1, \Omega) \right].$$

Therefore, using the partition function (2.2), we can write the free energy as

$$\begin{aligned}
\mathcal{F}_N[U_1, \Omega] &= -\beta^{-1} \ln \left[\frac{1}{N!} \int_{\Omega^N} \exp \left[-\beta \left(\sum_{i=1}^{N} U_1(x_i) + \sum_{1 \le i < j \le N} U_2(|x_i - x_j|) \right) \right] \mathrm{d}X_N \right] \\
&= \beta^{-1} \ln N! \\
&\quad - \beta^{-1} \ln \left[\int_{\Omega^N} \exp \left[-\beta \left(\sum_{i=1}^{N} U_1(x_i) + \sum_{1 \le i < j \le N} U_2(|x_i - x_j|) \right) \right] \mathrm{d}X_N \right].
\end{aligned} \tag{2.3}$$

2.2 The One-particle Density

A fundamental object in DFT is the one-particle density. We present three equivalent ways of defining it. In this section we only consider the equilibrium density. In a later section, Section 2.3, we will introduce notation that allows this to be generalised.

2.2.1 Using δ-functions

The canonical definition of the one-particle density (see e.g. [WGT+12, Equation (2)]) is as the average of N δ-functions centered at the particle positions, taken with respect to the canonical Gibbs measure (2.1):

$$\begin{aligned}
\rho_N(x) &= \rho_N(x; U_1, \Omega) \\
&= \int_{\Omega^N} \sum_{i=1}^{N} \delta(x - x_i) \hat{\rho}_N(X_N) \mathrm{d}X_N \\
&= \int_{\Omega^N} \sum_{i=1}^{N} \delta(x - x_i) \frac{\exp\left[-\beta H_N(X_N, U_1)\right]}{N! Z_N(U_1, \Omega)} \mathrm{d}X_N \\
&= \frac{1}{N! Z_N(U_1, \Omega)} \sum_{m=1}^{N} \int_{\Omega^N} \delta(x - x_1) \exp\left[-\beta H_N(X_N, U_1)\right] \mathrm{d}x_1 ... \mathrm{d}x_N.
\end{aligned}$$

Relabelling some of the terms leads to

$$\begin{aligned}
&\rho_N(x) \\
&= \frac{N}{N!Z_N(U_1,\Omega)} \int_{\Omega^N} \delta(x-x_1) \exp\left[-\beta\left(\sum_{i=1}^{N} U_1(x_i) + \sum_{1\le i<j\le N} U_2(|x_i-x_j|)\right)\right] \mathrm{d}x_1 ... \mathrm{d}x_N \\
&= \frac{N}{N!Z_N(U_1,\Omega)} \int_{\Omega^{N-1}} \exp\left[-\beta\left(\sum_{i=2}^{N} U_1(x_i) + \sum_{2\le i<j\le N} U_2(|x_i-x_j|)\right)\right] \\
&\quad \times \exp\left[-\beta\left(U_1(x) + \sum_{2\le j\le N} U_2(|x-x_j|)\right)\right] \mathrm{d}x_2 ... \mathrm{d}x_N.
\end{aligned} \tag{2.4}$$

We note that, since U_1 is an external potential and U_2 is rotationally and translationally invariant, the density is rotationally and translationally invariant as well.

2.2.2 Integrating the N-particle Density

We can define the one-particle density as a special case of the n-particle density $n \le N$ (this is the approach used by [WGT+12, Equation (26)]). In essence the n-particle density can be obtained by integrating the spatial density (2.1) over the other $N-n$ particle positions and then multiplying by the number of ways of choosing n particles from the total set of N, this factor being necessary since the particles are indistinguishable. Thus the one-particle density can be written as

$$\rho_N(x_1) = N \int_{\Omega^{N-1}} \hat{\rho}_N(X_N) \mathrm{d}x_2 \dots \mathrm{d}x_N. \tag{2.5}$$

One can see that the integral of the one-particle density over Ω gives the particle number, i.e.

$$N = \int_{\Omega} \rho_N(x) \mathrm{d}x. \tag{2.6}$$

The new definition of one-particle density (2.5) can be seen be equal to (2.4). Inserting the canonical Gibbs measure (2.1) into (2.5) yields

$$\begin{aligned}
\rho_N(x_1) &= N \int_{\Omega^{N-1}} \frac{\exp[-\beta H_N(X_1, U_1)]}{N! Z_N(U_1, \Omega)} \mathrm{d}x_2 \dots \mathrm{d}x_N \\
&= \frac{N}{N! Z_N(U_1, \Omega)} \\
&\quad \times \int_{\Omega^{N-1}} \exp\left[-\beta \left(\sum_{i=1}^{N} U_1(x_i) + \sum_{1 \le i < j \le N} U_2(|x_i - x_j|) \right)\right] \mathrm{d}x_2 \dots \mathrm{d}x_N \\
&= \frac{N}{N! Z_N(U_1, \Omega)} \int_{\Omega^{N-1}} \exp\left[-\beta \left(\sum_{i=2}^{N} U_1(x_i) + \sum_{2 \le i < j \le N} U_2(|x_i - x_j|) \right)\right] \\
&\quad \times \exp\left[-\beta \left(U_1(x_1) + \sum_{2 \le j \le N} U_2(|x_1 - x_j|) \right)\right] \mathrm{d}x_2 ... \mathrm{d}x_N .
\end{aligned}$$

Relabelling x_1 as x gives (2.4).

2.2.3 Functional Derivative

Finally, we can also write the one-particle density at equilibrium as the functional derivative of the free energy with respect to the external energy

$$\rho_N(x) = \frac{\delta \mathcal{F}_N[U_1, \Omega]}{\delta U_1(x)}. \tag{2.7}$$

In general this is defined in a distributional sense.

Using [Fre06, Equation (C.6)], some re-arrangement gives a variation on the definition of the Gâteaux derivative (see [Fre06, Equation (C.7)] or [BN08, Definition 3.1])

$$\int_\Omega \frac{\delta \mathcal{F}_N[U_1, \Omega]}{\delta U_1(x)} \varphi(x) \mathrm{d}x = \frac{\mathrm{d}}{\mathrm{d}\epsilon} \mathcal{F}_N[U_1 + \epsilon\varphi, \Omega] \Big|_{\epsilon=0}$$

where $\varphi(x)$ is an arbitrary test function.

Thus we have, using the formula for the free energy (2.3),

$$\begin{aligned}
&\int_\Omega \frac{\delta \mathcal{F}_N[U_1,\Omega]}{\delta U_1(x)}\varphi(x)\mathrm{d}x \\
&= \frac{\mathrm{d}}{\mathrm{d}\epsilon}\beta^{-1}\Bigg(\ln N! \\
&\quad - \ln\left[\int_{\Omega^N} \exp\left[-\beta\left(\sum_{i=1}^N (U_1(x_i)+\epsilon\varphi(x_i)) + \sum_{1\le i<j\le N} U_2(|x_i-x_j|)\right)\right]\mathrm{d}X_N\right]\Bigg)\Bigg|_{\epsilon=0} \\
&= \frac{-\beta^{-1}\frac{\mathrm{d}}{\mathrm{d}\epsilon}\int_{\Omega^N} \exp\left[-\beta\left(\sum_{i=1}^N (U_1(x_i)+\epsilon\varphi(x_i)) + \sum_{1\le i<j\le N} U_2(|x_i-x_j|)\right)\right]\mathrm{d}X_N\Big|_{\epsilon=0}}{\int_{\Omega^N} \exp\left[-\beta\left(\sum_{i=1}^N U_1(x_i) + \sum_{1\le i<j\le N} U_2(|x_i-x_j|)\right)\right]\mathrm{d}X_N} \\
&= \frac{\int_{\Omega^N} \sum_{i=1}^N \varphi(x_i)\exp\left[-\beta\left(\sum_{i=1}^N (U_1(x_i)+\epsilon\varphi(x_i)) + \sum_{1\le i<j\le N} U_2(|x_i-x_j|)\right)\right]\mathrm{d}X_N\Big|_{\epsilon=0}}{N!Z_N(U_1,\Omega)} \\
&= \frac{\int_{\Omega^N} \sum_{i=1}^N \varphi(x_i)\exp\left[-\beta\left(\sum_{i=1}^N U_1(x_i) + \sum_{1\le i<j\le N} U_2(|x_i-x_j|)\right)\right]\mathrm{d}X_N}{N!Z_N(U_1,\Omega)}
\end{aligned}$$

where we have used the definition of the partition function $Z_N(U_1,\Omega)$ (2.2) in the third equality.

We now split into N integrals, one for each of the $\varphi(x_i)$. By re-labelling the x_i we see that these integrals are equivalent. Hence we have, labelling x as x_1,

$$\begin{aligned}
&\int_\Omega \frac{\delta \mathcal{F}_N[U_1,\Omega]}{\delta U_1(x_1)}\varphi(x_1)\mathrm{d}x_1 \\
&= \frac{\int_\Omega N\varphi(x_1)\int_{\Omega^{N-1}} \exp\left[-\beta\left(\sum_{i=1}^N U_1(x_i) + \sum_{1\le i<j\le N} U_2(|x_i-x_j|)\right)\right]\mathrm{d}x_2\ldots\mathrm{d}x_N\mathrm{d}x_1}{N!Z_N(U_1,\Omega)},
\end{aligned}$$

comparing the left and right-hand sides gives that the functional derivative is equivalent to the definition of the one-particle density given in (2.4).

2.3 The Hohenberg-Kohn Functional

The idea of density functional theory is to construct a functional which is minimised by the equilibrium one-particle density given in Section 2.2 and at this density is equal to the free energy.

A function g has permutation invariance if for all π in the symmetry group S_n

$$g(x_1, ..., x_n) = g(x_{\pi(1)}, ..., x_{\pi(n)}). \tag{2.8}$$

Given an arbitrary N-body distribution g_N with permutation invariance (since the particles are taken to be indistinguishable) such that

$$\int_{\Omega^N} g_N(X_N) \mathrm{d}X_N = 1 \tag{2.9}$$

we define the associated one-particle density (following [DS11, Equation (56)]) by

$$\tilde{\rho}(x) = \int_{\Omega^N} g_N(X_N) \sum_{i=1}^{N} \delta(x - x_i) \mathrm{d}X_N. \tag{2.10}$$

Remark 2.3.1. *Comparing with the method of [DS11, Section VI] we have rescaled the N-body distribution by $N!$.*

A process analogous to the one first carried out in [Eva79, Section 2] for the grand canonical ensemble and detailed for the canonical ensemble in [DS11, Section IV], shows that there is a functional that depends on the density and the potential which is minimised by the equilibrium density. This functional can be split into a functional $\mathcal{F}_{\mathrm{HK}}$ (known as the Hohenberg-Kohn functional), which is purely a functional of density, and the product of the density and the internal potential, that is,

$$\mathcal{F}_N[U_1, \Omega] = \min_{\tilde{\rho}(x)} \left[\mathcal{F}_{\mathrm{HK}}[\tilde{\rho}] + \int_{\Omega} U_1(x) \tilde{\rho}(x) \mathrm{d}x \right] \tag{2.11}$$

where the minimum is over all the one-particle densities given by (2.10). The Hohenberg-Kohn functional is given by

$$\mathcal{F}_{\mathrm{HK}}[\tilde{\rho}] = \min_{g_N \to \tilde{\rho}} \left[\int_{\Omega^N} g_N(X_N) \left(\sum_{1 \le i < j \le N} U_2(|x_i - x_j|) + \beta^{-1} \ln[N! g_N(X_N)] \right) \mathrm{d}X_N \right] \tag{2.12}$$

where $g_N \to \tilde{\rho}$ indicates that $\tilde{\rho}$ is obtained from g_N via (2.10). The existence of such a functional is a standard result, which is detailed in Appendix A.

Remark 2.3.2. *If we define a functional*

$$\mathcal{G}[\tilde{\rho}] = \mathcal{F}_{\mathrm{HK}}[\tilde{\rho}] + \int_{\Omega} U_1(x) \tilde{\rho}(x) dx,$$

then as above we have three ways of finding the density $\tilde{\rho}$. The first is as the average of N δ-functions with respect to g_N, i.e. (2.10)*. The second is by multiplying the integral of g_N over all but one variable by N by analogue with* (2.5)*. The final method is the functional derivative of $\mathcal{G}$ with respect to U_1 by analogue with* (2.7)*.*

From (A.2) and (2.11) we know the minimisation problem (2.11) is solved when $\tilde{\rho}$ is the equilibrium density ρ_N. Therefore we can write the free energy as

$$\mathcal{F}_N[U_1, \Omega] = \mathcal{F}_{\mathrm{HK}}[\rho_N(x)] + \int_\Omega U_1(x)\rho_N(x)\mathrm{d}x.$$

This formula gives a simple way of obtaining the free energy from the Hohenberg-Kohn functional if the external potential and equilibrium density are known. Henceforth we will mostly ignore the external potential U_1 (essentially we are considering an isolated system), and concentrate on calculating the Hohenberg-Kohn functional.

There is often no way to obtain an exact formula for the Hohenberg-Kohn functional, hence we will introduce several approximations.

We split the Hohenberg-Kohn functional into two components,

$$\mathcal{F}_{\mathrm{HK}}[\rho_N(x)] = \mathcal{F}_{\mathrm{HK,id}}[\rho_N(x)] + \mathcal{F}_{\mathrm{HK,exc}}[\rho_N(x)],$$

where $\mathcal{F}_{\mathrm{HK,id}}$ is the Hohenberg-Kohn functional associated with the ideal gas.

2.4 Ideal Gas Contribution

We now consider the free energy for the ideal gas $\mathcal{F}_{N,\mathrm{id}}[U_1, \Omega]$. The ideal gas functional is both an initial example of a DFT functional and a contribution to the Hohenberg-Kohn PFC functional. The ideal gas in the canonical ensemble is considered in [WG02, Section 4]. In the ideal gas case there is no internal interaction between particles, i.e., $U_2(x_1, x_2) = 0$. Thus, using the formula for the free energy (2.3), we have

$$\begin{aligned}
\mathcal{F}_{N,\mathrm{id}}[U_1, \Omega] &= -\beta^{-1} \ln\left[Z_N(U_1, \Lambda)\right] \\
&= -\beta^{-1} \ln \left[\frac{\int_{\Omega^N} \exp\left[-\beta \sum_{i=1}^{N} U_1(x_i)\right] \mathrm{d}X_N}{N!} \right] \\
&= -\beta^{-1} \left(\ln\left[\int_{\Omega^N} \prod_{i=1}^{N} \exp\left[-\beta U_1(x_i)\right] \mathrm{d}x_i \right] - \ln[N!] \right) \\
&= \beta^{-1} \left(\ln[N!] - N \ln\left[\int_\Omega \exp\left[-\beta U_1(x)\right] \mathrm{d}x \right] \right). \qquad (2.13)
\end{aligned}$$

The product of exponentials in the third equality follows by separating out each term of the sum within the exponential in the previous line.

Using the characterisation (2.7) of the one-particle density as the functional deriva-

tive of the free energy we have

$$\begin{aligned}
&\int_\Omega \rho_N(x)\varphi(x)\mathrm{d}x \\
&= \frac{\mathrm{d}}{\mathrm{d}\epsilon}\left(\beta^{-1}\left(\ln[N!] - N\ln\left[\int_\Omega \exp\left[-\beta\left(U_1(x)+\epsilon\varphi(x)\right)\right]\mathrm{d}x\right]\right)\right)\Bigg|_{\epsilon=0} \\
&= -\beta^{-1}N\frac{\dfrac{\mathrm{d}}{\mathrm{d}\epsilon}\left(\displaystyle\int_\Omega \exp\left[-\beta\left(U_1(x)+\epsilon\varphi(x)\right)\right]\mathrm{d}x\right)\Bigg|_{\epsilon=0}}{\displaystyle\int_\Omega \exp\left[-\beta U_1(x)\right]\mathrm{d}x}.
\end{aligned}$$

Defining $z(\Omega)$ by

$$z(\Omega) := \int_\Omega \exp\left[-\beta U_1(x)\right]\mathrm{d}x$$

we have

$$\int_\Omega \rho_N(x)\varphi(x)\mathrm{d}x = \frac{\int_\Omega N\varphi(x)\exp\left[-\beta U_1(x)\right]\mathrm{d}x}{z(\Omega)}.$$

Therefore, the density is given by

$$\rho_N(x) = \frac{N\exp\left[-\beta U_1(x)\right]}{z(\Omega)}. \tag{2.14}$$

We now want to re-arrange the free energy (2.13) to isolate the U_1 dependent part. From (2.14) we have

$$\ln[z(\Omega)] = -\ln\left[\frac{\rho_N(x)}{N}\right] - \beta U_1(x).$$

Since $\int_\Omega \rho_N(x)\mathrm{d}x = N$ (2.6), we can substitute the formula for $z(\Omega)$ above into the free energy (2.13) to give

$$\begin{aligned}
\mathcal{F}_{N,\mathrm{id}}[U_1,\Omega] &= \beta^{-1}\left(\ln[N!] + \int_\Omega \rho_N(x)\left(\ln\left[\frac{\rho_N(x)}{N}\right] + \beta U_1(x)\right)\mathrm{d}x\right) \\
&= \beta^{-1}\left(\ln[N!] - N\ln N\right) + \beta^{-1}\int_\Omega \rho_N(x)\ln\left[\rho_N(x)\right]\mathrm{d}x \\
&\quad + \int_\Omega \rho_N(x)U_1(x)\mathrm{d}x.
\end{aligned} \tag{2.15}$$

2.4.1 Stirling's Approximation

A generalisation of Stirling's approximation from [Rob55] is

$$\sqrt{2\pi N}N^N\exp[-N]\exp\left[\frac{1}{12N+1}\right] \leq N! \leq \sqrt{2\pi N}N^N\exp[-N]\exp\left[\frac{1}{12N}\right].$$

Taking logarithms we obtain

$$\frac{1}{2}\ln N+\frac{1}{2}\ln[2\pi]+N\ln N-N+\frac{1}{12N+1}\leq\ln[N!]\leq\frac{1}{2}\ln N+\frac{1}{2}\ln[2\pi]+N\ln N-N+\frac{1}{12N}.$$

Using these bounds we can simplify the approximation of $\ln[N!]$ (using $N>0$) to give

$$\ln[N!]=N(\ln N-1)+O(\ln N).$$

Applying this approximation to the ideal gas free energy (2.15) we obtain

$$\begin{aligned}\mathcal{F}_{N,\mathrm{id}}[U_1,\Omega]&=\beta^{-1}\left(-N+O(\ln N)\right)+\beta^{-1}\int_\Omega\rho_N(x)\ln\left[\rho_N(x)\right]\mathrm{d}x+\int_\Omega\rho_N(x)U_1(x)\mathrm{d}x\\&=\beta^{-1}\int_\Omega\rho_N(x)\left(\ln\left[\rho_N(x)\right]-1\right)\mathrm{d}x+\int_\Omega\rho_N(x)U_1(x)\mathrm{d}x+O(\ln N),\end{aligned}$$

where we have used the relation between the density and the particle number (2.6) in the last line. This is the same form as found in [WG02, Equation (71)].

When the number of particles N is large the right-hand term grows faster than linearly and therefore it dominates and we discard the $O(\ln N)$ term. Hence we approximate the ideal gas contribution to the Hohenberg-Kohn functional by

$$\mathcal{F}_{\mathrm{HK,id}}[\rho_N(x)]=\widehat{\mathcal{F}_{\mathrm{HK,id}}}[\rho_N(x)]+O(\ln N)$$

where

$$\widehat{\mathcal{F}_{\mathrm{HK,id}}}[\rho_N(x)]=\beta^{-1}\int_\Omega\rho_N(x)\left(\ln\left(\rho_N(x)\right)-1\right)\mathrm{d}x \tag{2.16}$$

which agrees with the ideal gas Hohenberg-Kohn functional in the grand canonical ensemble derived in [AM00, Section II.C] (up to a constant in the logarithmic term that arises from consideration of particles with momentum and quantum considerations). This is what we expect since in the thermodynamic limit all ensembles are postulated to agree, see [Ada06, Section 5.3].

2.4.2 The Ideal Gas Contribution

We want to directly address the $\ln(\rho_N(x))$ term in the approximation of the ideal gas functional (2.16) by using a Taylor expansion on this term. We therefore assume that there is a constant reference density ρ_{ref} such that the density for N particles can be written as

$$\rho_N(x)=\rho_{\mathrm{ref}}(1+\psi(x)) \tag{2.17}$$

where $|\psi(x)|\ll 1$.

Substituting the approximation for the density (2.17) into the approximation of the

ideal gas functional (2.16) gives

$$\begin{aligned}\widehat{\mathcal{F}_{\mathrm{HK,id}}}[\rho] &= \beta^{-1}\int_\Omega \rho_{\mathrm{ref}}(1+\psi(x))\left(\ln\left(\rho_{\mathrm{ref}}(1+\psi(x))\right)-1\right)\mathrm{d}x \\ &= \beta^{-1}\int_\Omega \rho_{\mathrm{ref}}\left(\ln\left(\rho_{\mathrm{ref}}\right)-1\right)\mathrm{d}x + \beta^{-1}\int_\Omega \rho_{\mathrm{ref}}\psi(x)\left(\ln\left(\rho_{\mathrm{ref}}\right)-1\right)\mathrm{d}x \\ &\quad + \beta^{-1}\rho_{\mathrm{ref}}\int_\Omega \ln(1+\psi(x))+\psi(x)\ln(1+\psi(x))\mathrm{d}x.\end{aligned}$$

We take the Taylor expansion of the logarithm and curtail at fourth order,

$$\begin{aligned}\widehat{\mathcal{F}_{\mathrm{HK,id}}}[\rho] &= \beta^{-1}\int_\Omega \rho_{\mathrm{ref}}\left(\ln\left(\rho_{\mathrm{ref}}\right)-1\right)\mathrm{d}x + \beta^{-1}\rho_{\mathrm{ref}}\int_\Omega \psi(x)\left(\ln\left(\rho_{\mathrm{ref}}\right)-1\right)\mathrm{d}x \\ &+\beta^{-1}\rho_{\mathrm{ref}}\int_\Omega \psi(x)-\frac{\psi(x)^2}{2}+\frac{\psi(x)^3}{3}-\frac{\psi(x)^4}{4}+\psi(x)^2-\frac{\psi(x)^3}{2}+\frac{\psi(x)^4}{3}+O\left(\psi(x)^5\right)\mathrm{d}x \\ &= \beta^{-1}|\Omega|\rho_{\mathrm{ref}}\left(\ln\left(\rho_{\mathrm{ref}}\right)-1\right) \\ &\quad + \beta^{-1}\rho_{\mathrm{ref}}\int_\Omega \ln(\rho_{\mathrm{ref}})\psi(x)+\frac{\psi(x)^2}{2}-\frac{\psi(x)^3}{6}+\frac{\psi(x)^4}{12}+O\left(\psi(x)^5\right)\mathrm{d}x \\ &= \widehat{\mathcal{F}_{\mathrm{HK,id}}}[\rho_{\mathrm{ref}}] + \beta^{-1}\rho_{\mathrm{ref}}\int_\Omega a_0\psi(x)+\frac{\psi(x)^2}{2}-\frac{\psi(x)^3}{6}+\frac{\psi(x)^4}{12}+O\left(\psi(x)^5\right)\mathrm{d}x,\end{aligned}$$

where we use the notation

$$a_0 = \ln(\rho_{\mathrm{ref}}).$$

We have not stated the higher order terms explicitly as we will discard them in order to obtain the PFC functional. In later sections we are only interested in

$$\Delta\mathcal{F}_{\mathrm{HK,id}}[\rho] = \mathcal{F}_{\mathrm{HK,id}}[\rho] - \mathcal{F}_{\mathrm{HK,id}}[\rho_{\mathrm{ref}}]$$

the relative energy change from the reference density.

The fourth order expansion is the lowest order which enables the formation of stable crystalline phases, see [EG04, Section I.B]. We can discard terms linear in $\psi(x)$ as this contribution is constant, i.e. we know

$$\int_\Omega \psi(x)\mathrm{d}x = C, \tag{2.18}$$

where C is a constant. This follows from the definition of ψ (2.17) and the fact that the integral of density is constant.

Hence our approximation of the ideal gas contribution is

$$\Delta\mathcal{F}_{\mathrm{HK,id}}[\psi(x)] \approx \beta^{-1}\rho_{\mathrm{ref}}\int_\Omega \frac{\psi(x)^2}{2}-\frac{\psi(x)^3}{6}+\frac{\psi(x)^4}{12}\mathrm{d}x. \tag{2.19}$$

2.5 The Excess Energy Contribution

We now approximate $\mathcal{F}_{\mathrm{HK,exc}}[\rho_N(x)]$. First, recall the reference density ρ_{ref} from (2.17), and take a functional Taylor expansion (see [Fre06, Equation (C.6)]) about a uniform fluid density ρ_{ref} using (2.17)

$$\mathcal{F}_{\mathrm{HK,exc}}[\rho_N(x)] = \mathcal{F}^{(0)}_{\mathrm{HK,exc}}(\rho_{\mathrm{ref}}) + \beta^{-1}\sum_{n=1}^{\infty}\frac{1}{n!}\mathcal{F}^{(n)}_{\mathrm{exc}}[\rho_N(x)]$$

where the higher order terms in the expansion are given by

$$\mathcal{F}^{(n)}_{\mathrm{exc}}[\rho_N(x)] = -\rho^n_{\mathrm{ref}}\int_\Omega\dots\int_\Omega c^{(n)}(x_1,\dots,x_n)\prod_{i=1}^{n}\psi(x_i)\mathrm{d}x_1\dots\mathrm{d}x_n$$

with

$$c^{(n)}(x_1,\dots,x_n) = -\beta\frac{\delta^n\mathcal{F}_{\mathrm{HK,exc}}[\rho_N(x)]}{\delta\rho_N(x_1)\dots\delta\rho_N(x_n)}\bigg|_{\rho_{\mathrm{ref}}}.$$

This expansion of the energy was also used in [Eva79, Subsection 6.2]. The linearity of $\mathcal{F}_{\mathrm{HK,exc}}$ in temperature T means that $c^{(n)}$ is independent of temperature. Since $c^{(1)}$ is constant (see Appendix B.1) in space, by (2.18), the contribution $\mathcal{F}^{(1)}_{\mathrm{exc}}$ is constant and can be absorbed in the reference term.

We note that $c^{(2)}$ is radial

$$c^{(2)}(x_1,x_2) = c^{(2)}(|x_1-x_2|). \tag{2.20}$$

This follows from the fact that the density is translationally and rotationally invariant; see Appendix B.2.

Therefore, the simplest approximation of the excess part of the Hohenberg-Kohn functional which has any contribution from the density is (see [YR79])

$$\mathcal{F}_{\mathrm{HK,exc}}[\rho_N(x)] \approx \mathcal{F}^{(0)}_{HK,exc}(\rho_{\mathrm{ref}}) - \frac{1}{2}\beta^{-1}\int_\Omega\int_\Omega c^{(2)}(|x_1-x_2|)\psi(x_1)\psi(x_2)\mathrm{d}x_1\mathrm{d}x_2. \tag{2.21}$$

We again only care about the difference between the energy functional and the energy functional at the reference density, hence we only consider

$$\Delta\mathcal{F}_{\mathrm{HK,exc}}[\rho_N(x)] = \mathcal{F}_{\mathrm{HK,exc}}[\rho_N(x)] - \mathcal{F}^{(0)}_{HK,exc}(\rho_{\mathrm{ref}}).$$

2.5.1 Gradient Expansion

The approximation for $\mathcal{F}_{\mathrm{HK,exc}}[\psi]$ (2.21) is currently non-local we now wish to transform it to make it local. As remarked above, (2.20), $c^{(2)}$ depends only on the distance between

particles. We consider the non-constant part of the excess energy approximation (2.21) i.e.

$$\Delta\mathcal{F}_{\mathrm{HK,exc}}[\rho_N(x)] = -\frac{1}{2}\beta^{-1}\rho_{\mathrm{ref}}^2\int_\Omega\int_\Omega \psi(x_1)c^{(2)}(|x_1-x_2|)\psi(x_2)\mathrm{d}x_1\mathrm{d}x_2.$$

Using the definition of a convolution integral, we have (see [Gra08, Proposition 2.2.11 (12)])

$$\begin{aligned}\int_\Omega c^{(2)}(|x_1-x_2|)\psi(x_2)\mathrm{d}x_2 &= \left(c^{(2)}*\psi\right)(x_1)\\ &= \mathfrak{F}^{-1}[\hat{c}(k)\hat{\psi}(k)],\end{aligned}$$

where $\mathfrak{F}$ is the Fourier transform and $\hat{c}(k) = \mathfrak{F}[c](k)$ and $\hat{\psi}(k) = \mathfrak{F}[\psi](k)$. We now expand $\hat{c}(k)$ as a Taylor series in $|k|$ which is possible since $\hat{c}$ is radial (see Appendix B.3),

$$\Delta\mathcal{F}_{\mathrm{HK,exc}}[\psi] = -\frac{1}{2}\beta^{-1}\rho_{\mathrm{ref}}^2\int_\Omega \psi(x_1)\mathfrak{F}^{-1}\left[\left(\sum_{m=0}^{\infty}c_{2m}|k|^{2m}\right)\hat{\psi}(k)\right]\mathrm{d}x_1,$$

where terms of the form $|k|^{2n+1}, n\in\mathbb{N}$ vanish since $c^{(2)}$ is spherically symmetric. That is, $\mathfrak{F}[c^{(2)}(r)] = \sum_{m=0}^{\infty}c_m|k|^m = \mathfrak{F}[c^{(2)}(-r)] = \sum_{m=0}^{\infty}(-1)^m c_m|k|^m$ and hence $c_m = 0$ if $m = 2n+1$. Since

$$\mathfrak{F}^{-1}[k_i^n\hat{\psi}(k)] = i^n\partial_{x_i}^n\psi, \tag{2.22}$$

(see [Gra08, Proposition 2.2.11 (9)]) after applying the inverse Fourier transform to each term in the product, we obtain

$$\Delta\mathcal{F}_{\mathrm{HK,exc}}[\psi] = -\frac{1}{2}\beta^{-1}\rho_{\mathrm{ref}}^2\int_\Omega \psi(x_1)\left(\sum_{m=0}^{\infty}(-1)^m c_{2m}\nabla^{2m}\right)\psi(x_1)\mathrm{d}x_1.$$

Thus, the excess energy difference can be formally approximated by

$$\Delta\mathcal{F}_{\mathrm{HK,exc}}[\psi] \approx -\frac{1}{2}\beta^{-1}\rho_{\mathrm{ref}}^2\int_\Omega \psi(x_1)\left(\sum_{i=0}^{\infty}(-1)^m c_{2m}\nabla^{2m}\right)\psi(x_1)\mathrm{d}x_1 \tag{2.23}$$

The exact form of the constants c_{2m} in (2.23) is non-obvious and depends on the dimension and on U_2. The terms of the Fourier series for $\hat{c}$ can be found using successive derivatives evaluated at zero, i.e.

$$c_n = \frac{1}{n!}\frac{\partial^n\hat{c}}{\partial k^n}(0) = \int\frac{(ix)^n c^{(2)}(x)}{n!}\mathrm{d}x \tag{2.24}$$

where the second equation follows from the relation between derivatives and the variable in Fourier space (2.22). Hence as $c^{(2)}(r)$ depends on a variable r which is always positive the signs of the coefficients $\hat{c}_n$ will alternate. This is exactly the form required for the PFC functional. The reasons for this are considered in (2.26) where we give the form of the constants in the PFC functional.

We also curtail the gradient expansion at fourth order as this is the lowest one that makes stable periodic density fields possible, see the text above [EG04, Equation (6)] for some justification. Curtailing at fourth order in the gradient expansion we can re-write the approximate excess energy (2.23) as

$$\Delta\mathcal{F}_{\mathrm{HK,exc}}[\psi(x)] \approx -\frac{\rho_{\mathrm{ref}}}{2}\beta^{-1}\int_{\Omega} A_1\psi^2(x) + A_2\psi(x)\nabla^2\psi(x) + A_3\psi(x)\nabla^4\psi(x)\mathrm{d}x$$

where (in 3 dimensions)

$$A_1 = 4\pi\rho_{\mathrm{ref}}\int_0^\infty r^2c^2(r)\mathrm{d}r,$$
$$A_2 = \frac{2}{3}\pi\rho_{\mathrm{ref}}\int_0^\infty r^4c^2(r)\mathrm{d}r, \qquad A_3 = \frac{\rho_{\mathrm{ref}}\pi}{30}\int_0^\infty r^6c^2(r)\mathrm{d}r.$$

The form of these constants is taken from [WGT+12] and can be derived using (2.24).

2.6 Non-Dimensionalisation and the PFC Model

We now derive the PFC model by combining the ideal gas and excess energy contributions, see Sections 2.4 and 2.5, these are approximations of the two parts of the Hohenberg-Kohn functional of DFT. The link between DFT and PFC was suggested by [EPB+07], this paper also include binary alloys whilst we will only focus on pure materials. A cogent account of the derivation can also be found in [WGT+12]. We first follow [WGT+12, Section 2.3].

Combining the approximations of $\Delta F_{\mathrm{HK,id}}$, (2.19), and $\Delta F_{\mathrm{HK,exc}}$, (2.23), gives (this is slightly different from [WGT+12] where the authors consider the true functional rather then the difference from the reference functional)

$$\Delta\mathcal{F}_{\mathrm{HK}}[\psi(x)] \approx$$
$$\rho_{\mathrm{ref}}\beta^{-1}\int_{\Omega}\left(A_1'\psi(x)^2 + A_2'\psi(x)\nabla^2\psi(x) + A_3'\psi(x)\nabla^4\psi(x) - \frac{\psi(x)^3}{6} + \frac{\psi(x)^4}{12}\right)\mathrm{d}x \quad (2.25)$$

where the constants are given by

$$A_1' = \frac{1}{2}(1 - A_1) \qquad A_2' = -\frac{1}{2}A_2 \qquad A_3' = -\frac{1}{2}A_3. \quad (2.26)$$

[WGT+12] suggests A_2' should be positive in order to favour non-uniform phases, and $A_3' > 0$ for stability reasons. In particular the method used below (Theorem 3.2.1) for finding a minimum will not work if $A_3' < 0$. The existence of a maximum is excluded by the L^4-term and the negative coefficient on the highest derivative excludes the possibility of a minimum. Some heuristic justification of the form of the functional is given in [EG04, Section I.B] and the signs of the coefficients of the functional are motivated from a physical point of view in [EPB+07, Section III].

We wish to transform the functional (2.25) i.e. to reformulate the functional differ-

ence to be of the form

$$\tilde{\mathcal{F}} = \int_\Omega \left(\frac{\bar{\psi}}{2} \left(- ß + \left(k_0^2 + \nabla^2 \right)^2 \right) \bar{\psi} + \frac{\bar{\psi}^4}{4} \right) \mathrm{d}\bar{x}. \tag{2.27}$$

The reason for this transformation is to exhibit the multi-well structure of the functional and to allow easier comparison with existing literature on the PFC model, e.g. [WWL09], [EG04], [Ban11] and [EW13].

This is the form initially given for PFC theory in [EKHG02]. This form can be obtained by taking $p = 0$ in the normalised functional below (2.29) as in [WGT+12, Subsection 3.1.1.1]. However given the definition of p this seems to be unphysical so we use a transformation to remove this term.

In contrast to discarding the cubic term of (2.25) we show that we can obtain (2.27) from (2.25) by a change of variables. For simplicity we start with the desired functional (2.27). We then substitute the formula $\bar{\psi} = \alpha(1 - 2\psi(x))$ [2] into this functional. We can discard constant terms and terms linear in ψ using the same arguments as in Section 2.4. Our expansion of (2.27) then simplifies to the initial form of the functional (2.25). Substituting $\bar{\psi}$ in the desired form of the functional (2.27) we have

$$\tilde{\mathcal{F}} = \int_\Omega \left(\frac{\alpha(1 - 2\psi(x))}{2} \left(-ß + \left(k_0^2 + \nabla^2 \right)^2 \right) \alpha(1 - 2\psi(x)) + \frac{(\alpha(1 - 2\psi(x)))^4}{4} \right) \mathrm{d}x$$

expanding the quadratic in ψ and the square in ∇^2 we have

$$\begin{aligned} \tilde{\mathcal{F}} = \int_\Omega & \frac{\alpha^2(1 - 2\psi(x))^2}{2}(-ß + k_0^4) - 2k_0^2\alpha^2(1 - 2\psi(x))\nabla^2\psi(x) - \alpha^2(1 - 2\psi(x))\nabla^4\psi(x) \\ & + \frac{\alpha^4}{4} - 2\alpha^4\psi(x) + 6\alpha^4\psi(x)^2 - 8\alpha^4\psi(x)^3 + 4\alpha^4\psi(x)^4 \mathrm{d}x. \end{aligned}$$

Expanding out the first term we can write $\tilde{\mathcal{F}}$ in terms of powers of ψ and its derivatives, i.e.

$$\begin{aligned} \tilde{\mathcal{F}} = \int_\Omega & \frac{\alpha^2(-ß + k_0^4)}{2} + \frac{\alpha^4}{4} - 2\alpha^2(-ß + k_0^4)\psi(x) - 2\alpha^4\psi(x) - 2\alpha^2 k_0^2\nabla^2\psi(x) \\ & - \alpha^2\nabla^4\psi(x) + \left(2\alpha^2(-ß + k_0^4) + 6\alpha^4 \right)\psi(x)^2 - 8\alpha^4\psi(x)^3 + 4\alpha^4\psi(x)^4 \\ & + 4\alpha^2 k_0^2\psi(x)\nabla^2\psi(x) + 2\alpha^2\psi(x)\nabla^4\psi(x)\mathrm{d}x. \end{aligned}$$

We discard the first two terms as they will remain constant regardless of the density used. We use that linear multiplies of ψ are constant (2.18) to discard the next two terms. Finally since ψ and its derivatives are periodic we can discard the next two terms as well. The

[2] Physically this is 1 minus the density fluctuation scaled by the coefficient of the higher order derivative term.

functional $\tilde{\mathcal{F}}$ then simplifies to

$$\tilde{\mathcal{F}} = \int_\Omega \left(2\alpha^2(-ß + k_0^4) + 6\alpha^4\right)\psi(x)^2 - 8\alpha^4\psi(x)^3 + 4\alpha^4\psi(x)^4 + 4\alpha^2 k_0^2\psi(x)\nabla^2\psi(x) + 2\alpha^2\psi(x)\nabla^4\psi(x)\mathrm{d}x.$$

This is clearly of the desired form, that is we have completed the derivation of the PFC functional (2.27).

2.7 Discussion

We now follow [WGT+12, Section 3.1.1], this allows us to simplify the functional form and to give a physical intuition for the form of the constants involved. Consider the Taylor expansion of $\hat{c}(k)$

$$\hat{c}(k) = \tilde{c}_0^{(2)} + \tilde{c}_2^{(2)}|k|^2 + \dots$$

which has its first peak at $k = 2\pi R_p^{-1}$ [3] (R_p, the inter-particle distance). We re-scale $\hat{c}$ to include the reference density ρ_{ref} and the inter-atomic spacing R_p, i.e.

$$c(k) = \rho_{\text{ref}}\hat{c}(k) \approx \sum_{j=0}^{M} b_{2j}\left(|k|R_p\right)^{2j}.$$

We can now rewrite the functional (2.25) using this reformulation and using the new variables given in [WGT+12] (the authors state a relation to physical constants for B_1 and B_s which we will state and provide a justification for later)

$$\begin{aligned} B_1 &= 1 + |b_0| \\ B_s &= \frac{|b_2|^2}{4|b_4|} \\ R &= R_p\left(\frac{2|b_4|}{|b_2|}\right)^{\frac{1}{2}}. \end{aligned}$$

The functional difference we obtain is then

$$\Delta\mathcal{F}_{\text{HK}} \approx \rho_{\text{ref}}\beta^{-1}\int_\Omega \frac{\psi}{2}\left(B_1 + B_s\left(2R^2\nabla^2 + R^4\nabla^4\right)\right)\psi - \frac{\psi^3}{6} + \frac{\psi^4}{12}\mathrm{d}x.$$

By comparison to [WGT+12, Equation (52)] we have set $v = 1$ where v according to this source accounts for the zeroth order contribution for the particle correlations. By dimensional analysis (in three dimensions) we obtain, a relation for B_1, i.e.

$$B_1 = \frac{\beta}{\kappa\rho_{\text{ref}}},$$

[3] This gives peaks separated by atomic distance R_p

at least up to some dimensionless constant of proportionality, where κ is the compressibility.

We now use a second change of variables, i.e.

$$x_i = R\tilde{x}_i \qquad \psi = (3B_s)^{\frac{1}{2}}\,\tilde{\psi} \qquad \Delta\mathcal{F}_{\mathrm{HK}} = (3\rho_{\mathrm{ref}}\beta^{-1}R^dB_s^2)\Delta\tilde{\mathcal{F}}_{\mathrm{HK}}$$

substituting the above expressions for $\tilde{x}$, $\tilde{\psi}$ and $\Delta\tilde{\mathcal{F}}_{\mathrm{HK}}$ into the expression for $\Delta\mathcal{F}_{\mathrm{HK}}$ we have

$$\begin{aligned}\Delta\tilde{\mathcal{F}}_{\mathrm{HK}} &\approx \frac{1}{3B_s^2}\int_{\tilde{\Omega}} 3B_s\left(\frac{\tilde{\psi}}{2}\left(B_1 + B_s\left(1+\nabla^2\right)^2 - B_s\right)\tilde{\psi}\right) - 3\sqrt{3}B_s^{\frac{3}{2}}\frac{\tilde{\psi}^3}{6} + 9B_s^2\frac{\tilde{\psi}^4}{12}\mathrm{d}\tilde{x}\\ &\approx \int_{\tilde{\Omega}}\frac{\tilde{\psi}}{2}\left(\frac{B_1-B_s}{B_s} + \left(1+\nabla^2\right)^2\right)\tilde{\psi} - \frac{\sqrt{3}}{\sqrt{B_s}}\frac{1}{2}\frac{\tilde{\psi}^3}{3} + \frac{\tilde{\psi}^4}{4}\mathrm{d}\tilde{x} \qquad (2.28)\end{aligned}$$

where $\tilde{\Omega}$ is the appropriately rescaled domain. From this we can see that B_1 and B_s have the same dimensionality and thus (in three dimensions)

$$B_s = \frac{K\beta}{\rho_{\mathrm{ref}}}$$

at least up to a dimensionless constant of proportionality, where K is the bulk modulus.

Therefore we can re-write the above energy difference (2.28) as

$$\Delta\tilde{\mathcal{F}}_{\mathrm{HK}} \approx \int_{\tilde{\Omega}}\frac{\tilde{\psi}}{2}\left(-\epsilon + \left(1+\nabla^2\right)^2\right)\tilde{\psi} + p\frac{\tilde{\psi}^3}{3} + \frac{\tilde{\psi}^4}{4}\mathrm{d}\tilde{x} \qquad (2.29)$$

where the two constants are given by

$$\epsilon = \frac{B_s - B_1}{B_s} = 1 - \frac{K}{\kappa}, \qquad p = -\frac{\sqrt{3}}{\sqrt{B_s}}\frac{1}{2}.$$

ϵ is thus clearly dimensionless, [WGT+12] claims p is dimensionless.

2.8 Conclusion

In this chapter we have presented a formal derivation of the PFC model. We start with the canonical ensemble of statistical mechanics and from this restate the formulation of DFT. The DFT formulation means that we can formulate the free energy as a functional of the one-particle density. We then justify the formula for the free energy for the ideal gas and implement the splitting of the free energy into the ideal gas free energy and the excess free energy. Finally we approximate the density as a fluctuation around a reference density and expand the ideal gas energy using a Taylor series and the excess free energy using a gradient expansion, curtailing at fourth order gives the required PFC functional.

Chapter 3

Analysis of the PFC Model

In this chapter we consider the problem of minimising the PFC functional subject to a prescribed average of the variable. We first prove several properties of the PFC functional that will allow us to formulate the minimisation problem. We then prove the existence of a minimum of the PFC functional, formulate the associated PDE and prove smoothness of its solution.

Let $\Omega \subset \mathbb{R}^d, (d = 2, 3)$ be a domain (with periodic boundary conditions), given by

$$\Omega = \begin{cases} (0, L_x) \times (0, L_y), & \text{when } d = 2, \\ (0, L_x) \times (0, L_y) \times (0, L_z), & \text{when } d = 3, \end{cases}$$

where L_x, L_y and L_z are integer multiples of the length of the unit domain in the x, y and z directions respectively. For example, [EG04, Section II.C] suggests that, in two dimensions,

$$L_x = (2\pi/\sqrt{3})n, \quad L_y = 2\pi m \quad \text{for } n, m \in \mathbb{N}.$$

We impose periodic boundary conditions, since in Chapter 8 we will use Fourier spectral methods for discretisation in space. Fourier methods are useful as we can obtain super-algebraic convergence of the spatial discretisation to the solution (and possibly even exponential convergence, see Subsection 8.2.2). The focus of our thesis is the time discretisation and therefore we only consider Fourier spectral methods for the spatial discretisation; however, this discretisation could be undertaken using other methods, see [WWL09] for an example of alternative spatial discretisation of the PFC equation.

We will consider trial functions for the PFC functional drawn from subspaces of the space of periodic H^2-functions. The use of a subspace of $H^2(\Omega)$ rather than a subspace of another H^k-space will be justified in the next section.

For convenience we use the equivalence of $\|\Delta\eta\|_{L^2(\Omega)}$ and $\|\nabla^2\eta\|_{L^2(\Omega)}$ to give an alternative definition of the H^2-norm.

Definition 3.0.1. *The H^2-norm for η in $H^2(\Omega)$ is defined by*

$$\|\eta\|^2_{H^2(\Omega)} = \|\eta\|^2_{L^2(\Omega)} + \|\nabla\eta\|^2_{L^2(\Omega)} + \|\Delta\eta\|^2_{L^2(\Omega)}.$$

Recall the PFC functional (2.27)

$$\mathcal{F}[\eta] = \frac{1}{2}\|\Delta\eta + \eta\|^2_{L^2(\Omega)} - \frac{\delta}{2}\|\eta\|^2_{L^2(\Omega)} + \frac{1}{4}\|\eta\|^4_{L^4(\Omega)}, \tag{3.1}$$

where δ is a positive constant. In line with [EKHG02] we wish to minimise $\mathcal{F}$ over all trial functions with prescribed mean,

$$\bar{u} = \frac{1}{|\Omega|}\int_\Omega \eta \mathrm{d}x.$$

As mentioned in the previous chapter this constraint is equivalent to the requirement that mass is conserved within the system.

3.1 Preliminaries

For the sake of convenience we collect a series of inequalities that we will use for the proofs and lemmas throughout this chapter. We also state the function space that we will use to formulate our problem.

Definition 3.1.1. *The function space of periodic H^2-functions with fixed average $\bar{u}$ is defined by*

$$H^2_{\bar{u}}(\Omega) := \left\{ \eta \in H^2(\Omega) \;\middle|\; \eta = \bar{u} + \eta_0, \eta_0 \in H^2_\#(\Omega) \right\}$$

where $H^2_\#(\Omega)$ is defined in Definition C.1.2.

We now define a norm that will prove useful throughout this thesis.

Definition 3.1.2 (The A_1-norm)**.**

$$\|\eta\|^2_{A_1} := \|\eta\|^2_{L^2(\Omega)} + \|\Delta\eta + \eta\|^2_{L^2(\Omega)}.$$

We show this norm is equivalent to the H^2-norm on $H^2_{\mathrm{per}}(\Omega)$.

Lemma 3.1.1. *The A_1-norm is an equivalent norm to the H^2-norm, i.e.*

$$\frac{1}{5}\|\eta\|^2_{H^2(\Omega)} \leq \|\eta\|^2_{A_1} \leq 2\|\eta\|^2_{H^2(\Omega)}$$

for all η in $H^2_{\mathrm{per}}(\Omega)$.

Proof. Using the triangle inequality and Young's inequality we can bound

$$\|\Delta\eta\|^2_{L^2(\Omega)} \leq 2\|\Delta\eta + \eta\|^2_{L^2(\Omega)} + 2\|\eta\|^2_{L^2(\Omega)}.$$

Using integration by parts we can bound

$$\begin{aligned}\|\nabla\eta\|_{L^2}^2 &= \int_\Omega -\eta\Delta\eta + \eta^2 - \eta^2 \mathrm{d}x,\\ &\leq \left|\int_\Omega \eta\Delta\eta + \eta^2 \mathrm{d}x\right| + \|\eta\|_{L^2(\Omega)}^2,\\ &\leq \|\Delta\eta + \eta\|_{L^2(\Omega)}\|\eta\|_{L^2(\Omega)} + \|\eta\|_{L^2(\Omega)}^2,\\ &\leq \left(1 + \frac{1}{2\epsilon'}\right)\|\eta\|_{L^2(\Omega)}^2 + \frac{\epsilon'}{2}\|\Delta\eta + \eta\|_{L^2(\Omega)}^2, \end{aligned} \tag{3.2}$$

where we have used the triangle inequality in the second line and then used the Cauchy-Schwarz inequality and Young's inequality with ϵ' on the left-hand term of the upper bound.

Using the definition of the H^2-norm, Definition 3.0.1, we have a bound for the H^2-norm,

$$\begin{aligned}\|\eta\|_{H^2(\Omega)}^2 &= \|\eta\|_{L^2(\Omega)}^2 + \|\nabla\eta\|_{L^2(\Omega)}^2 + \|\Delta\eta\|_{L^2(\Omega)}^2,\\ &\leq \|\eta\|_{L^2(\Omega)}^2 + \left(1 + \frac{1}{2\epsilon'}\right)\|\eta\|_{L^2(\Omega)}^2 + \frac{\epsilon'}{2}\|\Delta\eta + \eta\|_{L^2(\Omega)}^2 + 2\|\Delta\eta + \eta\|_{L^2(\Omega)}^2\\ &\quad + 2\|\eta\|_{L^2(\Omega)}^2,\\ &\leq \left(4 + \frac{1}{2\epsilon'}\right)\|\eta\|_{L^2(\Omega)}^2 + \left(2 + \frac{\epsilon'}{2}\right)\|\Delta\eta + \eta\|_{L^2(\Omega)}^2. \end{aligned}$$

Equating the two coefficients gives $\epsilon' = 2 + \sqrt{5}$ and thus

$$\begin{aligned}\|\eta\|_{H^2(\Omega)}^2 &\leq \left(\frac{6+\sqrt{5}}{2}\right)\left(\|\eta\|_{L^2(\Omega)}^2 + \|\Delta\eta + \eta\|_{L^2(\Omega)}^2\right),\\ &\leq 5\left(\|\eta\|_{L^2(\Omega)}^2 + \|\Delta\eta + \eta\|_{L^2(\Omega)}^2\right). \end{aligned}$$

We now show that the A_1-norm is bounded above by the H^2-norm. Recall the definition of the A_1-norm, Definition 3.1.2, i.e.

$$\|\eta\|_{A_1}^2 = \left(\|\eta\|_{L^2(\Omega)}^2 + \|\Delta\eta + \eta\|_{L^2(\Omega)}^2\right).$$

We can expand the second term

$$\begin{aligned}\|\Delta\eta + \eta\|_{L^2(\Omega)}^2 &= \|\Delta\eta\|_{L^2(\Omega)}^2 + 2\int_\Omega \Delta\eta\eta \mathrm{d}x + \|\eta\|_{L^2(\Omega)}^2,\\ &\leq \|\Delta\eta\|_{L^2(\Omega)}^2 - 2\|\nabla\eta\|_{L^2(\Omega)}^2 + \|\eta\|_{L^2(\Omega)}^2,\\ &\leq \|\Delta\eta\|_{L^2(\Omega)}^2 + \|\eta\|_{L^2(\Omega)}^2, \end{aligned} \tag{3.3}$$

the second line follows from the periodicity of η.

Substituting this into the A_1-bound we have

$$\|\eta\|_{A_1}^2 \leq 2\|\eta\|_{L^2(\Omega)}^2 + \|\Delta\eta\|_{L^2(\Omega)}^2 \leq 2\|\eta\|_{H^2(\Omega)}^2.$$

□

We note that the spaces introduced, Definitions C.1.1, C.1.2 and 3.1.1, are all subspaces of H^2. We now show that $\mathcal{F}[\eta]$ is well-defined and real if and only if $\eta \in H^2(\Omega)$.

Lemma 3.1.2. *For all η in $H^2(\Omega)$ the PFC functional* (3.1) *is bounded above and below by*

$$\frac{1}{10}\|\eta\|_{H^2(\Omega)}^2 - (\delta+1)^2|\Omega| \leq \mathcal{F}[\eta] \leq \frac{1}{2}\|\eta\|_{H^2(\Omega)}^2 + \frac{1}{4}\|\eta\|_{H^2(\Omega)}^4.$$

In particular, $\mathcal{F}[\eta]$ is finite if and only if $\eta \in H^2(\Omega)$.

Proof. We first prove the upper bound. This follows with some obvious adaptations from [WW10, Lemma 3.1], however, we include the proof to emphasise the H^2-dependence which is not explicit in [WW10, Lemma 3.1].

By discarding the negative term in the PFC functional (3.1) we obtain

$$\mathcal{F}[\eta] \leq \frac{1}{2}\|\Delta\eta + \eta\|_{L^2(\Omega)}^2 + \frac{1}{4}\|\eta\|_{L^4(\Omega)}^4. \tag{3.4}$$

Recall from (3.3) that the first term of this bound can easily be bounded by the H^2-norm

$$\|\Delta\eta + \eta\|_{L^2(\Omega)}^2 \leq \|\eta\|_{H^2(\Omega)}^2.$$

Using Ladyzhenskaya's inequality, Lemma C.2.1, we can estimate

$$\|\eta\|_{L^4(\Omega)} \leq \|\eta\|_{L^2(\Omega)}^{1-\frac{d}{4}}\|\eta\|_{H^1(\Omega)}^{\frac{d}{4}} \leq \|\eta\|_{H^2(\Omega)}. \tag{3.5}$$

Combining this inequality with (3.3) and (3.4), we obtain

$$\mathcal{F}[\eta] \leq \frac{1}{2}\|\eta\|_{H^2(\Omega)}^2 + \frac{1}{4}\|\eta\|_{H^2(\Omega)}^4.$$

This completes the proof of the upper bound.

We now show that the PFC functional is bounded below for all η in $H^2(\Omega)$, which parallels the result of [WW10, Lemma 3.1]. A finite dimensional analogue is also considered in [WWL09, Lemma 3.7]. However, the bounds given here are more explicit and the exposition of the proof is extended to improve clarity.

The PFC functional (3.1) can be re-written by splitting it into a positive term and a double-well potential-like term,

$$\mathcal{F}[\eta] = \frac{1}{2}\|(\Delta + I)\eta\|_{L^2(\Omega)}^2 + \frac{1}{2}\int_\Omega \eta^2\left(\frac{\eta^2}{2} - \delta\right)\mathrm{d}x.$$

The first term on the right-hand side is always positive while the second term is positive outside the region were η is small, i.e. $\eta^2 \leq 2\delta$. Let $\epsilon > 0$, then we define the set $\Omega_\delta^\epsilon := \{\eta^2 \leq 2\delta + \epsilon\}$. We can now split the double-well term into

$$\mathcal{F}[\eta] = \frac{1}{2}\|(\Delta + I)\eta\|^2_{L^2(\Omega)} + \frac{1}{2}\int_{(\Omega_\delta^\epsilon)^c} \eta^2 \left(\frac{\eta^2}{2} - \delta\right) \mathrm{d}x - \frac{1}{2}\int_{\Omega_\delta^\epsilon} \eta^2 \left(\delta - \frac{\eta^2}{2}\right) \mathrm{d}x,$$

where $(\Omega_\delta^\epsilon)^c = \Omega \backslash \Omega_\delta^\epsilon$. Using $\eta^2 - 2\delta \geq \epsilon$ on $(\Omega_\delta^\epsilon)^c$, we have

$$\begin{aligned}
\mathcal{F}[\eta] &\geq \frac{1}{2}\|(\Delta + I)\eta\|^2_{L^2(\Omega)} + \frac{\epsilon}{4}\|\eta\|^2_{L^2((\Omega_\delta^\epsilon)^c)} - \frac{1}{2}\int_{\Omega_\delta^\epsilon} \eta^2 \left(\delta - \frac{\eta^2}{2}\right) \mathrm{d}x, \\
&= \frac{1}{2}\|(\Delta + I)\eta\|^2_{L^2(\Omega)} + \frac{\epsilon}{4}\|\eta\|^2_{L^2((\Omega_\delta^\epsilon)^c)} - \frac{1}{2}\int_{\Omega_\delta^\epsilon} \eta^2 \left(\delta - \frac{\eta^2}{2}\right) \mathrm{d}x \\
&\quad + \frac{\epsilon}{4}\|\eta\|^2_{L^2(\Omega_\delta^\epsilon)} - \frac{\epsilon}{4}\|\eta\|^2_{L^2(\Omega_\delta^\epsilon)}, \\
&= \frac{1}{2}\|(\Delta + I)\eta\|^2_{L^2(\Omega)} + \frac{\epsilon}{4}\|\eta\|^2_{L^2(\Omega)} - \frac{1}{2}\int_{\Omega_\delta^\epsilon} \eta^2 \left(\delta - \frac{\eta^2}{2}\right) \mathrm{d}x - \frac{\epsilon}{4}\|\eta\|^2_{L^2(\Omega_\delta^\epsilon)}.
\end{aligned}$$

Using $0 \leq \eta^2 \leq 2\delta + \epsilon$ in Ω_δ^ϵ to bound the third and fourth terms of the right-hand side, we have that the energy can be bounded below by

$$\begin{aligned}
\mathcal{F}[\eta] &\geq \frac{1}{2}\|(\Delta + I)\eta\|^2_{L^2(\Omega)} + \frac{\epsilon}{4}\|\eta\|^2_{L^2(\Omega)} - \left((2\delta + \epsilon)\frac{\delta}{2} + \frac{\epsilon}{4}(2\delta + \epsilon)\right)|\Omega_\delta^\epsilon|, \\
&\geq \frac{1}{2}\|(\Delta + I)\eta\|^2_{L^2(\Omega)} + \frac{\epsilon}{4}\|\eta\|^2_{L^2(\Omega)} - \frac{(2\delta + \epsilon)^2}{4}|\Omega_\delta^\epsilon| \qquad (3.6)
\end{aligned}$$

for any $\epsilon > 0$.

The lower bound (3.6), together with Lemma 3.1.1, gives

$$\mathcal{F}[\eta] \geq \frac{\min\left(1, \frac{\epsilon}{2}\right)}{10}\|\eta\|^2_{H^2(\Omega)} - \frac{(2\delta + \epsilon)^2}{4}|\Omega_\delta^\epsilon|.$$

Since $\Omega_\delta^\epsilon \subset \Omega$ for all $\epsilon > 0$ we have the uniform bound. For simplicity we set $\epsilon = 2$.

□

From the previous lemma we obtain L^∞-bounds on sublevels of $\mathcal{F}$.

Lemma 3.1.3. *There exist constants C_1, $C_2 > 0$ such that*

$$\|\eta\|_{L^\infty(\Omega)} \leq \sqrt{C_1\mathcal{F}[\eta] + C_2|\Omega|}, \qquad \forall \eta \in H^2_{\mathrm{per}}(\Omega).$$

Proof. We recall the upper bound for the H^2-norm in terms of the energy, Lemma 3.1.2 and re-arrange to give

$$\|\eta\|_{H^2(\Omega)} \leq \sqrt{10\mathcal{F}[\eta] + 10(\delta + 1)^2|\Omega|}. \qquad (3.7)$$

Since a rectangular or parallelepiped domain satisfies the cone condition, we can use the

result of [Ada75, Corollary 5.16] to bound the L^∞-norm by the H^2-norm, i.e.

$$\|\eta\|_{L^\infty(\Omega)} \leq C(\Omega)\|\eta\|_{H^2(\Omega)}. \tag{3.8}$$

Let Q be the unit domain, i.e. the smallest domain on which the solution is periodic. Clearly by (3.8) there exists a $C_Q > 0$ such that

$$\|\eta\|_{L^\infty(Q)} \leq C_Q\|\eta\|_{H^2(Q)} \leq C_Q\|\eta\|_{H^2(\Omega)}.$$

The domain Ω is constructed from N_x, N_y and N_z unit domains in the x,y and z directions respectively ($N_z = 1$ in 3 dimensions). Let $Q_{i,j,k}$ denote the unit domain with origin (iL_x, jL_y, kL_z) then clearly

$$\Omega = \bigcup_{0\leq i\leq N_x-1, 0\leq j\leq N_y-1, 0\leq k\leq N_z-1} Q_{i,j,k}.$$

Then we have

$$\|\eta\|_{L^\infty(\Omega)} = \sup_{0\leq i\leq N_x-1, 0\leq j\leq N_y-1, 0\leq k\leq N_z-1} \|\eta\|_{L^\infty(Q_{i,j,k})} = \|\eta\|_{L^\infty(Q)} \leq C_Q\|\eta\|_{H^2(\Omega)}.$$

Hence the constant C is independent of domain. (3.7) then implies a bound for the L^∞-norm,

$$\|\eta\|_{L^\infty(\Omega)} \leq C\sqrt{10\mathcal{F}[\eta] + 10(\delta+1)^2|\Omega|}.$$

□

In general we will consider minimisation of the PFC functional (3.1) by methods associated with gradient flows. As a prerequisite to this we define the first and second variations.

Lemma 3.1.4. *The PFC functional is infinitely Fréchet differentiable and its first and second variations are given, respectively, by*

$$\delta\mathcal{F}[\eta, v] = \int_\Omega (\Delta\eta + \eta)(\Delta v + v)\,dx - \delta\int_\Omega \eta v\,dx + \int_\Omega \eta^3 v\,dx, \quad \forall \eta, v \in H^2(\Omega), \tag{3.9}$$

$$\delta^2\mathcal{F}[\eta, v, v] = \|\,(\Delta + I)\,v\|^2_{L^2(\Omega)} - \delta\|v\|^2_{L^2(\Omega)} + 3\|\eta v\|^2_{L^2(\Omega)}, \qquad \forall \eta, v \in H^2(\Omega). \tag{3.10}$$

We will also use the notation $\delta\mathcal{F}[\eta] \in H^{-2}(\Omega)$ and $\delta^2\mathcal{F}[\eta] \in L(H^2(\Omega), H^{-2}(\Omega))$ to denote the operators associated with these multi-linear forms.

Proof. To prove this lemma we compute the Fréchet derivatives of all orders by comparing the difference in the PFC functional at two points along a given vector with the Taylor expansion of the functional. We then show that all these derivatives are bounded in the space $H^2(\Omega)$.

We consider the difference between the PFC functional evaluated at η and at $\eta + v$ where η, v in $H^2(\Omega)$, i.e.

$$\begin{aligned}\mathcal{F}[\eta + v] - \mathcal{F}[\eta] = \int_\Omega (\Delta + I)\eta(\Delta + I)v\mathrm{d}x + \frac{1}{2}\|\Delta v + v\|^2_{L^2(\Omega)} - \delta\int_\Omega \eta v\mathrm{d}x \\ - \frac{\delta}{2}\|v\|^2_{L^2(\Omega)} + \int_\Omega \eta^3 v\mathrm{d}x + \frac{3}{2}\|\eta v\|^2_{L^2(\Omega)} + \int_\Omega \eta v^3\mathrm{d}x + \frac{1}{4}\|v\|^4_{L^4(\Omega)}.\end{aligned} \tag{3.11}$$

Therefore the functional can be written as

$$\mathcal{F}[\eta + v] = \mathcal{F}[\eta] + \sum_{i=1}^{4} \frac{1}{i!}\delta^i\mathcal{F}[\eta, v, .., v]$$

where $\delta^i\mathcal{F}[\eta, v, .., v]$ are multi-linear forms corresponding to the ith-order Fréchet derivatives.

We can now see that the first and second variations are given by (3.9) and (3.10). The third and fourth variations are given by:

$$\delta^3\mathcal{F}[\eta, v_1, v_2, v_3] = 6\int_\Omega \eta v_1 v_2 v_3\mathrm{d}x \quad \text{and } \delta^4\mathcal{F}[\eta, v_1, v_2, v_3, v_4] = 6\int_\Omega v_1 v_2 v_3 v_4\mathrm{d}x.$$

It remains to show that these four non-zero variations are bounded in $H^2(\Omega)$ and hence are continuous. All four of these variations contain terms of the form $\int_\Omega f_1 f_2 f_3 f_4\mathrm{d}x$. Using the generalised Holder inequality, Lemma C.2.2, with $p_\alpha = 4$ for $\alpha = 1, 2, 3, 4$ we have

$$\int_\Omega f_1 f_2 f_3 f_4\mathrm{d}x \leq \|f_1\|_{L^4(\Omega)}\|f_2\|_{L^4(\Omega)}\|f_3\|_{L^4(\Omega)}\|f_4\|_{L^4(\Omega)}.$$

Using the bound for L^4-norms in terms of H^2-norms (3.5) we have

$$\int_\Omega f_1 f_2 f_3 f_4\mathrm{d}x \leq \|f_1\|_{H^2(\Omega)}\|f_2\|_{H^2(\Omega)}\|f_3\|_{H^2(\Omega)}\|f_4\|_{H^2(\Omega)}. \tag{3.12}$$

We note from (3.3) that

$$\|(\Delta + I)v\|^2_{L^2(\Omega)} \leq \|v\|^2_{H^2(\Omega)}.$$

Using this and (3.12), we can show that

$$\begin{aligned}|\delta\mathcal{F}[\eta, v]| &\leq \left[\left(1 + \delta + \|\eta\|^2_{H^2(\Omega)}\right)\|\eta\|_{H^2(\Omega)}\right]\|v\|_{H^2(\Omega)}, \\ |\delta^2\mathcal{F}[\eta, v, v]| &\leq \left(1 + \delta + 3\|\eta\|^2_{H^2(\Omega)}\right)\|v\|^2_{H^2(\Omega)}, \\ |\delta^3\mathcal{F}[\eta, v, v, v]| &\leq 6\|\eta\|_{H^2(\Omega)}\|v\|^3_{H^2(\Omega)}, \\ |\delta^4\mathcal{F}[\eta, v, v, v, v]| &\leq 6\|v\|^4_{H^2(\Omega)}.\end{aligned}$$

Hence the Fréchet derivatives are well defined for all orders and thus the PFC functional is infinitely Fréchet differentiable. □

Remark 3.1.1. *Using the Banach space analogue of analyticity (Definition 5.2.3) we can even see that $\mathcal{F}$ is in fact analytic; see Lemma 5.2.2.*

3.2 Minimisation Problem

As stated in the introduction to this chapter we wish to find a minimum of the PFC functional (3.1) over the function space $H^2_{\bar{u}}(\Omega)$:

$$\text{Find } u \text{ such that} \qquad \mathcal{F}[u] = \min_{\eta \in H^2_{\bar{u}}(\Omega)} \mathcal{F}[\eta], \qquad \textbf{(P)}.$$

We can prove the existence of a solution to **(P)**, using the direct method of calculus of variations (see for example [Eva10, Theorem 2, Section 8.2]).

Theorem 3.2.1. *There exists a solution to **(P)**.*

Proof. From the upper bound of the H^2-norm in Lemma 3.1.2,

$$\frac{1}{10}\|\eta\|^2_{H^2(\Omega)} - (\delta+1)^2|\Omega| \leq \mathcal{F}[\eta], \tag{3.13}$$

the energy is bounded below,

$$-(\delta+1)^2|\Omega| \leq \mathcal{F}[\eta], \qquad \forall \eta \in H^2_{\bar{u}}(\Omega).$$

Therefore, the infimum $d = \inf_{\eta \in H^2_{\bar{u}}(\Omega)} \mathcal{F}[\eta]$ exists.

We choose a minimising sequence $u_j \in H^2_{\bar{u}}(\Omega)$ such that $\lim_{j\to\infty} \mathcal{F}[u_j] = d$. Then (3.13) implies that the H^2-norm is bounded i.e. $\|u_j\|^2_{H^2(\Omega)} \leq C$, where C is independent of j. Since $H^2(\Omega)$ is a Hilbert space, u_j has a weakly convergent subsequence $u_{j_k} \rightharpoonup u^* \in H^2(\Omega)$. The Rellich-Kondrachov Compactness Theorem ([Eva10, Theorem 1, Section 5.7]) implies that $u_{j_k} \to u^*$ in $L^2(\Omega)$ and in $L^4(\Omega)$. By [KZ05, Theorem 7.2.3] we see that $\|\Delta\eta + \eta\|^2_{L^2(\Omega)}$ is weakly lower semi-continuous. Using this weak lower semi-continuity and the continuity of the L^2-, L^4-terms in the energy functional we obtain that $\mathcal{F}[u^*] \leq \liminf_j \mathcal{F}[u_j]$ and thus have shown that u^* satisfies (**P**). □

3.3 The Euler-Lagrange Equation

We now derive the Euler-Lagrange equation satisfied by the minimiser of the PFC functional (3.1) (the Euler-Lagrange equation for a more general functional is given in [Eva10, Subsection 8.1.2]). Initially we state the weak form of this equation.

Definition 3.3.1 (Euler-Lagrange Equation (Weak Form))**.** *A function u in $H^2_{\bar{u}}(\Omega)$ solves the Euler-Lagrange equation if*

$$\delta\mathcal{F}[u, v] = 0, \qquad \forall v \in H^2_{\#}(\Omega).$$

Existence of a solution to this equation is given by Theorem 3.2.1 and the following lemma.

Lemma 3.3.1. *The minima of the PFC functional* (3.1) *satisfy the Euler-Lagrange equation, Definition 3.3.1.*

Proof. Let u solve (**P**) (page 37) and choose v in $H^2_\#(\Omega)$, then let $i(\epsilon) = \mathcal{F}[u + \epsilon v]$ where clearly $u + \epsilon v \in H^2_{\bar{u}}(\Omega)$ and thus i has a critical point at $\epsilon = 0$. Since by Lemma 3.1.4 i is Fréchet differentiable so $i'(\epsilon)$ is well-defined and $i'(0) = 0$ which translates to

$$\delta\mathcal{F}[u, v] = \frac{\mathrm{d}}{\mathrm{d}\epsilon}\mathcal{F}[u + \epsilon v]\bigg|_{\epsilon=0} = i'(0) = 0,$$

and hence the first variation vanishes. □

We now wish to prove that solutions of the Euler-Lagrange equation (Definition 3.3.1) are smooth. We first prove an auxiliary regularity result for a linear PDE.

Lemma 3.3.2. *If* $\eta \in H^2_\#(\Omega)$, $f \in H^m_{\mathrm{per}}(\Omega), m \geq 0$ *and*

$$\langle \Delta\eta, \Delta v\rangle = \langle f, v\rangle, \qquad \forall v \in H^2_\#(\Omega) \tag{3.14}$$

then $\eta \in H^{m+4}_\#(\Omega)$.

Proof. Recall Parseval's Theorem (on periodic domains)

$$\langle f, g\rangle = \langle \hat{f}, \hat{g}\rangle$$

where $\hat{f}$ and $\hat{g}$ are the Fourier transforms of f and g respectively (this follows from [BO12, Equation (1.1)] with $s = 0$ applied to $f + g$). Using this on (3.14) we have

$$\langle \mathfrak{F}[\Delta\eta], \mathfrak{F}[\Delta v]\rangle = \langle \hat{f}, \hat{v}\rangle \qquad \forall \hat{v} \text{ such that } \mathfrak{F}^{-1}[\hat{v}] \in H^2_\#(\Omega).$$

Using that derivatives become multiples by k in Fourier space (2.22) we have

$$\langle -|k|^2\hat{\eta}, -|k|^2\hat{v}\rangle = \langle \hat{f}, \hat{v}\rangle \qquad \forall \hat{v} \text{ such that } \mathfrak{F}^{-1}[\hat{v}] \in H^2_\#(\Omega).$$

Therefore we have

$$\langle |k|^4\hat{\eta}, \hat{v}\rangle = \langle \hat{f}, \hat{v}\rangle \qquad \forall \hat{v} \text{ such that } \mathfrak{F}^{-1}[\hat{v}] \in H^2_\#(\Omega).$$

The inner product in Fourier space can be written as a sum (this follows from [Gra08, Equation (3.1.5)] with rescaling to generalise from $\mathbb{T}^d$ to Ω). Hence we have

$$\sum_{k\in\mathbb{Z}^d} |k|^4\hat{\eta}(k)\hat{v}(k) = \sum_{k\in\mathbb{Z}^d} \hat{f}(k)\hat{v}(k).$$

Consider

$$\hat{v}(0) = \int_\Omega v(x) e^{i0x} \mathrm{d}x = \int_\Omega v(x) \mathrm{d}x = 0.$$

Hence the first Fourier mode corresponds to the average and is thus already specified. Therefore we no longer consider the $k = 0$ case and we have

$$|k|^4 \hat{\eta}(k) = \hat{f}(k) \qquad \forall k \in \mathbb{Z}^d / \{0\}. \tag{3.15}$$

It is easy to see that

$$g \in H^s_{\mathrm{per}}(\Omega) \text{ iff } |k|^s \hat{g} \in l^2(\mathbb{Z}^d). \tag{3.16}$$

Therefore since $f \in H^s_{\mathrm{per}}(\Omega)$ we have from (3.15)

$$|k|^{s+4} \eta(k) \in l^2(\mathbb{Z}^d \backslash \{0\}).$$

Hence from (3.16) we have that

$$\eta \in H^{s+4}_{\#}(\Omega).$$

□

We can now prove that u is smooth.

Lemma 3.3.3. *Any solution to the Euler-Lagrange equation, Definition 3.3.1, belongs to* $C^\infty_{\mathrm{per}}(\Omega)$.

Proof. We show this result by using induction to show that $u \in H^k_{\bar{u}}(\Omega)$ for all k. From **(P)** (page 37) we already know that $u \in H^2_{\bar{u}}(\Omega)$, our inductive step is to show that, if we know that $u \in H^k_{\bar{u}}(\Omega)$, then we can deduce $u \in H^{k+2}_{\bar{u}}(\Omega)$ for all $k \geq 2$.

Consider the weak Euler-Lagrange equation, Definition 3.3.1, which we re-arrange to give

$$\langle \Delta\eta, \Delta v \rangle = \langle f, v \rangle, \qquad \forall v \in H^2_{\#}(\Omega)$$

where $\eta = u - \bar{u} \in H^{k+2}_{\#}(\Omega)$ for all $k \geq 0$ and

$$f = -2\Delta u + (\delta - 1)u - u^3. \tag{3.17}$$

Since $H^{k+2}_{\mathrm{per}}(\Omega)$ is a Banach algebra for $k \geq 0$ (see [Pel11, Appendix B.1]) it follows that $u^3 \in H^{k+2}_{\mathrm{per}}(\Omega)$. Therefore, from (3.17), $f \in H^k_{\mathrm{per}}(\Omega)$. Lemma 3.3.2 implies that $\eta \in H^{k+4}_{\mathrm{per}}(\Omega)$, and hence $u \in H^{k+4}_{\bar{u}}(\Omega)$. Starting from $k = 0$ induction gives that $u \in H^{k+4}_{\mathrm{per}}(\Omega)$ for all $k \geq 0$ taking the limit $k \to \infty$ gives that u is smooth.

□

To formulate the strong form of the Euler-Lagrange equation, we first note that for

any w in $H^2_{\text{per}}(\Omega)$, w can be written as

$$w = \bar{w} + \tilde{w}, \text{ where } \int_\Omega \tilde{w}\mathrm{d}x = 0.$$

Using this formulation in the weak form of the Euler-Lagrange equation, Definition 3.3.1, we have

$$\begin{aligned}
0 &= \delta\mathcal{F}[u, \tilde{w}], \\
&= \delta\mathcal{F}[u, w] - \delta\mathcal{F}[u, \bar{w}], \\
&= \delta\mathcal{F}[u, w] - \int_\Omega (\Delta + I)u(\Delta + I)\bar{w} - \delta u\bar{w} + u^3\bar{w}\mathrm{d}y.
\end{aligned}$$

Using that $u \in C^\infty(\Omega)$, which follows from Lemma 3.3.3, we have

$$\begin{aligned}
0 &= \delta\mathcal{F}[u, w] - \int_\Omega (\Delta + I)^2 u \frac{\int_\Omega w\mathrm{d}x}{|\Omega|} - \delta u \frac{\int_\Omega w\mathrm{d}x}{|\Omega|} + u^3 \frac{\int_\Omega w\mathrm{d}x}{|\Omega|}\mathrm{d}y, \\
&= \delta\mathcal{F}[u, w] - \frac{1}{|\Omega|}\int_\Omega\int_\Omega (\Delta_y + I)^2 u(y)w(x) - \delta u(y)w(x) + u(y)^3 w(x)\mathrm{d}x\mathrm{d}y, \\
&= \delta\mathcal{F}[u, w] - \int_\Omega w(x)\frac{1}{|\Omega|}\int_\Omega (\Delta + I)^2 u(y) - \delta u(y) + u(y)^3\mathrm{d}y\mathrm{d}x, \\
&= \int_\Omega (\Delta + I)\, u\, (\Delta + I)\, w\mathrm{d}x - \delta\int_\Omega uw\mathrm{d}x + \int_\Omega u^3 w\mathrm{d}x - \lambda\int_\Omega w\mathrm{d}x,
\end{aligned}$$

where since $1/|\Omega| \in H^2(\Omega)$, λ is given by

$$\lambda = \overline{\delta\mathcal{F}} = \left\langle \delta\mathcal{F}[\eta], \frac{1}{|\Omega|} \right\rangle = (1 - \delta)\bar{u} + \fint_\Omega u^3\mathrm{d}x.$$

We can now give the strong form of this equation.

Definition 3.3.2 (Euler-Lagrange Equation (Strong Form))**.** *A function $u \in H^4(\Omega)$, solves the strong form of the Euler-Lagrange equation if*

$$\begin{cases} (\Delta + I)^2 u - \delta u + u^3 - \lambda = 0, \\ \int u dx = \bar{u}. \end{cases}$$

It is clear that, if this equation is satisfied, then its weak form, Definition 3.3.1 is satisfied as well. Since from Lemma 3.3.3 the solutions of the weak form are sufficiently regular ($u \in H^4(\Omega)$) the reverse relation is true as well.

Remark 3.3.1. *The Euler-Lagrange equation can also be obtained by finding the critical points of the functional*

$$\mathcal{I}[\eta, \tilde{\lambda}] = \mathcal{F}[\eta] - \tilde{\lambda}\left(\int_\Omega \eta dx - |\Omega|\bar{u}\right)$$

over the space $\eta \in H^2_{\text{per}}(\Omega)$ *and* $\tilde{\lambda} \in \mathbb{R}$.

3.4 Conclusion

In this chapter we have formulated the minimisation problem for the PFC functional which we will focus on solving throughout the rest of this thesis. To achieve this we defined the space from which the minimiser is sought and proved properties of the PFC functional which will prove important in this and subsequent chapters. We also showed that the minimisation problem has a solution, i.e., there is a minimum of the PFC functional under the constraint that mass is conserved. The PDE problem associated with this minimisation is also formulated and we prove that the solution to this problem is smooth.

Chapter 4

Gradient Flow Analysis

In this chapter we introduce the method of gradient flows as a technique for finding a minimum of the problem **(P)** (page 37) and then prove results on the global existence, uniqueness and regularity of the solutions of three specific gradient flows, the L^2-, H^{-1}- and H^2-gradient flows.

4.1 Bochner Spaces

We now introduce spaces involving time, called the Bochner spaces. More detailed accounts on Bochner spaces can be found in [Eva10, Section 5.9.2] and [CF10, Section 5]. For the sake of generality we let X denote a real Banach space. We can define integrability and measurability of functions on Banach spaces in an analogous way to integrability and measurability of functions on subsets of $\mathbb{R}^d$ (see [Eva10, Appendix E]). Specifically, $u : [0,T] \to X$ is Bochner integrable if and only if $\|u\|_X$ is Lebesgue integrable [HP57, Definition 3.7.2]. Similarly, u is strongly measurable if and only if for all $v \in X^*$ the mapping $t \to \langle v, u(t)\rangle$ is Lebesgue measurable and u is almost separably valued [Eva10, Appendix E.5]. The first Bochner spaces we define are analogous to the L^p-spaces, see [Eva10, Section 5.9.2].

Definition 4.1.1 (The Bochner-Lebesgue Spaces)**.** *The space*

$$L^p(0,T;X)$$

consists of all strongly measurable functions $u : [0,T] \to X$ with

$$\|u\|_{L^p(0,T;X)} := \left(\int_0^T \|u(t)\|_X^p \, dt\right)^{\frac{1}{p}} < \infty$$

for $1 \leq p < \infty$, or, if $p = \infty$,

$$\|u\|_{L^\infty(0,T;X)} := \operatorname*{ess\,sup}_{0\leq t\leq T} \|u(t)\|_X < \infty.$$

We can also define the space of time continuous functions, see [Eva10, Section 5.9.2].

Definition 4.1.2. *The space*

$$C([0,T];X)$$

comprises all continuous functions $u : [0,T] \to X$ *with*

$$\|u\|_{L^\infty(0,T;X)} := \operatorname*{ess\,sup}_{0\le t\le T} \|u(t)\|_X < \infty.$$

Since we will consider derivatives with respect to time we need to define the weak time derivative, see [Eva10, Subsection 5.9.2].

Definition 4.1.3. *Let* $u \in L^1(0,T;X)$, $T > 0$. *We say* $v \in L^1(0,T;X)$ *is the weak derivative of* u, *written*

$$\partial_t u = v,$$

provided

$$\int_0^T \partial_t \phi(t) u(t)\,dt = -\int_0^T \phi(t) v(t)\,dt$$

for all scalar test functions $\phi \in C_c^\infty(0,T)$.

We can use this method inductively to define the j*-th weak derivative for* $j \in \mathbb{N}$, *i.e.* $\partial_t^j u$.

For the sake of simplicity we will use the notation $u_t = \partial_t u$ *for the rest of this thesis.*

Analogously to $C([0,T];X)$, we can define the spaces $C^k([0,T];X)$ for $k \in \mathbb{N}$, $k > 0$ (see [Pen13, Definition 2.55] or [MNRR96, Subsection 1.2.6]).

Definition 4.1.4. *The space*

$$C^k([0,T];X)$$

comprises all continuous functions $u : [0,T] \to X$ *where, for all* $j \in \mathbb{N}$, $0 \le j \le k$, $\partial_t^j u : [0,T] \to X$ *is continuous and*

$$\|u\|_{C^k(0,T;X)} := \sum_{j=0}^{k} \sup_{0\le t\le T} \|\partial_t^j u(t)\|_X < \infty.$$

Finally we define the analogue of the Sobolev spaces, i.e. the Bochner-Sobolev spaces, again following [Eva10, Section 5.9.2].

Definition 4.1.5. *The Sobolev space*

$$W^{1,p}(0,T;X)$$

consists of all functions $u \in L^p(0,T;X)$ *such that* u_t *exists in the weak sense and belongs*

to $L^p(0,T;X)$*. Furthermore*

$$\|u\|_{W^{1,p}(0,T;X)} := \begin{cases} \left(\int_0^T \|u(t)\|_X^p + \|u_t(t)\|_X^p \, dt\right)^{\frac{1}{p}} & \text{for } 1 \le p < \infty, \\ \operatorname*{ess\,sup}_{0\le t\le T} \left(\|u(t)\|_X + \|u_t(t)\|_X\right) & \text{for } p = \infty. \end{cases}$$

Following [CF10, Subsection 5.3] we define the k-th Bochner-Sobolev space inductively.

Definition 4.1.6 (The k-th Bochner-Sobolev Spaces)**.**

$$W^{k,p}(0,T;X) := \{u \in W^{1,p}(0,T;X) : u_t \in W^{k-1,p}(0,T;X)\}.$$

These are Banach spaces for the norms

$$\|u\|_{W^{k,p}(0,T;X)} := \begin{cases} \left(\sum_{j=0}^{k} \|\partial_t^j u\|_{L^p(0,T;X)}^p\right)^{\frac{1}{p}} & \text{for } 1 \le p < \infty, \\ \max\left\{\|u\|_{L^\infty(0,T;X)}, ..., \|\partial_t^k u\|_{L^\infty(0,T;X)}\right\} & \text{for } p = \infty. \end{cases}$$

For the sake of simplicity we define $H^k(0,T;X) := W^{k,2}(0,T;X)$.

Remark 4.1.1. *Throughout this thesis we will use the notation* $L^p(X)$*,* $H^k(X)$ *and* $W^{k,p}(X)$ *to denote the spaces* $L^p(0,\infty;X)$*,* $H^k(0,\infty;X)$ *and* $W^{k,p}(0,\infty;X)$ *respectively.*

4.2 Gradient Flows

As stated in the previous chapter we wish to solve the minimisation problem **(P)** (page 37), i.e. to find $\eta \in H^2_{\tilde{u}}(\Omega)$ that minimises the PFC functional (3.1). In Chapters 6, 7 and 8 we will introduce numerical schemes to obtain an approximation of the minimiser. These schemes are discrete versions of gradient flows as in [Bar15, Section 2.3]. Therefore we first study the corresponding continuous gradient flows,

$$\langle u_t, v\rangle_H = -\delta\mathcal{F}[u,v], \qquad \forall v \in H^2_{\#}(\Omega) \tag{4.1}$$

where the inner-product is over the Hilbert space defined by a positive definite operator $\hat{H}$, i.e.

$$\langle \eta, v\rangle_H = \langle \hat{H}\eta, v\rangle_{L^2(\Omega)}.$$

The idea of using a gradient flow method is that, as we follow the trajectory u, we reduce the value of the PFC functional. Formally, if u is a solution to (4.1) and sufficiently regular, which we show in Lemmas 4.3.2 and 4.4.1, then we have

$$\frac{\mathrm{d}}{\mathrm{d}t}\mathcal{F}[u(t)] = \delta\mathcal{F}[u,u_t] = -\|u_t\|_H^2.$$

Therefore we have that $\mathcal{F}[u(t)]$ is decreasing and, by integration,

$$\int_0^\infty \|u_t(s)\|_H^2 \mathrm{d}s < \infty.$$

Hence we expect that $u_t \to 0$ in H as $t \to \infty$, thus we also expect that $u(t) \to u^*$ in $H^2(\Omega)$ where u^* is a minimiser. We will prove this convergence and give an estimate of the rate in Chapter 5.

Remark 4.2.1. *In general, gradient flows are of interest in themselves (see for example the extensive literature on the similar Cahn-Hilliard and Allen-Cahn equations, e.g. [ES86],[CE94]), however for the purpose of this thesis we consider gradient flows primarily as methods for minimising the PFC functional* (3.1).

We will consider three distinct gradient flows. The first gradient flow we consider is the L^2-gradient flow where the associated partial differential equation is known as the Swift-Hohenberg equation.

Definition 4.2.1 (Swift-Hohenberg Equation, Weak Form)**.** $u \in \bar{u} + W^{1,1}(0,T;L^2(\Omega)) \cap L^\infty(0,T;H^2_\#(\Omega))$ *is a solution to the weak Swift-Hohenberg equation if*

$$\langle u_t, v\rangle_{L^2(\Omega)} = -\delta\mathcal{F}[u,v], \qquad \forall v \in H^2_\#(\Omega),$$

for a.e. t in $(0,T)$.

The second gradient flow we consider is the gradient flow typically used in PFC calculations, see e.g. [EKHG02], [EG04, Section II], [EW13, Section 1], [WGT$^+$12, Subsection 3.1.1.2], [Lar14] or [WWL09, Section 1.1]. This is the H^{-1}-gradient flow, known in the strong form as the PFC equation.

Definition 4.2.2 (PFC Equation, Weak Form)**.** $u \in \bar{u}+W^{1,1}(0,T;H^{-1}(\Omega))\cap L^\infty(0,T;H^2_\#(\Omega))$ *is a solution to the weak PFC equation if*

$$\langle u_t, v\rangle_{H^{-1}(\Omega)} = -\delta\mathcal{F}[u,v], \qquad \forall v \in H^2_\#(\Omega),$$

for a.e. t in $(0,T)$.

Remark 4.2.2. *We recall the H^{-1}-inner-product from Definition C.1.4 to obtain the strong form of Definition 4.2.2*

$$u_t = \Delta[(\Delta + I)^2 u - \delta u + u^3]. \tag{4.2}$$

This partial differential equation is known as the PFC equation and is the form considered in the physics literature, e.g. [EG04], [EKHG02] and [WGT$^+$12].

Remark 4.2.3. *Several papers, for example [EKHG02], argue that the H^{-1}-norm is the natural norm for the gradient flow since it automatically enforces mass conservation. This*

is true if the gradient flow is well formulated, i.e. we fix the zeroth mode of the transform of the variable to ensure the norm is well defined. This is equivalent to conserving the average.

In the L^2-case and the H^2-case (see Definition 4.2.4) we enforce conservation in the weak form by taking a test function in the zero average space $H^2_{\#}(\Omega)$.

As an alternative to the two established gradient flows introduced in Definitions 4.2.1 and 4.2.2 we introduce a gradient flow which can be thought of as a gradient flow in the H^2-norm. First consider a weak form of a Newton type descent flow

$$\delta\mathcal{F}[u, v] = -\delta^2\mathcal{F}[u, u_t, v]. \tag{4.3}$$

A similar flow for a different functional is considered in [Rin07, Equation (26a)].

Clearly the second variation is not positive definite for all u and v, we also desire the operator $\hat{H}$ to be easily invertible. This leads us to define the operator

$$A := (\Delta + I)^2 + \gamma I$$

where $\gamma > 0$ is a constant.

We also have an associated norm.

Definition 4.2.3 (A-norm)**.**

$$\|\eta\|_A^2 := \langle A\eta, \eta\rangle = \|\Delta\eta + \eta\|^2_{L^2(\Omega)} + \gamma\|\eta\|^2_{L^2(\Omega)}.$$

We consider the A-norm as it resembles the second variation (3.10), i.e. it is the closest approximation to the second variation that is independent of the solution u. This operator has two advantages over the second variation; (1) it is positive definite and thus unlike the second variation induces a norm; and (2) the operator is homogeneous and thus diagonalises Fourier space.

Lemma 4.2.1. *The A-norm is equivalent to the A_1-norm, Definition 3.1.2, (and hence to the H^2-norm),i.e., $\exists \tilde{C}_{\mathrm{b}}, \tilde{C}_{\mathrm{u}} > 0$ that depend only on γ such that*

$$\tilde{C}_{\mathrm{b}}\|v\|^2_{A_1} \leq \|v\|^2_A \leq \tilde{C}_{\mathrm{u}}\|v\|^2_{A_1}.$$

Remark 4.2.4. *In the numerical algorithms we introduce in Chapters 6, 8 and Appendix E we will use an adaptive version of γ. For the sake of simplicity in the following analysis we take γ to be constant. The numerical tests shown in Figure 8.3 suggest that a good choice of constant γ is*

$$\gamma_{\mathrm{om}} = 3\overline{u^2_{\mathrm{om}}} - \delta$$

where u_{om} is the one-mode solution (see (8.11)*). In the range where the one-mode approximation is valid, i.e. $0 < \delta < 1$ and $36\bar{u}^2 < 15\delta$, we can show that $\gamma_{\mathrm{om}} > 0$, the condition of Definition 4.2.3.*

We now have an equivalent norm to the H^2-norm and thus can define a new gradient flow equation.

Definition 4.2.4 (H^2-gradient flow equation)**.** *$u \in \bar{u}+W^{1,1}(0,T;H^2(\Omega))\cap L^\infty(0,T;H^2_\#(\Omega))$ is a solution to the H^2-gradient flow equation if*

$$\langle u_t, v\rangle_A = -\delta\mathcal{F}[u,v], \qquad \forall v \in H^2_\#(\Omega),$$

for a.e. t in $(0,T)$, where $\langle\cdot,\cdot\rangle_A$ is the inner product associated with the A-norm, Definition 4.2.3.

Remark 4.2.5. *Following [CF10, Equation (3.1)] we use the notation $\nabla_H\mathcal{F}$ for the unique element in H which represents the derivative $\delta\mathcal{F}[u]$ with respect to the inner product in H, i.e., $\nabla_H\mathcal{F}[u] \in H$ such that*

$$\delta\mathcal{F}[u,\varphi] = \langle\nabla_H\mathcal{F}[u],\varphi\rangle_H, \qquad \forall\varphi \in H^2_\#(\Omega).$$

We set

$$H = \begin{cases} L^2_\#(\Omega) & \text{for the SH equation,} \\ H^{-1}_\#(\Omega) & \text{for the PFC equation,} \\ H^2_\#(\Omega) & \text{for the H}^2\text{−gradient flow equation,} \end{cases} \tag{4.4}$$

where $L^2_\#(\Omega)$ and $H^{-1}_\#(\Omega)$ are defined in Definitions C.1.3 and C.1.5. Therefore Definitions 4.2.1, 4.2.2 and 4.2.4 can, formally, be written as

$$u_t + \nabla_H\mathcal{F}[u] = 0.$$

4.3 SH and PFC Equations

First we recall an embedding result from [Sim87] that that we will use to prove existence and a regularity result for the SH and PFC equations.

Lemma 4.3.1 ([Sim87, Corollary 4])**.** *Let X, B and Y be Banach spaces where $X \subset B \subset Y$ with the embedding X to B being compact.*

Let $(u^n)_{n\in\mathbb{N}}$ be a sequence bounded in $L^p(0,T;X)$ where $1 \le p < \infty$ and $(u^n_t)_{n\in\mathbb{N}}$ be bounded in $L^1(0,T;Y)$, then $(u^n)_{n\in\mathbb{N}}$ is relatively compact in $L^p(0,T;B)$.

Let $(u^n)_{n\in\mathbb{N}}$ be a sequence bounded in $L^\infty(0,T;X)$ and $(u^n_t)_{n\in\mathbb{N}}$ be bounded in $L^r(0,T;Y)$ where $r > 1$, then $(u^n)_{n\in\mathbb{N}}$ is relatively compact in $C(0,T;B)$.

We also recall Picard's theorem (see for example [Isl97, Theorem 2.2] and [Bre11, Theorem 7.3]). This is required for the existence proof of the SH and PFC equations (Lemma 4.3.2). Additionally, this theorem is also used to prove existence and uniqueness of the H^2-gradient flow (Definition 4.2.4) as well as giving the required regularity for this flow.

Theorem 4.3.1. *Let Y be a real Banach space and let $t_0 \in \mathbb{R}, y_0 \in Y$ and*

$$Q_b := \{(t, y) \in \mathbb{R} \times Y : |t - t_0| \leq a, \|y - y_0\|_Y \leq b\}$$

for fixed $a, b > 0$. Suppose $f : Q_b \to Y$ is continuous and

$$\|f(t, x) - f(t, y)\|_Y \leq L\|x - y\|_Y, \qquad \forall (t, x), (t, y) \in Q_b$$

and

$$\|f(t, y)\|_Y < K, \qquad \forall (t, y) \in Q_b,$$

where $L \geq 0$ and $K > 0$ are fixed real numbers. Choose c such that $0 < c < a$ and $c < \min\left\{\frac{b}{K}, \frac{1}{L}\right\}$. Then the

$$IVP : x_t(t) = f(t, x(t)), \qquad x(t_0) = y_0$$

has exactly one continuously differentiable solution on the interval $I_c = [t_0 - c, t_0 + c]$.

Remark 4.3.1. *We can not use Picard's theorem directly to prove the existence of a solution to the SH or PFC gradient flows since re-arranging these equations to the IVP form given in Theorem 4.3.1 gives an f that maps between two different Banach spaces. That is $f : H^2_{\text{per}}(\Omega) \to H^{-2}_{\text{per}}(\Omega)$ in the SH case and $f : H^2_{\text{per}}(\Omega) \to H^{-4}_{\text{per}}(\Omega)$ in the PFC case whereas $f : H^2_{\text{per}}(\Omega) \to H^2_{\text{per}}(\Omega)$ for the H^2-gradient flow.*

4.3.1 Existence

We now show the existence of a solution to the SH and PFC gradient flows. The reason for showing existence of these trajectories, beyond general interest, is that we also obtain corresponding regularity results, which will be of particular use in Chapter 5 to show convergence of the gradient flows to equilibrium.

Remark 4.3.2. *Proofs of the existence of a solution to the PFC equation can be found in [WWL09, Remark 3.12] and an adaptation ($\beta = 0$) of [WW10, Theorem 5.3]. These proofs rely on proving that solutions exist to a specific time-discretisation and taking the limit. It is worth noting that such a method could probably be adapted to prove the existence of alternative gradient flows.*

Conversely we use a Galerkin discretisation of the solution and prove the existence of a solution to the discretisation. We then show by taking the limit that we obtain a solution to the original gradient flow. The advantage of our method is that it is easier to obtain regularity results. Specifically, we can adapt this method in Lemma 4.3.3 to obtain the solution we need for Chapter 5.

We use one lemma to prove the existence of a solution to the L^2- and H^{-1}-gradient flows, Definitions 4.2.1 and 4.2.2, and another (in Section 4.4) to prove the existence of

a solution to the H^2-gradient flow, Definition 4.2.4. In principle the method of the first lemma, Lemma 4.3.2, could be applied to the H^2-gradient flow. However, we choose to prove the existence of a solution to the H^2-gradient flow separately as such a result can be obtained more easily from Picard's theorem, Theorem 4.3.1, and adapting the proof of Lemma 4.3.2 would be much more tedious.

Lemma 4.3.2. *Consider the initial value problem, written in the notation of Remark 4.2.5,*

$$\begin{aligned} u_t + \nabla_H \mathcal{F}[u] &= 0, \\ u(x,0) &= u_0(x), \end{aligned}$$

where $H = L^2_\#(\Omega)$ for the SH case and $H = H^{-1}_\#(\Omega)$ for the PFC case.

If $u_0 \in H^2(\Omega)$, then there exists a global weak solution,

$$u \in C(H^1(\Omega)) \cap H^1_{\text{loc}}(H) \cap L^\infty(H^2(\Omega)).$$

Proof. We adapt the proof of [KN14, Theorem 2.1].

This proof uses standard methods. However, we lay out the arguments in detail as we will use the regularity obtained here along with methods similar to Step 3 to prove the regularity result Lemma 4.3.3. This regularity result is required for the proof of the convergence of the SH and PFC equations given in Chapter 5.

To prove this result we use a Galerkin approximation. The proof is then split into three steps, first we prove the existence of a global solution to the Galerkin approximation. We then prove bounds on the Galerkin approximation. Finally we show convergence of the Galerkin approximation to the solution of the initial value problem.

We consider the gradient flow (4.1), for all $v \in H^2_\#(\Omega)$, i.e.

$$\langle u_t, v\rangle_H + \int_\Omega (\Delta + I)u, (\Delta + I)v - f'(u)v \mathrm{d}x = 0, \tag{4.5}$$

where

$$f'(u) = \delta u - u^3.$$

Step 1. We use a Galerkin method. Let $\{\phi_i\}_{i\in\mathbb{N}}$ be an L^2-orthonormal basis of $-\Delta$ with ordered eigenvalues $\{\lambda_i\}_{i\in\mathbb{N}}$. We note that the ϕ_i are in $C^\infty_{\text{per}}(\Omega)$ and define the associated space as (see [CHQZ88, Equation (9.7.2)])

$$S_N = \text{span}\left\{\phi_i(x) | i = 1, .., N\right\}.$$

We also define the space of zero average functions (i.e. $\phi_1(x)$ is constant)

$$S^\#_N = \text{span}\{\phi_i(x) | i > 1\}.$$

The Galerkin approximation

$$u^N(x,t) = \sum_{i=1}^{N} a_i^N(t)\phi_i(x), \tag{4.6}$$

satisfies the IVP

$$\begin{aligned} \left\langle u_t^N, v^N \right\rangle_H &= -\delta\mathcal{F}\left[u^N, v^N\right], \qquad \forall v^N \in S_N^{\#}, \\ u^N(x,0) &= \sum_{i=1}^{N} \langle u_0, \phi_i\rangle_{L^2(\Omega)}\phi_i(x). \end{aligned} \tag{4.7}$$

Since v^N can be written as

$$v^N = \sum_{i=2}^{N} b_i^N(t)\phi_i(x)$$

for some set of $b_i(t)$, (4.7) leads to a system of ODEs for the coefficients a_j^N. That is, since $\lambda_j > 0$, for $j \geq 2$ we have

$$\begin{cases} \frac{\mathrm{d}}{\mathrm{d}t}a_j^N(t) + (-\lambda_j)^\chi(-\lambda_j+1)^2 a_j^N(t) - \langle(-\lambda_j)^\chi f'(u^N), \phi_j\rangle_{L^2(\Omega)} = 0, \\ a_j^N(0) = \langle u_0, \phi_j\rangle_{L^2(\Omega)} \end{cases} \tag{4.8}$$

where

$$\chi = \begin{cases} 1 & \text{for the PFC equation} \\ 0 & \text{for the SH equation.} \end{cases}$$

Using Picard's theorem, Theorem 4.3.1,(with $x = a_j^N$, $Y = \mathbb{R}^N$ and where the local Lipschitz property and boundedness follow from the local Lipschitz property of f' and the boundedness of λ_j) these equations have a local in time solution. We take $\left(a_j^N(t)\right)_{i=1}^N$ to be a maximal solution, then to prove the ODE has a global solution we must show these coefficients are bounded. To do this we will prove $u^N \in L^\infty(0,T,H^2(\Omega))$.

Since $u_t^N \in S_N^{\#}$ we can test the first variation with u_t^N, using the notation of (4.4) (specifically we can also consider the norm $H = H^2(\Omega)$), to obtain

$$\left\langle \delta\mathcal{F}\left[u^N\right], u_t^N \right\rangle = -\left\|u_t^N\right\|_H^2 = \frac{\mathrm{d}}{\mathrm{d}t}\mathcal{F}\left[u^N\right]$$

integrating this, we have

$$\left\|u_t^N\right\|_{L^2(0,T;H)}^2 + \mathcal{F}\left[u^N(T)\right] \leq \mathcal{F}\left[u^N(0)\right]. \tag{4.9}$$

Recall the lower bound for $\mathcal{F}$, Lemma 3.1.2, then we have from (4.9)

$$\begin{aligned}\left\|u_t^N\right\|^2_{L^2(0,T;H)} + \frac{1}{10}\left\|u^N(T)\right\|^2_{H^2(\Omega)} &\leq \left\|u_t^N\right\|^2_{L^2(0,T;H)} + \mathcal{F}\left[u^N(T)\right] + (\delta+1)^2|\Omega| \\ &\leq \mathcal{F}\left[u^N(0)\right] + (\delta+1)^2|\Omega|. \end{aligned} \tag{4.10}$$

Since $u^N(0) \to u_0$ in $H^2(\Omega)$ as $N \to \infty$ and $\mathcal{F}$ is continuous, which follows from (3.11), we have $u^N \in L^\infty(H^2(\Omega))$ and thus by an embedding $u^N \in L^\infty(L^2(\Omega))$. Since the L^2-norm of u^N can be written as

$$\left\|u^N\right\|^2_{L^2(\Omega)} = \sum_{i=1}^{N}\left(a_i^N(t)\right)^2,$$

the bound on u^N in $L^\infty(L^2(\Omega))$ gives us an a-priori global bound on the a_j^N and hence the ODE (4.8) has a global solution.

Step 2. We now wish to prove bounds on the Galerkin solution and its derivative, namely $u^N \in L^2(0,T;H^2(\Omega))$ and $u_t^N \in L^2(0,T;H)$. The time derivative bound follows simply from (4.9). From this the u_t^N are bounded in $L^2(0,T;H)$. We can also see that

$$\left\|u^N\right\|^2_{L^2(0,T;H^2(\Omega))} \leq \left\|u^N\right\|^2_{L^\infty(0,T;H^2(\Omega))} T. \tag{4.11}$$

Step 3. Now there exists (u, u_t) and subsequences denoted $\{u^N\}, \{u_t^N\}$ such that

$$\begin{aligned} u^N &\to u \text{ weakly}^* \text{ in } L^\infty(0,T;H^2(\Omega)), \\ u_t^N &\rightharpoonup u_t \text{ weakly in } L^2(0,T;H). \end{aligned}$$

Using that $H^2(\Omega)$ is compactly embedded in H and $H^1(\Omega)$ is embedded in H and embeds $H^2(\Omega)$ we can use Lemma 4.3.1 ([Sim87, Corollary 4]) with $r = 2, X = H^2(\Omega), B = H^1(\Omega)$ and $Y = H$ to obtain relative compactness in $C(0,T;H^1(\Omega))$. Hence we can take a sub-sequence which we again rename u^N so that

$$u^N \to u \text{ strongly in } C(0,T;H^1(\Omega)).$$

$u^N \in L^2(0,T;H)$ follows from (4.11) by the embedding $H^2(\Omega) \subset H$. The weak convergence of u_t^N in $L^2(0,T;H)$ and u^N in $L^2(0,T;H)$ gives that

$$u \in H^1_{\text{loc}}(0,T;H).$$

We have $u^N \rightharpoonup u$ weakly in $L^2(0,T;H^2(\Omega))$ therefore to obtain a solution of the weak gradient flow (4.5) we only have to deal with the non-linearity $f'(u)$. Since $L^\infty(\Omega)$ embeds H and from [Ada75, Corollary 5.16] $L^\infty(\Omega)$ is compactly embedded in $H^2(\Omega)$, we can use Lemma 4.3.1 ([Sim87, Corollary 4]) with $r = 2, X = H^2(\Omega), B = L^\infty(\Omega)$ and $Y = H$ to obtain relative compactness in $C(0,T;L^\infty(\Omega))$. Hence we can take a sub-sequence which

we again rename u^N so that

$$u^N \to u \text{ strongly in } C(0,T;L^\infty(\Omega)).$$

Since $f'(u)$ is continuous we have that $f'(u^N(t))$ converges strongly to $f'(u(t))$ in $C(0,T;L^\infty(\Omega))$.

We now have the appropriate regularity for the approximation, i.e. $u^N \in C(H^1(\Omega)) \cap H^1_{\text{loc}}(H) \cap L^\infty(H^2(\Omega))$. Consider the Galerkin approximation (4.7) since we have weak convergence of u_t^N in $L^2(H)$ the left-hand side converges. For convergence of the right-hand side we separate the linear and non-linear ($f'(u)$) parts of the first variation. The weak convergence of u^N in $L^\infty(H^2(\Omega))$ gives that the linear part of the first variation converges. Finally the non-linear part converges by the convergence of $f'(u(t))$ in $C(0,T;L^\infty(\Omega))$.

Consequently we can pass to the limit in (4.7) and obtain a (u, u_t) that satisfies the initial value problem in the weak sense. The initial condition converges by the strong convergence of u^N in $C(H^1(\Omega))$. □

4.3.2 Regularity

We can now show that trajectories for the SH and PFC equations are continuously differentiable in $H^2(\Omega)$. In Chapter 5 this is one of the conditions we require for the convergence of these trajectories to equilibrium.

Lemma 4.3.3. *Suppose the initial condition u_0 for the Swift-Hohenberg equation (Definition 4.2.1) or the PFC equation (Definition 4.2.2) satisfies*

$$\begin{aligned} u_0 &\in H^8_{\bar{u}}(\Omega), && \text{for the SH case,} \\ u_0 &\in H^9_{\bar{u}}(\Omega), && \text{for the PFC case.} \end{aligned} \tag{4.12}$$

Then the weak solutions of the Swift-Hohenberg equation and of the PFC equation are continuously differentiable in $H^2(\Omega)$, that is, $u \in \bar{u} + C^1(H^2_\#(\Omega))$.

Proof. This proof is split into three steps. First we use the Galerkin approximation to show that $u_t^N(0)$ is bounded in $H^{4-\chi}(\Omega)$. Then we use the Galerkin approximation again to show $u \in H^2_{\text{loc}}(H^{-\chi}(\Omega)) \cap W^{1,\infty}_{\text{loc}}(H^{4-\chi}(\Omega))$ where $\chi = 0$ for the SH case and $\chi = 1$ for the PFC case. Finally we use the result of Lemma 4.3.1 to prove that $u \in C^1(H^2(\Omega))$.

Step 1. Recall the Galerkin approximation of Lemma 4.3.2, i.e. (4.7). This can be rewritten as

$$\langle(-\Delta)^{-\chi}u_t^N, v^N\rangle + \langle(\Delta + I)u^N, (\Delta + I)v^N\rangle = \delta\langle u^N, v^N\rangle - \langle(u^N)^3, v^N\rangle \qquad \forall v^N \in S_N^\#, \tag{4.13}$$

which holds for all time t and in particular $t = 0$.

We now test (4.13) at $t = 0$ with $v^N = (-\Delta)^{\chi+j}u_t^N(0) \in H^2_\#(\Omega)$, where $0 \le j \le$

$4-\chi$, to obtain

$$\begin{aligned}
&\|(-\Delta)^{\frac{j}{2}}u_t^N(0)\|^2_{L^2(\Omega)}\\
&= (\delta-1)\langle(-\Delta)^{\frac{j}{2}+\chi}u^N(0),(-\Delta)^{\frac{j}{2}}u_t^N(0)\rangle - \langle(-\Delta)^{2+\frac{j}{2}+\chi}u^N(0),(-\Delta)^{\frac{j}{2}}u_t^N(0)\rangle\\
&\quad + 2\langle(-\Delta)^{1+\frac{j}{2}+\chi}u^N(0),(-\Delta)^{\frac{j}{2}}u_t^N(0)\rangle - \langle(-\Delta)^{\frac{j}{2}+\chi}(u^N(0))^3,(-\Delta)^{\frac{j}{2}}u_t^N(0)\rangle\\
&\leq 2\left[\|(-\Delta)^{\frac{j}{2}+\chi}u^N(0)\|^2_{L^2(\Omega)} + \|(-\Delta)^{2+\frac{j}{2}+\chi}u^N(0)\|^2_{L^2(\Omega)}\right]\\
&\quad + 2\left[4\|(-\Delta)^{1+\frac{j}{2}+\chi}u^N(0)\|^2_{L^2(\Omega)} + \|(-\Delta)^{\frac{j}{2}+\chi}(u^N(0))^3\|^2_{L^2(\Omega)}\right] + \frac{1}{2}\|(-\Delta)^{\frac{j}{2}}u_t^N(0)\|^2_{L^2(\Omega)}\\
&\leq 2\left[6\|u^N(0)\|^2_{H^{4+j+2\chi}(\Omega)} + \|u^N(0)^3\|^2_{H^{4+j+2\chi}(\Omega)}\right] + \frac{1}{2}\|(-\Delta)^{\frac{j}{2}}u_t^N(0)\|^2_{L^2(\Omega)},
\end{aligned}$$

where we use Young's inequality in the first inequality and that the $H^{4+j+2\chi}$-norm bounds the $H^{j+2\chi}$-,$H^{2+j+2\chi}$- and $H^{4+j+2\chi}$-semi-norms in the final line.

Re-arranging and using that $H^{4+j+2\chi}(\Omega)$ is a Banach algebra (see [Ada75, Theorem 5.23]) we have

$$\|(-\Delta)^{\frac{j}{2}}u_t^N(0)\|^2_{L^2(\Omega)} \leq 4\left[6\|u^N(0)\|^2_{H^{4+j+2\chi}(\Omega)} + \|u^N(0)\|^6_{H^{4+j+2\chi}(\Omega)}\right]. \tag{4.14}$$

If $u(0)\in H^{4+j+2\chi}(\Omega)$ then $u^N(0)\to u_0\in H^{4+j+2\chi}(\Omega)$ as $N\to\infty$, hence $u^N(0)$ is bounded in $H^{4+j+2\chi}(\Omega)$ and $u_t^N(0)$ is bounded in $H^j(\Omega)$.

Step 2. In the Galerkin approximation (4.6) the coefficients in $\{a_i^N\}_{i=1}^N$ are smooth functions of t. We can therefore differentiate (4.13) with respect to time and re-arrange to obtain, for all $v^N\in S_N^{\#}$,

$$\int_\Omega (-\Delta)^{-\chi}u_{tt}^N v^N + (\Delta+I)^2u_t^N v^N + u_t^N v^N \mathrm{d}x = \int_\Omega (\delta+1)u_t^N v^N - 3(u^N)^2u_t^N v^N \mathrm{d}x. \tag{4.15}$$

We test (4.15) with $v^N = (-\Delta)^p u_{tt}^N$, where $p\geq 0$, which is clearly in $S_N^{\#}$ since $u_{tt}=\eta_{tt}$, where $\eta = u-\bar{u}\in S_N^{\#}$. Therefore we obtain

$$\begin{aligned}
&\|\nabla^p u_{tt}^N\|^2_{H^{-\chi}(\Omega)} + \frac{1}{2}\frac{\mathrm{d}}{\mathrm{d}t}\left[\|(\Delta+I)\nabla^p u_t^N\|^2_{L^2(\Omega)} + \|\nabla^p u_t^N\|^2_{L^2(\Omega)}\right]\\
&= (\delta+1)\langle u_t^N,(-\Delta)^p u_{tt}^N\rangle - 3\langle(-\Delta)^p u_{tt}^N, u_t^N(u^N)^2\rangle.
\end{aligned} \tag{4.16}$$

Consider the non-linear term

$$\begin{aligned}
|3\langle(-\Delta)^p u_{tt}^N, u_t^N(u^N)^2\rangle| &= |3\langle\nabla^p u_{tt}^N, \nabla^p\left(u_t^N(u^N)^2\right)\rangle|\\
&\leq \frac{\left\|\nabla^p u_{tt}^N\right\|^2_{H^{-\chi}(\Omega)}}{4} + 9\left\|\nabla^p\left(u_t^N\left(u^N\right)^2\right)\right\|^2_{H^{\chi}(\Omega)}\\
&\leq \frac{\left\|\nabla^p u_{tt}^N\right\|^2_{H^{-\chi}(\Omega)}}{4} + 9\left\|u_t^N\left(u^N\right)^2\right\|^2_{H^{p+\chi}(\Omega)}
\end{aligned}$$

where we use Young's inequality in the second line and that the $H^{p+\chi}$-norm bounds the H^p- and $H^{p+\chi}$-semi-norms in the last line.

Choosing $p+\chi \leq 2$ then we have

$$\begin{aligned}|3\langle(-\Delta)^p u_{tt}^N, u_t^N (u^N)^2\rangle| &\leq \frac{\left\|\nabla^p u_{tt}^N\right\|_{H^{-\chi}(\Omega)}^2}{4} + 9\left\|u_t^N \left(u^N\right)^2\right\|_{H^2(\Omega)}^2 \\ &\leq \frac{\left\|\nabla^p u_{tt}^N\right\|_{H^{-\chi}(\Omega)}^2}{4} + 9\left\|u_t^N\right\|_{H^2(\Omega)}^2 \left\|u^N\right\|_{H^2(\Omega)}^4 \end{aligned} \tag{4.17}$$

where we use that $H^2(\Omega)$ is a Banach algebra in the last line.

Substituting (4.17) into (4.16) we have

$$\begin{aligned}&\|\nabla^p u_{tt}^N\|_{H^{-\chi}(\Omega)}^2 + \frac{1}{2}\frac{\mathrm{d}}{\mathrm{d}t}\left[\|(\Delta+I)\nabla^p u_t^N\|_{L^2(\Omega)}^2 + \|\nabla^p u_t^N\|_{L^2(\Omega)}^2\right] \\ &\leq (\delta+1)\langle u_t^N, (-\Delta)^p u_{tt}^N\rangle + \frac{\left\|\nabla^p u_{tt}^N\right\|_{H^{-\chi}(\Omega)}^2}{4} + 9\left\|u_t^N\right\|_{H^2(\Omega)}^2 \left\|u^N\right\|_{H^2(\Omega)}^4 \\ &\leq \frac{\left\|\nabla^p u_{tt}^N\right\|_{H^{-\chi}(\Omega)}^2}{2} + \left(9\left\|u^N\right\|_{H^2(\Omega)}^4 + (\delta+1)^2\right)\left\|u_t^N\right\|_{H^2(\Omega)}^2.\end{aligned}$$

We know that $u^N \in L^\infty(H^2(\Omega))$ (see Lemma 4.3.2) thus for $p+\chi \leq 2$ there exists a $C > 0$ such that

$$\|\nabla^p u_{tt}^N\|_{H^{-\chi}(\Omega)}^2 + \frac{\mathrm{d}}{\mathrm{d}t}\left[\|(\Delta+I)\nabla^p u_t^N\|_{L^2(\Omega)}^2 + \|\nabla^p u_t^N\|_{L^2(\Omega)}^2\right] \leq C\left\|u_t^N\right\|_{H^2(\Omega)}^2. \tag{4.18}$$

Given this inequality we define

$$e_N(t) = \|(\Delta+I)\nabla^p u_t^N(t)\|_{L^2(\Omega)}^2 + \|\nabla^p u_t^N(t)\|_{L^2(\Omega)}^2.$$

Since $p \geq 0$ we have, from Lemma C.2.3, that

$$\begin{aligned}\|u_t^N\|_{H^2(\Omega)}^2 &\leq C_1\|u_t^N\|_{H^{-\chi}(\Omega)}^2 + c_2\|\Delta\nabla^p u_t^N\|_{L^2(\Omega)}^2 \\ &\leq C_1\|u_t^N\|_{H^{-\chi}(\Omega)}^2 + c_2 e_N(t)\end{aligned} \tag{4.19}$$

where the last line follows from the triangle inequality. We define

$$\varphi_N(t) := \|u_t^N\|_{H^{-\chi}(\Omega)}^2.$$

Substituting (4.19) into (4.18) we have

$$\dot{e}_N(t) \leq C_1\varphi_N(t) + c_2 e_N(t).$$

Therefore by Grönwall's inequality, and using $\varphi_N(t) \in L^1(0,\infty)$ by Lemma 4.3.2, we have

$$e_N(T) \leq \exp(c_2 T)e_N(0) + C_3\exp(c_2 T). \tag{4.20}$$

Using Lemma 3.1.1 and then (4.20) we have

$$\begin{aligned}\frac{1}{5}\|\nabla^p u_t^N(T)\|^2_{H^2(\Omega)} &\leq \|(\Delta+I)\nabla^p u_t^N(T)\|^2_{L^2(\Omega)} + \|\nabla^p u_t^N(T)\|^2_{L^2(\Omega)} \\ &\leq \exp(c_2T)\left[\|(\Delta+I)\nabla^p u_t^N(0)\|^2_{L^2(\Omega)} + \|\nabla^p u_t^N(0)\|^2_{L^2(\Omega)}\right] + C_3\exp(c_2T) \\ &\leq \exp(c_2T)\left[2\|\nabla^p u_t^N(0)\|^2_{H^2(\Omega)} + C_3\right]\end{aligned}$$

where we use Lemma 3.1.1 in the final inequality.

Summing $p = 0$ to $p = 2 - \chi$ we have

$$\|u_t^N(T)\|^2_{H^{4-\chi}(\Omega)} \leq 5(3-\chi)\exp(c_2T)\left[2\|u_t^N(0)\|^2_{H^{4-\chi}(\Omega)} + C_3\right]$$

where we use that the $H^{4-\chi}$-norm bounds the H^2-,H^3- and $H^{4-\chi}$-semi-norms.

From (4.14) we have that $u_t^N(0) \in H^{4-\chi}(\Omega)$ if $u^N(0) \in H^{8+\chi}(\Omega)$, i.e. (4.12). We have shown that $u_t^N \in L^\infty_{\text{loc}}(H^{4-\chi}(\Omega))$ and hence by integration $u^N \in L^\infty_{\text{loc}}(H^{4-\chi}(\Omega))$. Using this, integration on (4.18) gives $u_{tt}^N \in L^2_{\text{loc}}(H^{-\chi}(\Omega))$. Therefore we have u^N is bounded in $H^2_{\text{loc}}(H^{-\chi}(\Omega)) \cap W^{1,\infty}_{\text{loc}}(H^{4-\chi}(\Omega))$.

Since u^N is bounded in $H^2_{\text{loc}}(H^{-\chi}(\Omega)) \cap W^{1,\infty}_{\text{loc}}(H^{4-\chi}(\Omega))$ by taking the limit $N \to \infty$, $u \in H^2_{\text{loc}}(H^{-\chi}(\Omega)) \cap W^{1,\infty}_{\text{loc}}(H^{4-\chi}(\Omega))$.

Step 3. Using that $H^{4-\chi}(\Omega)$ is compactly embedded in $H^{-\chi}(\Omega)$ and $H^2(\Omega)$ is embedded in $H^{-\chi}(\Omega)$ and embeds $H^{4-\chi}(\Omega)$ we can use Lemma 4.3.1 ([Sim87, Corollary 4]) with $r = 2, X = H^{4-\chi}(\Omega), B = H^2(\Omega)$ and $Y = H^{-\chi}(\Omega)$ to obtain relative compactness in $C(0,T;H^2(\Omega))$. Hence we can take a sub-sequence which we again rename u^N so that

$$u^N \to u \text{ strongly in } C(0,T;H^2(\Omega)).$$

Also we can take a subsequence u_t^N so that

$$u_t^N \to u_t \text{ strongly in } C(0,T;H^2(\Omega))$$

so that we have $u \in C^1(0,T;H^2(\Omega))$. □

Remark 4.3.3. *It may be possible to remove the assumption* (4.12) *using the smoothing property of the PFC and SH equations. For the sake of simplicity we did not pursue this option.*

4.3.3 Uniqueness

Finally, we show that the solutions of the L^2- and the H^{-1}-gradient flows starting from given initial data are unique.

Lemma 4.3.4. *The solution u of the gradient flows defined in Definitions 4.2.1 and 4.2.2 are unique for given initial conditions $u_0(x) \in H^2_{\bar{u}}(\Omega)$.*

Proof. Assume there exist two solutions u_1, u_2 that satisfy the weak form (4.1) with

$$u_1(x,0) = u_0(x) = u_2(x,0).$$

We define the difference as

$$\tilde{u} = u_1 - u_2.$$

Then clearly $\tilde{u}(x,0) = 0$. Inserting u_1 and u_2 into the weak form (4.1) and subtracting one from the other we have

$$\langle \tilde{u}_t, v\rangle_H = -\langle(\Delta + I)\tilde{u}, (\Delta + I)v\rangle + \delta\langle\tilde{u}, v\rangle - \langle u_1^3 - u_2^3, v\rangle$$

for all $v \in H^2_\#(\Omega)$. Testing with $v = \tilde{u}(t) \in H^2_\#(\Omega)$ we obtain

$$\frac{1}{2}\frac{\mathrm{d}}{\mathrm{d}t}\|\tilde{u}\|_H^2 \leq \delta\|\tilde{u}\|^2_{L^2(\Omega)} - \|(\Delta + I)\tilde{u}\|^2_{L^2(\Omega)} - \langle u_1^3 - u_2^3, \tilde{u}\rangle. \tag{4.21}$$

We can see that the cross-term is positive i.e.,

$$\begin{aligned}\langle u_1^3 - u_2^3, \tilde{u}\rangle &= \langle\left(u_1^2 + u_1u_2 + u_2^2\right)(u_1 - u_2), \tilde{u}\rangle \\ &= \frac{1}{2}\langle\left[u_1^2 + u_2^2 + (u_1 + u_2)^2\right], \tilde{u}^2\rangle \\ &\geq 0.\end{aligned}$$

We can thus discard the cross-term from (4.21) to obtain

$$\frac{1}{2}\frac{\mathrm{d}}{\mathrm{d}t}\|\tilde{u}\|_H^2 \leq \delta\|\tilde{u}\|^2_{L^2(\Omega)} - \|(\Delta + I)\tilde{u}\|^2_{L^2(\Omega)}. \tag{4.22}$$

Consider the L^2-norm

$$\|\tilde{u}\|^2_{L^2(\Omega)} = \int_\Omega \tilde{u}^2 \mathrm{d}x \leq \frac{1}{2}\|\tilde{u}\|^2_{H^{-1}(\Omega)} + \frac{1}{2}\|\nabla\tilde{u}\|^2_{L^2(\Omega)}.$$

Using (3.2) with $\epsilon = 1$ we have

$$\|\tilde{u}\|^2_{L^2(\Omega)} \leq \frac{1}{2}\|\tilde{u}\|^2_{H^{-1}(\Omega)} + \frac{3}{4}\|\tilde{u}\|^2_{L^2(\Omega)} + \frac{1}{4}\|\Delta u + u\|^2_{L^2(\Omega)}.$$

Re-arranging we have

$$\|\tilde{u}\|^2_{L^2(\Omega)} - \|\Delta\tilde{u} + \tilde{u}\|^2_{L^2(\Omega)} \leq 2\|\tilde{u}\|^2_{H^{-1}(\Omega)}. \tag{4.23}$$

Hence we can bound the right-hand side of (4.22) by the H^{-1}- or L^2-norm depending on H. Therefore we can write

$$\frac{\mathrm{d}}{\mathrm{d}t}\|\tilde{u}\|_H^2 \leq 2C\|\tilde{u}\|_H^2,$$

where the constant C is defined

$$C = \begin{cases} \delta, & \text{for the Swift-Hohenberg equation,} \\ 2, & \text{for the PFC equation.} \end{cases}$$

Applying Grönwall's lemma, recalling from Lemmas 4.3.3 that $u \in C^1(0,T;H^2(\Omega))$, yields the result. □

4.4 H^2-gradient Flow

Using Picard's theorem, Theorem 4.3.1, we can show that the solution of the H^2-gradient flow equation, Definition 4.2.4, is continuous. We use Picard's theorem for the H^2-gradient flow as it is much simpler than the Galerkin method of Lemma 4.3.2 and gives the additional regularity required for Chapter 5.

Lemma 4.4.1. *For each $u_0 \in H^2(\Omega)$. There exists a unique $u \in C^1(H^2(\Omega))$ that satisfies Definition 4.2.4.*

Proof. Recall that we have chosen $u \in H^2_{\bar{u}}(\Omega)$ therefore $\eta = u - \bar{u} \in H^2_{\#}(\Omega)$ and we can rewrite Definition 4.2.4 as

$$\langle \eta_t, v \rangle_A = -\delta\mathcal{F}[\bar{u} + \eta, v], \qquad \forall v \in H^2_{\#}(\Omega).$$

Since, from Lemma 4.2.1, the A-norm is equivalent to the H^2-norm we can use the A-inner product to define an operator $G : H^2_{\#}(\Omega) \to H^2_{\#}(\Omega)$,

$$\langle AG[\eta], v \rangle = -\delta\mathcal{F}[\bar{u} + \eta, v] \qquad \forall v \in H^2_{\#}(\Omega). \tag{4.24}$$

From Lemma 3.1.4 $\delta\mathcal{F}[\bar{u}+\eta] \in H^{-2}(\Omega)$, hence the variational problem (4.24) is well-posed. That is, for each $\eta \in H^2_{\#}(\Omega)$ the variational problem (4.24) defines a $G[\eta] \in H^2_{\#}(\Omega)$.

Since, from Lemma 3.1.4, $\mathcal{F} \in C^4(H^2(\Omega))$ in the sense of Fréchet we immediately have that G is locally bounded and locally Lipschitz. Therefore we can use Picard's theorem, Theorem 4.3.1, to obtain a $T > 0$ and a $\eta \in C^1(0,T;H^2_{\#}(\Omega))$ such that $\eta_t = G[\eta]$ and η is the unique solution on this interval.

Since we have chosen u_0 in $H^2(\Omega)$ then we can define the set

$$S := \{v \in H^2_{\#}(\Omega) | \mathcal{F}[v + \bar{u}] \leq \mathcal{F}[u_0]\}.$$

Since $\mathcal{F}$ is decreasing along our trajectory we have that

$$\{\eta(t)\} \subseteq S.$$

Since $\mathcal{F} \in C^4(H^2(\Omega))$ we have that $G : S \to H^2_{\#}(\Omega)$ is Lipschitz and bounded where the bounds depend on u_0.

Recall Theorem 4.3.1 since we know that for $v_0 \in S$, L and K depend only on u_0 therefore for all $v_0 \in S$ we can choose the same $c > 0$. Let T be maximal. For T maximal we consider the solution at time $T - c/2$, i.e. $v_0 = u(T - c/2)$. By Theorem 4.3.1 we have that the solution u exists in the interval $[T - 3c/2, T + c/2]$ in particular the solution exists at $T + c/2 > T$ which contradicts the assumption that T is maximal. Therefore there is no maximal t, i.e. we have global existence of u. □

4.5 Conclusion

In this chapter we discuss several methods to find the minimiser of the PFC functional by finding the solution to the associated Euler-Lagrange equation. The technique chosen in this thesis to compute the solution to the Euler-Lagrange equation is the gradient flow technique. Other minimisation techniques can be seen in [NW06], we also show a trust region method in Appendix E. We introduce three gradient flows in the norms H^{-1}, L^2 and H^2. We then prove existence, uniqueness and regularity results for the solutions to each of these gradient flows.

Chapter 5

Convergence to Equilibrium

In this chapter we obtain rates of convergence to equilibrium for the solution of the gradient flows introduced in the previous chapter. The technique we employ is based on the Łojasiewicz gradient inequality. This method is used for the modified phase-field crystal equation in [GW14]. Similarly to [GW14] we split our proof into two steps: first we prove the Łojasiewicz inequality, second we prove that the trajectory of our gradient flow is compact (here, we use a different method to [GW14]).

We will show in Section 5.2 that the PFC functional (3.1) satisfies the Łojasiewicz gradient inequality:

Theorem 5.0.1. *The PFC functional* (3.1) *satisfies the Łojasiewicz inequality. That is, for every* $\varphi \in H^2_{\bar{u}}(\Omega)$ *such that* $\delta\mathcal{F}[\varphi, v] = 0$ *for all* $v \in H^2_{\#}(\Omega)$*, there exist constants* $\theta \in \left(0, \frac{1}{2}\right], c \geq 0$ *and* $\sigma > 0$ *such that, for all* $\eta \in H^2_{\bar{u}}(\Omega)$*, with* $\|\eta - \varphi\|_{H^2(\Omega)} \leq \sigma$*,*

$$\|\delta\mathcal{F}[\eta]\|_{H^{-2}(\Omega)} \geq c|\mathcal{F}[\eta] - \mathcal{F}[\varphi]|^{1-\theta}.$$

The constant θ *is called a Łojasiewicz exponent.*

We now state the convergence theorem which is the main result of this chapter.

Theorem 5.0.2. *Let* u *be a trajectory that satisfies Definition 4.2.1, Definition 4.2.2 or Definition 4.2.4 with* $u_0 \in H^s_{\bar{u}}(\Omega)$ *where* $s = 8, 9$ *or* 4 *respectively. Then there exists* $\varphi \in H^2_{\bar{u}}(\Omega)$ *such that* $\delta\mathcal{F}[\varphi, v] = 0$ *for all* $v \in H^2_{\#}(\Omega)$ *and*

$$\lim_{t\to\infty} \|u(t) - \varphi\|_{H^2(\Omega)} = 0.$$

Moreover, let θ *be any Łojasiewicz exponent of the PFC functional* $\mathcal{F}$ *at* φ*. Then we have*

$$\|u(t) - \varphi\|_H \leq \begin{cases} Ce^{-\beta t} \text{ for some } \beta > 0 \text{ if } \theta = \frac{1}{2}, \\ Ct^{-\frac{\theta}{1-2\theta}} \text{ if } 0 < \theta < \frac{1}{2}, \end{cases}$$

where $C > 0$ *and the* H*-norm is defined by the spaces* H *given in* (4.4)*.*

5.1 Abstract Convergence Theory

In this section we review an abstract convergence theorem which we employ in the proof of Theorem 5.0.2. First we take two Hilbert spaces V and H such that

$$V \subset H = H^* \subset V^*$$

where the embeddings are continuous and dense. In our case, we take $V = H^2_{\#}$ (see Definition C.1.2) and H is determined by (4.4).

The principle results we use are [HJ15, Theorem 11.3.1] and [CF10, Theorem 12.2] for the case $V = H$. We recall a version of these theorems here for convenience. Let $\mathcal{E} \in C^1(V, \mathbb{R})$, we define $\delta\mathcal{E}[\eta]$ by $\delta\mathcal{E}[u, v] = \langle \delta\mathcal{E}[u], v\rangle$. Using the notation of Remark 4.2.5 we have the following result.

Theorem 5.1.1 ([HJ15, Theorem 11.3.1] and [CF10, Theorem 12.2] for the case $V = H$)**.** *Let $\eta \in C^1(V)$ be a solution of the gradient system*

$$\eta_t + \nabla_H \mathcal{E}[\eta] = 0.$$

Assume that

i) $\bigcup_{t\geq 1}\{\eta(t)\}$ is compact in V;

ii) $\mathcal{E}$ satisfies the Łojasiewicz inequality near every point $\varphi \in V, \nabla_H \mathcal{E}[\varphi] = 0$, that is there exist $\theta \in (0, \frac{1}{2}], \sigma > 0$ and $C \geq 0$ such that for every $v \in V$ with $\|v - \varphi\|_V \leq \sigma$ one has

$$|\mathcal{E}[v] - \mathcal{E}[\varphi]|^{1-\theta} \leq C\|\delta\mathcal{E}[v]\|_{V^*}.$$

Then $\lim_{t\to\infty} \|\eta(t) - \varphi\|_V = 0$. Moreover,

$$\|\eta(t) - \varphi\|_H \leq \begin{cases} C_{ae}e^{-ct} & \text{for some } c > 0, \text{ if } \theta = \frac{1}{2}, \\ C_{at}t^{-\frac{\theta}{1-2\theta}} & \text{if } \theta \in (0, \frac{1}{2}), \end{cases}$$

where $C_{ae}, C_{at} > 0$.

We consider the functional $\mathcal{E} : H^2_{\#}(\Omega) \to \mathbb{R}$ defined by

$$\mathcal{E}[\eta] = \mathcal{F}[\eta + \bar{u}]. \tag{5.1}$$

Then the problem **(P)** (see page 37) can be written as

$$\min_{\tilde{\eta}\in H^2_{\#}(\Omega)} \mathcal{E}[\tilde{\eta}].$$

If we let $u = \bar{u} + \eta$ where $\eta \in H^2_{\#}(\Omega)$, then $\eta_t = u_t$. Therefore the weak gradient flow (4.1) can be written in abstract form as

$$\eta_t + \nabla_H \mathcal{E}[\eta] = 0.$$

If $\mathcal{E}$ and η satisfy the assumptions of Theorem 5.1.1 we can use this theorem to prove Theorem 5.0.2. Therefore we now have to prove four assumptions: two on the energy; $\mathcal{E} \in C^1(H^2_\#(\Omega), \mathbb{R})$ and the Łojasiewicz inequality, and two on the trajectory; $\eta \in C^1(H^2_\#(\Omega))$ and $\bigcup_{t\geq 1}\{\eta(t)\}$ is compact in $H^2_\#(\Omega)$.

The requirement that $\mathcal{E}[\eta] \in C^1(H^2_\#(\Omega), \mathbb{R})$ is established in Lemma 3.1.4.

Regularity of η follows from that of u. We have already proved that $u \in \bar{u} + C^1(H^2_\#(\Omega))$ for the H^2-gradient flow in Lemma 4.4.1 and for the PFC- and SH-gradient flows in Lemma 4.3.3.

Therefore we have two assumptions to check before we can use Theorem 5.1.1. These are that the translated PFC functional (5.1) satisfies the Łojasiewicz inequality and that $\bigcup_{t\geq 1}\{\eta(t)\}$ is relatively compact in $H^2_\#(\Omega)$. We first prove the Łojasiewicz inequality for $\mathcal{E}$ in Section 5.2. We then prove the compactness of the trajectories η in Section 5.3.

5.2 The Łojasiewicsz Gradient Inequality

We wish to prove that the translated PFC functional (5.1) satisfies the Łojasiewicz inequality, Theorem 5.0.1. This is also shown in [GW14, Lemma 6.1]; however we lay out the argument in more detail. We first give a version of [HJ15, Theorem 11.2.7] which gives general conditions under which the Łojasiewicz gradient inequality holds. We then show that in the specific case of the translated PFC functional (5.1) these conditions are satisfied.

To facilitate the rest of this section we recall the definition of the Łojasiewicz gradient inequality (see [Sim83, Theorem 3] and also [HJ15, Definition 11.0.3]).

Definition 5.2.1 (The Łojasiewicz gradient inequality)**.** *We say that the functional $\mathcal{E}_0 \in C^1(V, \mathbb{R})$ satisfies the Łojasiewicz gradient inequality near some $\varphi \in V$, if there exist constants $\theta \in \left(0, \frac{1}{2}\right], c \geq 0$ and $\sigma > 0$ such that, for all $\eta \in V$ with $\|\eta - \varphi\|_V \leq \sigma$,*

$$\|\delta\mathcal{E}_0[\eta]\|_{V^*} \geq c|\mathcal{E}_0[\eta] - \mathcal{E}_0[\varphi]|^{1-\theta}. \tag{5.2}$$

In order to prove the Łojasiewicz gradient inequality we will need the second variation to be a semi-Fredholm operator. Therefore we recall the relevant definition. Let E, F be two Banach spaces and $B : E \to F$ be a linear operator. We denote by $N(B)$ and $R(B)$ the null space and the range of B, respectively.

Definition 5.2.2 ([HJ15, Definition 2.2.1])**.** *A bounded linear operator $B \in L(E, F)$ is said to be semi-Fredholm if*

- *$N(B)$ is finite dimensional, and*
- *$R(B)$ is closed.*

We then say $B \in \mathrm{SF}(E,F)$.

We also define a Banach-space analogue of analyticity.

Definition 5.2.3 ([HJ15, Definition 2.3.1])**.** *Let* X, Y *be two real Banach spaces and* $a \in X$*. Let* U *be an open neighbourhood of* a *in* X*. A map* $f : U \to Y$ *is called analytic at* a *if there exists* $r > 0$ *and a sequence of* n*-linear continuous symmetric maps* $(M_n)_{n\in\mathbb{N}}$ *fulfilling the following conditions:*

- $\sum_{n\in\mathbb{N}} \|M_n\|_{\mathcal{L}_n(X,Y)} r^n < \infty$
  where $\|M_n\|_{\mathcal{L}_n(X,Y)} = \sup\{\|M_n(x_1,..,x_n)\|_Y, \sup_i \|x_i\|_X \leq 1\}$,
- $\bar{B}(a,r) \subset U$,
- $\forall h \in \bar{B}(0,r),\ f(a+h) = f(a) + \sum_{n\geq 1} M_n(h^{(n)})$ *where* $h^{(n)} = \underbrace{(h,..,h)}_{n \text{ times}}$.

If $\mathcal{E}_0$ is analytic and $\mathcal{E}_0 \in C^1(V,\mathbb{R})$ then we can see from [HJ15, Proposition 2.3.4] that $\delta\mathcal{E}_0 : V \to V^*$ is analytic as well.

We can then obtain the Łojasiewicz inequality needed for convergence (see Theorem 5.1.1) from the following abstract theorem. For any $\mathcal{E}_0 \in C^2(V,\mathbb{R})$ and fixed $\eta_0 \in H^2(\Omega)$ such that $\delta\mathcal{E}_0[\eta_0] = 0$ this theorem follows directly from [HJ15, Theorem 11.2.7] by applying the result of that theorem to $\mathcal{G}[v] = \mathcal{E}_0[v+\eta_0] - \mathcal{E}_0[\eta_0]$.

Theorem 5.2.1. *Let* $\mathcal{E}_0 \in C^2(V,\mathbb{R})$ *and let* $\eta_0 \in V$*. Assume that* $\hat{A} = \delta^2\mathcal{E}_0[\eta_0]$ *is a semi-Fredholm operator and that* $N := ker\hat{A} \subset Z$ *and* $Z \subset H$ *where this embedding is continuous and dense. Let the operator* $\mathcal{L}$ *be defined by* $\mathcal{L} = \Pi + \hat{A}$ *where* $\Pi : V \to ker\hat{A}$ *is the* H*-orthogonal-projection. We define the space* $W = \mathcal{L}^{-1}(Z)$.

Assume that:

• *(H2)* $\mathcal{E}_0 : U \to \mathbb{R}$ *is analytic in the sense of Definition 5.2.3 where* $U \subset W$ *is an open neighbourhood of* η_0*, such that* $\delta\mathcal{E}_0(U) \subset Z$.

Then there exist $\theta \in \left(0, \frac{1}{2}\right]$, $\sigma > 0$ *and* $c > 0$ *such that, for all* $\eta \in V$,

$$\|\eta - \eta_0\|_V < \sigma \Rightarrow \|\delta\mathcal{E}_0[\eta]\|_{V^*} \geq c|\mathcal{E}_0[\eta] - \mathcal{E}_0[\eta_0]|^{1-\theta}.$$

In order to prove that $\delta^2\mathcal{E}_0[\eta_0]$ is a semi-Fredholm operator for a specific $\mathcal{E}_0$ we recall two abstract theorems of [HJ15] which state properties that a bounded operator satisfies if it is a semi-Fredholm operator.

Theorem 5.2.2 ([HJ15, Theorem 2.2.3])**.** *Let* E, F *be two Banach spaces. Let* $B \in L(E,F)$ *and assume that* $N(B)$ *is finite dimensional. Then we have* $B \in \mathrm{SF}(E,F)$ if and only if

$$\exists \rho > 0,\ \forall u \in X\ \|Bu\|_F \geq \rho\|u\|_E,$$

where X is a closed subset of E such that $E = N(B) \oplus X$.

Theorem 5.2.3 ([HJ15, Theorem 2.2.5])**.** *Let E, F be two Banach spaces. Let $B \in \mathrm{SF}(E,F)$* and let $G \in L(E,F)$ be a compact operator, then $B+G \in \mathrm{SF}(E,F)$.

We now consider the specific case of the shifted PFC functional (5.1). To obtain the Łojasiewicz gradient inequality in this case, using Theorem 5.2.1, we have two hypotheses to check: that $\delta^2\mathcal{E}[\eta]$ is a semi-Fredholm operator for all $\eta \in H^2_{\#}(\Omega)$ and that $\mathcal{E}$ and $\delta\mathcal{E}$ are analytic. Clearly these hypotheses follow from the equivalent hypotheses on $\mathcal{F}$, i.e., that $\delta^2\mathcal{F}[\bar{u}+\eta]$ is a semi-Fredholm operator and that $\mathcal{F}$ and $\delta\mathcal{F}$ are analytic.

Recalling the abstract Theorems 5.2.2 and 5.2.3 we are able to prove that $\delta^2\mathcal{F}[u]$ is a semi-Fredholm operator for any $u \in H^2_{\mathrm{per}}(\Omega)$.

Lemma 5.2.1. *For all $u \in H^2_{\mathrm{per}}(\Omega)$, $\delta^2\mathcal{F}[u] \in \mathrm{SF}(H^2_{\mathrm{per}}(\Omega), H^{-2}_{\mathrm{per}}(\Omega))$.*

Proof. Recall the second variation (3.10), the associated operator can be written as

$$\delta^2\mathcal{F}[u] = A_1 - (\delta+1)I + 3u^2 I, \tag{5.3}$$

where

$$A_1 := (\Delta + I)^2 + I \tag{5.4}$$

is an isomosphism from $H^2_{\mathrm{per}}(\Omega)$ to $H^{-2}_{\mathrm{per}}(\Omega)$. Hence the conditions of Theorem 5.2.2 are satisfied and the operator A_1 is semi-Fredholm.

Following the splitting (5.3) we define

$$p(x) = 3u(x)^2 - (\delta+1).$$

If $u \in H^2_{\mathrm{per}}(\Omega)$ then $u \in L^\infty(\Omega)$ and therefore $p \in L^\infty(\Omega)$. We define $Gv := pv$ for all $v \in H^2_{\mathrm{per}}(\Omega)$. Since $p \in L^\infty(\Omega)$, $G : H^2_{\mathrm{per}}(\Omega) \to L^2_{\mathrm{per}}(\Omega)$ is bounded ($G : H^2_{\mathrm{per}}(\Omega) \to L^2_{\mathrm{per}}(\Omega)$ as $\|Gv\|_{L^2(\Omega)} \le \|p\|_{L^\infty(\Omega)}\|v\|_{L^2(\Omega)} \le \|p\|_{L^\infty(\Omega)}\|v\|_{H^2(\Omega)}$) and since $L^2_{\mathrm{per}}(\Omega) \subset\subset H^{-2}_{\mathrm{per}}(\Omega)$, it follows that G is compact.

We have by the splitting (5.3) that $\delta^2\mathcal{F}[u] = A_1 + G$. Since G is compact and $A_1 \in \mathrm{SF}(H^2_{\mathrm{per}}(\Omega), H^{-2}_{\mathrm{per}}(\Omega))$ by Theorem 5.2.3 we have $\delta^2\mathcal{F}[u] \in \mathrm{SF}(H^2_{\mathrm{per}}(\Omega), H^{-2}_{\mathrm{per}}(\Omega))$. □

We now prove that the PFC functional is analytic.

Lemma 5.2.2. *The PFC functional* (3.1) *is analytic at every point $\eta \in H^2(\Omega)$.*

Proof. Recall the PFC functional difference (3.11),

$$\begin{aligned}\mathcal{F}[a+h] - \mathcal{F}[a] = \langle \Delta a + a, \Delta h + h\rangle - \delta\langle a, h\rangle + \langle a^3, h\rangle + \frac{1}{2}\|\Delta h + h\|^2_{L^2(\Omega)} - \frac{\delta}{2}\|h\|^2_{L^2(\Omega)} \\ + \frac{3}{2}\|ah\|^2_{L^2(\Omega)} + \langle a, h^3\rangle + \frac{1}{4}\|h\|^4_{L^4(\Omega)}.\end{aligned}$$

Then by comparison with Definition 5.2.3, we have

$$\begin{aligned}
M_1(x_1) &= \langle \Delta a + a, \Delta x_1 + x_1\rangle - \delta\langle a, x_1\rangle + \langle a^3, x_1\rangle,\\
M_2(x_1, x_2) &= \frac{1}{2}\left[\langle \Delta x_1 + x_1, \Delta x_2 + x_2\rangle - \delta\langle x_1, x_2\rangle + 3\langle a^2 x_1, x_2\rangle\right],\\
M_3(x_1, x_2, x_3) &= \langle a, x_1 x_2 x_3\rangle,\\
M_4(x_1, x_2, x_3, x_4) &= \frac{1}{4}\langle x_1 x_2 x_3, x_4\rangle,\\
M_n(x_1, ..., x_n) &= 0, \qquad\qquad \forall n > 4.
\end{aligned}$$

These are exactly the same, up to multiplicative constants, as the variations of $\mathcal{F}$ given in Lemma 3.1.4. Since in this lemma we show that these variations are all bounded if $x_1, x_2, x_3, x_4 \in H^2(\Omega)$, we now have that $\mathcal{F}$ is analytic. □

Since we are considering the translated PFC functional (5.1) we consider the case where $V = H^2_\#(\Omega)$ and thus we have $\eta_0 \in H^2_\#(\Omega)$. We can show that for $-2 \le k \le 2$ $\delta^2\mathcal{E}[\eta_0] : H^{k+4}_\#(\Omega) \to H^k_\#(\Omega)$.

Lemma 5.2.3. *For $-2 \le k \le 2$, $\delta^2\mathcal{E}[\eta_0] : H^{k+4}_\#(\Omega) \to H^k_\#(\Omega)$ is bounded.*

Proof. The $k = -2$ case follows from the definition of $\delta^2\mathcal{E}[\eta_0]$.

From Lemma 3.1.4 we have

$$\delta^2\mathcal{E}[\eta_0] = (\Delta + I)^2 - \delta + 3(\eta_0 + \bar{u})^2.$$

For all $v \in H^{k+4}(\Omega)$ we have

$$\begin{aligned}
\|\delta^2\mathcal{E}[\eta_0]v\|_{H^k(\Omega)} &= \|\Delta^2 v + 2\Delta v + (1-\delta)v + 3(\eta_0 + \bar{u})^2 v\|_{H^k(\Omega)}\\
&\le \|\Delta^2 v\|_{H^k(\Omega)} + 2\|\Delta v\|_{H^k(\Omega)} + \|v\|_{H^k(\Omega)} + 3\|(\eta_0 + \bar{u})^2 v\|_{H^k(\Omega)}\\
&\le 4\|v\|_{H^{4+k}(\Omega)} + 3\|(\eta_0 + \bar{u})^2 v\|_{H^2(\Omega)}\\
&\le 4\|v\|_{H^{4+k}(\Omega)} + 3\|\eta_0 + \bar{u}\|^2_{H^2(\Omega)}\|v\|_{H^2(\Omega)}\\
&\le \left(4 + 3\|\eta_0 + \bar{u}\|^2_{H^2(\Omega)}\right)\|v\|_{H^{4+k}(\Omega)}
\end{aligned}$$

where we use that the H^{4+k}-norm bounds the H^k-, H^{2+k}- and H^{4+k}-semi-norms in the third and final lines and that $H^2(\Omega)$ is a Banach algebra (see [Pel11, Appendix B.1]) in the fourth line. □

By comparison with Theorem 5.2.1, for $-2 \le k \le 2$ we define $\mathcal{L} : H^{k+4}_\#(\Omega) \to H^k_\#(\Omega)$. We can find a stricter embedding for $\ker(\delta^2\mathcal{E}[\eta_0])$.

Lemma 5.2.4. *Let $\eta_0 \in H^2_\#(\Omega)$ then $ker(\delta^2\mathcal{E}[\eta_0]) \subseteq H^6_\#(\Omega)$.*

Proof. By definition, $z \in \ker(\delta^2\mathcal{E}[\eta_0])$ if

$$\delta^2\mathcal{E}[\eta_0]z = 0. \tag{5.5}$$

From the definition of (3.10) we know that $z \in H^2_{\#}(\Omega)$. The weak form of (5.5) is

$$\langle \delta^2 \mathcal{E}[\eta_0] z, \varphi \rangle = 0 \qquad \forall \varphi \in H^2_{\#}(\Omega)$$

using (3.10) we can re-arrange to obtain

$$\langle \Delta z, \Delta \varphi \rangle = -2\langle \Delta z, \varphi \rangle + (\delta - 1)\langle z, \varphi \rangle - 3\langle (\eta_0 + \bar{u})^2 z, \varphi \rangle.$$

This is clearly an equation of the form (3.14) with $\eta = z$ and

$$f = -2\Delta z + (\delta - 1)z - 3(\eta_0 + \bar{u})^2 z.$$

Clearly since $z \in H^2_{\#}(\Omega)$ then $\Delta z \in L^2_{\#}(\Omega)$. We also know that $\eta_0 \in H^2_{\#}(\Omega)$ and hence $\eta_0 + \bar{u} \in H^2_{\text{per}}(\Omega)$ therefore $3(\eta_0 + \bar{u})^2 z \in H^2_{\text{per}}(\Omega)$ since $H^2_{\text{per}}(\Omega)$ is a Banach algebra. Therefore we have $f \in L^2_{\text{per}}(\Omega)$.

Using Lemma 3.3.2 we therefore obtain that $z \in H^4_{\#}(\Omega)$. Since $z \in H^4_{\#}(\Omega)$, $\Delta z \in H^2_{\#}(\Omega)$ and therefore $f \in H^2_{\text{per}}(\Omega)$. Hence we can use Lemma 3.3.2 again to obtain that $z \in H^6_{\#}(\Omega)$. □

Since $H^6_{\#}(\Omega) \subset H^2_{\#}(\Omega)$ then $\ker \delta^2 \mathcal{E}[\eta_0] \subset H^2_{\#}(\Omega)$. Also since in (4.4) we choose $H^2_{\#}(\Omega) \subseteq H$, for an analogy of Theorem 5.2.1 we need $Z = H^2_{\#}(\Omega)$. From the definition of $\mathcal{L}$ (see Theorem 5.2.1) we have, for $-2 \leq k \leq 2$, $\mathcal{L}^{-1} : H^k_{\#}(\Omega) \to H^{k+4}_{\#}(\Omega)$ hence $W = \mathcal{L}^{-1}(Z) = H^6_{\#}(\Omega)$. From the method of Lemma 3.3.3, if $u \in H^k(\Omega)$ then $\delta\mathcal{E}[u] \in H^{k-4}(\Omega)$. Therefore, $\delta\mathcal{E}[\eta_0] \subset H^2_{\#}(\Omega)$ for all $\eta_0 \in H^6_{\#}(\Omega)$.

We are now in a position to use Theorem 5.2.1 with $\mathcal{E} = \mathcal{E}_0$, $V = Z = H^2_{\#}(\Omega)$ and $W = H^6_{\#}(\Omega)$. Since Theorem 5.2.1 holds for all $\eta_0 \in H^2_{\#}(\Omega)$ such that $\delta\mathcal{E}_0[\eta_0] = 0$ we choose $\eta_0 = u_0$ such that $\delta\mathcal{E}[u_0] = 0$. Then we use Theorem 5.2.1 to prove the Łojasiewicz inequality in $H^2_{\#}(\Omega)$.

Theorem 5.2.4. *The translated PFC functional* (5.1) *satisfies the Łojasiewicz inequality* (5.2). *That is, near any* $u_0 \in H^2_{\#}(\Omega)$ *such that* $\delta\mathcal{E}[u_0] = 0$, *there exist constants* $\theta \in \left(0, \frac{1}{2}\right]$, $c \geq 0$ *and* $\sigma > 0$ *such that, for all* $\eta \in H^2_{\#}(\Omega)$ *with* $\|\eta - u_0\|_{H^2_{\#}(\Omega)} \leq \sigma$,

$$\|\delta\mathcal{E}[\eta]\|_{H^{-2}_{\#}(\Omega)} \geq c|\mathcal{E}[\eta] - \mathcal{E}[u_0]|^{1-\theta}.$$

Proof. From Lemma 5.2.1, picking $u = u_0 + \bar{u}$ we have that $\delta^2\mathcal{F}[u_0 + \bar{u}]$ is a semi-Fredholm operator. From Lemma 5.2.2 and [HJ15, Proposition 2.3.4] we see that $\mathcal{E}$ and $\delta\mathcal{E}$ are analytic. Hence the conditions of Theorem 5.2.1 are fulfilled and we have that the translated PFC functional (5.1) obeys a Łojasiewicz gradient inequality on $H^2_{\#}(\Omega)$ at u_0, i.e. Theorem 5.2.4. □

5.3 Compactness

Having established the Łojasiewicz inequality, the remaining condition in Theorem 5.1.1 is compactness of trajectories in $H^2(\Omega)$. We use a different argument here from the one in [GW14] as we want to avoid the more involved method of attractors that is necessary to deal with the u_{tt}-term in the MPFC equation, see [GW14, Section 5]. Furthermore, we also require a different method to prove compactness for the H^2-gradient flow.

To prove that the trajectory η is compact, we first prove that u_t is bounded for $t > 1$, in an appropriate space. We then rearrange the gradient-flow equation (5.6) to show that boundedness of u_t implies $u \in L^\infty([1,\infty); H^4(\Omega))$. The compact embedding of $H^4(\Omega)$ in $H^2(\Omega)$ gives that the trajectory is compact in $H^2(\Omega)$. We use a separate lemma to prove $u \in L^\infty(H^4(\Omega))$ for the H^2-gradient flow.

We take $\mathcal{E}[\eta] = \mathcal{F}[\bar{u} + \eta] \in C^1(H^2_\#(\Omega), \mathbb{R})$ then we have the abstract evolution equation

$$\eta_t(t) + \nabla_H \mathcal{E}[\eta(t)] = 0, \qquad \forall t \geq 0. \tag{5.6}$$

We use a positive operator $\tilde{H}$ which is defined as

$$\tilde{H} = \begin{cases} I, & \text{for the SH case,} \\ (-\Delta)^{-1}, & \text{for the PFC case,} \\ A, & \text{for the } H^2\text{-gradient flow case.} \end{cases}$$

Hence we can rewrite (5.6) in weak form, using $u = \eta + \bar{u}$, as

$$\langle \tilde{H} u_t(t), v\rangle + \langle \delta\mathcal{F}[u(t)], v\rangle = 0, \qquad \forall v \in H^2_\#(\Omega). \tag{5.7}$$

As the first stage of proving compactness we show that u_t is bounded for all $t > 1$.

Lemma 5.3.1. *For the solutions of the weak partial differential equations Definition 4.2.1, 4.2.2 and 4.2.4 u_t is bounded for all $t > 1$. That is,*

$$\begin{aligned} &u_t \in L^\infty([1,\infty); L^2_\#(\Omega)) \quad \textit{for the Swift-Hohenberg case,} \\ &u_t \in L^\infty([1,\infty); H^{-1}_\#(\Omega)) \quad \textit{for the PFC case,} \\ &u_t \in L^\infty([1,\infty); H^2_\#(\Omega)) \quad \textit{for the } H^2\textit{-gradient flow case.} \end{aligned} \tag{5.8}$$

Proof. We use a Galerkin method and split this proof into two steps. We first prove that for each interval $[j, j+1]$ there exists a $t_j^N \in [j, j+1]$ such that $\|\tilde{H}^{\frac{1}{2}} u_t^N(t_j^N)\|_{L^2(\Omega)}$ is uniformly bounded for all N and j. We then prove that for $t - t_j^N \leq 2$ we can bound $\|\tilde{H}^{\frac{1}{2}} u_t(t)\|_{L^2(\Omega)}$ by $\|\tilde{H}^{\frac{1}{2}} u_t(t_j^N)\|_{L^2(\Omega)}$. This allows us to show that $\|\tilde{H}^{\frac{1}{2}} u_t(t)\|_{L^2(\Omega)}$ is bounded for all $t > 1$.

Step 1. We prove that for the interval $[j, j+1]$ there exists a $t_j^N \in [j, j+1]$ such that $\|\tilde{H}^{\frac{1}{2}} u_t^N(t_j^N)\|_{L^2(\Omega)}$ is bounded uniformly in N and j.

From (4.9) we obtain

$$\int_0^\infty \|\tilde{H}^{\frac{1}{2}} u_t^N(s)\|^2_{L^2(\Omega)} \mathrm{d}s \leq \mathcal{F}[u^N(0)] - \inf_{t\in[0,\infty)} \mathcal{F}[u^N(t)] \leq \tilde{C}$$

where $\tilde{C} > 0$ and is independent of N, since $\mathcal{F}$ is bounded below (see Lemma 3.1.2). By splitting the integral into partitions of size 1 we obtain the following bound

$$\int_{j-1}^{j} \|\tilde{H}^{\frac{1}{2}} u_t^N(s)\|^2_{L^2(\Omega)} \mathrm{d}s \leq \tilde{C}. \tag{5.9}$$

It follows from (5.9) that for every interval $[j, j+1]$ there exists a t_j^N such that

$$\sup_{N,j} \|\tilde{H}^{\frac{1}{2}} u_t^N(t_j^N)\|^2_{L^2(\Omega)} \leq \tilde{C}. \tag{5.10}$$

Step 2. Recall the Galerkin approximation (4.6) and (4.15) from Lemma 4.3.3. From this we test with $v^N = u_t^N$ to obtain

$$\frac{1}{2}\frac{\mathrm{d}}{\mathrm{d}t}\|\tilde{H}^{\frac{1}{2}} u_t^N\|^2_{L^2(\Omega)} + \left\|(\Delta + I)u_t^N\right\|^2_{L^2(\Omega)} + 3\left\|u_t^N u^N\right\|^2_{L^2(\Omega)} \leq \delta \left\|u_t^N\right\|^2_{L^2(\Omega)}.$$

Therefore we have

$$\frac{1}{2}\frac{\mathrm{d}}{\mathrm{d}t}\|\tilde{H}^{\frac{1}{2}} u_t^N\|^2_{L^2(\Omega)} \leq 2\|\tilde{H}^{\frac{1}{2}} u_t^N\|^2_{L^2(\Omega)} \tag{5.11}$$

which follows immediately for the L^2- and H^2-flows since $\delta \leq 2$. For the H^{-1}- gradient flow we recall (4.23), replacing $\tilde{u}$ with u^N and recalling that $\delta \leq 1$ we have

$$\delta \left\|u^N\right\|^2_{L^2(\Omega)} - \left\|(\Delta + I)u^N\right\|^2_{L^2(\Omega)} \leq 2\left\|u^N\right\|^2_{H^{-1}(\Omega)}.$$

Hence (5.11) follows for the H^{-1}-norm as well.

From the inequality (5.11), for any $t_0 < t$, we integrate from t_0 to t to obtain a bound on u_t^N, using Grönwall's inequality,

$$\|\tilde{H}^{\frac{1}{2}} u_t^N(t)\|^2_{L^2(\Omega)} \leq C_1 \exp[C_2(t - t_0)]\|\tilde{H}^{\frac{1}{2}} u_t^N(t_0)\|^2_{L^2(\Omega)}, \tag{5.12}$$

for constant $C_1, C_2 > 0$.

For any $t > 1$ there exists $j \in \mathbb{N}$ such that $t \in [j+1, j+2]$, from (5.10) we know that there exists $t_j^N \in [j, j+1]$ so that

$$\sup_N \|\tilde{H}^{\frac{1}{2}} u_t^N(t_j^N)\|^2_{L^2(\Omega)} \leq \tilde{C}.$$

Hence recalling the relation between the u_t^N-norm at t and the u_t^N-norm at t_0 (5.12)

and (5.10) if we choose $t_0 = t_j^N$ then we have

$$\begin{aligned}\|\tilde{H}^{\frac{1}{2}} u_t^N(t)\|_{L^2(\Omega)} &\leq \sqrt{C_1 \exp[C_2(t - t_j^N)]}\sqrt{\tilde{C}}, \\ &\leq \sqrt{C_1 \tilde{C} \exp[2C_2]},\end{aligned}$$

where the second line follows from the fact that $t - t_j^N \leq 2$.

Therefore we have that u_t^N is bounded, i.e., there exists a $\hat{C} > 0$ such that

$$\|\tilde{H}^{\frac{1}{2}} u_t^N(t)\|_{L^2(\Omega)} \leq \hat{C}.$$

Since this result holds independent of N we take the limit $N \to \infty$ and we obtain the stated result. □

We can now prove the compactness of the trajectories. In all cases we will show that $u \in L^\infty([1,\infty); H^4_{\bar{u}}(\Omega))$ and then use the compact embedding of $H^4(\Omega)$ in $H^2(\Omega)$. Since both the PFC and SH equations have a smoothing property we can prove compactness for both using a similar method. The smoothing property gives us the required increase in regularity needed for compactness. However, the H^2-gradient flow does not have a smoothing property and hence we need a different proof. We first prove compactness for the SH and PFC cases.

Lemma 5.3.2. *For the SH and PFC equations $\eta = u - \bar{u} \in L^\infty([1,\infty); H^4_\#(\Omega))$ and in particular $\bigcup_{t\geq 1}\{\eta(t)\}$ is compact in $H^2_\#(\Omega)$.*

Proof. We recall (5.7), which can be written as

$$\langle \tilde{H} u_t, v\rangle + \langle \Delta u, \Delta v\rangle + 2\langle \Delta u, v\rangle + \langle u, v\rangle - \delta\langle u, v\rangle + \langle u^3, v\rangle = 0, \qquad \forall v \in H^2_\#(\Omega),$$

or, equivalently,

$$\langle \Delta u, \Delta v\rangle = \langle f, v\rangle, \qquad \forall v \in H^2_\#(\Omega) \tag{5.13}$$

where

$$f = -2\Delta u - (1-\delta)u - u^3 - (-\Delta)^{-\chi} u_t$$

(this is an equality in $L^2(\Omega)$ since $u \in C^1(H^2(\Omega)))$ and $\chi = 0, 1$ for the SH and PFC cases respectively.

We have $u \in L^\infty(H^2_{\text{per}}(\Omega))$ and hence $\Delta u \in L^\infty(L^2_{\text{per}}(\Omega))$ and $u^3 \in L^\infty(H^2_{\text{per}}(\Omega))$ since $H^2_{\text{per}}(\Omega)$ is a Banach algebra. From (5.8) we have $u_t \in L^\infty([1,\infty); L^2_\#(\Omega))$ for the SH case ($\chi = 0$). For the PFC case ($\chi = 1$) we have $u_t \in L^\infty([1,\infty); H^{-1}_\#(\Omega))$ and by the embedding $H^{-1}_\#(\Omega) \subseteq H^{-2}_\#(\Omega)$, $(-\Delta)^{-\chi} u_t \in L^\infty([1,\infty); L^2(\Omega))$. Therefore we have shown that $f \in L^\infty([1,\infty); L^2(\Omega))$.

We now use Lemma 3.3.2 to obtain $u - \bar{u} \in L^\infty([1,\infty); H^4_\#(\Omega))$.

By the compact embedding of $H^4(\Omega)$ in $H^2(\Omega)$, u is pre-compact in $H^2(\Omega)$ and thus since the space is closed $u(t)$ is compact in $H^2(\Omega)$ for $t > 1$ and hence $\eta(t)$ is compact in $H^2_\#(\Omega)$ for $t > 1$. □

Remark 5.3.1. *Since for the PFC case we already have $u \in L^\infty([1,\infty); H^3_{\bar{u}}(\Omega))$ we can differentiate* (5.13) *to obtain an equation of the form* (3.14) *with $f = -2(-\Delta)^{\frac{3}{2}}u - (1-\delta)(-\Delta)^{\frac{1}{2}}u - (-\Delta)^{\frac{1}{2}}(u^3) - (-\Delta)^{-\frac{1}{2}}u_t$. Since $H^2_{\text{per}}(\Omega)$ is a Banach algebra and thus $u^3 \in H^2_{\text{per}}(\Omega)$. Therefore since $u \in H^3_{\bar{u}}(\Omega)$ and from the strong form of* (5.7) *u is periodic, finally from* (5.8) *we have $u_t \in L^\infty([1,\infty); H^{-1}_{\#}(\Omega))$ then $f \in L^\infty([1,\infty); L^2_{\text{per}}(\Omega))$. Choosing $\eta = (-\Delta)^{\frac{1}{2}}u \in L^\infty([1,\infty); H^2_{\#}(\Omega))$ and $f \in L^\infty([1,\infty); L^2_{\text{per}}(\Omega))$ we have $\eta \in L^\infty([1,\infty); H^4_{\#}(\Omega))$ and thus we even obtain $u - \bar{u} \in L^\infty([1,\infty); H^5_{\#}(\Omega))$.*

We can also prove for the H^2-gradient flow equation, Definition 4.2.4, that the trajectory is bounded in $H^4(\Omega)$. The technique used in this case is different from the method used in the SH and PFC cases, Lemma 5.3.2, since in this case the differential equation no longer has a smoothing property.

Lemma 5.3.3. *Assume that $u_0 \in H^4_{\bar{u}}(\Omega)$ then for $\eta = u - \bar{u}$ where u is the trajectory for the H^2-gradient flow equation, $\eta \in L^\infty(H^4_{\#}(\Omega))$ and in particular $\bigcup_{t\geq 1}\{\eta(t)\}$ is compact in $H^2_{\#}(\Omega)$.*

Proof. For simplicity, without loss of generality, we take $\gamma = 1$. We can then rewrite Definition 4.2.4 as

$$\langle [(\Delta + I)^2 + I]u_t + [(\Delta + I)^2 + I]u, v\rangle = \langle (\delta + 1)u - u^3, v\rangle \qquad \forall v \in H^2_{\#}(\Omega). \tag{5.14}$$

We use the Galerkin approximation (4.6).

Testing the Galerkin approximation of (5.14) with $A_1\eta^N = A_1(u^N - \bar{u}) \in H^2_{\#}(\Omega)$ we obtain

$$\langle A_1 u^N_t + A_1 u^N, A_1\eta^N\rangle = \left\langle (\delta+1)u^N - \left(u^N\right)^3, A_1\eta^N \right\rangle.$$

Since $A_1\eta^N \in H^2_{\#}(\Omega)$ we have

$$\langle A_1\eta^N_t + A_1\eta^N, A_1\eta^N\rangle = \langle f^N, A_1\eta^N\rangle \tag{5.15}$$

where

$$f^N = (\delta+1)u^N - \left(u^N\right)^3.$$

Using Young's inequality on (5.15) we have

$$\frac{1}{2}\frac{\mathrm{d}}{\mathrm{d}t}\left\|A_1\eta^N\right\|^2_{L^2(\Omega)} + \left\|A_1\eta^N\right\|^2_{L^2(\Omega)} \leq \frac{1}{2}\left\|f^N\right\|^2_{L^2(\Omega)} + \frac{1}{2}\left\|A_1\eta^N\right\|^2_{L^2(\Omega)},$$

which rearranges as

$$\begin{aligned}\frac{\mathrm{d}}{\mathrm{d}t}\left\|A_1\eta^N\right\|^2_{L^2(\Omega)} + \left\|A_1\eta^N\right\|^2_{L^2(\Omega)} &\leq \left\|f^N\right\|^2_{L^2(\Omega)} \\ &\leq \left\|f^N\right\|^2_{H^2(\Omega)} \\ &\leq \left((\delta+1)\left\|u^N\right\|_{H^2(\Omega)} + \left\|u^N\right\|^3_{H^2(\Omega)}\right)^2 \\ &\leq C_0,\end{aligned}$$

where we have used that $H^2(\Omega)$ is a Banach algebra in the third line and we have used that $\|u^N\|_{H^2(\Omega)}$ is bounded uniformly in t and N, which follows by taking the $N \to \infty$ limit of (4.10), in the final line.

Applying Grönwall's inequality we obtain

$$\left\|A_1\eta^N\right\|^2_{L^2(\Omega)} \leq \left\|A_1\eta^N(0)\right\|^2_{L^2(\Omega)} + C_0. \tag{5.16}$$

We can bound the right-hand norm by

$$\begin{aligned}\left\|A_1\eta^N(0)\right\|_{L^2(\Omega)} &\leq \left\|\Delta^2\eta^N(0)\right\|_{L^2(\Omega)} + 2\left\|\Delta\eta^N(0)\right\|_{L^2(\Omega)} + 2\left\|\eta^N(0)\right\|_{L^2(\Omega)} \\ &\leq 2\left\|\eta^N(0)\right\|_{H^4(\Omega)}.\end{aligned} \tag{5.17}$$

From the assumption $\eta_0 = u_0 - \bar{u} \in H^4_\#(\Omega)$ we can use (5.17) and take the limit $N \to \infty$ in (5.16) to obtain that for all $t > 0$ there exists a $C > 0$ such that

$$\|A_1\eta(t)\|_{L^2(\Omega)} \leq C. \tag{5.18}$$

We can also find a bound for the H^4-norm of η

$$\begin{aligned}\|\eta\|^2_{H^4(\Omega)} &\leq C_4\left(\|(\Delta+I)^2\eta\|^2_{L^2(\Omega)} + \|\eta\|^2_{L^2(\Omega)}\right) \\ &\leq C_4\left(\left\|(\Delta+I)^2\eta\right\|^2_{L^2(\Omega)} + 2\|(\Delta+I)\eta\|^2_{L^2(\Omega)} + \|\eta\|^2_{L^2(\Omega)}\right) \\ &= C_4\|A_1\eta\|^2_{L^2(\Omega)}\end{aligned} \tag{5.19}$$

where the first inequality follows from Lemma C.2.4.

Therefore from (5.18) and (5.19) we have $\eta \in H^4_\#(\Omega)$. Since η is bounded in $H^4_\#(\Omega)$, by the compact embedding of $H^4_\#(\Omega)$ in $H^2_\#(\Omega)$, the union of η is pre-compact in $H^2_\#(\Omega)$ and thus since the space is closed $\bigcup_{t\geq 1}\{\eta(t)\}$ is compact in $H^2_\#(\Omega)$. □

Remark 5.3.2. *If we use the test function $v^N = A_1\Delta^p\eta^N$ for $0 < p \leq 2$ in (5.15) we can prove $\eta \in H^{4+p}(\Omega)$ if we choose $u_0 \in H^{4+p}(\Omega)$.*

5.4 Conclusion

In this chapter we have demonstrated that the trajectories produced by the L^2-, H^{-1}- and H^2-gradient flows introduced in the previous chapter converge to critical points.

Chapter 6

Semi-Discretisation of H^2-Flow

We wish to discretise the gradient flow given by Definition 4.2.4 in both space and time so that we can implement a computational scheme for the minimisation problem **(P)** (page 37). We first discretise in time. Space discretisation is undertaken in Chapter 8. After introducing a time-discrete formulation of the H^2-gradient flow equation we give the conditions under which this algorithm is stable and converges a critical point. The method we formulate is a variable-metric steepest descent algorithm, see [NW06, Equation (3.2)].

6.1 Steepest Descent-Type Algorithm

6.1.1 Forward Euler Method

A simple method for discretising partial differential equations is the forward Euler method. In this case we approximate u_t as $v_n = (u_{n+1} - u_n)/\tau_n$ where $\tau_n > 0$. The discretisation of the gradient flow equation (4.1) using the forward Euler method is

$$\left\langle \frac{u_{n+1} - u_n}{\tau_n}, w \right\rangle_H = \left\langle -\left(\Delta + I\right)^2 u_n + \delta u_n - (u_n)^3, w \right\rangle \qquad \forall w \in H^2_{\#}(\Omega) \qquad (6.1)$$

where, on the left hand side, we use the L^2-, H^{-1}- and A-inner-products for the SH, PFC and H^2-gradient flow cases respectively. In this case, in the notation of Remark 4.2.5, this scheme can be seen to be a steepest descent algorithm of the form discussed in [NW06, Section 2.2].

The forward Euler method means that the u_{n+1}-term is only included in the H-inner product on the left-hand side. This means that u_{n+1} is no longer confined to the space $H^2_{\bar{u}}(\Omega)$ but is in the space $H^{-2-2\chi}(\Omega)$, $\chi = 0$ for the SH case, $\chi = 1$ for the PFC case and $\chi = -2$ for the H^2-gradient flow case. In the H^2-gradient flow case the H-inner-product is equivalent to the H^2-inner-product so we have no problem; however, in the SH and PFC cases the H-inner product is not equivalent to the H^2-inner product so the forward Euler method is ill-defined. That is, in the case of the forward Euler discretisation of the Swift-

Hohenberg and PFC equations, even for an initial condition $u_0 \in H^2_{\bar{u}}(\Omega)$, u_n is no longer in a subset of $H^2(\Omega)$ and hence we no longer have iterates for which the PFC functional is bounded.

It can also be seen that, for the PFC and SH equations, the associated strong equation is very stiff. We can use the same argument as [EW13]. An analogue of the Courant-Friedrichs-Lewy condition, using a finite difference approximation of the Laplacian, gives restrictive conditions on the time step in relation to the grid size (e.g. for the PFC equation the time step is restricted by the sixth power of the grid size). For the remainder of the chapter we investigate a variant of the forward Euler discretisation of the H^2-flow.

6.1.2 Adaptive Forward Euler/ Line Search Method

In this chapter, rather than using a constant γ as in the previous chapters, we use an adaptive γ that changes at each time-step. Recall that the aim of this thesis is to formulate algorithms to minimise the PFC functional (3.1), i.e. to solve problem **(P)** (page 37). Changing γ at each time-step means that our method is no longer a discretisation of Definition 4.2.4, but we are able to show, in Figure 8.3, that an adaptive γ method is significantly faster than a fixed γ method. The results of this chapter only require that γ is bounded, hence these results also apply to the case where γ is fixed. Therefore we could just use a direct discretisation of Definition 4.2.4 (e.g. (6.1)) but such a method would take longer to reach a solution to (**P**)(page 37).

Given u_n we now define the discrete $A^{(n)}$-norm and the adaptive constant γ_n.

Definition 6.1.1 (The $A^{(n)}$-norm)**.** *For $u_n \in L^\infty(\Omega)$ we define the $A^{(n)}$-norm by*

$$\|\eta\|^2_{A^{(n)}} := \|\Delta\eta + \eta\|^2_{L^2(\Omega)} + \gamma_n \|\eta\|^2_{L^2(\Omega)},$$

where

$$\gamma_n = \max\left(\gamma_{\min}, 3\overline{u_n^2} - \delta\right). \tag{6.2}$$

The choice of γ_n is motivated by the form of the second variation (3.10). In Chapter 9 we show that in the pre-asymptotic regime, using a variable γ_n leads to a significant numerical improvement, when compared to using an appropriately chosen constant γ (see Figure 9.6). If, however, we are in the asymptotic regime then the effect of a variable γ is less pronounced (see Figure 9.4).

By analogy with (6.1), we can now define a variable metric steepest descent iteration

$$\left\langle \frac{u_{n+1} - u_n}{\tau_n}, w \right\rangle_{A^{(n)}} = -\delta\mathcal{F}\left[u_n, w\right], \qquad \forall w \in H^2_{\#}(\Omega) \tag{6.3}$$

where $\langle \cdot, \cdot \rangle_{A^{(n)}}$ is the inner product associated with the $A^{(n)}$ -norm, Definition 6.1.1. For future reference we define $v_n := (u_{n+1} - u_n)/\tau_n$. We note that this method is essentially a method of the form of [NW06, Equation (3.2)].

We now prove that the $A^{(n)}$-norm is an equivalent norm to the H^2-norm and therefore that (6.3) is well-defined.

Lemma 6.1.1. *For $u_n \in H^2(\Omega)$ the $A^{(n)}$-norm is equivalent to the A_1-norm, Definition 3.1.2, (and hence to the H^2-norm). More precisely, $\exists \tilde{C}_\mathrm{b}, \tilde{C}_\mathrm{u} > 0$ that depend on $\gamma_{\min}$ and on $\|u_n\|_{L^\infty(\Omega)}$, such that for all $v \in H^2(\Omega)$,*

$$\tilde{C}_\mathrm{b}\|v\|_{A_1}^2 \leq \|v\|_{A^{(n)}}^2 \leq \tilde{C}_\mathrm{u}\|v\|_{A_1}^2.$$

In particular, (6.3) *is well-posed.*

Proof. Recalling that the A-norm, Definition 4.2.3, is equivalent to the H^2-norm (Lemma 4.2.1), therefore all we require is that γ_n is bounded.

We can show that for all $C_1 > 0$ there exists a $C = C(C_1)$ such that $\gamma_n \leq C$ in $\{\|u\|_{L^\infty(\Omega)} \leq C_1\}$.

Recall the definition of γ_n (6.2) for this to be bounded we need to bound $3\overline{u_n^2}$. Clearly

$$\overline{u_n^2} = \frac{1}{|\Omega|}\int_\Omega u_n^2 \mathrm{d}x \leq \|u_n\|_{L^\infty(\Omega)}^2,$$

therefore

$$|\gamma_n| \leq \max(\gamma_{\min}, 3C_1^2 - \delta) =: C. \qquad \square$$

6.1.3 Algorithm

We briefly describe the algorithm used for finding the sequence $\{u_n\}_{n\in\mathbb{N}}$ generated by (6.3). This algorithm is similar to [NW06, Algorithm 11.4]. Recall that δ and $\bar{u}$ are fixed model parameters.

Algorithm 6.1.1.

(0) INPUT $u_0, \tau_{\max} < 2, \gamma_{\min} > 0, 0 < \Theta < 1/2$

(1) FOR $n = 0, 1, 2, \ldots$

(2) $\gamma_n = \max\left(\gamma_{\min}, 3\overline{u_n^2} - \delta\right),\ \tau_n = \tau_{\max}$

(3) SOLVE $\langle v_n, w\rangle_{A^{(n)}} = -\delta\mathcal{F}[u_n, w]$ *for all* $w \in H^2_\#(\Omega)$

(4) WHILE $\mathcal{F}[u_n + \tau_n v_n] > \mathcal{F}[u_n] - \Theta\tau_n\|\delta\mathcal{F}[u_n]\|^2_{(A^{(n)})^{-1}}$

(5) $\tau_n \leftarrow \tau_n/2$

(6) $u_{n+1} = u_n + \tau_n v_n$

The condition for energy reduction such that the while condition of step (4) is satisfied is known as the Armijo condition. Steps (4) and (5) are equivalent to the backtracking line search of [NW06, Algorithm 3.1].

In the numerical implementation of Chapter 8 we will use a more refined method in step (5). In particular we will use a cubic interpolation to find τ_n and we will use τ_n to formulate our initial guess for τ_{n+1} in step (2).

We now state a theorem that gives us the rate of convergence of a sequence defined through Algorithm 6.1.1. This theorem is the main result of this chapter and the rest of the chapter will be dedicated to proving it.

Theorem 6.1.1. *Let $u_0 \in H^4_{\tilde{u}}(\Omega)$ then we have*

(a) *Algorithm 6.1.1 is well-defined. That is, it produces a sequence $\{u_n\}_{n\in\mathbb{N}} \subset H^2_{\tilde{u}}(\Omega)$.*

(b) *There exists $\theta \in \left(0, \frac{1}{2}\right]$ and $\tilde{u} \in H^2_{\tilde{u}}(\Omega)$ such that $\delta\mathcal{F}[\tilde{u}] = 0$ and*

$$\|u_n - \tilde{u}\|_{H^2(\Omega)} \leq C \begin{cases} \nu^n, & \theta = \frac{1}{2} \\ n^{-\frac{\theta}{1-2\theta}}, & \theta < \frac{1}{2} \end{cases}$$

where $C > 0$ and $\nu \in (0, 1)$.

6.2 Energy Stability and Convergence of Residual

We want to show that Algorithm 6.1.1 produces a sequence u_n that converges to a critical point of the PFC functional. First we need to show that for, a given n and u_n, the while loop starting at line (4) terminates. This means that for small enough τ_n we want to show that the Armijo condition of line (4) is fulfilled.

We therefore seek bounds for the energy difference.

Proposition 6.2.1. *Let $u_n \in H^2_{\tilde{u}}(\Omega)$, $\tau_n > 0$ and $\tilde{v} \in H^2_{\#}(\Omega)$, then*

$$\begin{aligned} \mathcal{F}[u_n + \tau_n\tilde{v}] - \mathcal{F}[u_n] \leq \frac{\tau_n^2}{2}\|\Delta\tilde{v} + \tilde{v}\|^2_{L^2(\Omega)} + \frac{3\tau_n^2}{2}\|u_n\|^2_{L^\infty(\Omega)}\|\tilde{v}\|^2_{L^2(\Omega)} \\ + \tau_n^3\|u_n\|_{L^\infty(\Omega)}\|\tilde{v}\|^3_{L^3(\Omega)} + \frac{\tau_n^4}{4}\|\tilde{v}\|^4_{L^4(\Omega)} + \tau_n\delta\mathcal{F}[u_n, \tilde{v}]. \end{aligned} \tag{6.4}$$

Proof. Using the first variation (3.9) we can write the energy difference (3.11), for all $\tilde{v} \in H^2_{\#}(\Omega)$, as

$$\begin{aligned} \mathcal{F}[u_n + \tau_n\tilde{v}] - \mathcal{F}[u_n] = \frac{{\tau_n}^2}{2}\|\Delta\tilde{v} + \tilde{v}\|^2_{L^2(\Omega} - \frac{{\tau_n}^2\delta}{2}\|\tilde{v}\|^2_{L^2(\Omega)} + \frac{3{\tau_n}^2}{2}\|u_n\tilde{v}\|^2_{L^2(\Omega)} \\ + {\tau_n}^3\int_\Omega u_n\tilde{v}^3\mathrm{d}x + \frac{{\tau_n}^4}{4}\|\tilde{v}\|^4_{L^4(\Omega)} + \tau_n\delta\mathcal{F}[u_n, \tilde{v}]. \end{aligned}$$

We can re-write this energy decrease as an inequality. For all $\tilde{v} \in H^2_{\#}(\Omega)$, we have

$$\mathcal{F}[u_n + \tau_n \tilde{v}] - \mathcal{F}[u_n] \leq \frac{{\tau_n}^2}{2}\|\Delta\tilde{v} + \tilde{v}\|^2_{L^2(\Omega)} + \frac{3{\tau_n}^2}{2}\|u_n\|^2_{L^\infty(\Omega)}\|\tilde{v}\|^2_{L^2(\Omega)} + {\tau_n}^3\|u_n\|_{L^\infty(\Omega)}\|\tilde{v}\|^3_{L^3(\Omega)} + \frac{{\tau_n}^4}{4}\|\tilde{v}\|^4_{L^4(\Omega)} + \tau_n\delta\mathcal{F}[u_n, \tilde{v}],$$

where we have discarded the purely negative term associated with δ. □

To obtain our desired energy reduction we have the following proposition (which follows from the Riesz representation theorem), which links v_n to the first variation.

Proposition 6.2.2. *Let $h \supseteq H^2_{\#}(\Omega)$ be a Hilbert space where the embedding is dense. Let v_n be given by $\langle v_n, \varphi\rangle_h = -\delta\mathcal{F}[u_n, \varphi]$ for all $\varphi \in H^2_{\#}(\Omega)$ then*

$$\|v_n\|_h = \|\delta\mathcal{F}[u_n]\|_{h^*}.$$

We can now obtain stability of the sequence $\{u_n\}$ given by Algorithm 6.1.1.

Proposition 6.2.3. *Let $u_n \in H^2_{\tilde{u}}(\Omega)$, then there exist constants $c_1 = c_1(\|u_n\|_{L^\infty(\Omega)})$, $c_2 = c_2(\|u_n\|_{L^\infty(\Omega)})$ such that, if*

$$\tau_n \leq c_1$$
$$\tau_n\|v_n\|_{A^{(n)}} \leq c_2$$

then the Armijo condition is satisfied with $\Theta = 1/2$ (and hence for any $\theta \in (0, 1/2)$), i.e.,

$$\mathcal{F}[u_n + \tau_n v_n] - \mathcal{F}[u_n] \leq -\frac{1}{2}\tau_n\|v_n\|^2_{A^{(n)}} = -\frac{1}{2}\tau_n\|\delta\mathcal{F}[u_n]\|^2_{(A^{(n)})^{-1}}. \tag{6.5}$$

Proof. From Lemmas 3.1.1 and 6.1.1 we obtain the following bounds

$$\begin{aligned}\|\Delta v + v\|_{L^2(\Omega)} \leq \|v\|_{H^2(\Omega)} \leq C_H\|v\|_{A^{(n)}},\\ \|v\|_{L^2(\Omega)} \leq \|v\|_{H^1(\Omega)} \leq C_H\|v\|_{A^{(n)}},\end{aligned} \tag{6.6}$$

where $C_H > 0$ is a constant and the second set of inequalities follows by the fact that $H^2(\Omega) \subset H^1(\Omega) \subset L^2(\Omega)$.

Consider Proposition 6.2.1 and recall the interpolation of Hölder's inequality which allows us to approximate the L^3-term, Lemma C.2.5, we can therefore write the change in the energy functional as, for all $\tilde{v} \in H^2_{\#}(\Omega)$,

$$\begin{aligned}\mathcal{F}[u_n + \tau_n\tilde{v}] - \mathcal{F}[u_n] \leq \frac{{\tau_n}^2}{2}\|\Delta\tilde{v} + \tilde{v}\|^2_{L^2(\Omega)} + \frac{3{\tau_n}^2}{2}\|u_n\|^2_{L^\infty(\Omega)}\|\tilde{v}\|^2_{L^2(\Omega)}\\ + {\tau_n}^3\|u_n\|_{L^\infty(\Omega)}\|\tilde{v}\|_{L^2(\Omega)}\|\tilde{v}\|^2_{L^4(\Omega)} + \frac{{\tau_n}^4}{4}\|\tilde{v}\|^4_{L^4(\Omega)}\\ + \tau_n\delta\mathcal{F}[u_n, \tilde{v}].\end{aligned}$$

Recall Ladyzhenskaya's inequality in d-dimensions, Lemma C.2.1, using this and defining $\tilde{v} = v_n$ by (6.3) we have

$$\begin{aligned}\mathcal{F}[u_n + \tau_n v_n] - \mathcal{F}[u_n] \leq \frac{{\tau_n}^2}{2}\|\Delta v_n + v_n\|^2_{L^2(\Omega)} + \frac{3{\tau_n}^2}{2}\|u_n\|^2_{L^\infty(\Omega)}\|v_n\|^2_{L^2(\Omega)} \\ + {\tau_n}^3\|u_n\|_{L^\infty(\Omega)}\|v_n\|^3_{H^1(\Omega)} + \frac{{\tau_n}^4}{4}\|v_n\|^4_{H^1(\Omega)} - \tau_n\|v_n\|^2_{A^{(n)}}.\end{aligned} \tag{6.7}$$

where we have used $H^1(\Omega) \subset L^2(\Omega)$ in the cubic term.

We desire the energy decrease to be proportional to the $\|v_n\|^2_{A^{(n)}}$-term, i.e. (6.5). Using (6.7) with (6.6) to bound the v_n-norms we can obtain an upper bound for the functionals. Setting this upper bound to less than the right-hand side of (6.5) and re-arranging we have

$$\begin{aligned}&\frac{\tau_n^2\left(1 + 3\|u_n\|^2_{L^\infty(\Omega)}\right)}{2}\left(C_H\|v\|_{A^{(n)}}\right)^2 + \frac{\tau_n^4}{4}\left(C_H\|v\|_{A^{(n)}}\right)^4 + \tau_n^3\|u_n\|_{L^\infty(\Omega)}\left(C_H\|v\|_{A^{(n)}}\right)^3 \\ &\leq \frac{1}{2}\|v_n\|^2_{A^{(n)}}\tau_n.\end{aligned}$$

Cancellation of $\|v_n\|^2_{A^{(n)}}\tau_n$ gives

$$\frac{\tau_n\left(1 + 3\|u_n\|^2_{L^\infty(\Omega)}\right)C_H^2}{2} + \frac{\tau_n^3 C_H^4}{4}\|v_n\|^2_{A^{(n)}} + C_H^3\tau_n^2\|u_n\|_{L^\infty(\Omega)}\|v_n\|_{A^{(n)}} \leq \frac{1}{2}.$$

We can reduce this to two conditions

$$\tau_n\left(1 + 3\|u_n\|^2_{L^\infty(\Omega)}\right)C_H^2 \leq \frac{1}{2}, \tag{6.8}$$

$$\frac{C_H^4}{4}(\tau_n\|v_n\|_{A^{(n)}})^2 + \|u_n\|_{L^\infty(\Omega)}C_H^3(\tau_n\|v_n\|_{A^{(n)}}) \leq \frac{1}{4\tau_n}. \tag{6.9}$$

Clearly the first condition gives us the existence of the upper bound for τ_n. (6.8) also gives us a lower bound for τ_n^{-1}. Hence (6.9) simplifies to

$$\frac{C_H^4}{4}(\tau_n\|v_n\|_{A^{(n)}})^2 + \|u_n\|_{L^\infty(\Omega)}C_H^3(\tau_n\|v_n\|_{A^{(n)}}) \leq \frac{\left(1 + 3\|u_n\|^2_{L^\infty(\Omega)}\right)C_H^2}{2}$$

which is satisfied if $\tau_n\|v_n\|_{A^{(n)}}$ is small enough. □

Remark 6.2.1. *Using Definition 6.1.1 and Lemma 3.1.2 we can find an explicit value for C_H. Then following through the proof of Proposition 6.2.3 with explicit upper bounds gives*

us the conditions

$$\tau_n \leq \frac{\min(1, \gamma_{\min})}{10\left(1 + 3\|u_n\|^2_{L^\infty(\Omega)}\right)},$$
$$\tau_n \|v_n\|_{A^{(n)}} \leq \frac{\sqrt{3\min(1, \gamma_{\min})\left(1 + 3\|u_n\|^2_{L^\infty(\Omega)}\right)}}{4\sqrt{5}}.$$

Statement (a) of Theorem 6.1.1 now follows from Proposition 6.2.3.

Remark 6.2.2. *The constants c_1 and c_2 of Proposition 6.2.3 depend on $\|u_n\|_{L^\infty(\Omega)}$. Specifically, we have $c_1 \to 0$ as $\|u_n\|_{L^\infty(\Omega)} \to \infty$. In practice, e.g. in the simulations of Chapters 8 and 9, we see that $\|u_n\|_{L^\infty(\Omega)} = O(\|u_0\|_{L^\infty(\Omega)})$. Therefore we expect that the constants c_1 and c_2 of Proposition 6.2.3 depend only on $\|u_0\|_{L^\infty(\Omega)}$. Since the energy is decreasing* (6.5) *and the $\|u_n\|_{L^\infty(\Omega)}$ is bounded by the energy (Proposition 3.1.3) we know that $\|u_n\|_{L^\infty(\Omega)}$ is bounded for all n, however this bound may depend on $|\Omega|$.*

We want the sequence $\{u_n\}_{n\in\mathbb{N}}$ generated by Algorithm 6.1.1 to converge to an equilibrium point. As a first step we prove that $\delta\mathcal{F}[u_n] \to 0$.

Lemma 6.2.1. *For any sequence $\{u_n\}_{n\in\mathbb{N}}$ generated by Algorithm 6.1.1, we have*

$$\|\delta\mathcal{F}[u_n]\|_{H^{-2}_{\#}(\Omega)} \to 0 \qquad \text{as } n \to \infty.$$

Moreover, there exists $\tau_{\min} > 0$ such that $\tau_n \geq \tau_{\min}$ for all $n \in \mathbb{N}$.

Proof. The method used is similar to that used for a general line search algorithm, see [NW06, Pages 38-39]. An interesting aspect is that we obtain $\tau_n \geq \tau_{\min}$ as a consequence of $\|\delta\mathcal{F}[u_n]\|_{H^{-2}_{\#}(\Omega)} \to 0$, whereas normally one obtains $\|\delta\mathcal{F}[u_n]\|_{H^{-2}_{\#}(\Omega)} \to 0$ from the fact that $\tau_n \geq \tau_{\min}$.

Re-arranging the bound on the difference between the functionals, from Proposition 6.2.3, and using that $\mathcal{F}[u_n]$ is decreasing in n we have

$$\frac{1}{2}\sum_{n=0}^{\infty} \tau_n \|v_n\|^2_{A^{(n)}} \leq \mathcal{F}[u_0] - \inf_n \mathcal{F}[u_n]. \tag{6.10}$$

We want the right-hand side to be bounded. This is clearly true in a bounded domain using the fact that the PFC energy functional (3.1) is bounded below in this case, i.e.

$$\mathcal{F}[u] \geq -(\delta + 1)^2|\Omega|.$$

This bound follows from the lower bound for the energy in Lemma 3.1.2 by discarding the purely positive term.

Therefore from (6.10) we have

$$\sum_{n=0}^{\infty} \tau_n \|v_n\|^2_{A^{(n)}} < \infty. \tag{6.11}$$

From Proposition 6.2.3 we know that if $\tau_n \leq c_1$ and $\tau_n \|v_n\|_{A^{(n)}} \leq c_2$ or equivalently if

$$\tau_n \|v_n\|_{A^{(n)}} \leq \min(c_2, c_1 \|v_n\|_{A^{(n)}}, \tau_{\max} \|v_n\|_{A^{(n)}})$$

then the Armijo condition (6.5) is satisfied. By inspecting steps (4) and (5) of Algorithm 6.1.1, we deduce that

$$\tau_n \|v_n\|_{A^{(n)}} \geq \frac{1}{2} \min(c_2, c_1 \|v_n\|_{A^{(n)}}, \tau_{\max} \|v_n\|_{A^{(n)}}). \tag{6.12}$$

Using this lower bound and (6.11) we obtain

$$\sum_{n=0}^{\infty} \frac{1}{2} \min\left(c_1, c_2 \|v_n\|_{A^{(n)}}, \tau_{\max} \|v_n\|_{A^{(n)}}\right) \|v_n\|_{A^{(n)}} \leq \sum_{n=0}^{\infty} \tau_n \|v_n\|^2_{A^{(n)}} < \infty.$$

Therefore we have that $\|v_n\|_{A^{(n)}} \min(c_1 \|v_n\|_{A^{(n)}}/2, , \tau_{\max} \|v_n\|_{A^{(n)}}/2, c_2/2)$ converges to 0 and hence $\|v_n\|_{A^{(n)}} \to 0$ and also, by Proposition 6.2.2, $\|\delta \mathcal{F}[u_n]\|_{(A^{(n)})^{-1}}$ converges to 0. Since, from Proposition 6.2.2 and $v_n \in H^2_{\#}(\Omega)$, the $(A^{(n)})^{-1}$-norm is an equivalent norm to the $H^{-2}_{\#}$-norm we have $\|\delta \mathcal{F}[u_n]\|_{H^{-2}_{\#}(\Omega)} \to 0$.

Using (6.12) and $\|v_n\|_{A^{(n)}} \to 0$ we have for sufficiently large n

$$\begin{aligned} \tau_n &\geq \frac{1}{2} \min\left(c_2, \tau_{\max}, \frac{c_1}{\|v_n\|_{A^{(n)}}}\right) \\ &\geq \frac{\min(c_2, \tau_{\max})}{2}. \end{aligned}$$

Hence τ_n is bounded below. □

6.3 Convergence to Equilibrium

As in Theorem 5.0.2 we want to use a Łojasiewicz inequality to obtain rates of convergence. By analogy with Theorem 5.1.1 in addition to the Łojasiewicz inequality, Theorem 5.0.1, we need compactness of the sequence $\{u_n\}_{n\in\mathbb{N}}$.

Lemma 6.3.1. *Consider the sequence generated by Algorithm 6.1.1. If $u_0 \in H^4_{\bar{u}}(\Omega)$ then the iterates $\eta_n = u_n - \bar{u}$ are bounded in $H^4_{\#}(\Omega)$ for all $n \in \mathbb{N}$ and hence the sequence $\{\eta_n\}_{n\in\mathbb{N}}$ is compact in $H^2_{\#}(\Omega)$.*

Proof. The H^2-gradient flow (6.3) can be rewritten as, $\forall \varphi \in H^2_{\#}(\Omega)$,

$$\begin{aligned}\langle \Delta u_{n+1}, \Delta\varphi\rangle = &-2\langle \Delta u_{n+1}, \varphi\rangle - (1+\gamma_n)\langle u_{n+1}, \varphi\rangle + (1-\tau_n)\langle \Delta u_n, \Delta\varphi\rangle \\ &+ 2(1-\tau_n)\langle \Delta u_n, \varphi\rangle + ((1+\gamma_n) - \tau_n(1-\delta))\langle u_n, \varphi\rangle - \langle \tau_n u_n^3, \varphi\rangle.\end{aligned}$$

This is clearly an equation of the form (3.14) where $\eta_{n+1} = u_{n+1} - \bar{u}$ and

$$f_n = -2\Delta u_{n+1} - (1+\gamma_n)u_{n+1} + (1-\tau_n)\Delta^2 u_n + 2(1-\tau_n)\Delta u_n + ((1+\gamma_n) - \tau_n(1-\delta))u_n - \tau_n u_n^3.$$

Consider the case $n = 0$ we know that $u_1 \in H^2_{\bar{u}}(\Omega)$ (by the construction in step (6) of Algorithm 6.1.1 and the fact that $v_n \in H^2_{\#}(\Omega)$ through Proposition 6.2.2 and Lemma 3.1.4) and by assumption $u_0 \in H^4_{\bar{u}}(\Omega)$. From Algorithm 6.1.1 we know that $|\tau_n|$ is bounded. Hence, $f_n \in L^2_{\text{per}}(\Omega)$ and therefore through Lemma 3.3.2 $u_1 - \bar{u} \in H^4_{\#}(\Omega)$ and thus $u_1 \in H^4_{\bar{u}}(\Omega)$. Induction gives us that $u_n \in H^4_{\bar{u}}(\Omega)$ for all $n \in \mathbb{N}$.

We also know that (6.3) can be rewritten as

$$\langle A_1 u_{n+1}, \varphi\rangle = (1-\tau_n)\langle A_1 u_n, \varphi\rangle + \langle g_n, \varphi\rangle \qquad \forall \varphi \in H^2_{\#}(\Omega) \tag{6.13}$$

where

$$g_n = -(\gamma_n - 1)u_{n+1} + ((\gamma_n - 1) + \tau_n(1+\delta))u_n - \tau_n u_n^3.$$

Since we have a uniform bound on the u_n in $H^2(\Omega)$ for all $n \in \mathbb{N}$ and $H^2(\Omega)$ is a Banach algebra then we have a uniform bound on g_n in $L^2(\Omega)$, i.e. $\|g_n\|_{L^2(\Omega)} \leq C$ for all $n \in \mathbb{N}$.

Taking the L^2-norms of both sides of the strong form of (6.13) we have

$$\|A_1 u_{n+1}\|_{L^2(\Omega)} \leq (1-\tau_n)\|A_1 u_n\|_{L^2(\Omega)} + C. \tag{6.14}$$

From Lemma 6.2.1, we have $\tau_n \geq \tau_{\min}$ for $n \in \mathbb{N}$. From step (0) of Algorithm 6.1.1 we have $\tau_n \leq \tau_{\max} < 2$ for all $n \in \mathbb{N}$. Therefore, for all i, we have

$$|1 - \tau_i| \leq \max(|1-\tau_{\min}|, |1-\tau_{\max}|) =: \theta < 1.$$

Using θ to bound $(1-\tau_n)$ for all n induction on (6.14) gives us

$$\|A_1 u_{n+1}\|_{L^2(\Omega)} \leq \theta^{n+1}\|A_1 u_0\|_{L^2(\Omega)} + C\left(1 + \sum_{i=1}^{n}\theta^i\right).$$

Using this, (5.17) and (5.19), we have

$$\frac{1}{C_4}\|u_{n+1}\|_{H^4(\Omega)} \leq 2\theta^{n+1}\|u_0\|_{H^4(\Omega)} + C\left(1 + \frac{1}{1-\theta}\right).$$

□

We now follow the method of [Lev12, Theorems 4.1 and 4.2] to prove a general

result on the rate of convergence. We establish this more general result as we can also use it directly in Chapter 7.

Lemma 6.3.2. *Consider a sequence $\{u_n\}_{n\in\mathbb{N}}$ which is compact in $H^2_{\bar{u}}(\Omega)$ and obeys the conditions*

$$C_{\mathrm{en}}\|u_{n+1}-u_n\|^2_{H^2(\Omega)} \leq \mathcal{F}[u_{n+1}]-\mathcal{F}[u_n] \tag{6.15}$$

$$\|\delta\mathcal{F}[u_n]\|_{H^{-2}_{\#}(\Omega)} \leq C_{\mathrm{dF}}\|u_{n+1}-u_n\|_{H^2(\Omega)} \tag{6.16}$$

where $C_{\mathrm{en}}, C_{\mathrm{dF}} > 0$.

There exists $\theta \in \left(0, \frac{1}{2}\right]$ and $\tilde{u} \in H^2_{\bar{u}}(\Omega)$ such that $\delta\mathcal{F}[\tilde{u}] = 0$ and

$$\|u_n - \tilde{u}\|_{H^2(\Omega)} \leq C \begin{cases} \nu^n, & \theta = \frac{1}{2} \\ n^{-\frac{\theta}{1-2\theta}}, & \theta < \frac{1}{2} \end{cases}$$

where $C > 0$ and $\nu \in (0,1)$.

Proof. We first prove the compactness of the ω-limit set. We then prove a uniform Lojasiewicz inequality for points in this set. We can use the Łojasiewicz inequality, (6.15) and (6.16) to show the sequence converges to the minima. Finally we can obtain the stated rates of convergence.

Step 1. Compactness of the ω-limit set.

We define the set of limit points

$$\Gamma := \left\{ \lim_{j\to\infty} u_{n_j} \,\middle|\, \{u_{n_j}\} \text{ converges in } H^2(\Omega) \right\}.$$

Γ is closed (since this is an ω-limit set; this follows from [Chi06, Proposition 1.167]). Since the sequence u_n is compact, Γ is non-empty.

Using (6.15) and (6.16) and summing, since $\mathcal{F}[u_n]$ is decreasing in n, we have

$$\frac{C_{\mathrm{en}}}{C_{\mathrm{dF}}} \sum_{n=0}^{\infty} \|\delta\mathcal{F}[u_n]\|^2_{H^{-2}_{\#}(\Omega)} \leq \mathcal{F}[u_0] - \inf_n \mathcal{F}[u_n] < \infty.$$

Since the PFC functional has a minimum, Theorem 3.2.1, we have

$$\frac{C_{\mathrm{en}}}{C_{\mathrm{dF}}} \sum_{n=0}^{\infty} \|\delta\mathcal{F}[u_n]\|^2_{H^{-2}_{\#}(\Omega)} < \infty$$

and hence $\|\delta\mathcal{F}[u_n]\|_{H^{-2}_{\#}(\Omega)} \to 0$.

By definition for all $\tilde{u} \in \Gamma$, there exists a sequence $u_{n_j} \to \tilde{u}$ in $H^2_{\bar{u}}(\Omega)$. Therefore $\delta\mathcal{F}[\tilde{u}] = \lim_{j\to\infty} \delta\mathcal{F}[u_{n_j}] = 0$.

For all $\tilde{u} \in \Gamma$, since $\mathcal{F}[u_n]$ is decreasing in n, we have

$$\mathcal{F}[\tilde{u}] = \lim_{j\to\infty} \mathcal{F}[u_{n_j}] = \lim_{n\to\infty} \mathcal{F}[u_n] =: \tilde{\mathcal{F}}.$$

If $\tilde{u} \in \Gamma$ we have $\delta\mathcal{F}[\tilde{u}] = 0$ this can be re-arranged to the weak form of $\Delta^2\eta = f$ (i.e. (3.14)) where $\eta = \tilde{u} - \bar{u}$ and

$$f = -2\Delta\tilde{u} - (1-\delta)\tilde{u} - \tilde{u}^3. \tag{6.17}$$

Therefore from Lemma 3.3.2 we have $\tilde{u} \in H^4(\Omega)$. From (3.7) we have that, for $\tilde{u} \in \Gamma$, $\|\tilde{u}\|_{H^2(\Omega)} \leq C\|u_0\|_{H^2(\Omega)}$, for some $C > 0$. Using that $H^2(\Omega)$ is a Banach algebra and (6.17) we have a uniform bound on f, that is

$$\|f\|_{L^2(\Omega)} \leq (2 + |1-\delta|)\|\tilde{u}\|_{H^2(\Omega)} + \|\tilde{u}\|^3_{H^2(\Omega)}.$$

Hence we have a uniform bound on the H^4-semi-norm and on $\|\tilde{u}\|_{H^2(\Omega)}$ and thus we have a uniform bound on $\|\tilde{u}\|_{H^4(\Omega)}$. Therefore Γ is compact in $H^2_{\tilde{u}}(\Omega)$ and non-empty.

Step 2. Uniform Łojasiewicz inequality.

Since the Łojasiewicz inequality holds for critical points, Theorem 5.0.1, we can apply it to every point in Γ. Therefore for all $\tilde{u} \in \Gamma$ there exist constants $\theta_{\tilde{u}}, c_{\tilde{u}}, \rho_{\tilde{u}} > 0$ such that

$$\forall v \in H^2_{\tilde{u}}(\Omega)\ \|\tilde{u} - v\|_{H^2(\Omega)} \leq \rho_{\tilde{u}} \ \Rightarrow\ c_{\tilde{u}}|\mathcal{F}[v] - \tilde{\mathcal{F}}|^{1-\theta_{\tilde{u}}} \leq \|\delta\mathcal{F}[v]\|_{H^{-2}_{\#}(\Omega)}.$$

Since Γ is compact we can obtain a finite subcover of Γ. That is there exist $\tilde{u}_i \in \Gamma$, $i = 1, \ldots, I$ and constants $\theta_i, c_i, \rho_i > 0$ such that

$$\Gamma \subseteq \bigcup_{i=1}^{I} B_{\frac{\rho_i}{2}}(\tilde{u}_i)$$

and $\forall v \in H^2_{\tilde{u}}(\Omega)$, $i = 1, \ldots, I$ we have

$$\|\tilde{u}_i - v\|_{H^2(\Omega)} \leq \rho_i \ \Rightarrow\ c_i|\mathcal{F}[v] - \tilde{\mathcal{F}}|^{1-\theta_i} \leq \|\delta\mathcal{F}[v]\|_{H^{-2}_{\#}(\Omega)}. \tag{6.18}$$

Let $\theta = \min\theta_i$, for $0 < s \leq 1$ we have

$$\frac{s^{1-\theta_i}}{s^{1-\theta}} = \frac{s^{-\theta_i}}{s^{-\theta}} \geq 1. \tag{6.19}$$

Let $s_0 = 2\max((\delta+1)^2|\Omega|, |\mathcal{F}[u_0]|)$ from (6.19) we have there exists $\hat{c}_i$ such that for all $s \in (0, s_0)$ we have

$$s^{1-\theta_i} \geq \hat{c}_i s^{1-\theta}. \tag{6.20}$$

From (3.13) we have $\mathcal{F}[v], \tilde{\mathcal{F}} \geq -(\delta+1)^2|\Omega|$. Since from (6.15) the energy is decreasing we have $\mathcal{F}[u_n] \leq \mathcal{F}[u_0]$ for all $n \in \mathbb{N}$. Using this we have $|\mathcal{F}[v] - \tilde{\mathcal{F}}| \leq$

$2\max((\delta+1)^2|\Omega|, |\mathcal{F}[u_0]|)$. Therefore from (6.20) for any $i \in I$ we have

$$\hat{c}_i|\mathcal{F}[v] - \tilde{\mathcal{F}}|^{1-\theta} \leq |\mathcal{F}[v] - \tilde{\mathcal{F}}|^{1-\theta_i}.$$

From this and (6.18), for all $i \in I$ and $v \in H^2(\Omega)$ such that $\|\tilde{u}_i - v\|_{H^2(\Omega)} \leq \rho_i$, we have

$$\hat{c}_i|\mathcal{F}[v] - \tilde{\mathcal{F}}|^{1-\theta} \leq \frac{1}{\min_i c_i}\|\delta\mathcal{F}[v]\|_{H^{-2}_{\#}(\Omega)}.$$

Therefore if we define $c = 1/(\min c_i \min \hat{c}_i)$ we have

$$\|\tilde{u}_i - v\|_{H^2(\Omega)} \leq \rho_i \;\Rightarrow |\mathcal{F}[v] - \tilde{\mathcal{F}}|^{1-\theta} \leq c\|\delta\mathcal{F}[v]\|_{H^{-2}_{\#}(\Omega)}.$$

Finally, let $\operatorname{dist}(v, \Gamma) \leq \min\left(\frac{\rho_i}{2}\right) := \rho_\Gamma$, then we have

$$\operatorname{dist}(v, \Gamma) \leq \rho_\Gamma \;\Rightarrow |\mathcal{F}[v] - \tilde{\mathcal{F}}|^{1-\theta} \leq c\|\delta\mathcal{F}[v]\|_{H^{-2}_{\#}(\Omega)}.$$

Step 2′. We wish to show that $d(u_n, \Gamma) \to 0$ as $n \to \infty$.

Assume this is not true then there exists a subsequence u_{n_j} and a constant $\epsilon > 0$ such that, $\forall n_j$ and $\forall \tilde{u} \in \Gamma$

$$\|\tilde{u} - u_{n_j}\|_{H^2(\Omega)} \geq \epsilon. \tag{6.21}$$

Using that the sequence $\{u_n\}$ is compact in $H^2_{\tilde{u}}(\Omega)$ the subsequence u_{n_j} is compact and hence has a convergent subsequence $\{u_{n_{j_k}}\}$ with $\lim_{k\to\infty} u_{n_{j_k}} \in \Gamma$. Therefore there exists a $\tilde{u}$ such that $\lim \|u_{n_{j_k}} - \tilde{u}\|_{H^2(\Omega)} \to 0$ which contradicts (6.21).

In conclusion, there is an $n_0 \in \mathbb{N}$ such that for $n > n_0$,

$$|\mathcal{F}[u_n] - \tilde{\mathcal{F}}|^{1-\theta} \leq c\|\delta\mathcal{F}[u_n]\|_{H^{-2}_{\#}(\Omega)}. \tag{6.22}$$

Step 3. Convergence to equilibrium.

We now wish to show that there exists a $\tilde{u} \in \Gamma$ such that $u_n \to \tilde{u}$ strongly in $H^2(\Omega)$.

First we define

$$e_k = \sum_{l=k}^{\infty} \|u_{l+1} - u_l\|_{H^2(\Omega)}. \tag{6.23}$$

From Step (1) we know there exists $u_{n_j} \to \tilde{u}$ such that $\tilde{u} \in \Gamma$ using this, the triangle inequality and (6.23) we have

$$\|u_k - \tilde{u}\|_{H^2(\Omega)} \leq e_k \qquad \forall k. \tag{6.24}$$

It remains to prove that e_k is finite for all k.

Consider the decreasing energy $\mathcal{R}[u] = \mathcal{F}[u] - \tilde{\mathcal{F}} > 0$. From Young's inequality we have

$$\mathcal{R}[u_k]^{1-\theta}\mathcal{R}[u_{k+1}]^{\theta} \leq (1-\theta)\mathcal{R}[u_k] + \theta\mathcal{R}[u_{k+1}].$$

Re-arranging this and using that $\mathcal{R}$ is always positive, we have

$$\mathcal{R}[u_k]^\theta - \mathcal{R}[u_{k+1}]^\theta \geq \frac{\theta}{\mathcal{R}[u_k]^{1-\theta}} \left(\mathcal{R}[u_k] - \mathcal{R}[u_{k+1}]\right).$$

If we choose $k \geq k_0 = n_0$ then the Łojasiewicz inequality (6.22) holds and we have

$$\begin{aligned}
\mathcal{R}[u_k]^\theta - \mathcal{R}[u_{k+1}]^\theta &\geq \frac{\theta \left(\mathcal{R}[u_k] - \mathcal{R}[u_{k+1}]\right)}{c\|\delta\mathcal{F}[u_k]\|_{H^{-2}_\#(\Omega)}} \\
&\geq \theta C_{\text{en}} \frac{\|u_{k+1} - u_k\|^2_{H^2(\Omega)}}{c\|\delta\mathcal{F}[u_k]\|_{H^{-2}_\#(\Omega)}} \\
&\geq \frac{\theta C_{\text{en}}}{cC_{\text{dF}}} \|u_{k+1} - u_k\|_{H^2(\Omega)} \qquad (6.25)
\end{aligned}$$

where we use (6.15) in the second line and (6.16) in the last line.

We can see from (6.23) and (6.25), since $\mathcal{R}$ is decreasing, that

$$\begin{aligned}
\frac{\theta C_{\text{en}}}{cC_{\text{dF}}} e_k &\leq \mathcal{R}[u_k]^\theta - \inf_k \mathcal{R}[u_k]^\theta \\
&\leq \mathcal{R}[u_k]^\theta \\
&\leq \left[c\|\delta\mathcal{F}[u_k]\|_{H^{-2}_\#(\Omega)}\right]^{\frac{\theta}{1-\theta}}, \qquad (6.26)
\end{aligned}$$

where we have used that $\lim_{k\to\infty} \mathcal{F}[u_k] = \tilde{\mathcal{F}}$ in the second inequality and the Łojasiewicz inequality (6.22) in the third inequality.

Since $\|\delta\mathcal{F}[u_n]\|_{H^{-2}_\#(\Omega)} \to 0$ it follows that $e_k \to 0$.

Step 4 Convergence rates.

We now use the relationship (6.26) to obtain the stated rates of convergence.

Substituting (6.16) into (6.26) we have

$$\begin{aligned}
\frac{\theta c C_{\text{en}}}{C_{\text{dF}}} e_k &\leq \left[cC_{\text{dF}}\|u_{k+1} - u_k\|_{H^2(\Omega)}\right]^{\frac{\theta}{1-\theta}} \\
&\leq \left[cC_{\text{dF}}\right]^{\frac{\theta}{1-\theta}} \left[e_k - e_{k+1}\right]^{\frac{\theta}{1-\theta}}.
\end{aligned}$$

Taking the $(1-\theta)/\theta$ power of both sides and rearranging we have that there is a constant $\nu > 0$ such that

$$e_{k+1} \leq e_k - \nu e_k^{\frac{1-\theta}{\theta}}. \qquad (6.27)$$

In the case $\theta = 1/2$ by induction we obtain

$$e_{k+1} \leq (1-\nu)^k e_0.$$

Using (6.15), (6.23) and (6.24) we have

$$\|u_k - \tilde{u}\|_{H^2(\Omega)} \leq (1-\nu)^k \sqrt{\frac{\mathcal{F}[u_0] - \tilde{\mathcal{F}}}{C_{\text{en}}}}$$

and thus since $|\tilde{\mathcal{F}}| \leq \max(|\mathcal{F}[u_0]|, (\delta+1)^2|\Omega|)$ we have the $\theta = 1/2$ rate.

In the case $\theta \neq 1/2$ we define

$$y_k := \tilde{c}k^{-p}.$$

Hence we have

$$\begin{aligned} y_{k+1} &= \tilde{c}(k+1)^{-p} \\ &\geq \tilde{c}k^{-p}\left(1 - \frac{p}{k}\right) \\ &\geq y_k\left(1 - p\tilde{c}^{-\frac{1}{p}} y_k^{\frac{1}{p}}\right). \end{aligned} \tag{6.28}$$

Let $p = \theta/(1-2\theta)$ then from (6.27) we have

$$e_{k+1} \leq e_k\left(1 - \nu e_k^{\frac{1}{p}}\right).$$

If we choose k_0 and let $y_{k_0} \geq e_{k_0}$ then from (6.28) we have

$$y_{k_0+1} \geq y_{k_0}\left(1 - p\tilde{c}^{-\frac{1}{p}} y_{k_0}^{\frac{1}{p}}\right).$$

We choose $\tilde{c} > (\nu/p)^{-p}$ and then choose $\tilde{c}$ large enough so that

$$1 - \nu e_{k_0}^{\frac{1}{p}} \leq 1 - p\tilde{c}^{-\frac{1}{p}} y_{k_0}^{\frac{1}{p}}.$$

Therefore we have that

$$\begin{aligned} y_{k_0+1} &\geq y_{k_0}\left(1 - p\tilde{c}^{-\frac{1}{p}} y_{k_0}^{\frac{1}{p}}\right) \\ &\geq e_{k_0} - \nu e_{k_0}^{\frac{1-\theta}{\theta}} \\ &\geq e_{k_0+1} \end{aligned}$$

where the final line follows from (6.27). Using induction we have that $y_k \geq e_k$ for $k \geq k_0$. Fixing e_{k_0} we can then increase $\tilde{c}$ so that $y_k \geq e_k$ for $k < k_0$.

Defining $y_0 = y_1 = \tilde{c}$ and (6.24) then we have

$$\|u_k - \tilde{u}\|_{H^2(\Omega)} \leq \tilde{c}k^{-\frac{\theta}{1-2\theta}}$$

and hence we obtain the result. □

We can now draw together the results of Sections 6.2 and 6.3 to prove part (b) of Theorem 6.1.1.

Proof of Theorem 6.1.1 (b)

Proof. Consider the sequence given by the Algorithm 6.1.1. Clearly this is compact from Lemma 6.3.1. From Lemma 6.2.1 and step (0) of Algorithm 6.1.1, τ_n is bounded above and below for all $n \in \mathbb{N}$. Using this, the equivalence of the $A^{(n)}$-norm and the H^2-norm, Lemma 6.1.1, gives us (6.15) from Proposition 6.2.3 and (6.16) from Proposition 6.2.2. Hence by Lemma 6.3.2 we have part (b) of Theorem 6.1.1. □

Remark 6.3.1. *Consider an h-norm which is an equivalent norm to the H^2-norm. Then for the sequence u_n given by*

$$\left\langle \frac{u_{n+1} - u_n}{\tau_n}, w \right\rangle_h = -\delta\mathcal{F}[u_n, w] \qquad \forall w \in H^2_{\#}(\Omega)$$

with $u_0 \in H^4_{\tilde{u}}(\Omega)$ we can obtain exact analogues to the results of this chapter. As noted above, our choice of h-norm, Definition 6.1.1, is motivated by its relation to the second variation (3.10).

6.4 Conclusion

In this chapter we introduced a time discretisation for the H^2-gradient flow given by Definition 4.2.4. We introduced an adaptive method for choosing γ and defined an inductive algorithm for finding the discrete solution u_n. We then proved that this iterative scheme is stable and that the residual converges to zero. Finally we used the Łojasiewicz inequality to show the iterate converges to a critical point and gave rates of convergence.

Chapter 7

Convex-Concave Splitting

In the previous chapter we introduced a time discretisation for the H^2-gradient flow given by Definition 4.2.4. We now wish to discretise the gradient flows given by Definitions 4.2.1 and 4.2.2 in time so that we can implement analogous computational schemes for the minimisation problem **(P)** (page 37). (As noted in Chapter 6 we undertake space discretisation for (4.1) in Chapter 8). In this chapter we introduce a time-discrete formulation of both the SH and PFC equations (Definitions 4.2.1 and 4.2.2) and give the conditions under which this algorithm is stable and convergent. We will also show that, qualitatively, the methods developed in this chapter are similar to that of Chapter 6.

7.1 Time Discretisation

In Subsection 6.1.1 we introduced the forward Euler method as a way of discretising (4.1). In that section we argued that this method can not be used to discretise the PFC or Swift-Hohenberg equations since the discretisation is ill-defined. We also noted that after space discretisation these equations are stiff and that a restriction on the time-step can be derived from the CFL condition.

Therefore, in this section, we consider different methods of discretising Definitions 4.2.1 and 4.2.2. We first consider the implicit method of time discretisation and then proceed to consider two semi-implicit methods based on a convex-concave splitting.

7.1.1 Backward Euler Method

A method for unconditional stability is the backward Euler method. Using the backward Euler method with $H = L^2(\Omega)$ for the Swift-Hohenberg case and $H = H^{-1}(\Omega)$ for the PFC case we have

$$\left\langle \frac{u_{n+1} - u_n}{\tau_n}, w \right\rangle_H = \langle -(\Delta + I)^2 u_{n+1} + \delta u_{n+1} - (u_{n+1})^3, w \rangle \qquad \forall w \in H^2_{\#}(\Omega).$$

Since the non-linear term is one of the implicit terms, at each iteration we have to use Newton's method to find the variable at the new time step and thus each iteration will be computationally expensive. Also, since we are now solving a weak equation of the form $f(u_{n+1}) = u_n$ where f is not convex we only have a locally unique solution if the time-step is small.

7.1.2 Convex-Concave Splitting

We want a scheme that is stable for any τ_n, therefore we consider a different method for time discretisation of the two gradient flows, the Swift-Hohenberg equation, Definition 4.2.1, and the PFC equation, Definition 4.2.2. Specifically, since we have excluded the fully implicit (backward Euler) and fully explicit (forward Euler) schemes, we consider a semi-implicit scheme.

A common approach, used for the Cahn-Hilliard equation in [Eyr98] and used for the PFC equation in [EW13] and [WWL09], is the convex-concave splitting. We focus on the approach of [EW13]. The idea is to write the functional as the sum of a concave and convex part. Taking the convex part implicitly and the concave part explicitly gives us energy stability of the solution. The fact that the implicit part is now a convex function means the non-linear equation to be solved at each time-step has a unique solution and hence we no longer have the time-step restriction of the backward Euler method.

A simple convex-concave splitting, used in [WWL09, Equation (1.5)], is $\mathcal{F}[u] = \mathcal{F}_{\mathrm{c}}[u] - \mathcal{F}_{\mathrm{e}}[u]$, where

$$\begin{aligned}\mathcal{F}_{\mathrm{c}}[u] &= \frac{1}{2}\|\Delta u\|^2_{L^2(\Omega)} + \frac{1-\delta}{2}\|u\|^2_{L^2(\Omega)} + \frac{1}{4}\|u\|^4_{L^4(\Omega)},\\ \mathcal{F}_{\mathrm{e}}[u] &= \|\nabla u\|^2_{L^2(\Omega)}\end{aligned}$$

are clearly convex functionals (the notation $\mathcal{F}_{\mathrm{c}}$ and $\mathcal{F}_{\mathrm{e}}$ is borrowed from [WWL09] and [Eyr98] where c refers to the contractive part of the energy and e refers to the expansive part of the energy). In this case the semi-implicit time-stepping, with $H = L^2(\Omega)$ for the Swift-Hohenberg case and $H = H^{-1}(\Omega)$ for the PFC case, can be written as

$$\left\langle \frac{u_{n+1}-u_n}{\tau_n}, w \right\rangle_H = \langle -\Delta^2 u_{n+1} - (1-\delta)u_{n+1} - (u_{n+1})^3 - 2\Delta u_n, w\rangle \qquad \forall w \in H^2_{\#}(\Omega).$$

Unconditional stability of such schemes is given in [WWL09, Theorem 3.6] and an error estimate is given in [WWL09, Theorem 3.11]. However, this scheme requires us to solve a non-linear equation, which is expensive, particularly for spectral methods.

To deal with this issue [EW13] suggest a different convex-concave splitting by adding and subtracting an L^2-norm.

Definition 7.1.1 (Convex-Concave Splitting)**.**

$$\mathcal{F}[u] = \mathcal{F}_{\mathrm{C},C_{\mathrm{stab}}}[u] - \mathcal{F}_{\mathrm{E},C_{\mathrm{stab}}}[u],$$

where, for $C_{\text{stab}} > 0$, we have

$$\mathcal{F}_{\text{C},C_{\text{stab}}}[u] = \frac{1}{2}\|\Delta u + u\|^2_{L^2(\Omega)} - \frac{\delta}{2}\|u\|^2_{L^2(\Omega)} + \frac{C_{\text{stab}}}{2}\|u\|^2_{L^2(\Omega)},$$
$$\mathcal{F}_{\text{E},C_{\text{stab}}}[u] = \frac{C_{\text{stab}}}{2}\|u\|^2_{L^2(\Omega)} - \frac{1}{4}\|u\|^4_{L^4(\Omega)},$$

which is equivalent to [EW13, Equations (1.7) and (1.8)].

Remark 7.1.1. *This convex-concave splitting can be generalised by using a stabilisation term $\|Lu\|_{L^2(\Omega)}$ instead of $\|u\|_{L^2(\Omega)}$. L is a general differential operator such that $\|Lu\|_{L^2(\Omega)} \geq c\|u\|_{L^2(\Omega)}$ for some $c > 0$. A version of this generalisation, where the stabilisation term is replaced by the H^1-semi-norm, is seen in [EW13, Equation (1.7) and (1.8)] .*

We now give two lemmas on the properties of these functionals.

Lemma 7.1.1. *For large enough C_{stab} the functional $\mathcal{F}_{\text{C},C_{\text{stab}}}[u]$ is convex.*

Lemma 7.1.2. *If $C_1 > 0$ and $C_{\text{stab}} \geq 3C_1^2$ then $\mathcal{F}_{\text{E},C_{\text{stab}}}$ is convex in $\{\|u\|_{L^\infty(\Omega)} \leq C_1\}$.*

Proof. We follow the method outlined in the proof of [EW13, Theorem 2.1].

We calculate the second variation by finding the second order terms in v of the Taylor expansion of $\mathcal{F}_{\text{E},C_{\text{stab}}}$ at $u + \epsilon v$. The functional expansion is then

$$\begin{aligned}\mathcal{F}_{\text{E},C_{\text{stab}}}[u+\epsilon v] = \frac{C_{\text{stab}}}{2}\|u\|^2_{L^2(\Omega)} + C_{\text{stab}}\epsilon\int_\Omega uv\mathrm{d}x + \frac{C_{\text{stab}}}{2}\epsilon^2\|v\|^2_{L^2(\Omega)} - \frac{1}{4}\|u\|^4_{L^2(\Omega)} \\ - \epsilon\int_\Omega u^3 v\mathrm{d}x - \frac{3}{2}\epsilon^2\|uv\|^2_{L^2(\Omega)} - \epsilon^3\int_\Omega uv^3\mathrm{d}x - \frac{1}{4}\epsilon^4\|v\|^4_{L^2(\Omega)}.\end{aligned}$$

Thus the second variation is

$$\begin{aligned}\langle\delta^2\mathcal{F}_{\text{E},C_{\text{stab}}}[u]v, v\rangle &= \left(C_{\text{stab}}\|v\|^2_{L^2(\Omega)} - 3\|uv\|^2_{L^2(\Omega)} - 6\epsilon\int_\Omega uv^3\mathrm{d}x - 3\epsilon^2\|v\|^4_{L^2(\Omega)}\right)_{\epsilon=0} \\ &= C_{\text{stab}}\|v\|^2_{L^2(\Omega)} - 3\|uv\|^2_{L^2(\Omega)}.\end{aligned}$$

We have a lower bound for the second variation, using that u has a maximum, Lemma 3.1.3, which follows from the boundedness of the energy. That is,

$$\begin{aligned}\langle\delta^2\mathcal{F}_{\text{E},C_{\text{stab}}}[u]v, v\rangle &\geq C_{\text{stab}}\|v\|^2_{L^2(\Omega)} - 3\|u\|^2_{L^\infty(\Omega)}\|v\|^2_{L^2(\Omega)} \\ &\geq 0,\end{aligned}$$

if $\|u\|^2_{L^\infty(\Omega)} \leq \frac{C_{\text{stab}}}{3}$. Therefore if $\|u\|_{L^\infty(\Omega)} \leq C_1$ we have that $\mathcal{F}_{\text{E},C_{\text{stab}}}[u]$ is convex if $C_{\text{stab}} \geq 3C_1^2$. □

On a bounded domain we have that u has a maximum, Lemma 3.1.3; therefore, from Lemmas 7.1.1 and 7.1.2, for a sufficiently large constant C_{stab} both $\mathcal{F}_{\text{C},C_{\text{stab}}}$ and $\mathcal{F}_{\text{E},C_{\text{stab}}}$ are convex on $\{\|u\|_{L^\infty(\Omega)} \leq C_1\}$ (see also [EW13, pages 4-5]). Hence we have stability and we no longer have to solve the non-linear part implicitly.

We note that the first variation of the functionals of Definition 7.1.1 are given as

$$\delta\mathcal{F}_{\mathrm{C},C_{\mathrm{stab}}}[u,v] = \langle(\Delta+I)^2u - \delta u + C_{\mathrm{stab}}u, v\rangle,$$
$$\delta\mathcal{F}_{\mathrm{E},C_{\mathrm{stab}}}[u,v] = \langle C_{\mathrm{stab}}u - u^3, v\rangle.$$

At each step we want to choose C_{stab} as small as possible whilst preserving the convexity of $\mathcal{F}_{\mathrm{E},C_{\mathrm{stab}}}[u_{n+1}]$ and $\mathcal{F}_{\mathrm{C},C_{\mathrm{stab}}}[u_{n+1}]$. The sufficient condition on C_{stab} for convexity obtained from Lemma 7.1.2 depends on the iteration number. Therefore we choose a C_{stab} that depends on the iteration number and relabel this $C_n = C_{\mathrm{stab}}$.

Since C_n now depends on the iteration number it acts like an inverse time step. Therefore, and also for the sake of simplicity, we take a constant $\tau = \tau_n$.

The time-stepping scheme for gradient flow in a general H-norm can be written, using the notation $v_n = (u_{n+1} - u_n)/\tau$, as

$$\langle v_n, w\rangle_H = -\delta\mathcal{F}_{\mathrm{C},C_n}[u_{n+1}, w] + \delta\mathcal{F}_{\mathrm{E},C_n}[u_n, w] \qquad \forall w \in H^2_{\#}(\Omega). \tag{7.1}$$

We can now write the weak form of the discretised Swift-Hohenberg equation.

Definition 7.1.2 (Discrete Convex-Concave SH Equation)**.** $\forall v \in H^2_{\#}(\Omega)$

$$\left\langle \frac{u_{n+1}-u_n}{\tau}, v \right\rangle_{L^2(\Omega)} = -\left\langle (\Delta+I)^2u_{n+1} - \delta u_{n+1} + C_n(u_{n+1}-u_n) + u_n^3, v\right\rangle.$$

We can also write the weak form of the discretised PFC equation.

Definition 7.1.3 (Discrete Convex-Concave PFC Equation)**.** $\forall v \in H^2_{\#}(\Omega)$

$$\left\langle \frac{u_{n+1}-u_n}{\tau}, v \right\rangle_{H^{-1}(\Omega)} = -\left\langle (\Delta+I)^2u_{n+1} - \delta u_{n+1} + C_n(u_{n+1}-u_n) + u_n^3, v\right\rangle.$$

In [EW13, Equation (2.6)] the constant C_n appears to be domain dependent. By contrast in Remark 6.2.2 we suggested that the corresponding n-dependent parameter τ_n has an upper bound that depends only on $\|u_0\|_{L^\infty(\Omega)}$. We show in Lemma 7.2.1 that we actually have similar constraints on C_n in the asymptotic regime.

We first recall theorems for stability and convergence (see also [EW13]). We first state the theorem for stability from [EW13, Theorem 2.1].

Theorem 7.1.1. *[([EW13, Theorem 2.1]) Stability].*

Let $\delta < 1$. For any $u_0 : \Omega \to \mathbb{R}$ with finite energy $\mathcal{F}$ there exists a C_n such that the schemes given by Definition 7.1.2 and Definition 7.1.3 are stable for any $\tau > 0$. That is,

$$\mathcal{F}[u_{n+1}] \le \mathcal{F}[u_n], \qquad \forall n \in \mathbb{N}$$
$$\exists\, U > 0 \text{ such that } \|u_n\|_{L^\infty(\Omega)} \le U \qquad \forall n \in \mathbb{N}.$$

We also state the theorem that gives an error estimate for the discretisation, from [EW13, Theorem 2.3].

Theorem 7.1.2. *[[EW13, Theorem 2.3]) Error Estimate].*

Suppose the Swift-Hohenberg or Phase Field Crystal equation is solved by a smooth spatially periodic function $u : [0,T] \times \Omega \to \mathbb{R}$ for some $T \in (0,\infty)$. We denote the solution to the scheme Definition 7.1.2 or 7.1.3 by u_n, $n = 0, 1, \dots$ where $u_0 = u(0)$ and C_n is chosen according to Theorem 7.1.1. Then there exists a constant $\tilde{C} > 0$ independent of τ such that

$$\|u(n\tau) - u_n\|_{L^2(\Omega)} \leq \tilde{C}\tau$$

for all n with $n\tau \leq T$.

Despite this theorem, most practitioners are only interested in the case of large τ (even in [EW13, Section 5] $\tau = 1$ is used).

We note that the proofs of Theorems 7.1.1 and 7.1.2 are analogous to those in [EW13], however care must be taken to ensure the average of u is conserved in the SH case.

In the following discussion we show that we can rewrite the discrete convex-concave flow as a discrete gradient flow in a norm equivalent to the H^2-norm. In Chapter 6 we considered a discrete H^2-gradient flow given by (6.3). This means that there is a close qualitative link between the two schemes (6.3) and (7.1).

Fix $\tau > 0$. Let $H = L^2(\Omega)$ for the Swift-Hohenberg case and $H = H^{-1}(\Omega)$ for the PFC case. For $C_n \geq \delta$ we can define a new norm

$$\|v\|^2_{H_{\text{con,n}}} := \|v\|^2_H + \tau\left[\|\Delta v + v\|^2_{L^2(\Omega)} + (C_n - \delta)\|v\|^2_{L^2(\Omega)}\right]. \tag{7.2}$$

We first show that the convex-concave splitting scheme (7.1) can be rewritten as a discrete gradient flow in the $H_{\text{con},n}$-norm. We then show in Lemma 7.1.3 that, for $C_n > \delta$, the $H_{\text{con},n}$-norm is an equivalent norm to the H^2-norm. This means that (7.3) can be considered as a discrete gradient flow for $v_n = (u_{n+1} - u_n)/\tau$ in a norm equivalent to the H^2-norm.

The convex-concave splitting (7.1) can be rearranged as, $\forall \varphi \in H^2_{\#}(\Omega)$,

$$\left\langle \frac{u_{n+1} - u_n}{\tau}, \varphi \right\rangle_H + \langle(\Delta + I)u_{n+1}, (\Delta + I)\varphi\rangle + (C_n - \delta)\langle u_{n+1}, \varphi\rangle = C_n\langle u_n, \varphi\rangle - \langle u_n^3, \varphi\rangle$$

this can be rewritten using the first variation as, $\forall \varphi \in H^2_{\#}(\Omega)$,

$$\langle v_n, \varphi\rangle_H + \tau\langle(\Delta + I)v_n, (\Delta + I)\varphi\rangle + \tau(C_n - \delta)\langle v_n, \varphi\rangle = -\delta\mathcal{F}[u_n, \varphi] \tag{7.3}$$

where $v_n = (u_{n+1} - u_n)/\tau$. Using the definition of the $H_{\text{con},n}$-norm (7.2) we can re-write (7.3) as

$$\langle v_n, \varphi\rangle_{H_{\text{con},n}} = -\delta\mathcal{F}[u_n, \varphi] \qquad \forall \varphi \in H^2_{\#}(\Omega).$$

To highlight the similarity to the H^2-gradient flow we now show that the $H_{\text{con},n}$-

norm is equivalent to the H^2-norm which is the result of the following lemma.

Lemma 7.1.3. *There exists $\mathfrak{C} > 0$ such that for all $C_n < \infty$ with $C_n \geq \mathfrak{C} + \delta$, $\|v\|_{H_{\mathrm{con,n}}}$ is equivalent to the H^2-norm. That is, for fixed n, there exist $C_{\mathrm{con,l}}, C_{\mathrm{con,u},n} > 0$ such that for all $v \in H^2(\Omega)$*

$$C_{\mathrm{con,l}}\|v\|^2_{H^2(\Omega)} \leq \|v\|^2_{H_{\mathrm{con,n}}} \leq C_{\mathrm{con,u},n}\|v\|^2_{H^2(\Omega)}.$$

We note that $C_{\mathrm{con,l}}$ is independent of n for $C_n > \mathfrak{C} + \delta$.

Also from this we can show that

$$\|\delta\mathcal{F}[u_n]\|_{H^{-1}_{\mathrm{con,n}}} \leq \sqrt{\frac{1}{C_{\mathrm{con,l}}}}\|\delta\mathcal{F}[u_n]\|_{H^{-2}_{\#}(\Omega)}. \tag{7.4}$$

Proof. Since for the PFC ($H = H^{-1}(\Omega)$) and SH ($H = L^2(\Omega)$) case, $H^2(\Omega) \subset H$ we have, $\forall v \in H^2(\Omega)$,

$$\|v\|^2_{H^2(\Omega)} \leq \|v\|^2_H + \|v\|^2_{H^2(\Omega)} \leq C(\Omega)\|v\|^2_{H^2(\Omega)} \tag{7.5}$$

where $C(\Omega) > 0$ is a domain dependent constant.

Let $0 < \epsilon \leq 1$, therefore using Lemma 3.1.1, (7.5) and (7.2) we have an equivalent-norm to $H^2(\Omega)$

$$\begin{aligned}\frac{\epsilon\tau}{5}\|v\|^2_{H^2(\Omega)} &\leq \|v\|^2_H + \tau\epsilon\left[\|(\Delta + I)v\|^2_{L^2(\Omega)} + \|v\|^2_{L^2(\Omega)}\right] \\ &\leq \|v\|^2_{H_{\mathrm{con},n}} \\ &\leq (\max(2\tau, 1)C(\Omega) + \tau(C_n - \delta))\,\|v\|^2_{H^2(\Omega)}.\end{aligned} \tag{7.6}$$

where from the second line onwards we use that C_n is sufficiently large, i.e. $C_n > \delta + \epsilon$. In the final line we use Lemma 3.1.1 and (7.5).

Consider the dual norm

$$\begin{aligned}\|\delta\mathcal{F}[u_n]\|_{H^{-1}_{\mathrm{con,n}}} &= \sup_{\varphi\in H^2_{\#}(\Omega)} \frac{|\langle\delta\mathcal{F}[u_n], \varphi\rangle|}{\|\varphi\|_{H_{\mathrm{con,n}}}} \\ &\leq \sup_{\varphi\in H^2_{\#}(\Omega)} \sqrt{\frac{5}{\tau\epsilon}}\frac{|\langle\delta\mathcal{F}[u_n], \varphi\rangle|}{\|\varphi\|_{H^2(\Omega)}}\end{aligned}$$

where we have used the lower bound (7.6) in the second line. Using Cauchy-Schwartz on our upper bound for the dual yields the result, that is

$$\begin{aligned}\|\delta\mathcal{F}[u_n]\|_{H^{-1}_{\mathrm{con,n}}} &\leq \sup_{\varphi\in H^2_{\#}(\Omega)} \sqrt{\frac{5}{\tau\epsilon}}\frac{\|\delta\mathcal{F}[u_n]\|_{H^{-2}_{\#}(\Omega)}\|\varphi\|_{H^2(\Omega)}}{\|\varphi\|_{H^2(\Omega)}} \\ &\leq \sqrt{\frac{5}{\tau\epsilon}}\|\delta\mathcal{F}[u_n]\|_{H^{-2}_{\#}(\Omega)}.\end{aligned}$$

□

Remark 7.1.2. *Since both* (6.3) *and* (7.1) *can be reformulated as discrete gradient flows in a norm that is equivalent to the H^2-norm we might expect both methods to perform*

similarly. However, the simulations of Chapters 8 and 9 suggest that the discretisation of Algorithm 6.1.1 reaches a minimum faster than the discretisation of Algorithm 7.1.1. Also we see that for the large simulations undertaken in Sections 9.1 and 9.2 the method of (7.1) *converges faster in the pre-asymptotic regime whereas Algorithm 6.1.1 converges faster in the asymptotic regime. In Section 9.2 we also obtain qualitatively different minima for Algorithm 6.1.1 and the method of* (7.1).

7.1.3 Algorithm

We briefly describe the algorithm used for finding the sequence $\{u_n\}_{n\in\mathbb{N}}$ generated by (7.1). We assume a fixed δ, $\bar{u}$ and $\tau > 0$. We let $H = L^2(\Omega)$ for the Swift-Hohenberg case and $H = H^{-1}(\Omega)$ for the PFC case.

Algorithm 7.1.1.

(0) INPUT $u_0, \tau > 0, 0 < \Theta < 1/2$

(1) FOR $n = 0, 1, 2, ..$

(2) $C_n = 3\|u_n\|^2_{L^\infty(\Omega)} + \delta$

(3) SOLVE $\langle v_n, w\rangle_{H_{\text{con},n}} = -\delta\mathcal{F}[u_n, w] \qquad \forall w \in H^2_\#(\Omega)$

(4) WHILE $\mathcal{F}[u_n + \tau v_n] > \mathcal{F}[u_n] - \tau\Theta\|\delta\mathcal{F}[u_n]\|^2_{H^{-1}_{\text{con},n}}$

(5) $C_n \leftarrow 2C_n$

(6) SOLVE $\langle v_n, w\rangle_{H_{\text{con},n}} = -\delta\mathcal{F}[u_n, w] \qquad \forall w \in H^2_\#(\Omega)$

(7) $u_{n+1} = u_n + \tau v_n$

This algorithm is very similar to Algorithm 6.1.1. Again the while condition is an Armijo condition. Step (5) is equivalent to the backtracking of Algorithm 6.1.1 since from (7.3) C_n acts like an inverse time-step. The main difference between Algorithm 6.1.1 and 7.1.1 is that in the while loop of Algorithm 7.1.1 we have to recalculate v_n every time we change C_n whereas in Algorithm 6.1.1 for each while loop v_n is independent of τ_n.

We now state a theorem that gives us the rate of convergence of a sequence defined through Algorithm 7.1.1. The method of obtaining this result is very similar to the method for obtaining Theorem 6.1.1. This theorem is the main result of this chapter and the rest of the chapter is dedicated to its proof.

Theorem 7.1.3. *Let $u_0 \in H^2_{\bar{u}}(\Omega)$, then we have*

(a) *Algorithm 7.1.1 is well-defined. That is, it produces a sequence $\{u_n\}_{n\in\mathbb{N}} \subset H^2_{\bar{u}}(\Omega)$.*

(b) *There exists* $\theta \in \left(0, \frac{1}{2}\right]$ *and* $\tilde{u} \in H^2_{\tilde{u}}(\Omega)$ *such that* $\delta\mathcal{F}[\tilde{u}] = 0$ *and*

$$\|u_n - \tilde{u}\|_{H^2(\Omega)} \leq C \begin{cases} \nu^n, & \theta = \frac{1}{2} \\ n^{-\frac{\theta}{1-2\theta}}, & \theta < \frac{1}{2} \end{cases}$$

where $C > 0$ *and* $\nu \in (0, 1)$.

7.2 Energy Stability and Convergence of Residual

To obtain analogous results to those obtained for the H^2-gradient flow in Chapter 6 we need to prove energy decrease. This also ensures that step (4) of Algorithm 7.1.1 will be fulfilled.

Lemma 7.2.1. *Let the sequence* $\{u_n\}_{n\in\mathbb{N}}$ *be defined through* (7.1). *Also take* $0 < \Theta < 1/2$ *and fix the constant* $\tau > 0$.

There exists a $\tilde{C} = \tilde{C}(\delta, \|u_n\|_{L^\infty(\Omega)}) > 0$ *such that for* $C_n \geq \tilde{C}$ *we have energy decrease, i.e.,*

$$\mathcal{F}[u_n + \tau v_n] - \mathcal{F}[u_n] \leq -\Theta\tau\|v_n\|^2_{H_{con,n}} = -\Theta\tau\|\delta\mathcal{F}[u_n]\|^2_{H^{-1}_{con,n}}. \tag{7.7}$$

In particular we have

$$\mathcal{F}[u_n + \tau v_n] - \mathcal{F}[u_n] \leq -\tilde{\Theta}\tau\|\delta\mathcal{F}[u_n]\|^2_{H^{-2}_{\#}(\Omega)} \tag{7.8}$$

and

$$\mathcal{F}[u_n + \tau v_n] - \mathcal{F}[u_n] \leq -\tilde{\Theta}\tau\|v_n\|^2_{H^2(\Omega)} \tag{7.9}$$

where $\tilde{\Theta}(\tau) > 0$.

Proof. We split the proof into two steps. First we show that the energy decrease (7.7) is satisfied if we satisfy certain bounds on C_n and the L^3- and L^4-norms. We then show that for large enough C_n the bounds on L^3- and L^4-norms are satisfied.

Step 1. Let $H = L^2(\Omega)$ for the SH case and $H = H^{-1}(\Omega)$ for the PFC case. We recall the definition of the $H_{\mathrm{con},n}$-norm (7.2), that is

$$\|v\|^2_{H_{\mathrm{con},n}} = \|v\|^2_H + \tau\|\Delta v + v\|^2_{L^2(\Omega)} + \tau(C_n - \delta)\|v\|^2_{L^2(\Omega)}.$$

We want the energy decrease of (7.7). Clearly the equality in this line follows from Proposition 6.2.2, hence we now prove (7.7) with the $\|v\|_{H_{\mathrm{con},n}}$ form of the right hand side. We recall (6.4) with $\tilde{v} = v_n$ defined by $\langle v_n, w\rangle_{H_{\mathrm{con},n}} = -\delta\mathcal{F}[u_n, w]$ for all $w \in H^2_{\#}(\Omega)$ and $\tau_n = \tau$ for all n. Setting this upper bound for the energy difference as less than the upper bound

we desire for (7.7) and re-arranging we obtain

$$\frac{\tau^2}{2}\|\Delta v_n + v_n\|^2_{L^2(\Omega)} + \frac{3\tau^2}{2}\|u_n\|^2_{L^\infty(\Omega)}\|v_n\|^2_{L^2(\Omega)} + \tau^3\|u_n\|_{L^\infty(\Omega)}\|v_n\|^3_{L^3(\Omega)} + \frac{\tau^4}{4}\|v_n\|^4_{L^4(\Omega)}$$
$$\leq (1-\Theta)\tau\|v_n\|^2_{H_{\mathrm{con},n}}.$$

If we substitute in the definition of the $H_{\mathrm{con},n}$-norm (7.2) we have

$$\frac{\tau^2}{2}\|\Delta v_n + v_n\|^2_{L^2(\Omega)} + \frac{3\tau^2}{2}\|u_n\|^2_{L^\infty(\Omega)}\|v_n\|^2_{L^2(\Omega)} + \tau^3\|u_n\|_{L^\infty(\Omega)}\|v_n\|^3_{L^3(\Omega)} + \frac{\tau^4}{4}\|v_n\|^4_{L^4(\Omega)}$$
$$\leq (1-\Theta)\tau\left[\|v_n\|^2_H + \tau\|\Delta v_n + v_n\|^2_{L^2(\Omega)} + \tau(C_n-\delta)\|v_n\|^2_{L^2(\Omega)}\right]$$

which simplifies to

$$\frac{\left(3\|u_n\|^2_{L^\infty(\Omega)} - (C_n-\delta)\right)\tau^2}{2}\|v_n\|^2_{L^2(\Omega)} + \tau^3\|u_n\|_{L^\infty(\Omega)}\|v_n\|^3_{L^3(\Omega)} + \frac{\tau^4}{4}\|v_n\|^4_{L^4(\Omega)}$$
$$\leq \left(\frac{1}{2}-\Theta\right)\left[\tau^2\|\Delta v_n + v_n\|^2_{L^2(\Omega)} + \tau^2(C_n-\delta)\|v_n\|^2_{L^2(\Omega)} + \tau\|v_n\|^2_H\right] + \frac{\tau}{2}\|v_n\|^2_H. \tag{7.10}$$

We use the $H_{\mathrm{con,n}}$-norm to simplify this condition. The three conditions

$$3\|u_n\|^2_{L^\infty(\Omega)} \leq (C_n-\delta), \tag{7.11}$$
$$\|v_n\|^3_{L^3(\Omega)} \leq \frac{(1-2\Theta)}{4\tau^2\|u_n\|_{L^\infty(\Omega)}}\|v_n\|^2_{H_{\mathrm{con},n}}, \tag{7.12}$$
$$\|v_n\|^4_{L^4(\Omega)} \leq \frac{(1-2\Theta)}{\tau^3}\|v_n\|^2_{H_{\mathrm{con},n}}. \tag{7.13}$$

are now sufficient to obtain (7.10). We note that condition (7.11) is automatically satisfied for a sequence generated by Algorithm 7.1.1 due to line (2).

Step 2. To prove that, for C_n sufficiently large, (7.12) and (7.13) are satisfied we first show that $\|v_n\|_{L^2(\Omega)}\|v_n\|_{H^2(\Omega)}$ decreases as C_n increases. We then show that both $\|v_n\|_{L^3(\Omega)}$ and $\|v_n\|_{L^4(\Omega)}$ can be bounded by powers of $\|v_n\|_{L^2(\Omega)}\|v_n\|_{H^2(\Omega)}$. Finally we can combine these to show that, for C_n sufficiently large, (7.12) and (7.13) are satisfied.

Step 2 a) We wish to show that $\|v_n\|_{L^2(\Omega)}\|v_n\|_{H^2(\Omega)} \to 0$ as $C_n \to \infty$. We first prove an upper bound $\|v_n\|_{L^2(\Omega)}\|v_n\|_{H^2(\Omega)}$ in terms of C_n and $\|v_n\|_{H_{\mathrm{con},n}}$ and then prove that there is a uniform upper bound for $\|v_n\|_{H_{\mathrm{con},n}}$.

Let $0 < \epsilon \leq 1$. From Young's inequality we have

$$2\tau\sqrt{\frac{(C_n-\epsilon-\delta)\epsilon}{5}}\|v_n\|_{H^2(\Omega)}\|v_n\|_{L^2(\Omega)} \leq \tau(C_n-\epsilon-\delta)\|v_n\|^2_{L^2(\Omega)} + \frac{\tau\epsilon}{5}\|v_n\|^2_{H^2(\Omega)}$$
$$\leq \|v_n\|^2_{H_{\mathrm{con},n}}$$

where the final inequality follows from Lemma 3.1.1 and (7.2). This re-arranges to

$$\|v_n\|_{H^2(\Omega)}\|v_n\|_{L^2(\Omega)} \leq \frac{\sqrt{5}}{2\tau\sqrt{\epsilon(C_n-\epsilon-\delta)}}\|v_n\|^2_{H_{\mathrm{con},n}}. \tag{7.14}$$

In order to justify the claim that $\|v_n\|_{H^2(\Omega)}\|v_n\|_{L^2(\Omega)} \to 0$ as $C_n \to \infty$ we must show that $\|v_n\|_{H_{\mathrm{con},n}}$ has a uniform upper bound for u_n uniformly bounded in $H^2(\Omega)$. From Proposition 6.2.2 we have

$$\|v_n\|_{H_{\mathrm{con},n}} = \|\delta\mathcal{F}[u_n]\|_{H^{-1}_{\mathrm{con},n}}.$$

Using this with (7.4) we have

$$\|v_n\|_{H_{\mathrm{con},n}} \leq \sqrt{\frac{1}{C_{\mathrm{con},l}}}\|\delta\mathcal{F}[u_n]\|_{H^{-2}_{\#}(\Omega)} \tag{7.15}$$

using this bound in (7.14) we have

$$\|v_n\|_{H^2(\Omega)}\|v_n\|_{L^2(\Omega)} \leq \frac{\sqrt{5}}{2\tau C_{\mathrm{con},l}\sqrt{\epsilon(C_n-\epsilon-\delta)}}\|\delta\mathcal{F}[u_n]\|^2_{H^{-2}_{\#}(\Omega)}. \tag{7.16}$$

From Lemma 3.1.4 we can see

$$\|\delta\mathcal{F}[u_n]\|_{H^{-2}_{\#}(\Omega)} \leq \left(2+|\delta|+\|u_n\|^2_{H^2(\Omega)}\right)\|u_n\|_{H^2(\Omega)}. \tag{7.17}$$

Therefore in the set $\|u_n\|_{H^2(\Omega)} \leq C$, $C > 0$ we have that $\|\delta\mathcal{F}[u_n]\|_{H^{-2}_{\#}(\Omega)}$ is bounded. Therefore from (7.15) and (7.17) there exists a $\hat{C} > 0$ such that

$$\|v_n\|_{H_{\mathrm{con},n}} \leq \hat{C}.$$

Substituting this bound into (7.14) we have

$$\|v_n\|_{H^2(\Omega)}\|v_n\|_{L^2(\Omega)} \leq \frac{\sqrt{5}\hat{C}^2}{2\tau\sqrt{\epsilon(C_n-\epsilon-\delta)}} \tag{7.18}$$

and therefore clearly $\|v_n\|_{H^2(\Omega)}\|v_n\|_{L^2(\Omega)} \to 0$ as $C_n \to \infty$.

Step 2 b) We now wish to show that both $\|v_n\|_{L^3(\Omega)}$ and $\|v_n\|_{L^4(\Omega)}$ are bounded by powers of $\|v_n\|_{L^2(\Omega)}\|v_n\|_{L^4(\Omega)}$.

Recall the L^3-norm, from Lemma C.2.5 we have

$$\|v_n\|^3_{L^3(\Omega)} \leq \|v_n\|_{L^2(\Omega)}\|v_n\|^2_{L^4(\Omega)} \tag{7.19}$$

We therefore consider the L^4-norm, from Ladyzhenskaya's inequality (Lemma C.2.1) and

$H^2(\Omega) \subset H^1(\Omega) \subset L^2(\Omega)$ we have (see Lemma C.2.6)

$$\|v_n\|_{L^4(\Omega)} \leq \sqrt[8]{2}\|v_n\|^{\frac{1}{2}}_{H^2(\Omega)}\|v_n\|^{\frac{1}{2}}_{L^2(\Omega)}. \tag{7.20}$$

Using this upper bound and $H^2(\Omega) \subset L^2(\Omega)$ in (7.19) we have (see Lemma C.2.7)

$$\|v_n\|^3_{L^3(\Omega)} \leq \sqrt[4]{2}\|v_n\|^{\frac{3}{2}}_{H^2(\Omega)}\|v_n\|^{\frac{3}{2}}_{L^2(\Omega)}. \tag{7.21}$$

Clearly substituting (7.14) and (7.18) into (7.21) and (7.20) we obtain

$$\|v_n\|^3_{L^3(\Omega)} \leq \frac{\sqrt[4]{2}(5)^{\frac{3}{2}}\hat{C}\|v_n\|^2_{H_{\mathrm{con},n}}}{(2\tau)^{\frac{3}{2}}\left(\epsilon(C_n-\epsilon-\delta)\right)^{\frac{3}{4}}},$$
$$\|v_n\|^4_{L^4(\Omega)} \leq \frac{5\sqrt{2}\hat{C}^2\|v_n\|^2_{H_{\mathrm{con},n}}}{(2\tau)^2\epsilon(C_n-\epsilon-\delta)}.$$

From these equations it is clear that if C_n is large enough (7.12) and (7.13) are satisfied.

We now show that we can obtain (7.8) and (7.9) from (7.7).

Since we can choose a finite C_n such that (7.12) and (7.13) are satisfied, the second form of the energy decrease (7.8) follows from (7.7) by using (7.1) and the equivalence of the $H_{\mathrm{con},n}$-norm and the H^2-norm for C_n sufficiently large, Lemma 7.1.3. In particular this means $\tilde{\Theta} > 0$.

The third inequality (7.9) follows simply from the lower bound of Lemma 7.1.3 and $0 < \epsilon \leq 1$.

□

Statement (a) of Theorem 7.1.3 now follows.

We want the sequence $\{u_n\}_{n\in\mathbb{N}}$ generated by Algorithm 7.1.1 to converge to an equilibrium point. We can obtain this result using Lemma 7.2.1 from the following lemma.

Lemma 7.2.2. *For any sequence $\{u_n\}_{n\in\mathbb{N}}$ generated by Algorithm 7.1.1, we have*

$$\|\delta\mathcal{F}[u_n]\|_{H^{-2}_{\#}(\Omega)} \to 0 \qquad \text{as } n \to \infty.$$

Proof. As in Lemma 6.2.1, the method used is similar to that used for a general line search algorithm, see [NW06, Pages 38-39].

Re-arranging the bound on the difference between the functionals from Lemma 7.2.1 (7.8), since $\mathcal{F}$ is decreasing, we have

$$\tilde{\Theta}\tau\sum_{n=0}^{\infty}\|\delta\mathcal{F}[u_n]\|^2_{H^{-2}_{\#}(\Omega)} \leq \mathcal{F}[u_0] - \inf_n \mathcal{F}[u_n].$$

The result follows since we have chosen a fixed $\tau > 0$ and from Lemma 7.2.1 $\tilde{\Theta} > 0$.

□

Remark 7.2.1. *Let* $0 < \epsilon \leq 1$. *From* (7.14), (7.16), (7.20) *and* (7.21) *since* $\|\delta\mathcal{F}[u_n]\|_{H^{-2}_{\#}(\Omega)} \to 0$, *for large enough* n *the conditions* (7.12) *and* (7.13) *will be satisfied for any* $C_n > \delta + \epsilon$. *Therefore, in the asymptotic regime, only* (7.11) *is required for stability (as we can choose* $\epsilon \leq 3\|u_n\|^2_{L^\infty(\Omega)}$ *since* $|\bar{u}| \leq \|u_n\|_{L^\infty(\Omega)}$*) which justifies the initial choice of* C_n *in line (2) of Algorithm 7.1.1.*

7.3 Convergence to Equilibrium

We are able to prove that the sequence $\{u_n\}$ generated by Algorithm 7.1.1 is compact using a similar method to Lemma 5.3.2.

Lemma 7.3.1. *For all* $n \in \mathbb{N}$, $n \geq 1$ *the terms of the sequence* u_n *defined by Algorithm 7.1.1 are bounded in* $H^4(\Omega)$. *That is for* $\eta_n = u_n - \bar{u}$ *in the case* $n \geq 1$ *we have* $\sup_{n\in\mathbb{N}} \|\eta_n\|_{H^4_{\#}(\Omega)} < \infty$ *and thus the sequence* $\{\eta_n\}_{n\in\mathbb{N}, n\geq 1}$ *is compact in* $H^2_{\#}(\Omega)$.

Proof. Let $\chi = 0$ for the SH case and $\chi = 1$ for the PFC case and define

$$H_1 := C_n I + \frac{(-\Delta)^{-\chi}}{\tau}.$$

From (7.14), (7.16), (7.20) and (7.21) we have that, for $0 < \epsilon \leq 1$, there exists $c_3(\|\delta\mathcal{F}[u_n]\|_{H^{-2}_{\#}(\Omega)}) \geq 0$ such that (7.12) and (7.13) are satisfied if $C_n \geq \delta + \epsilon + c_3$. Using (7.11) we have that the Armijo condition (7.8) is satisfied if

$$C_n \geq \max(\delta + \epsilon + c_3, 3\|u_n\|^2_{L^\infty(\Omega)} + \delta).$$

Inspecting steps (4) and (5) of Algorithm 7.1.1 we have

$$C_n \leq 2\max(\delta + \epsilon + c_3, 3\|u_n\|^2_{L^\infty(\Omega)} + \delta). \tag{7.22}$$

Therefore, C_n is bounded above and below.

Now (7.1) can be re-written as, $\forall v \in H^2_{\#}(\Omega)$,

$$\langle \Delta u_{n+1}, \Delta v\rangle = -2\langle \Delta u_{n+1}, v\rangle - \langle((1-\delta)I + H_1)u_{n+1}, v\rangle + \langle H_1 u_n, v\rangle - \langle u_n^3, v\rangle. \tag{7.23}$$

Using $\eta_{n+1} = u_{n+1} - \bar{u} \in H^2_{\#}(\Omega)$, we can rewrite this equation as the weak form of $\Delta^2\eta_{n+1} = f_n$ (i.e. (3.14)), where

$$f_n = -2\Delta u_{n+1} - ((1-\delta)I + H_1)u_{n+1} + H_1 u_n - u_n^3. \tag{7.24}$$

We have $u_n \in H^2_{\text{per}}(\Omega)$ for all $n \in \mathbb{N}$, hence $\Delta u_n \in L^2_{\text{per}}(\Omega)$ and $H_1 u_n \in H^2_{\text{per}}(\Omega)$ for all $n \in \mathbb{N}$. Additionally, since $H^2_{\text{per}}(\Omega)$ is a Banach algebra, $u_n^3 \in H^2_{\text{per}}(\Omega)$ for all $n \in \mathbb{N}$. Therefore, we have $f_n \in L^2_{\text{per}}(\Omega)$ for all $n \in \mathbb{N}$.

We now use Lemma 3.3.2 to obtain $u_{n+1} - \bar{u} \in H^4_\#(\Omega)$ for all $n \in \mathbb{N}$. Therefore for $n \geq 1$ we have $u_n \in H^4_{\bar{u}}(\Omega)$.

Given (3.8), (7.17), (7.22), that $H^2(\Omega)$ is a Banach algebra, and (7.24), there exists a constant $c_4(\|u_n\|_{H^2(\Omega)})$ such that $\|f_n\|_{L^2(\Omega)} \leq c_4$.

From (3.7), for a fixed domain size $|\Omega|$, $\mathcal{F}[u_{n+1}] \leq \mathcal{F}[u_n]$ implies $\|u_{n+1}\|_{H^2(\Omega)} \leq \|u_n\|_{H^2(\Omega)}$. The fact the energy is reducing follows from (7.8), therefore we know that $\|u_n\|_{H^2(\Omega)} \leq \|u_0\|_{H^2(\Omega)}$ for all $n \in \mathbb{N}$. Hence we have a uniform bound for f_n that is there exists a constant $c_5(\|u_0\|_{H^2(\Omega)})$ such that

$$\|f_n\|_{L^2(\Omega)} \leq c_5 \qquad n \in \mathbb{N}.$$

Using this bound from (7.23) and Lemma 3.3.2 we have a uniform bound on the H^4-seminorm of u_n for all $n \in \mathbb{N}$ and since we already have a uniform bound on $\|u_n\|_{H^2(\Omega)}$ for all $n \in \mathbb{N}$ we now have a uniform bound on $\|u_n\|_{H^4(\Omega)}$ for all $n \in \mathbb{N}$.

By the compact embedding of $H^4_{\bar{u}}(\Omega)$ in $H^2_{\bar{u}}(\Omega)$, the sequence $\{u_n\}_{n\in\mathbb{N},n\geq 1}$ is compact in $H^2_{\bar{u}}(\Omega)$. □

The results that we have obtained in this chapter mean that we are now in a position to use Lemma 6.3.2 to obtain convergence rates for the sequence $\{u_n\}_{n\in\mathbb{N}}$ given by Algorithm 7.1.1, that is part (b) of Theorem 7.1.3.

Proof of Theorem 7.1.3 (b)

Proof. We use Lemma 6.3.2. We have three conditions to prove. The first is compactness of the sequence $\{u_n\}_{n\in\mathbb{N}}$ in $H^2_{\bar{u}}(\Omega)$ which, since we are only interested in the $n \to \infty$ limit, follows from Lemma 7.3.1. The second condition is a lower bound for the difference in the PFC functional evaluated at successive elements of the sequence $\{u_n\}_{n\in\mathbb{N}}$ in terms of the H^2-norm of the difference of these elements, i.e. (6.15), this is just the statement (7.9). The final condition to check is an upper bound for $\|\delta\mathcal{F}[u_n]\|_{H^{-2}_\#(\Omega)}$ in terms of the H^2-norm of the difference between successive iterates u_{n+1} and u_n, i.e. (6.16). From Proposition 6.2.2 we have $\|v_n\|_{H_{\mathrm{con},n}} = \|\delta\mathcal{F}[u_n]\|_{H^{-1}_{\mathrm{con},n}}$, the lower bound (7.6) and the upper bound (7.4) together with the fact that τ is constant then give us (6.16). □

7.4 Conclusion

In this chapter we developed a variation on a numerical method proposed in [EW13] for obtaining the solution of **(P)** (page 37). We obtained energy stability and convergence results for this method using similar techniques to in Chapter 6. We also showed that this scheme can be formulated as a semi-discrete gradient flow in a norm equivalent to the H^2-norm. We therefore note that the methods of Chapters 6 and 7 are qualitatively very similar.

Chapter 8

Implementation

In this chapter we describe an implementation of Algorithms 6.1.1 and 7.1.1 introduced in Chapters 6 and 7. We first introduce the pseudo-spectral method, which we will use to discretise our algorithms in space, and review the associated notation. We then describe the implementation of the fully discrete schemes on some test problems. For all simulations undertaken in this thesis we use MATLAB. We look at the convergence of the schemes with respect to the number of spatial grid points and investigate a striking issue that arises when the number of grid points is low. Finally we consider the convergence of the residual with domain size.

8.1 Spatial Discretisations

Having discussed several methods of time discretisation in Chapters 6 and 7 we now proceed with the discretisation in space. Space discretisation is necessary in order to implement our algorithms computationally and therefore be able to numerically compare the different time discretisation. For the purpose of clarity we will confine ourselves to two space dimensions. Formulations in three space dimensions are completely analogous and we show basic three dimensional simulations in Section 9.3.

As a first stage recall the periodic domain we introduced in Chapter 3, that is

$$\Omega = (0, L_x) \times (0, L_y)$$

where L_x and L_y are integer multiples of the length of the unit domain in the x and y directions.

We let a be the unit length in the x-direction, i.e. the difference between two areas of high density (which we call atoms) along the x-direction. We expect the minimum solution will be a periodic triangular lattice. We consider the periodic cubic unit cell (see Figure 8.1a), i.e. the minimal rectangular subset of the lattice (henceforth we call this the unit cell). Since we know this is the unit cell of a triangular lattice, we can see the difference

between two successive atoms along the y-axis is $\sqrt{3}a$ (the source of this $\sqrt{3}$ scaling can be seen in Figure 8.1b, the distance between two rows of atoms can be seen to be twice the height of an equilateral triangle of side length a, which is $(\sqrt{3}/2)a$ by Pythagoras' theorem). Hence the unit domain can be written as

$$\Omega_{\text{uc}} = (0, a) \times (0, \sqrt{3}a). \tag{8.1}$$

We also wish to consider larger domains. It is clear that any domain composed of an integer number of unit cells in the x- and y-directions has the right periodicity. We wish our domains to be roughly square therefore, since $\sqrt{3}/2 \approx 0.87$, we take half the number of unit domains in the y-direction that we take in the x-direction. We therefore define our domain, for an even integer L, by

$$\Omega_L = L(0, a) \times \frac{L}{2}(0, \sqrt{3}a). \tag{8.2}$$

For convenience we define Ω_1 as the unit cell that is $\Omega_1 = \Omega_{\text{uc}}$.

We now wish to discretise the domains. Since $L/2 \in \mathbb{N}$, we can see that, if we discretise the unit cell (8.1) we can translate this discretisation to the general domain (8.2). For the unit cell we take the number of grid points to be

$$(N, M)$$

where $N \in 2\mathbb{N}$ is the number of spatial grid points along the x-axis and considering (8.1) we define $M = 2\left\lceil \sqrt{3}N/2 \right\rceil$. We require M and N to be powers of 2 in order to obtain the $\mathrm{O}(N \log N)$ computation time of MATLAB's FFT function (a similar point is made on [Tre00, page 24]).

Using N and M we now define the grid spacing along the x- and y-axes by

$$h_x = \frac{a}{N}, \qquad h_y = \frac{\sqrt{3}a}{M}.$$

A co-ordinate point in our discrete domain is now given by (x_i, y_j) where $i, j \in \mathbb{N}$ and $x_i = ih_x$ and $y_j = jh_y$.

Having defined a discrete domain we can now introduce our method of obtaining a spatially discrete approximation.

Due to the C^∞-regularity (possibly even analyicity) of equilibria (see Lemma 3.3.3, we discuss this issue more in Subsection 8.2.2), and the periodic boundary conditions we use Fourier spectral methods. We also recall that the Fourier transform diagonalises the Laplace operator (see (8.4)) which makes this method particularly convenient.

Because we have chosen a different scaling between the x-axis and the y-axis in the case of the unit cell (8.1) as compared to the scaling used for the general domain (8.2) we

define a new function M' where

$$LM' = \begin{cases} M, & L = 1 \text{ (unit cell)} \\ \frac{LM}{2}, & L > 1. \end{cases}$$

Since we have imposed periodic boundary conditions we know that our Fourier modes are integers. To correspond to our discretisation of the domain we have the following conditions on the two modes

$$\begin{aligned} -\frac{LN}{2} + 1 \leq & k_1 \leq \frac{LN}{2} \\ -\frac{LM'}{2} + 1 \leq & k_2 \leq \frac{LM'}{2} \end{aligned}$$

where we note that we have chosen $N, M \in 2\mathbb{N}$.

We can now define a basis for our approximations,

$$\varphi_{k_1,k_2}(x_i, y_j) = \exp\left(2\pi i \left(\frac{1}{a} k_1 x_i + \frac{1}{\sqrt{3}a} k_2 y_j\right)\right),$$

where $x_i = ih_x$ for $i \in [0, LN]$, $y_j = jh_y$ for $j \in [0, LM']$.

Following the one-dimensional example of [Tre00, Equations (3.2) and (3.3)] and the equal-axis (i.e. $N = M$) example of [CHQZ88, Equation (9.7.6)] we can define the discrete Fourier transform of u and then use this to give the spectral approximation of u ([LSL15, Equation (6)] uses the same form but rescaled by $1/h_x h_y$). That is,

$$\begin{aligned} \hat{U}(k_1, k_2) &= h_x h_y \sum_{i=1}^{LN} \sum_{j=1}^{LM'} u(x_i, y_j) \overline{\varphi_{k_1,k_2}(x_i, y_j)} \\ U(x_i, y_j) &= \frac{2}{\sqrt{3}a^2 L'^2} \sum_{-\frac{NL}{2}+1 \leq k_1 \leq \frac{NL}{2}} \sum_{-\frac{LM'}{2}+1 \leq k_2 \leq \frac{LM'}{2}} \hat{U}(k_1, k_2) \varphi_{k_1,k_2}(x_i, y_j) \end{aligned} \tag{8.3}$$

where

$$L' = \begin{cases} \sqrt{2} & \text{for the unit cell} \\ L & \text{for the general domain.} \end{cases}$$

We note the difference between the solution evaluated at the discrete points $u(x_i, y_j)$ in the first line of (8.3) and the discrete approximation $U(x_i, y_j)$ in the second line of (8.3).

As noted in [Tre00, Page 24] for the purposes of implementation, in our notation, MATLAB stores wavenumbers in the order 0,1, ..., $LN/2$, - $LN/2$ +1, - $LN/2$ +2, ...,-1.

Henceforth we choose our iterates U_n from the set S_N (see [CHQZ88, Equation (9.7.2)] and Lemma 4.3.2) defined by, $k_1, k_2, i, j \in \mathbb{N}$, $i \in [0, LN]$, $j \in [0, LM']$

$$S_N = \text{span}\left\{ \varphi_{k_1,k_2}(x_i, y_j) \,\middle|\, \begin{array}{c} -LN/2 + 1 \leq k_1 \leq LN/2, -LM'/2 + 1 \leq k_2 \leq LM'/2, \\ x_i = ih_x, y_j = jh_y \end{array} \right\}.$$

Differentiation in real space then becomes multiplication by polynomials of k in Fourier space (see [Tre00, page 23]) which is a reason for choosing the method.

Following [EW13, Section 4.2] we wish to define the discrete analogues of the energy and some of the norms introduced in Chapters 3, 6 and 7.

Definition 8.1.1 (The Discrete Inner Product and L^p-norms)**.** *For simplicity we index our inner-products and norms by N where implicitly they depend on N and L.*

Consider two $LN \times LM'$ matrices, U and V. The discrete inner product is given by

$$(U,V)_N = h_x h_y \sum_{i=1}^{LN} \sum_{j=1}^{LM'} U(x_i, y_j) V(x_i, y_j)$$

where $x_i = ih_x$, $y_j = jh_y$.

The discrete L^p-norm for $1 \leq p < \infty$ are given by (see [EW13, Equations (4.5)-(4.6)])

$$\|U\|_{L_N^p}^p = (|U|^p, I)_N\,, \qquad \text{where } I \text{ is the } LN \times LM' \text{ identity matrix}$$

and for $p = \infty$ we have

$$\|U\|_{L_N^\infty} = \max_{i,j} |U(x_i, y_j)|.$$

The application of the Laplacian in discrete space can be obtained through the discrete Fourier transform using (8.3),

$$\begin{aligned} &\Delta U(x_i, y_j) \\ &= -\frac{2}{\sqrt{3}a^2 L'^2} \left(\frac{2\pi}{a}\right)^2 \sum_{-\frac{NL}{2}+1 \leq k_1 \leq \frac{NL}{2}} \sum_{-\frac{LM'}{2}+1 \leq k_2 \leq \frac{LM'}{2}} \left(k_1^2 + \frac{k_2^2}{3}\right) \hat{U}(k_1, k_2) \varphi_{k_1,k_2}(x_i, y_j). \end{aligned} \tag{8.4}$$

Next, we define the discrete energy, as in [EW13, Equation (4.11)].

Definition 8.1.2 (Discrete PFC Functional)**.**

$$\mathcal{F}_N[U] = \frac{1}{2}\|\Delta U + U\|_{L_N^2}^2 - \frac{\delta}{2}\|U\|_{L_N^2}^2 + \frac{1}{4}\|U\|_{L_N^4}^4.$$

Again, implicitly $\mathcal{F}_N$ depends on the domain size L.

By direct analogy with Lemma 3.1.4, we can define the discrete first and second variations, $\langle \delta \mathcal{F}_N[U], V\rangle$ and $\langle \delta^2 \mathcal{F}_N[U]V, V\rangle$.

By analogy, with Definition 7.1.1 we define the discrete convex-concave splittings.

Definition 8.1.3 (Discrete Convex-Concave Splitting)**.**

$$\mathcal{F}_N[U] = \mathcal{F}_{C,C_n}^N[U] - \mathcal{F}_{E,C_n}^N[U],$$

where, for $C_n > 0$, we have

$$\mathcal{F}^N_{\mathrm{C},C_n}[U] = \frac{1}{2}\|\Delta U + U\|^2_{L^2_N} - \frac{\delta}{2}\|U\|^2_{L^2_N} + \frac{C_n}{2}\|U\|^2_{L^2_N},$$
$$\mathcal{F}^N_{\mathrm{E},C_n}[U] = \frac{C_n}{2}\|U\|^2_{L^2_N} - \frac{1}{4}\|U\|^4_{L^4_N}.$$

Again, implicitly these functionals depend on the domain size L.

Finally we define the discrete analogue of the $A^{(n)}$-norm defined in Definition 6.1.1.

Definition 8.1.4 (Discrete $A^{(n)}$-norm)**.**

$$\|U\|^2_{A^{(n)}_N} = \|\Delta U + U\|^2_{L^2_N} + \gamma_n\|U\|^2_{L^2_N}$$

where for $\gamma_{\min} > 0$ we have

$$\gamma_n = \max\left(\gamma_{\min}, 3\overline{U_n^2} - \delta\right).$$

Again, implicitly this norm depends on the domain size L. For $v \in H^{-2}(\Omega)$ we denote the inverse norm by

$$\|v\|_{N,n} = \|v\|_{\left(A^{(n)}_N\right)^{-1}}. \tag{8.5}$$

Remark 8.1.1. *Using this form of spatial discretisation one should be able to prove convergence results for the fully discrete scheme that are analogous to the results we obtained for the time discrete schemes in Theorems 6.1.1 and 7.1.3. Since the focus of this thesis is time discretisation we don't address this issue.*

8.2 Review of Time Discretisations

We now consider the numerical implementation of the discrete versions of Algorithms 6.1.1 and 7.1.1. We will first consider methods of ensuring convergence through the choice of C_n for the PFC and Swift-Hohenberg algorithms and through the choice of τ_n for the H^2-gradient flow based algorithm. Finally we use some simple numerical tests to compare the methods outlined above and to choose an appropriate point to terminate the resulting algorithms.

8.2.1 Adaptive Convex-Concave Splitting

The proof of [EW13, Theorem 2.1] and Theorem 7.2.1 show that if the constant C_n is large enough then Algorithm 7.1.1 is well-defined. However, for the purposes of numerical simulations we require a way to calculate an initial estimate for C_n. It is important to try to optimise C_n as numerical tests suggest the larger the value of C_n the slower the rate of convergence (which is also suggested by [EW13, Theorem 3.1]).

Remark 7.2.1 motivates us to initially choose C_n as

$$C_n = 3\|U_n\|^2_{L^\infty_N} + \delta. \tag{8.6}$$

In the numerical simulations we undertake the initial choice of C_n (8.6) already ensures energy decrease except in the case, given in Section 9.2, of random initial conditions on a large domain. Even in the case of Section 9.2 the choice (8.6) ensures energy decrease down to a residual of approximately 10^{-6}.

We can see that for this numerical implementation the only change we need to make to Algorithm 7.1.1 is discretisation in space. Hence, in the remainder of the thesis, when we refer to Algorithm 7.1.1 we implicitly mean the discrete in space version of this algorithm.

8.2.2 Exponential Convergence

From [Tre00, Chapter 4] we know that for analytic functions we would obtain exponential convergence of the spectral approximation and for C^∞ functions the order of convergence is super-algebraic. We know from Lemma 3.3.3 that the solution to the problem **(P)** (page 37) is C^∞; however, we do not prove that the solution is analytic. Nevertheless, the numerical test shown in Figure 8.2 suggest exponential convergence of the energy.

For our first numerical simulations the basic test environment we use is the rectangular unit cell (8.1). This test environment is shown below in Figure 8.1a.

Figure 8.1

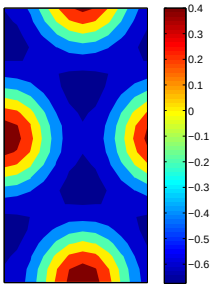

(a) We show the unit cell for $\delta = -\bar{u} = 0.3$. This is generated using the Swift-Hohenberg equation on the initial condition given in (8.11).

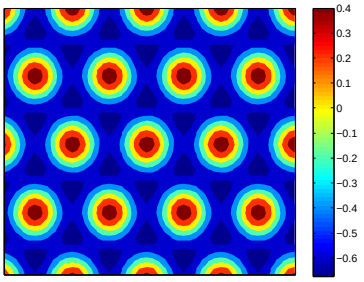

(b) We show four unit cells (i.e. the domain Ω_4 given by (8.2)) for $\delta = -\bar{u} = 0.3$. This is also generated using the Swift-Hohenberg equation on the initial condition given in (8.11). From this diagram we can more easily see the triangular form of the lattice.

We can see the convergence of the difference between minimum of the discrete PFC functional $\mathcal{F}_N[U]$ at N and at $N = N + 2$ against the number of grid points in Figure 8.2, which appears to be exponential. The increase near the end is probably due to the energy

difference stagnating because we have reached computational accuracy.

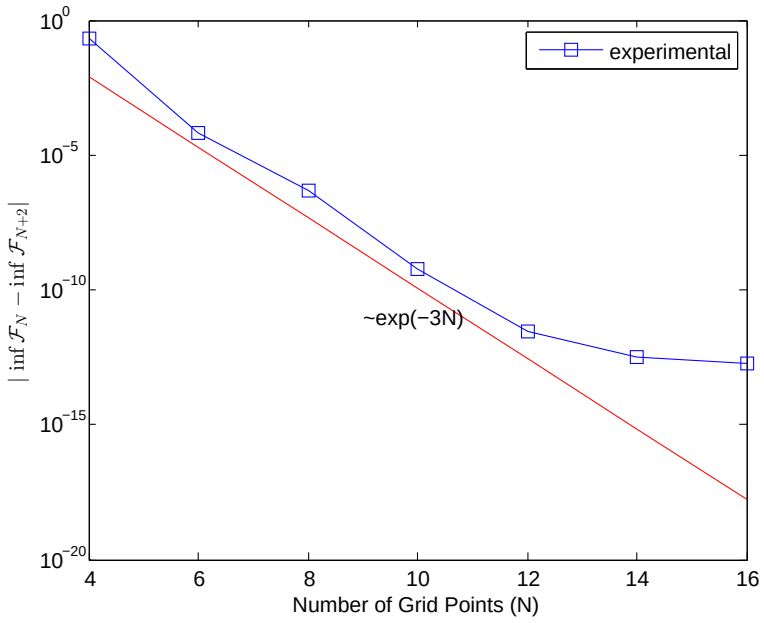

Figure 8.2: We show the reduction of energy with grid points. The error is calculated by finding the difference between the energy of the minimiser at N grid points and the energy of the minimiser at $N+2$ grid points. The decline in error appears to be roughly exponential. An exponential reduction is shown as a guide to the eye.

8.2.3 Line Search Method

We consider the case of the H^2-gradient flow based approach of Chapter 6. As mentioned in Subsection 6.1.3, we wish to improve the time-step selection in Algorithm 6.1.1. We make two changes, first we change the initial choice of τ in line (2) and secondly we change how we update τ in line (5).

We consider the case where in line (2) the initial choice of τ is motivated by the value of τ at the previous time-step. Our initial choice of τ_n is motivated by [NW06, Page 59]. Specifically, we initialise the line search with

$$\tau_n = \begin{cases} \min\left(1, \frac{1}{\|\delta\mathcal{F}_N[U_0]\|_{N,0}}\right) & \text{if } n = 0 \\ \tau_{n-1} \frac{\|\delta\mathcal{F}_N[U_{n-1}]\|_{N,n}}{\|\delta\mathcal{F}_N[U_n]\|_{N,n-1}} & \text{otherwise,} \end{cases} \tag{8.7}$$

where the dual norm is defined through (8.5).

To find a suitable τ we could use a back-tracking approach (e.g. [NW06, Algorithm 3.1]) or a more sophisticated cubic interpolation (see for example [NW06, Section 3.5]). In the numerical simulations below, we choose the cubic interpolation, that is, at each iterate

of the line search loop we update τ_n using

$$\tau_n \leftarrow \tau_n - \tau_n \left(\frac{\langle \delta\mathcal{F}_N[U_n + \tau_n V_n], \delta\mathcal{F}_N[U_n] \rangle_{N,n} + h_2 - h_1}{\langle \delta\mathcal{F}_N[U_n + \tau_n V_n], \delta\mathcal{F}_N[U_n] \rangle_{N,n} - \|\delta\mathcal{F}_N[U_n]\|^2_{N,n} + 2h_2} \right) \tag{8.8}$$

where

$$h_1 = \|\delta\mathcal{F}_N[U_n]\|^2_{N,n} + \langle \delta\mathcal{F}_N[U_n + \tau_n V_n], \delta\mathcal{F}_N[U_n] \rangle_{N,n} - \frac{3\left[\mathcal{F}_N[U_n + \tau_n V_n] - \mathcal{F}_N[U_n]\right]}{\tau_n},$$
$$h_2 = \sqrt{h_1^2 - \langle \delta\mathcal{F}_N[U_n + \tau_n V_n], \delta\mathcal{F}_N[U_n] \rangle_{N,n} \|\delta\mathcal{F}_N[U_n]\|^2_{N,n}}$$

and again the dual norm is defined through (8.5).

In Chapter 6 we showed that the back-tracking method is sufficient to ensure stability; however, we obtain faster convergence by using the cubic interpolation method, see Figure 8.4. For convenience we now state the cubic line search algorithm we will use throughout the rest of this thesis. Again δ and $\bar{u}$ are fixed constants.

Algorithm 8.2.1.

(0) INPUT $U_0, \gamma_{\min} > 0, 0 < \Theta < 1/2$
(1) FOR $n = 0, 1, 2, \ldots$
(2) $\quad \gamma_n = \max\left(\gamma_{\min}, 3\overline{U_n^2} - \delta\right)$
(3) $\quad$ INITIALISE τ_n using (8.7)
(4) $\quad$ UPDATE $V_n = -\left(A_N^{(n)}\right)^{-1} \Pi\delta\mathcal{F}_N[U_n]$
(5) $\quad$ WHILE $\mathcal{F}_N[U_n + \tau_n V_n] > \mathcal{F}_N[U_n] - \Theta\tau_n \|\delta\mathcal{F}_N[U_n]\|^2_{N,n}$
(6) $\quad\quad$ UPDATE τ_n using (8.8)
(7) $\quad U_{n+1} = U_n + \tau_n V_n$

Π in line (4) is defined by

$$\Pi d := d - \fint_\Omega d \mathrm{d}x \tag{8.9}$$

and the dual norm in line (5) is defined through (8.5).

Motivated by (6.1) with $H = A$ we want to consider the effect of the constant γ on the rate of convergence. We define the constant γ as a function of u, i.e.

$$\gamma(u) = 3\overline{u^2} - \delta. \tag{8.10}$$

Definition 6.1.1 and (3.10) suggest that our choice for γ should be $\gamma = \gamma(u^*)$ where u^* is the solution to **(P)** (page 37). Obviously, we can not know a priori what u^* is. As an

approximation to u^* we use the one mode solution of the PFC equation (see for example [EG04, Equation (37)]), that is

$$u_{\text{om}}(x,y) = -\frac{4}{5}\left(|\bar{u}| + \frac{1}{3}\sqrt{15\delta - 36\bar{u}^2}\right)\left(\cos\left(\frac{2\pi y}{a}\right)\cos\left(\frac{2\pi x}{a\sqrt{3}}\right) - 0.5\cos\left(\frac{4\pi x}{a\sqrt{3}}\right)\right) + \bar{u} \tag{8.11}$$

where again a is the unit length along the x-axis. The one mode solution lets us define the fixed value of γ, $\gamma_{\text{om}} = \gamma(u_{\text{om}})$ which can be shown to be positive.

The performance of an algorithm is measured using the number of fast Fourier transforms (FFTs) as we expect this to be the slowest process in our algorithms if they are fully optimised. We do not use the iteration number as in Algorithm 7.1.1 the while loop (line (4)-(6)) may be very expensive since we may have to continually solve (7.3). Also we will introduce a trust region (Algorithm E.1.1) which requires us to solve a sub-problem (Definition E.0.1) at each iteration which can be very expensive. To clarify this issue for the complex domain simulations (Subsection 8.2.6) and random initial condition simulations (Section 9.2) we reproduce the convergence plots Figure 8.9 and 9.6 with time measured in iteration number. For these simulations we also show that for the trust region algorithms the number of FFTs per iteration changes dramatically. Since we are looking for critical points, i.e. $\|\delta\mathcal{F}[u]\|_{H^{-2}_{\#}(\Omega)} = 0$, we consider the residual, i.e.

$$\|\delta\mathcal{F}_N[U_n] - \overline{\delta\mathcal{F}_N[U_n]}\|_{L^\infty_N}$$

and look for values of U_n where this residual is small. We use the L^∞-norm as this norm is independent of the domain size, is relatively easy to compute, and is also independent of the numerical discretisation choice.

In Figure 8.3 we show the decrease of the residual plotted against the number of fast Fourier transforms for $\gamma = \gamma_{\text{om}}$, $\gamma = 1$ and γ adaptive as in Definition 6.1.1. We start on a unit domain with random initial conditions given by $\text{rand}(x,y) - 0.5 + \bar{u}$ and set $N = 16$. As noted in Remark 4.2.4 the rate of convergence for $\gamma = \gamma_{\text{om}}$ constant is similar to the rate of convergence for adaptive γ but slightly slower.

8.2.4 Choice of Line Search Algorithm

We wish to justify our choice of algorithms by comparing the speed of convergence for a test problem on a small domain.

Specifically, we wish to show that the line search algorithm (Algorithm 8.2.1) is a good choice. To do this we will compare Algorithm 8.2.1 to its analogue where line (6) is replaced by a back-tracking scheme (i.e. $\tau_n \leftarrow \tau_n/2$) or by a quadratic approximation (see [NW06, Equation (3.58)]). Finally we will compare these three line search algorithms to their analogues with line (2) replaced by $\gamma_n = \gamma_{\text{om}}$ for all n.

To compare these algorithms we look at the rates of convergence of the different

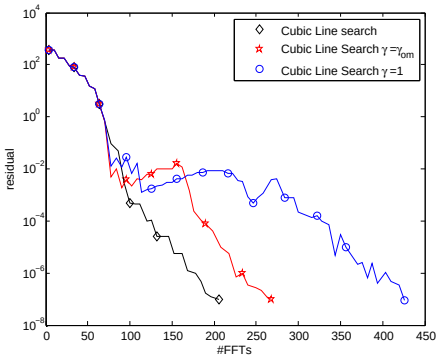

Figure 8.3: Residual of the solution against number of FFTs, from random initial conditions on a unit cell, using adaptive γ, $\gamma = \gamma_{\text{om}}$ and $\gamma = 1$. For $N = 16$ and residual tolerence 10^{-7}.

algorithms detailed above against the number of grid points. We take the initial number of grid points to be 12, this will be justified in the next subsection. We start with random initial conditions generated by the MATLAB function rand, i.e. rand$-0.5 + \bar{u}$. The same initial conditions are used for all methods. We use the same termination criterion for all algorithms,

$$\left\|\delta\mathcal{F}_N - \overline{\delta\mathcal{F}_N}\right\|_{L_N^\infty} \leq 10^{-7}. \tag{8.12}$$

For more stringent termination criteria, numerical round-off prevents us from checking the Armijo condition. Hence this is the lowest residual tolerance we can sensibly use. We show the number of FFTs required to satisfy (8.12) against grid size for the different line search algorithms in Figure 8.4.

We can see, from Figure 8.4, that for all the methods of interpolating τ_n choosing an adaptive γ_n rather than a fixed γ leads to a reduction in the number of FFTs required to converge. Therefore, henceforth, we always use an adaptive γ_n. We can also see, from Figure 8.4, that the cubic interpolation is generally better than the other interpolation methods. Also, since calculating the energy and the first variation can be done at the same cost (in fast Fourier transforms) as just calculating the PFC functional, there is no real disadvantage in using the cubic interpolation over using the quadratic interpolation.

Therefore, for the numerical simulations undertaken in the rest of this thesis we chiefly consider three algorithms:

- Algorithm 8.2.1 for the line search method, with the cubic interpolation of [NW06, Section 3.5]
- the discrete form of Algorithm 7.1.1 with $H = L^2(\Omega)$ for the Swift-Hohenberg case,
- the discrete form of Algorithm 7.1.1 with $H = H^{-1}(\Omega)$ for the PFC case.

In the next section we encounter an issue with the number of grid points which leads us to

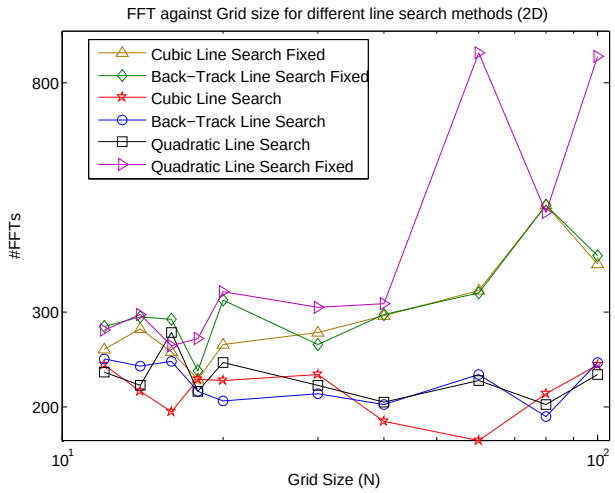

Figure 8.4: Number of FFTs required for convergence of the solution against grid size, starting from random initial conditions, using the six line search methods generated from Algorithms 8.2.1 by fixing $\gamma_n = \gamma_{\text{om}}$ and replacing line (6) by a back tracking or quadratic interpolation. For fixed residual tolerence 10^{-7}.

introduce a trust region algorithm (Algorithm E.1.1) which will we also include in all the remaining simulations.

In the simulations of Chapter 9 we will include simulations using Algorithm 8.2.1 with $\gamma_n = \gamma_{\text{om}}$ for all $n \in \mathbb{N}$ in line (2) to justify the assertions of Subsection 6.1.2.

8.2.5 Convergence with Number of Grid Points

We now wish to compare the speed of convergence for the Algorithms 7.1.1 and 8.2.1 against the number of grid points. We use exactly the same test problem as detailed in Subsection 8.2.4 with the termination criterion (8.12). However, as well as comparing the different algorithms, we also start from a lower number of grid points, that is $N = 4$. The results are shown in Figure 8.5.

We can see that for all the methods there is a drastic increase in the number of FFTs when the number of grid points is small. This is the justification for starting at $N = 12$ for Figure 8.4. To demonstrate that this issue can not be resolved simply by using the full second variation we also tested a trust region method. More detail on the trust region method used is given in Appendix E. The trust region algorithm, Algorithm E.1.1, is also shown in Figure 8.5 and this demonstrates that for this method we still encounter the same effect. For the purposes of comparison we include this algorithm in all the remaining simulations.

We believe this "divergence" occurs because the translational invariance of the PFC functional is broken by the discretisation. The translational invariance of the original PFC

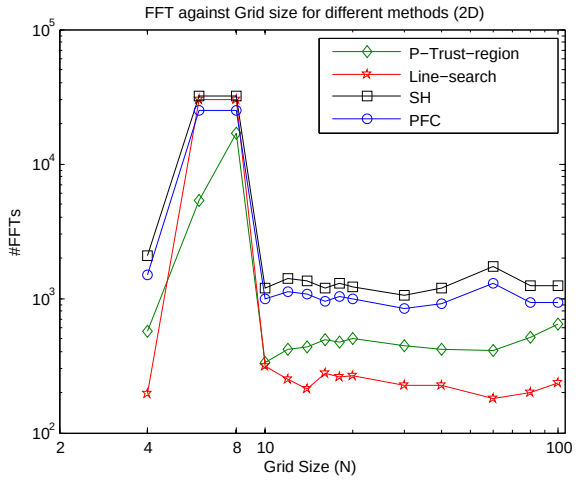

Figure 8.5: Number of FFTs required for convergence of the solution against grid size, starting from random initial conditions, using the four different methods described in Algorithms 7.1.1, 8.2.1 and E.1.1. For fixed residual tolerence 10^{-7}.

functional follows from Appendix B.The discretised PFC functional therefore has a minimum associated with each of the grid points, while between each minimum there lies a saddle. As the number of points grows the energy barrier between minima becomes smaller (and eventually vanishes at the continuum) therefore the oscillation between different states ceases to be an issue. The existence of a saddle point and the dependence of its energy on the number of grid points are shown in the figure below, Figure 8.6a. We take one converged solution U and translate all the points by one grid point U_T, we then plot the energy of the linear combination of the two solutions $tU + (1-t)U_T$ against $t \in (0, 1)$. We plot the figure for 6, 8 and 10 grid points.

We see that the initial minimum and the perturbed solution have the same energy and that between them lies a saddle. We also see that the saddle is less pronounced for higher numbers of grid points as suggested in the previous paragraph. The second figure, Figure 8.6b, shows that the difference between successive maxima of the interpolation declines with the number of grid points. Since we interpolate between two minima we do not necessarily find the true saddle and hence the decline in energy difference is not exponential.

The "divergence" in the number of FFTs when the number of grid points is low can be treated in several ways. The first and most obvious method is to take the number of grid points to be large enough so that this problem never occurs, e.g. greater than ten (this is what we did in Subsection 8.2.4). The issue with only using a relatively large number of grid points is that we wish to consider large domain sizes and if we require ten grid points on the x-axis per unit cell, which is much larger than the minimum required (at least two according to [Tre00, page 67]), then calculations especially in three dimensions will be very

Figure 8.6

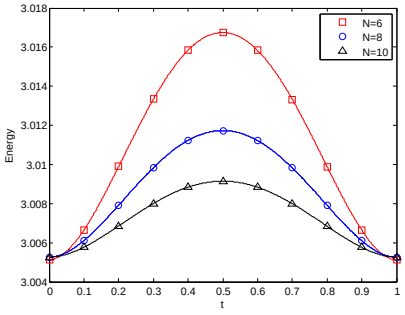

(a) Energy of the linear combinations of the initial minima U and translated minima U_T, $tU + (1-t)U_T$ against the linear parameter t in 2D. We plot the results for 6, 8 and 10 grid points.

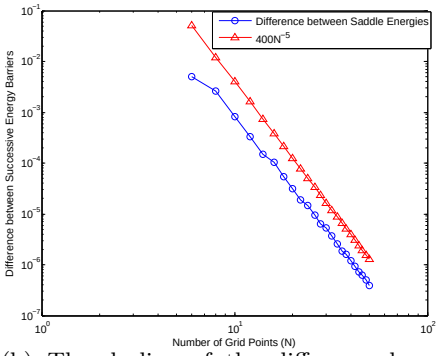

(b) The decline of the difference between successive maxima of the interpolation between two minima. Since we use an interpolation we do not necessarily find the true saddle so the decline is not necessarily exponential.

computationally expensive. A second possible solution and the one we adopt in this chapter is to choose the residual tolerance large enough so that the algorithm terminates before an accuracy where the saddle affects the iteration. The obvious disadvantage of increasing the residual tolerance we terminate the algorithm at when the number of grid points is low is that it affects the accuracy of the solution.

To negate this issue of accuracy we choose the residual we converge at to get smaller with increasing number of grid points until the residual becomes so small that the energy change reaches computational accuracy, i.e. 10^{-7}. Experimentally, we found that

$$\left\|\delta\mathcal{F}_N - \overline{\delta\mathcal{F}_N}\right\|_{L^\infty_N} \leq \max\left(10^{-2} \times \exp\left[-\frac{6}{h_x}\right], 2 \times 10^{-7}\right) \tag{8.13}$$

is a suitable choice.

The corresponding graph is shown in Figure 8.7. We can see that the preconditioned line search method introduced in Chapter 6 scales in a similar way to the other methods. An appropriate choice of parameters could mean the other methods perform substantially better; however, the results here are at least indicative that this method is promising.

From Figure 8.7 we can see that the number of FFTs required for convergence seems to increase with grid size N. This is even the case at high grid point numbers when the upper bound (8.13) is uniformly 2×10^{-7} (this occurs for $h_x < 0.52$ which translates to $N > 14$). We believe that this increase occurs because the fluctuations we have chosen are only bounded uniformly in $L^\infty(\Omega)$ and not necessarily in $H^2(\Omega)$. We therefore repeat this test with random fluctuations that are bounded in $H^2(\Omega)$.

To facilitate quick convergence we start from the equilibrium solution (u^*) to which we then add random fluctuations. To obtain the equilibrium solution we start from an initial

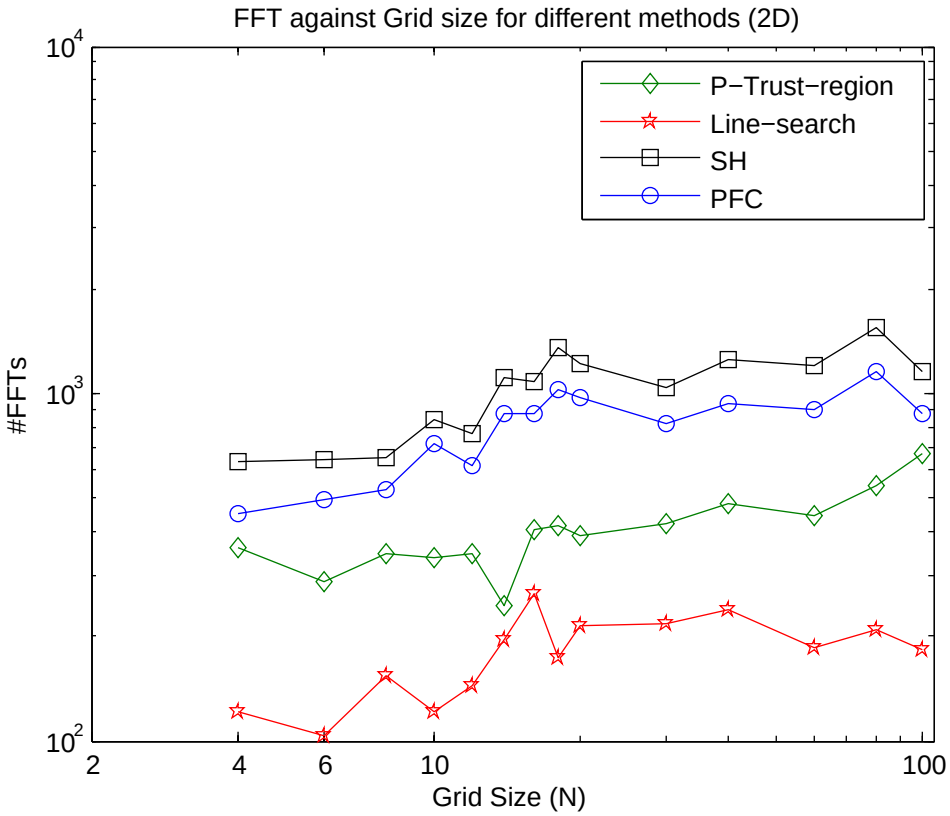

Figure 8.7: Number of FFTs required for convergence of the solution against grid size, from random initial conditions, using the four different methods described in Algorithms 7.1.1, 8.2.1 and E.1.1. For adaptive residual tolerance given by $\max\left(10^{-2} \times \exp\left[-6/h_x\right], 2 \times 10^{-7}\right)$.

condition of the one mode solution (8.11) and run the trust region algorithm (Algorithm E.1.1) until (8.13) is satisfied.

To obtain the random fluctuations we first need to ensure that we are bounded in $H^2(\Omega)$. We start with a scaled random fluctuation in Fourier space, that is

$$\hat{v}(k_1, k_2) = (1 + |k|^2)^{-2}\text{rand}(k_1, k_2). \tag{8.14}$$

We know that $\|v\|_{H^2(\Omega)}$ is an equivalent norm to $\|(1 + |k|^2)\hat{v}\|_{L^2(\Omega)}$ therefore for the scaled random fluctuation given by (8.14) we have $\|v\|_{H^2(\Omega)} \leq C$, for $C > 0$. To ensure the fluctuation is not too large we divide v by its maximum. That is, we define a scaled random H^2-fluctuation

$$\zeta(x, y) = \frac{v(x, y)}{2 \max\limits_{\Omega_L}[v(x, y)]} \tag{8.15}$$

where v is defined through (8.14). We want to mollify this fluctuation to ensure that our initial condition has the right continuity. We use the C^2-mollifier of [Mur12, Page 58],

$$\phi(r) = \begin{cases} -6r^5 + 15r^4 - 10r^3 + 1 & r \in [0,1] \\ 0 & r > 1. \end{cases} \tag{8.16}$$

We want our mollifier to be centred at the middle of our domain. To do this for the domain Ω_L we define the normalised radial distance from the centre of the domain, that is

$$r_{a,L}(x,y)^2 = \left(x - \frac{La}{2}\right)^2 + \left(y - \frac{\tilde{L}\sqrt{3}a}{4}\right)^2$$

where

$$\tilde{L} = \begin{cases} 2 & \text{for the unit cell } (L = 1) \\ L & \text{for the general domain.} \end{cases}$$

To obtain our centred fluctuation we combine the mollifier (8.16) with our fluctuation (8.15). We now modify our equilibrium solution by multiplying u^* by the identity minus our centred fluctuation, that is

$$u_0(x,y) = u^*(x,y)(1 - \phi(r_{a,L})\zeta(x,y)).$$

This solution is essentially equivalent to subtracting some random fluctuations from the centre of the lattice. This means our initial condition is a lattice with a vacancy. To ensure the average is conserved we prescribe the average of u_0 that is

$$\mathfrak{F}[u_0(x,y)](k_1,k_2) = \begin{cases} \bar{u}|\Omega_L| & k_1 = k_2 = 0, \\ \mathfrak{F}[u^*(x,y)(1 - \phi(r_{a,L})\zeta(x,y))](k_1,k_2) & \text{otherwise,} \end{cases} \tag{8.17}$$

where $\mathfrak{F}$ denotes the Fourier transform.

We then rerun the simulation of Figure 8.7 with this initial condition and the adaptive termination criterion (8.13). The results are shown in Figure 8.8. The slight increase for high grid point numbers seems to have disappeared, in fact there seems to be a decrease. This decrease is probably due to the higher resolution of our model when the number of grid points is high. We can see that the algorithms remain in the same order, in terms of FFTs required to reach a minimum, and therefore there is still evidence that the line search is a promising method.

8.2.6 Domain Convergence

We shall now use the new initial condition (8.17) to test the effect of domain size on our algorithms. The initial simulations used to show grid size convergence were taken on the unit cell. We now wish to consider larger domains, i.e. (8.2).

Given the section on grid convergence above (Subsection 8.2.5) we take the number

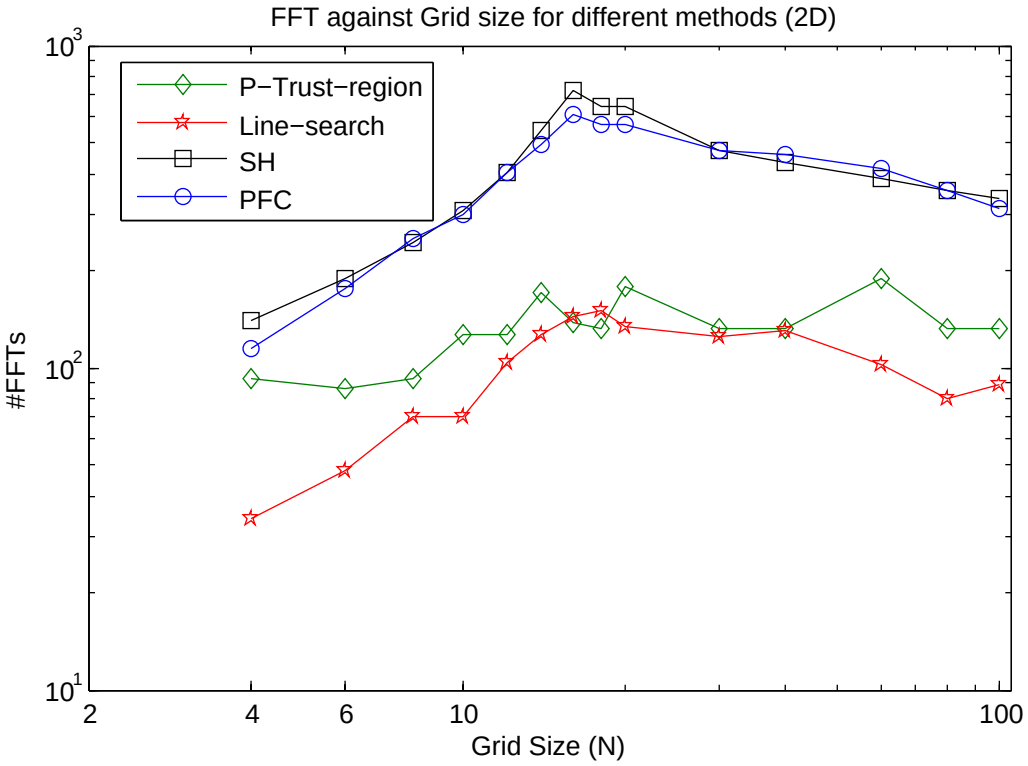

Figure 8.8: Number of FFTs required for convergence of the solution against grid size, from the initial condition (8.17), using the four different methods described in Algorithms 7.1.1, 8.2.1 and E.1.1. For adaptive residual tolerance given by $\max\left(10^{-2} \times \exp\left[-6/h_x\right], 2 \times 10^{-7}\right)$.

of points along the x-axis, N, to be sixteen and the convergence criterion to be (8.13). As remarked above the initial condition is given by (8.17). The results are shown in Figure 8.9.

We can see that the number of FFTs required for the convergence of the solution increases with domain size before plateauing for all methods. All the algorithms seem to plateau between $L = 16$ and $L = 32$. We suspect that the increase in the pre-asymptotic regime is due to resolving the high wavelengths that are not present in a small domain. All four methods scale similarly and again the convex-concave schemes (Algorithm 7.1.1) seem to take an order of magnitude more FFTs than the line search algorithm (Algorithm 8.2.1). We note that the PFC algorithm is significantly slower than the SH algorithm; however it may be that a different choice of parameters would eliminate this effect.

We can see that for all our domains the line search algorithm is significantly faster than the two convex-concave splitting schemes. The line search algorithm and the trust

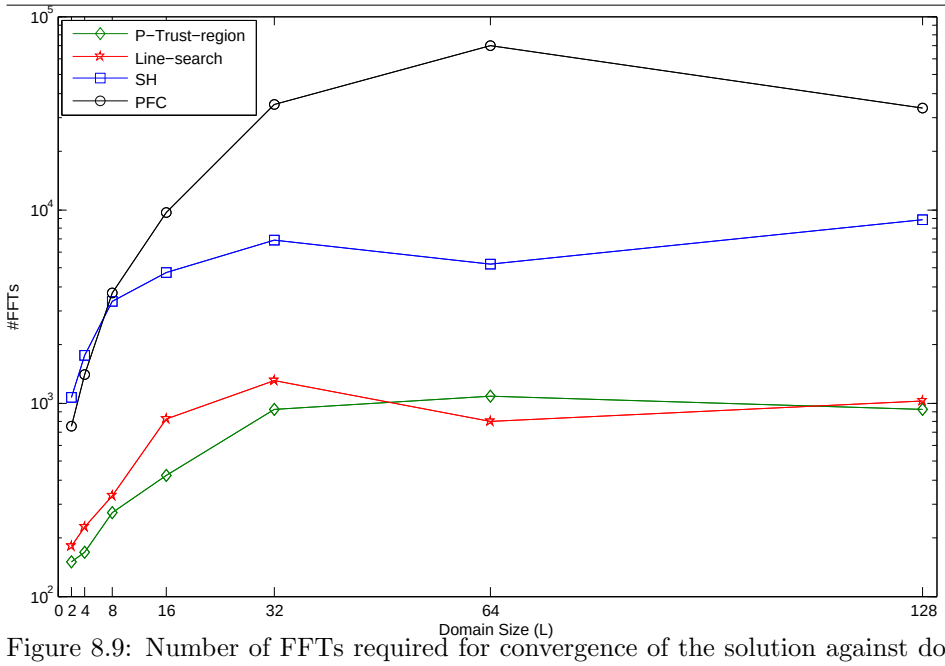

Figure 8.9: Number of FFTs required for convergence of the solution against domain size. The initial condition is given by (8.17) and we use the four different methods described by Algorithms 7.1.1, 8.2.1 and E.1.1. For adaptive residual tolerence (8.13) and $N = 16$.

region algorithm (Algorithm E.1.1) seem to take roughly the same number of FFTs to converge. These two facts demonstrate that the line search maybe a promising alternative scheme for solving problem (**P**) (see page 37). Even though the trust region method seems to be roughly the same speed as the line search algorithm, there is some indication that the line search algorithm may be more reliable. Specifically, we show in Section 9.2 that, in contrast to Algorithm 8.2.1, the trust region method Algorithm E.1.1 fails to reach the expected minima, that is, it behaves qualitatively differently.

In Subsection 8.2.3 we argued that the speed of our algorithms should be measured using the number of FFTs. The domain simulations undertaken above are some of the most complex undertaken in this thesis as the domain size is larger than the one generally used in Chapter 9. Therefore we reproduce these simulations with the speed of our algorithms measured using iteration number (see Figure 8.10a). We can see that the graph is qualitatively similar for all the algorithms except the trust region. To highlight the difference between using the number of FFTs and using the iteration number to measure the speed of convergence we plot the average number of FFTs per iteration (see Figure 8.10b). We can see that the number of FFTs per iteration is constant for the line search algorithm. We would expect this as the only difference between iterations is the amount of time spent in the while loop (lines (5) and (6) of Algorithm 8.2.1) and no FFTs are undertaken in this loop. The average number of FFTs per iteration is also constant for the SH and PFC algorithms. Since, again, the only difference between iterations is the amount of time spent in the while loop (lines (4)-(6) of Algorithm 7.1.1) this suggests that the initial value of C_n

(8.6) is normally accepted. By contrast, the average number of FFTs per iteration varies widely for the trust region algorithm, this is because the sub-problem Definition E.0.1 may require many FFTs to solve. This graph (Figure 8.10b) demonstrates part of the reason for using FFTs to measure the speed of our algorithms.

Figure 8.10

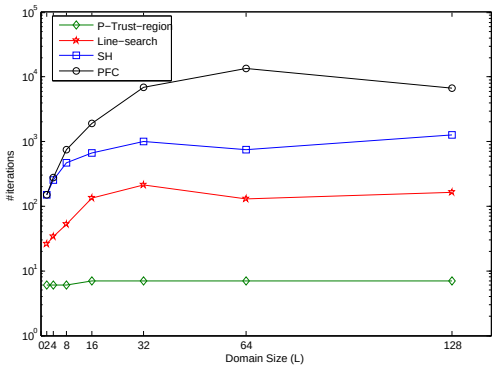

(a) Number of iterations required for convergence of the solution against domain size. The initial condition is given by (8.17) and we use the four different methods described by Algorithms 7.1.1, 8.2.1 and E.1.1. For adaptive residual tolerence (8.13) and $N = 16$. This graph is qualitively similar to Figure 8.9.

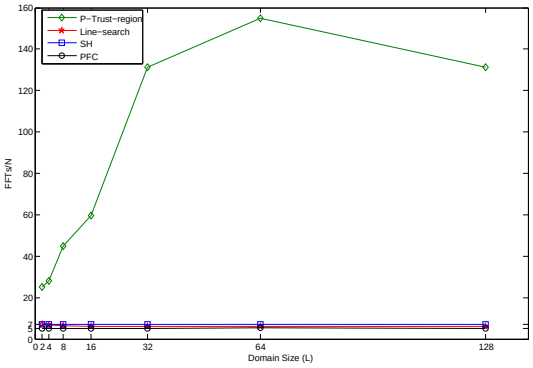

(b) Average number of FFTs per iterations against domain size. We note that for the PFC, SH and line search algorithms the number of FFTs per iteration is constant, However, for the trust region algorithm the number of FFTs per iteration varies widely. This explains the difference between Figure 8.9 and 8.10a

8.3 Conclusion

In this chapter we introduced the spatial discretisation used for our numerical tests. We use a pseudo-spectral method as in this case we expect exponential convergence. We then detailed the adaptive methods for choosing the constants τ_n and C_n so that the discrete forms of Algorithms 6.1.1 and 7.1.1 respectively are well-defined and perform well. We discussed an issue that arises with the "divergence" of convergence time at a low number of spatial grid points and possible methods for resolving this issue. Finally, we studied the convergence of the residual with domain size.

Chapter 9

Model Problems

Having considered the minimisation problem **(P)** (page 37) on a unit cell we now consider simulations on larger domains. These simulations are closer to problems that practitioners consider and they demonstrate interesting properties of and differences between the algorithms used.

In principle we expect the minima reached by each algorithm to be the same but the process by which we reach the minima may differ. We wish to compare the behaviour of the different methods after a long time (a large number of FFTs) or near a critical point (i.e. when the residual is small), in this case it may be possible to show that the qualitative behaviour of the four methods (Algorithms 8.2.1, E.1.1, and the discrete version of Algorithm 7.1.1 with $H = L^2(\Omega)$ and $H = H^{-1}(\Omega)$) have similarities.

9.1 Rotated Crystal

We consider the case of a rotated crystal, i.e. where the initial condition is the reference lattice with a small central portion rotated out of orientation. This was previously studied using the PFC model, for example in [Lar14, Chapter 5].

9.1.1 Numerics

In this case to generate the initial condition there are several steps. We start with a $L = 64$ lattice (defined by (8.2)), generated by periodically repeating the solution with residual 10^{-7} on a unit cell, i.e. 64 unit cells along the x-direction and 32 in the y-direction. We then rotate a central circle of diameter one (in terms of the period of the unit cell a) through $\pi/6$. This initial condition is shown below in Figure 9.1. We consider the four algorithms, Algorithms E.1.1, 8.2.1 and the discrete version of Algorithm 7.1.1 with $H = L^2(\Omega)$ and $H = H^{-1}(\Omega)$. To justify the choice of adaptive γ, introduced in Subsection 6.1.2, we also use Algorithm 8.2.1 with fixed γ, i.e. $\gamma_n = \gamma_{\text{om}}$ for all n.

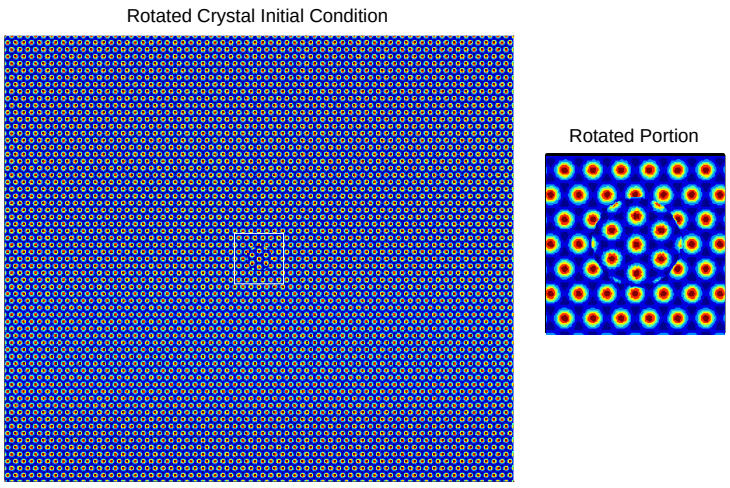

Figure 9.1: The initial condition for the rotated crystal. A $L = 64$ lattice is generated and a central circle of diameter one is rotated through $\pi/6$. The inset on the right highlights the rotated portion, demarked on the larger diagram by a rectangle.

We run the algorithms for 10^5 FFTs. After this time, the rotated defect is absorbed and we obtain the standard lattice. This final condition is shown below in Figure 9.2.

We plot the reduction of the residual for the five algorithms. We see that the residual initially reduces quickly before stagnating; however, for this initial condition the line search (both fixed and adaptive γ) and trust-region methods converge faster than the other two methods. In contrast the PFC and the Swift-Hohenberg methods initially perform better. Figure 9.3 shows the reduction of the residual where the y-axis is plotted on a logarithmic scale and the x-axis is plotted on a linear scale. After the initial reduction, all algorithms get stuck in a metastable state before reducing further, this effect can be seen more clearly in Figure 9.4 where both axes are plotted on a logarithmic scale. We note that terminating at a residual of 10^{-5} should be sufficient; however, we curtail at 10^{-7} to make the convergence clearer.

9.1.2 Discussion

Here we can see that in contrast to the case of random initial conditions below, Section 9.2, we spend very little time in the metastable state for the line search or trust region algorithms. The Swift-Hohenberg and PFC algorithms enter a metastable state for longer but even they do not persist there for very long. This contrast suggests that the problem of metastability is reduced when one chooses an initial condition which is not far from the reference lattice, which under no strain should be the true minimum. In this case all

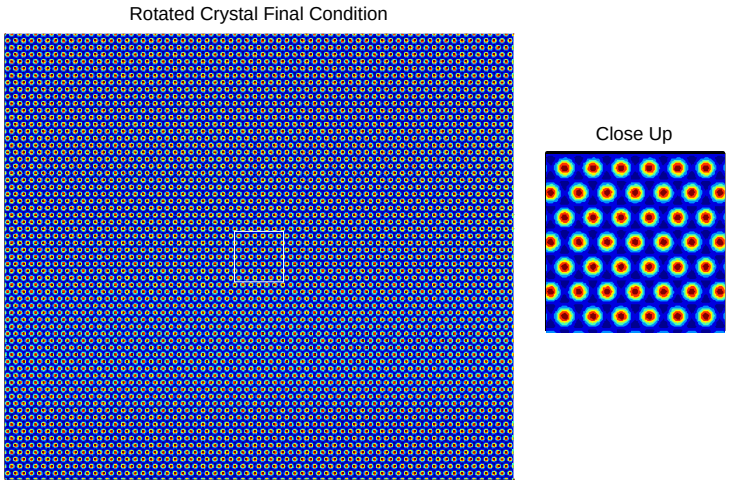

Figure 9.2: The final state of the rotated crystal, whose initial condition is given by Figure 9.1. The solution is given after 10^5 FFTs or when the residual is less than 10^{-7}. We thus have the standard lattice, the solutions of Section 9.2 are close to this. The inset zooms in the central portion to highlight the hexagonal lattice structure.

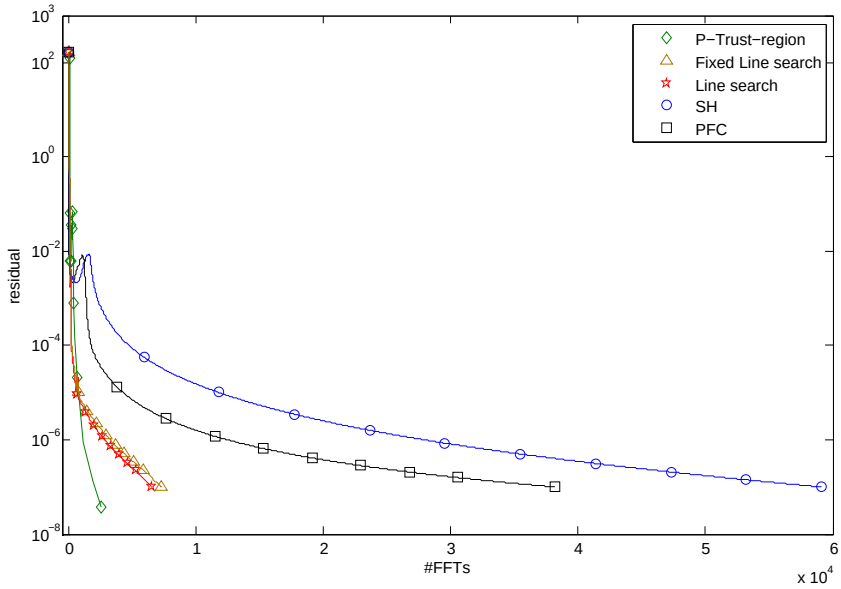

Figure 9.3: The reduction in residual for the rotated crystal, whose initial condition is given by Figure 9.1. We note that the residuals initially converge quickly before stagnating and then finally converging to a low residual with the line search and trust-region methods performing better. The x-axis is linear and the y-axis logarithmic.

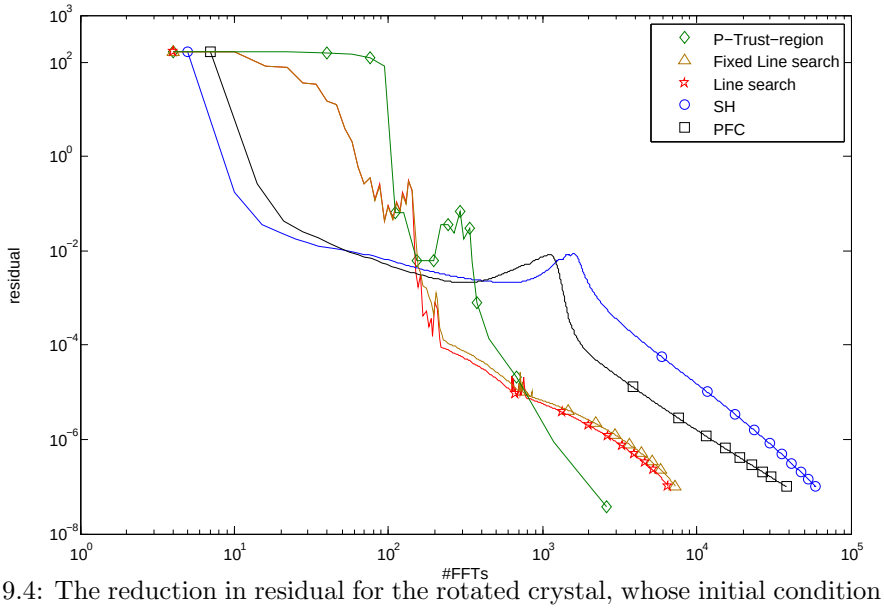

Figure 9.4: The reduction in residual for the rotated crystal, whose initial condition is given by Figure 9.1. Both axes are given on a logarithmic scale. This image emphaisises the behaviour around the metastable state. We can also see that the PFC and Swift-Hohenberg algorithms perform better initially.

algorithms obtain the same final state, as predicted, although the speed of the line search algorithm demonstrates that it may be potentially useful. We can see that there is little difference between the adaptive and fixed line search algorithms. We believe this is because we are in the asymptotic regime as mentioned in Subsection 6.1.2.

9.2 Random Initial Conditions

We start with one of the simplest possible initial conditions, i.e. where the domain is filled with random fluctuations around the average $\bar{u}$.

9.2.1 Numerics

We start with a large, $L = 64$, domain with random initial conditions, i.e.

$$u_0(x, y) = \text{rand}(x, y) - 0.5 + \bar{u}. \tag{9.1}$$

The initial condition is shown below in Figure 9.5. We then run all the five algorithms (Algorithm E.1.1, Algorithm 8.2.1 with $\gamma = \gamma_n$ and $\gamma_n = \gamma_{\text{om}}$ for all n and the discrete form of Algorithm 7.1.1 with $H = L^2(\Omega)$ and $H = H^{-1}(\Omega)$) for 5×10^6 FFTs or until the residual is less than 10^{-7} and compare the results.

Figure 9.6 shows that the residuals for all the algorithms initially converge quickly before stagnating. The residual then reduces slowly suggesting that, as we would expect, we

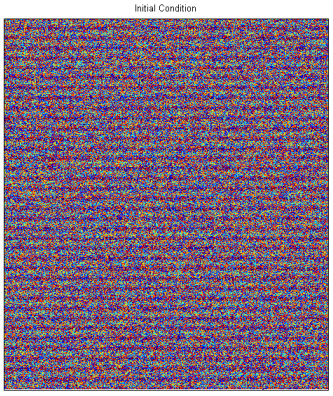

Figure 9.5: The initial condition for the algorithms, a $L = 64$ domain with random initial condition given by (9.1).

are not at a minimum. Both the trust region method and the line search then enter a regime where the residual again decreases faster; however, this happens earlier and the decrease is faster for the trust region method. In the case of the fixed line search this final decrease is much later than for the line search. The SH and PFC equation methods eventually decrease so that they reach the termination criterion. All the algorithms terminate before the end of the five million FFTs; however, they do not reach the reference lattice which is expected to be the minimum state. Figure 9.7 gives the residual decrease where both axes are plotted on a logarithmic scale as this makes the initial behaviour clearer.

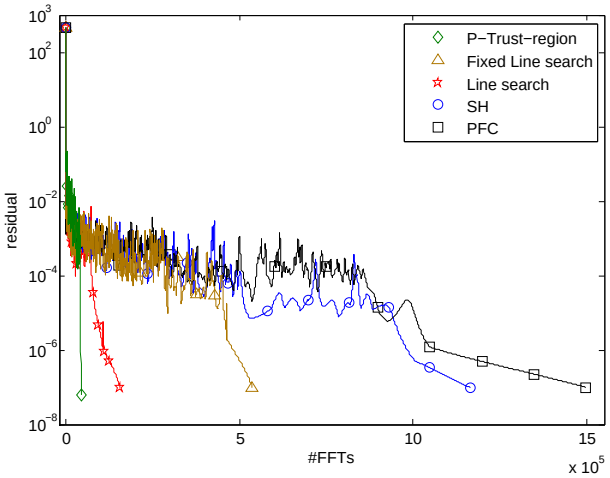

Figure 9.6: We show the convergence of the residual upto 5×10^6 FFTs starting from the random initial conditions given by (9.1). We note the residual converges quickly before stagnating, it then appears to reduce slowly. The adaptive line search and trust region methods then relatively quickly enter a phase where they reduce further. We note that in this case the fixed line search is much worse than the adaptive line search. All the algorithms eventually reach a point where their residual is low enough that they are taken to have converged.

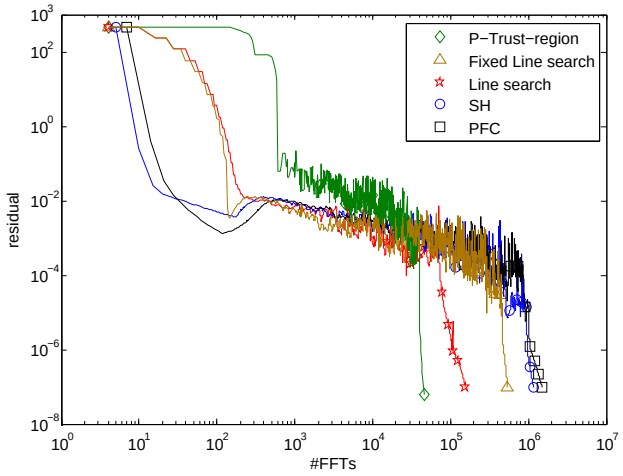

Figure 9.7: We show the convergence of the residual upto 5×10^6 FFTs starting from random initial conditions given by (9.1). In this case both axes are plotted on a logarithmic scale. We note the residual converges quickly before stagnating particularly for the Swift-Hohenberg and PFC methods.

In Subsection 8.2.3 we argued that the speed of our algorithms should be measured using the number of FFTs. The simulations undertaken above are some of the most complex undertaken in this thesis as the initial conditions are deliberately chosen to be far away from the expected solution. Therefore we reproduce these simulations with the speed of our algorithms measured using iteration number (see Figure 9.8a). We can see that the graph is qualitatively similar for all the algorithms except the trust region. To highlight the difference between using the number of FFTs and using the iteration number to measure the speed of convergence we plot the average number of FFTs per iteration (see Figure 9.8b). We can see that the number of FFTs per iteration is constant for the line search algorithm. We would expect this as the only difference between iterations is the amount of time spent in the while loop (lines (5) and (6) of Algorithm 8.2.1) and no FFTs are undertaken in this loop. The average number of FFTs per iteration is also constant for the SH and PFC algorithms. Since, again, the only difference between iterations is the amount of time spent in the while loop (lines (4)-(6) of Algorithm 7.1.1) this suggests that the initial value of C_n (8.6) is normally accepted. By contrast, the average number of FFTs per iteration varies widely for the trust region algorithm, this is because the sub-problem Definition E.0.1 may require many FFTs to solve. This graph (Figure 9.8b) along with Figure 8.10b demonstrates part of the reason for using FFTs to measure the speed of our algorithms.

Figure 9.8

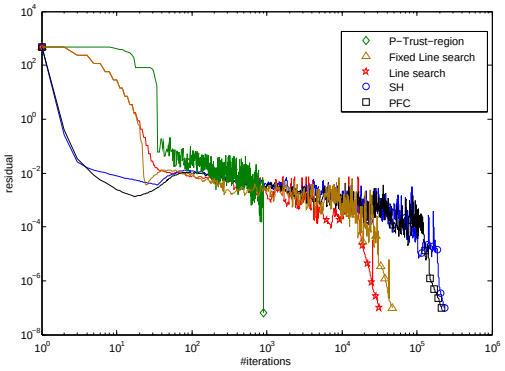

(a) Convergence of residue against iteration number. The initial condition is given by (9.1) and we use the four different methods described by Algorithms 7.1.1, 8.2.1 and E.1.1. This graph is qualitively similar to Figure 9.7.

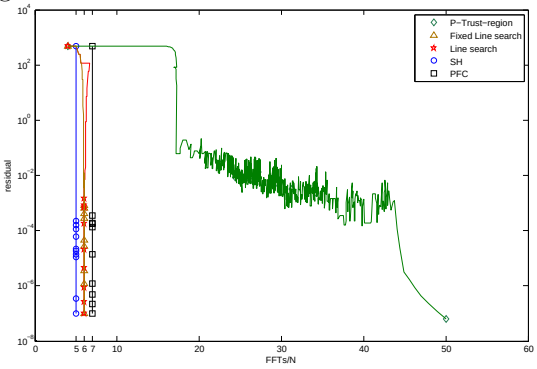

(b) Residue against average number of FFTs per iterations . We note that for the PFC, SH and line search algorithms the number of FFTs per iteration is constant, However, for the trust region algorithm the number of FFTs per iteration varies widely. This explains the difference between Figure 9.7 and 9.8a

From the residue plots Figures 9.6 and 9.7 we can see that all our methods enter a region where the residue decreases slowly. This is a metastable region. As mentioned in Chapter 1 much of the current PFC literature is interested in metastable states, see e.g. [Lar14] and [WV12]. Therefore we show the solutions of the various algorithms within their metastable regimes. As expected none of the algorithms have reached the expected minima, i.e. the lattice. However we have chosen a number of FFTs so that all the solutions have a lattice like structure. We show the solution of the cubic line search algorithm (Algorithm 8.2.1) after 1200FFTs (see Figure 9.11), the solution resembles a lattice with multiple dislocations. The final solution of the line search algorithm (see Figure 9.17) suggests that the dislocations pair up to recover the true lattice. We have therefore chosen the number of FFTs for the line search algorithm so that it looks most qualitatively similar to the solutions obtained for the other algorithms (see below, i.e. Figures 9.9, 9.10, 9.12 9.13). We show the solution for the other four algorithms (i.e. Algorithm E.1.1, Algorithm 8.2.1 with $\gamma_n = \gamma_{\text{om}}$ for all n and the discrete form of Algorithm 7.1.1 with $H = L^2(\Omega)$ and $H = H^{-1}(\Omega)$) after 3500FFTs. The trust region solution is shown in Figure 9.9, the fixed line search solution is shown in 9.10, the SH solution is shown in Figure 9.12 and the PFC solution is shown in Figure 9.13. For all these algorithms multiple grains are formed and they look qualitatively similar. However all these metastable solutions differ significantly from the metastable solution obtained for the cubic line search (see Figure 9.11). We show the residue against the number of FFTs for the various algorithms in Figure 9.14 to demonstrate that we are in the metastable state and to show the relative progress of the algorithms.

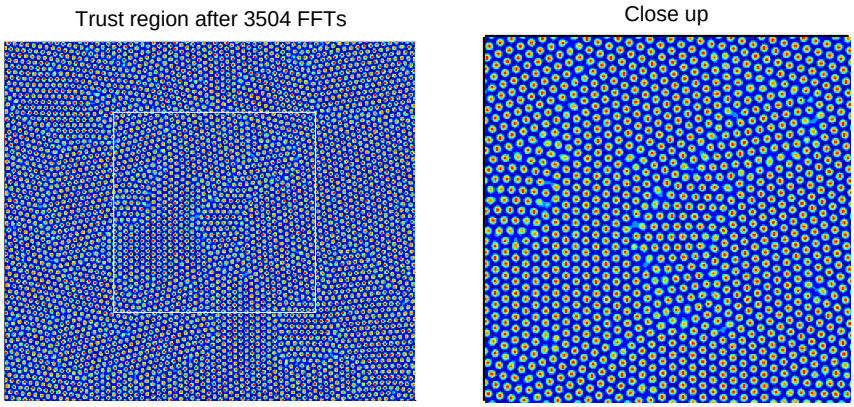

Figure 9.9: Solution for the trust region algorithm after 3504 FFTs starting from random initial conditions given by (9.1). We note the formation of grains. The area highlighted by the white rectangle in the left image is enlarged in the right image can see multiple grain boundaries. The grains look qualitively similar to the fixed line search solution Figure 9.10, the SH solution Figure 9.12 and the PFC solution Figure 9.13.

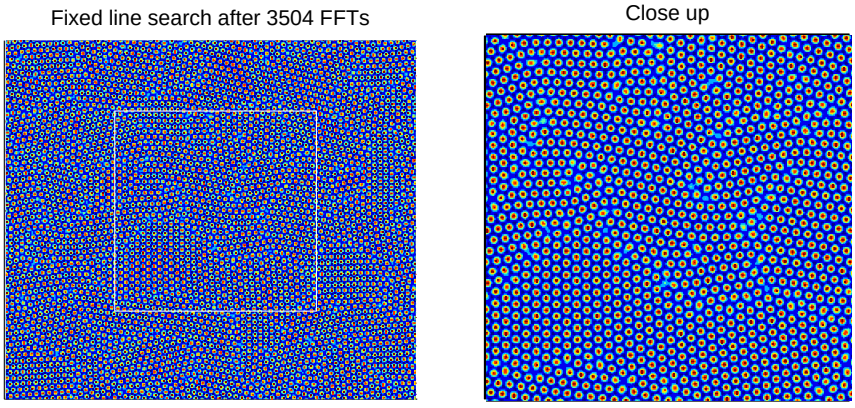

Figure 9.10: Fixed line search algorithm ($\gamma = \gamma_{\text{om}}$) after 3504 FFTs starting from random initial conditions given by (9.1). We note the formation of grains. The area highlighted by the white rectangle in the left image is enlarged in the right and we can see multiple grain boundaries. The grains look qualitively similar to the trust region solution Figure 9.9, the SH solution Figure 9.12 and the PFC solution Figure 9.13.

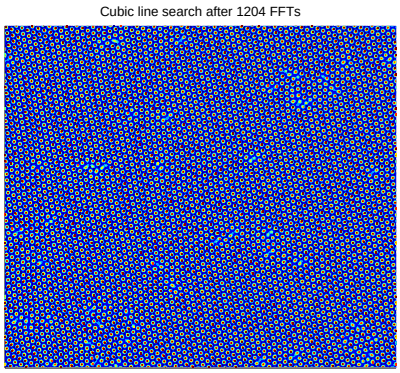

Figure 9.11: Line search algorithm after 1204 FFTs starting from random initial conditions given by (9.1). We note that in general we have a uniform lattice, however there are multiple dislocations. There are no grain boundaries unlike the trust region solution Figure 9.9, the fixed line search solution Figure 9.10, the SH solution Figure 9.12 and the PFC solution Figure 9.13.

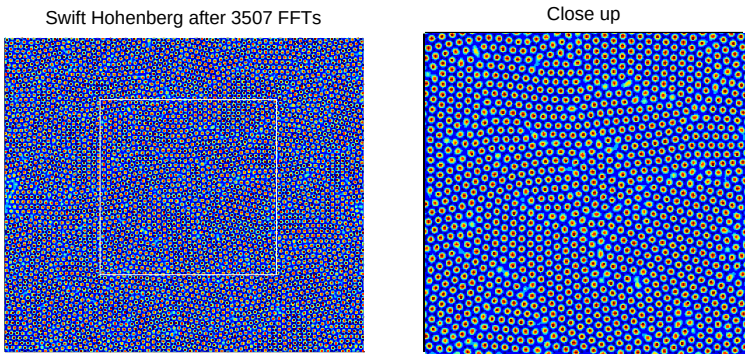

Figure 9.12: Swift-Hohenberg algorithm after 3507 FFTs starting from random initial conditions given by (9.1). We note the formation of grains. The area highlighted by the white rectangle in the left image is enlarged in the right image and we can see multiple grain boundaries. The grains look qualitively similar to the trust region solution Figure 9.9, the fixed line search solution Figure 9.10 and the PFC solution Figure 9.13.

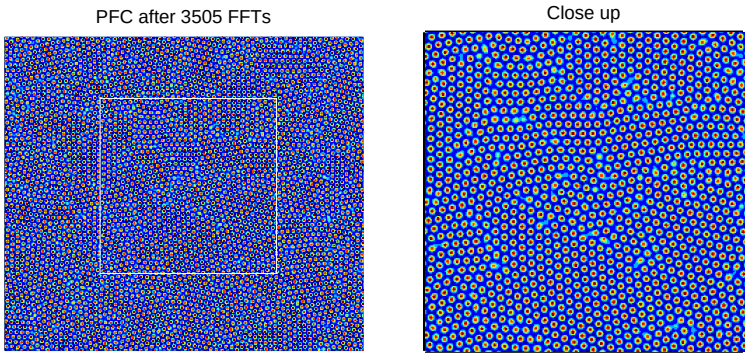

Figure 9.13: PFC algorithm after 3505 FFTs starting from random initial conditions given by (9.1). We note the formation of grains. The area highlighted by the white rectangle in the left image is enlarged in the right image and we can see multiple grain boundaries. The grains look qualitively similar to the trust region solution Figure 9.9, the fixed line search solution Figure 9.10 and the SH solution Figure 9.12

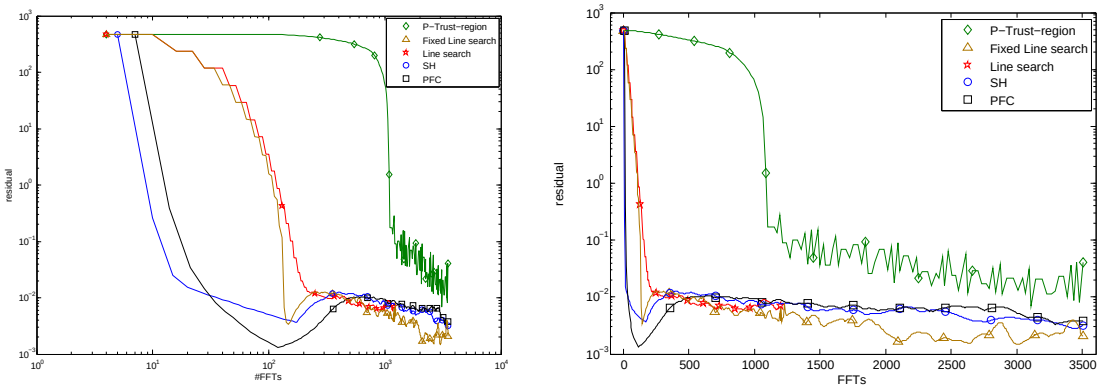

Figure 9.14: We show the convergence of the residual upto 3500 FFTs for the trust region, fixed line search, SH and PFC algorithms and 1200 FFTs for the cubic line search algorithm starting from the random initial conditions given by (9.1). We note the residual converges quickly before stagnating, it then appears to reduce slowly. The trust region method is much slower than the others. A log-log plot is shown on the left and a log linear plot is shown on the right.

As mentioned above all the algorithms converge, i.e. the residue is less than 10^{-7} for a number of FFTs less than 5×10^6. For completeness we show the final solution obtained by each algorithm. From Figure 9.15 we can see that two large grains are formed for the trust region algorithm (Algorithm E.1.1). Figures 9.16, 9.18 and 9.19 show the results of the fixed line search (Algorithm 8.2.1 with $\gamma_n = \gamma_{\text{om}}$ for all $n \in \mathbb{N}$), the Swift-Hohenberg and the PFC algorithms respectively (the discrete form of Algorithm 7.1.1 with $H = L^2(\Omega)$ and $H = H^{-1}(\Omega)$ respectively), here we see that multiple grains are formed. For the Swift-Hohenberg and PFC algorithms we also see the formation of isolated dislocations (see Figures 9.18 and 9.19) that we do not see with the fixed line search algorithm. For the adaptive line search method (Algorithm 8.2.1) we recover the reference lattice; however, the lattice is mis-orientated, see Figure 9.17. As compared to the metastable states shown above (Figures 9.9-9.13) the line search algorithm has reached the true minimum. By contrast the solutions for the other algorithms still have multiple grains but the number of grains seem to be fewer.

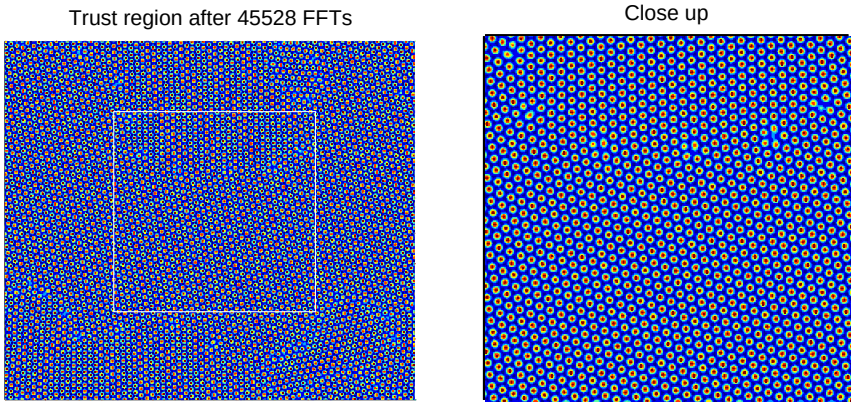

Figure 9.15: Solution for the trust region algorithm after 45528 FFTs starting from random initial conditions given by (9.1). We note the formation of grains. The area highlighted by the white rectangle in the left image is enlarged in the right image and we can see two grain boundaries, towards the centre at the top and towards the bottom left.

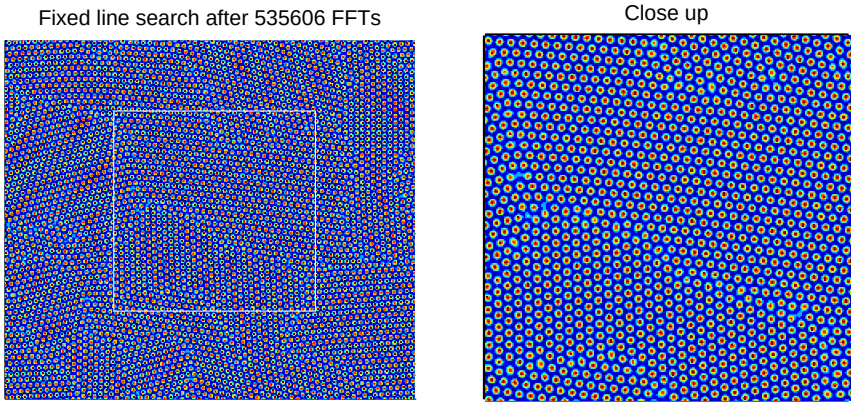

Figure 9.16: Fixed line search algorithm ($\gamma = \gamma_{\text{om}}$) after 535606 FFTs starting from random initial conditions given by (9.1). We note the formation of grains. The area highlighted by the white rectangle in the left image is enlarged in the right and we can see multiple grain boundaries, towards the top right and bottom left and running through the centre.

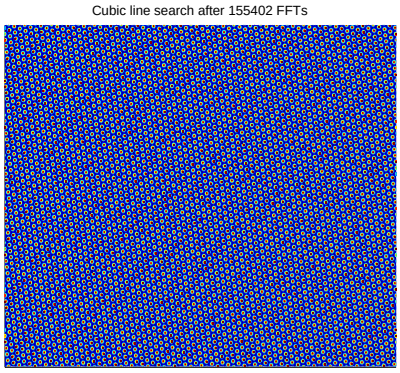

Figure 9.17: Line search algorithm after 155402 FFTs starting from random initial conditions given by (9.1). We note that in general we have a uniform lattice. However the oreintation is different from the basic lattice shown in Figure 9.2

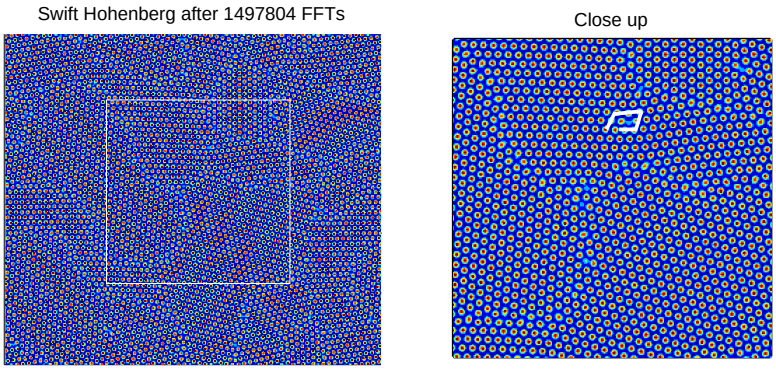

Figure 9.18: Swift-Hohenberg algorithm after 1497804 FFTs starting from random initial conditions given by (9.1). We note the formation of grains. The area highlighted by the white rectangle in the left image is enlarged in the right image and we can see multiple grain boundaries. An isolated dislocation is highlighted by white lines.

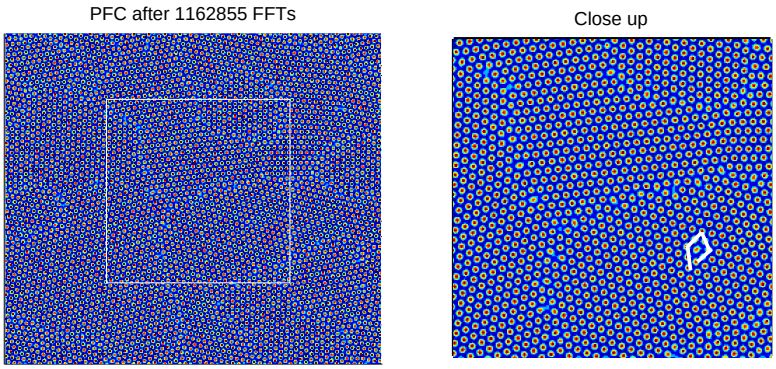

Figure 9.19: PFC algorithm after 1162855 FFTs starting from random initial conditions given by (9.1). We note the formation of grains. The area highlighted by the white rectangle in the left image is enlarged in the right image and we can see multiple grain boundaries. An isolated dislocation is highlighted by white lines.

9.2.2 Orientational Ordering

In the previous subsection we showed that the adaptive line search algorithm (Algorithm 8.2.1) is the only algorithm that reaches the true minimum. We wish to investigate whether this effect persists for different domain sizes.

For our minimisation problem (**P**) (see page 37) the true solution is the lattice. Considering the PFC functional (3.1) we see that grain boundaries increase energy compared to the lattice. Therefore we suspect that a smaller number of grains will be more energetically favourable than a large number of grains.

We first reconsider the line search algorithm on the $L = 64$ domain with initial conditions given by (9.1).We rerun the simulation multiple times with the rand function giving us different initial conditions. In some cases we initially have a large number of dislocations and we appear to almost form to grains, see Figure 9.20 which shows the result of the algorithm after 1200FFTs . However all the cases simulated the dislocations pair up and eventually we obtain the true lattice (with possibly some misorientation), see Figure 9.17.

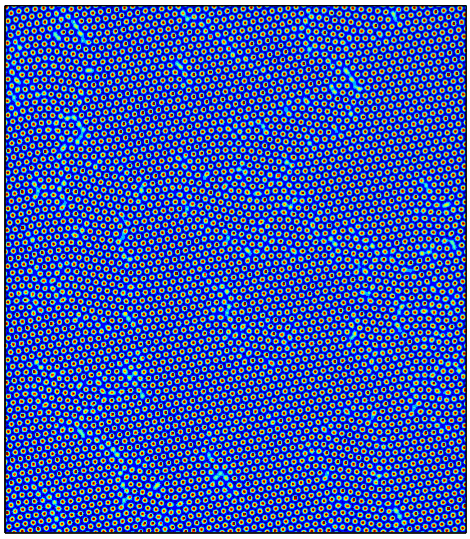

Figure 9.20: Line search algorithm after 1200 FFTs starting from random initial conditions given by (9.1). We note the large number of dislocations

This effect of orientational ordering does appear to be domain dependent. As shown in Figures 1.2 and 9.21 if we start on an $L = 32$ domain with random initial conditions given by (9.1) we obtain a grain boundary. However in this case we still have a degree of ordering as we seem to only ever generate two grains. The other four algorithms (Algorithm E.1.1, Algorithm 7.1.1 or Algorithm 8.2.1 with $\gamma_n = \gamma_{\text{om}}$ for all n), obtain the same or a greater number of grain boundaries.

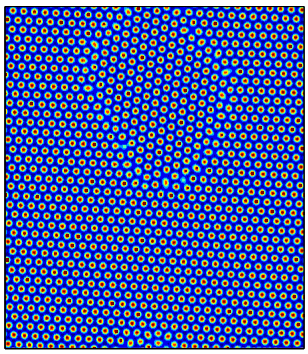

Figure 9.21: Line search algorithm after 10^5 FFTs starting from random initial conditions given by (9.1). We note the large single grain

If we start with random initial conditions (9.1) on a $L = 128$ domain we obtain a large number of dislocations. In some cases these dislocations join up to form a grain boundary however we only ever seem to form one grain. We show the $L = 128$ domain domain starting from random initial conditions (9.1) after 10^5 FFTs in Figure 9.22. In Figure 9.23 we show the fixed line search algorithm (Algorithm 8.2.1 with $\gamma_n = \gamma_{\text{om}}$ for all n) for $L = 128$ after 5×10^5 FFTs. This image is quantitatively similar to those produced by the trust region algorithm and the SH and PFC algorithms after 5×10^5 FFTs. By contrast with Figure 9.22 instead of isolated dislocations we see true grain boundaries. This means that even in this case the adaptive line search imposes more orientational ordering than the other algorithms.

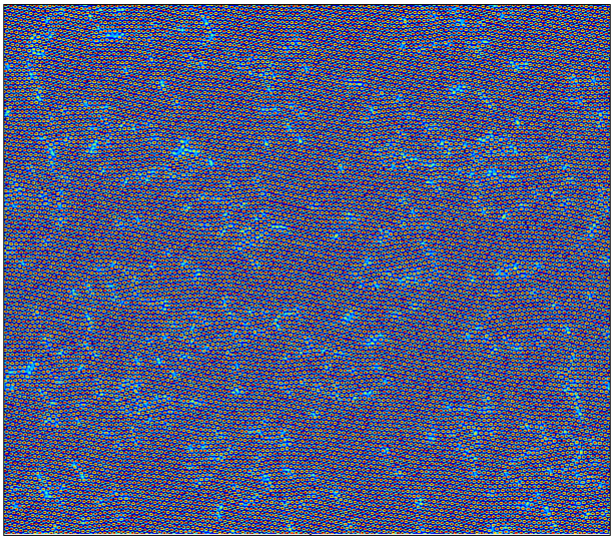

Figure 9.22: Line search algorithm after 10^5 FFTs starting from random initial conditions given by (9.1). We note the large number of dislocations

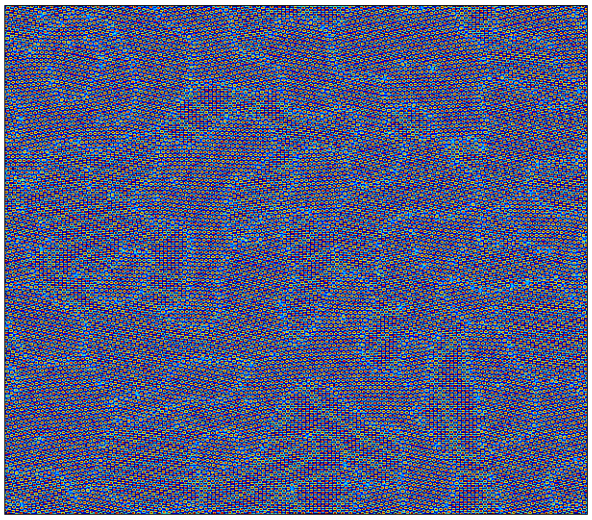

Figure 9.23: Fixed line search algorithm after 5×10^5 FFTs starting from random initial conditions given by (9.1). We note the formation of many grains.

Finally we look at the $L = 256$ domain. If we start with random initial conditions (9.1) on a $L = 128$ domain we obtain a large number of dislocations. These dislocations join up to form multiple grain boundaries. We show the $L = 256$ domain domain starting from random initial conditions (9.1) after 10^5 FFTs in Figure 9.24.

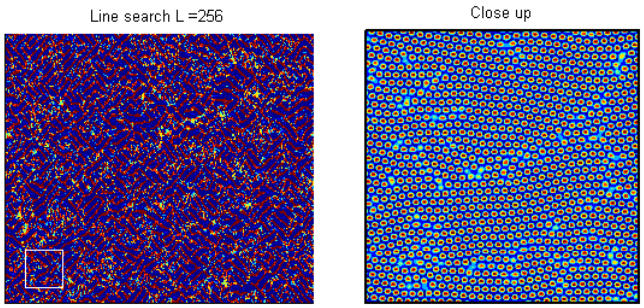

Figure 9.24: Line search algorithm after 10^5 FFTs starting from random initial conditions given by (9.1). The area highlighted by the white rectangle in the left image is enlarged in the right image and we can see multiple dislocations.

In conclusion the orientational ordering seen in Figure 9.17 does not occur for the $L = 32$ or $L = 256$ case and may not occur for the $L = 128$ case. However, in the $L = 32$, $L = 64$ and $L = 128$ the line search algorithm forms an equal number of fewer grains than the other algorithms (Algorithm E.1.1, Algorithm 7.1.1 or Algorithm 8.2.1 with $\gamma_n = \gamma_{\text{om}}$ for all n) which is more energetically favourable. We suspect that this trend continues although

is less pronounced for $L = 256$ and larger domains; however simulations demonstrating this are unfeasibly expensive.

9.2.3 Discussion

This model problem demonstrates the issue of metastability, i.e. the algorithm reaches a point where the reduction in residual at each step is small and so it stagnates. The numerical tests demonstrated above suggest this is less of an issue for the adaptive line search method we have implemented. The vast difference in final outcome and the speed of convergence between the adaptive and fixed line search is a justification for our introduction of this variable metric technique in Subsection 6.1.2.

This model problem shows that, as noted above, although all the algorithms are discretisations of the problem (**P**) (page 37), the process by which they reach the minima is not necessarily the same. This raises an issue over the comparison of numerical tests as although we suspect all algorithms will eventually obtain the reference lattice, it appears that it would take an infeasibly long time to demonstrate this numerically. We might be able to refine our algorithms to reach lower residuals which are currently available due to the limitations imposed by computational precision.

In terms of the metastable state we can see, from Figure 9.14, that the fixed line search algorithm (Algorithm 8.2.1 with $\gamma_n = \gamma_{\text{om}}$ for all $n \in \mathbb{N}$) seems to reach the same metastable state as the PFC, SH and trust region algorithms. However, it appears that the cubic line search algorithm (Algorithm 8.2.1) never passes through this metastable state. The PFC and SH algorithms seem to reach the metastable state faster than the other algorithms. However, the relative speed of the adaptive line search method suggests that this may allow us to find equilibrium configurations that are infeasible by other methods. In addition the fixed line search algorithm appears to reach a similar final condition to the SH and PFC algorithms in approximately half the number of FFTs.

For the $L = 64$ domain the line search algorithm imposes an orientational order on the solution and therefore avoids grain boundaries. For different domain sizes the solutions of the line search algorithm still have a high degree of order but can now produce grain boundaries with the frequency of such boundaries roughly increasing with domain size.

9.3 3D Simulations

An obvious advantage of undertaking calculations in three dimensions is that we should be able to simulate a much greater variety of physical phenomena. Three dimensional simulations are considered in [EW13] and [WGT$^+$12].

In Chapters 4 and 5 we derived analytical results that hold in both two and three dimensions. The time discretisations of Chapters 6 and 7 are also valid for both two and three dimensions. It is therefore justifiable to consider analogues to our numerical algorithms in three dimensions.

The spatially discrete norms and gradients introduced in Section 8.1 are only valid for calculations in two dimensions; however, these discretisations can easily be adapted to the three dimensional case (using similar notation to that of [EW13, Section 4.2]). In fact some three dimensional simulations are undertaken in [EW13, Sections 5.5 and 5.6].

Following the work of [EW13] we can reformulate the algorithms for the PFC and SH equations in three dimensions (i.e. we reformulate Algorithm 7.1.1). We are also able to formulate a three dimensional version of the line search algorithm (i.e. we reformulate Algorithm 8.2.1).

9.3.1 Vacancy Diffusion

To demonstrate the feasibility of three dimensional simulations we undertake a basic simulation.

Initially, since we expect our minimal solution to be a body centered cubic (BCC) lattice (see the phase diagram [WGT$^+$12, Figure 9 b)] as we use $-\bar{u} = \delta = 0.3$), we start with a cubic domain whose side-length is the expected period of the lattice (in the x, y and z-directions). To avoid the issue of divergence at low grid points (see Subsection 8.2.5), which we assume will be analogous in 3 dimensions, we take $N = 16$ along each axis. We then take an initial condition of random fluctuations around our prescribed average and run the Swift-Hohenberg equation until a residual of 10^{-7} is obtained (i.e. the residual is given by the 3 dimensional analogue of (8.12)). From this simulation we obtain the unit cube.

We then create a three dimensional lattice by taking two unit cubes in each of the three dimensions. We then remove the central atom to obtain a vacancy which we fill with the constant value $u(x, y, z) = 0$, this initial condition is shown in Figure 9.25.

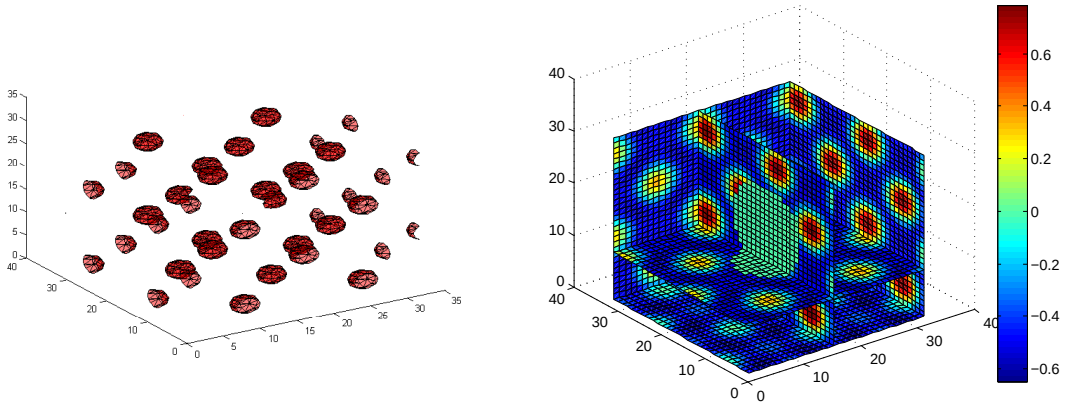

Figure 9.25: The initial condition for our three dimensional simulations. A lattice is generated by taking two unit cells in each of the three dimensions. The central atom is then removed. The left figure shows the level set plot and the right figure shows a composition of contour plot slices.

We run the three algorithms (the PFC, SH and line search algorithms) until a residual of 10^{-7} is obtained. In all three cases we obtain the same final condition which is a homogeneous lattice, shown in Figure 9.26. We note that the vacancy has been absorbed, this is the analogous result to the result seen in two dimensions, see e.g. [EG04, Figure 7]. The physical justification for the vacancy being absorbed is that the PFC model acts on a diffusive time-scale and therefore, since the vacancy moves through the lattice, each site is equally likely to be a vacancy site so that, on average, no site is empty.

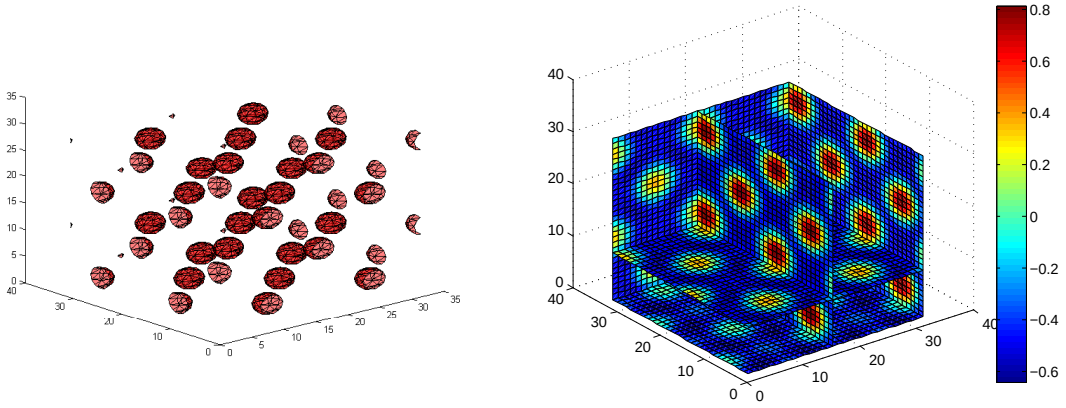

Figure 9.26: The final condition for our three dimensional simulations. This lattice is obtained by running the algorithms until a residual of 10^{-7} is obtained. The initial condition is given in Figure 9.25. The left figure shows the level set plot and the right figure shows a composition of contour plot slices.

We can compare the three algorithms by looking at the number of fast Fourier transforms needed to obtain a given residual. From Figure 9.27 we can see that the SH and PFC algorithms have faster initial convergence; however, the line search algorithm then becomes much faster and overall takes about an order of magnitude fewer FFTs to reach the desired residual (10^{-7}). The superior speed of the line search algorithm yet again provides a justification for considering this method. Since three dimensional simulations will in general require many more grid points than a two dimensional simulation, choosing the fastest method is particularly advantageous in three dimensions.

9.4 Conclusion

In this chapter we demonstrated the performance of the various numerical algorithms on large test problems. We considered two 2D problems defined by their initial conditions. The first test problem's initial condition is a large lattice with a rotated crystal at the centre and the second problem has an initial condition of random fluctuations around the average of u. We demonstrated that for the first problem all our algorithms converge to the same final

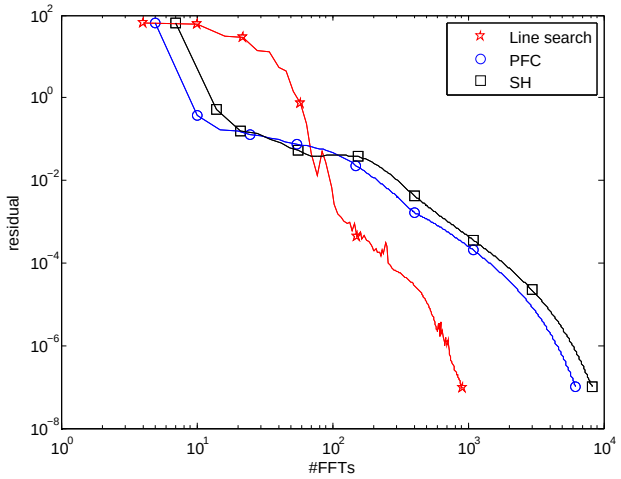

Figure 9.27: We show the residual plotted against the number of FFTs for the SH and PFC algorithms as well as for the line search algorithm. The residual and number of FFTs are plotted on a log-log scale. The initial condition is given in Figure 9.25 and the final condition is given in Figure 9.26.

state. However, for the second problem the algorithms converge to different final states. We also included a three dimensional test where the initial condition is a lattice with a vacancy. In this case we only compare three algorithms the SH, PFC and adaptive line search algorithm. All three algorithms converge to the same final state of a BCC lattice.

In all three cases we showed that Algorithms E.1.1 and 8.2.1 obtain a small residual in a much smaller number of FFTs than the methods from Algorithm 7.1.1. However, in the case of the second problem where we have a persistent metastable state the adaptive line search does not appear to pass through the same metastable state as all the other algorithms. The adaptive line search seems to recover the true lattice in this case, for different domain sizes this adaptive line search produces more highly ordered states but may not recover the true solution. In the case of Section 9.2, by contrast the fixed line search appears to obtain the same metastable state as the PFC, SH and trust region algorithms. The fixed line search algorithm also lies between the three algorithms in the sense that it obtains the metastable state faster than the trust region algorithm but slower than the SH and PFC algorithms, but persists in the metastable state for longer than the trust region algorithm but for less FFTs than the SH and PFC algorithms.

Chapter 10

Conclusions and Further Work

In this chapter we summarise the results of the thesis and outline related areas for possible further work.

10.1 Conclusions

We recall that the aim of this thesis is to develop and analyse various gradient-flow type algorithms to minimise the PFC functional whilst conserving the average of the variable. That is we formulate gradient-flow type methods to solve problem (**P**) (see page 37). We analysed and developed two kinds of time-discrete gradient-type algorithms (see Chapters 6 and 7). We concluded this thesis with a series of numerical tests to demonstrate the performance of the various schemes surveyed (Chapters 8 and 9).

The rest of this section is split into four subsections each of which highlights a significant aspect of this thesis which appears to be novel.

10.1.1 Novel Algorithms

In this thesis all our minimisation algorithms for problem (**P**) are based around solving gradient flow equations, i.e. equations of the form (4.1).

In this thesis we introduced a novel H^2-like gradient flow, i.e. Definition 4.2.4. We proved existence and uniqueness of this flow in Lemma 4.4.1.

This gradient flow is discretised in Chapter 6. In this chapter we also introduced a variable metric version of this flow, i.e. Definition 6.1.1. This variable metric flow is shown to converge in a smaller number of FFTs than its fixed metric analogue in the simulations of Chapter 9. Finally, we formulated a line search algorithm based on this gradient flow, Algorithm 6.1.1, we then showed that such an algorithm is energy stable and converges to equilibrium.

In Chapter 7 we use the convex-concave splitting method of [EW13] (see Definition 7.1.1) to discretise the SH and PFC equations. In contrast to [EW13] we give a formula

for initialising the stabilisation constant C_n at each iteration step (see line (2) of Algorithm 7.1.1). This allows us to formulate an algorithm for this convex-concave splitting method, that is Algorithm 7.1.1.

Chapters 8 and 9 are dedicated to testing the validity and performance of the various algorithms. We tested the H^2-gradient flow against the discretisation of the SH and PFC equations from [EW13] and the trust region algorithm, Algorithm E.1.1. In all our simulations the new H^2-flow algorithm seem to reach equilibrium in roughly the same number of FFTs as the trust region algorithm and in significantly fewer FFTs than the SH and PFC algorithms. The relatively fast convergence of the line search algorithm, in terms of FFTs, compared to these other methods suggests that this algorithm might be useful in further studies.

10.1.2 Łojasiewicz Method

In Chapter 5 we used the Łojasiewicz inequality to prove the convergence of the H^{-1}- and L^2-gradient flows and of our H^2-gradient flow to an equilibrium point of the PFC functional. We also used this inequality to prove the convergence of our line search algorithm (Algorithm 6.1.1), in Theorem 6.1.1, and the SH and PFC algorithms from [EW13], in Theorem 7.1.3.

The Łojasiewicz inequality for the PFC functional has been proved in [GW14, Lemma 6.1] and this technique has been used to prove the convergence of the MPFC equation in [GW14] and a discretisation of the MPFC in [GP15]. However, the use of this inequality to prove the convergence of the H^2- and L^2-gradient flows seems to be new.

Since, as described in the subsection above, our formulation of the H^2-gradient flow is new, the proof that the discrete H^2-gradient flow converges to an equilibrium point of the PFC functional is new. We note that Lemma 6.3.2 allows us to formulate a more general convergence result than is strictly necessary and may therefore be generally useful.

Finally, we used the Łojasiewicz inequality to extend the results of [EW13]. In particular we were able to prove convergence to equilibrium for these schemes and give rates of convergence.

10.1.3 Equivalence of Discrete Algorithms

In Chapter 7 we were able to prove that the discretisations of the PFC and SH equations from [EW13] can both be formulated in the gradient flow form (7.3). As noted in this chapter this form of the gradient flow is qualitatively similar to an H^2-gradient flow.

The fact that these formulas are closely linked to the H^2-gradient flow may provide more justification for using the H^2-flow. That is, since there is already interest in minimisation algorithms for the PFC functional that are similar to the H^2-flow, it is reasonable to study the true H^2-flow.

Additionally, although this link suggests that Algorithms 7.1.1 and 8.2.1 should behave similarly, in practice we do not always observe this. In particular, in the simulations of Section 9.2 a different metastable state is obtained using Algorithm 8.2.1. This seems to

be a consequence of using an adaptive metric (see Definition 6.1.1) since if we fix $\gamma_n = \gamma_{\text{om}}$ for all $n \in \mathbb{N}$ in Algorithm 8.2.1 we seem to obtain the same metastable states as the SH, PFC and trust region algorithms. This unexpected difference is an interesting avenue for further research. Furthermore, we have demonstrated that the orientational ordering imposed by the adaptive line search algorithm becomes less pronounced when the domain is larger. However, it seems likely that even on larger domains the adaptive line search will reach a more energetically favourable state than the other algorithms tested. This could also be investigated further.

10.1.4 Divergence at Low Grid Point Numbers

In Subsection 8.2.5 we highlighted an issue that arises when the number of spatial grid points is low. That is, the number of FFTs required to reach a low residual increases drastically when the number of grid points is low. This issue does not seem to have been highlighted by previous work; however, Figure 8.5 shows that this issue occurs for all our methods and thus we believe it arises from the translational invariance of the functional. The fact this divergence problem arises from the spatial discretisation of the PFC functional rather than from the schemes themselves suggests that this problem may be an issue for most spatially discrete schemes that attempt to minimise the PFC functional, or indeed any translation invariant energy functional.

We suggested two ad hoc ways of avoiding this issue. The first was essentially to ignore the issue by taking the number of grid points high enough (i.e. $N > 10$). The second method was to have a residual tolerance that adapts to the number of grid points, i.e. (8.13).

Although the methods we have introduced deal with the issue, see Figure 8.7, we are still unable to reach low residuals at low grid point numbers which might affect the simulation of meta-stable phenomena. Resolving the low grid point issue might also be another area for further research.

10.2 Further Work

In Subsection 10.1.3 we suggested that further research could be conducted into why Algorithms 7.1.1 and 8.2.1 are qualitatively similar but produce quantitatively different results. Also in Subsection 10.1.4 we mentioned the issue that the number of FFTs required to reach a low residual increases drastically when the number of grid points is low. Since for large simulations to be efficient we need a small number of grid points per atom we suspect that it may be worthwhile to reformulate our algorithms so that this issue does not occur even when the residual is low.

In Remark 6.2.2 we noted that for energy stability of Algorithm 6.1.1 we need $\|u_n\|_{L^\infty(\Omega)} < \infty$. This is also the case for Algorithm 7.1.1. Our numerical simulations demonstrated that $\|u_n\|_{L^\infty(\Omega)} = O(\|u_0\|_{L^\infty(\Omega)})$; however, we were unable to prove a rigorous result confirming this observation.

Finally, in Subsection 8.2.2 we noted that to obtain exponential convergence of our spatially discrete scheme we need the solution of the weak Euler-Lagrange equation to be analytic. We proved in Lemma 3.3.3 that the solution to the weak Euler-Lagrange equation is C^∞. Figure 8.2 gives numerical evidence that our solution is analytic; however, again, we were unable to prove a rigorous result confirming this observation.

We now briefly outline two extensions of the PFC model and suggest how they could be linked to the work of this thesis. To maintain clarity and to keep this section short we focus on methods that are derived from the PFC functional (3.1). We note that many successful extensions of the PFC model exist which are based around a subtly different functional, e.g. the 2M-PFC model, the EOF-PFC model, the VPFC model, and the binary PFC model (see [WGT$^+$12, Equation (54), (56), (58) and (67)] respectively).

10.2.1 Coarse-Graining the Solution

In Chapter 1 we noted that although the PFC model acts on a diffusive time-scale it is atomic on the spatial scale. The fact that the model has to resolve the spatial scale atomically means that stimulating large crystalline structures is still very computationally expensive. To resolve this issue we wish to spatially coarse-grain the PFC model.

We briefly survey a popular method for coarse-graining the PFC equation using renormalistion group techniques. This technique was introduced in [GAD05] to simulate grain boundaries and more rigourously justified using multi-scale techniques in [GAD06b, Section V] or for 1D in [GAD06b, Section VII].

As an example we give a heuristic justification of coarse-graining of the PFC equation (4.2) in two dimensions using renormalisation group techniques (see [CGO96, Section V] where they use similar techniques on the Swift-Hohenberg equation). We borrow the re-scaling technique [GAD06b] to re-write (4.2), using $\hat{\psi} = \sqrt{\delta}u$ to obtain

$$\hat{\psi}_t = \Delta\left[(\Delta + I)^2\,\hat{\psi} - \delta\hat{\psi} + \delta\hat{\psi}^3\right]. \tag{10.1}$$

Assume that $\hat{\psi}$ is a fluctuation around the average i.e. $\hat{\psi} = \bar{\psi} + \psi$ where $|\psi| \ll \bar{\psi}$ and $\bar{\psi} = \sqrt{\delta}\bar{u}$. Using this approximation and the fact that $\bar{u}$ is constant the linearised version of (10.1) is

$$\psi_t = \Delta\left[(\Delta + I)^2\,\psi - \delta\psi + \delta 3\overline{\psi}^2\psi\right]. \tag{10.2}$$

Appealing to the hexagonal symmetry of the solution we consider a splitting motivated by the one mode approximation

$$\psi = \sum_{j=1}^{3} A_j(x,y,t)e^{ik_j x} + A_j^*(x,y,t)e^{-ik_j x}, \tag{10.3}$$

where the k_i are the directions associated with the hexagonal lattice

$$k_1 = \frac{-\vec{i}\sqrt{3}}{2} - \frac{\vec{j}}{2}, \qquad k_2 = \vec{j}, \qquad k_3 = \frac{\vec{i}\sqrt{3}}{2} - \frac{\vec{j}}{2}.$$

The idea we shall use in approximating (10.3) is that the coefficients A_i vary on a larger scale than the lattice structure described by the exponentials (see [GAD05, Page 1]). This idea is where the power of this technique comes from since we can coarse-grain the A_i. We now want to find an equation for the coefficients A_i. Substitution of the approximation (10.3) in the linear equation (10.2) and considering only the coefficients of $e^{ik_i x}$ (other terms can be ignored as they are non-resonant see [GAD06b, Page 5] or [CGO96]) gives

$$\frac{\partial A_i}{\partial t} - \Delta^3 A_i - 6ik_i\cdot\nabla^5 A_i + 13\Delta^2 A_i + 12ik_i\cdot\nabla^3 A_i - 4\Delta A_i + \delta(1-3\overline{\psi}^2)[\Delta A_i + 2ik_i\cdot\nabla A_i - A_i] = 0 \tag{10.4}$$

(see [GAD06b, Section III] for an alternative derivation).

Following [GAD06b, Equation (9)] we define the linear operator

$$\mathcal{L}_{k_i} = \Delta + 2ik_i\cdot\nabla.$$

Then we can re-write (10.4) as

$$\frac{\partial A_i}{\partial t} + (1-\mathcal{L}_{k_i})\mathcal{L}_{k_i}^2 A_i + \delta(1-3\overline{\psi}^2)\mathcal{L}_{k_i}A_i - \delta(1-3\overline{\psi}^2)A_i = 0. \tag{10.5}$$

If we rewrite the linear spatial operator as

$$\hat{\mathcal{M}}_{k_i} = (1-\mathcal{L}_{k_i})(\delta(1-3\overline{\psi}^2) - \mathcal{L}_{k_i}^2)$$

then (10.5) simplifies to

$$\frac{\partial A_i}{\partial t} = \hat{\mathcal{M}}_{k_i} A_i$$

where the operator $\hat{\mathcal{M}}_{k_i}$ is a rotationally covariant operator (see [AGD$^+$07, Equation (8)]).

To obtain (10.2) we discarded the non-linear terms associated with $\hat{\psi}^3$. Therefore we consider the non-linear term in (10.1), i.e.

$$\Delta(\hat{\psi}^3). \tag{10.6}$$

We consider a version of the one mode approximation (10.3)

$$\psi_0 = \sum_{j=1}^{3} A_j(t)e^{ik_j x} + A_j^*(t)e^{-ik_j x} + \overline{\psi}.$$

The term associated with $e^{ik_1 x}$ in (10.6) (see [GAD06a, Equation (13)]) is

$$-3\overline{\psi}^2 A_1 - 6\overline{\psi}A_2^* A_3^* - 3A_1(|A_1|^2 + 2|A_2|^2 + 2|A_3|^2)$$

using this to replace the term not associated with the differential operator (i.e. $-3\bar{\psi}^2 A_i$) in (10.5) we have (for the coefficient A_1)

$$\begin{aligned}&\frac{\partial A_1}{\partial t} + (1-\mathcal{L}_{k_1})\mathcal{L}_{k_1}^2 A_1 + \delta(1-3\overline{\psi}^2)\mathcal{L}_{k_1} A_1 - \delta(1-3\overline{\psi}^2)A_1\\ &= -6\delta\overline{\psi}A_2^* A_3^* - 3\delta A_1(|A_1|^2 + 2|A_2|^2 + 2|A_3|^2)\end{aligned}$$

see [GAD06b, Equation (15)], similar equations can be derived for A_2 and A_3. We can also obtain this by starting with the rescaled equation (10.1) and substituting in (10.3) and then discarding terms associated with the non-linear action of differential operators, e.g. terms such as $A_1 \Delta A_1$.

The results obtained using this approximation seem quite promising, a 10 times speed up in the CPU time required to undertake the Read-Shockley tests is obtained in [GAD05]. In [AGD+07] they split the A_i into phase amplitude equations (see [AGD+07, Equations (9)-(11)]) and use the frozen gradient approximation ([AGD+07, Section D]) to obtain a mesh refinement algorithm ([AGD+07, Table 1]). Using this approximation the authors obtain a 1000 times speed up (quantified by [AGD+07, Equation (15)]) in some situations (see [AGD+07, Equations (17) and (19)]).

The derivation above seems rather ad hoc; however, more justification is given in [GAD06b] and it may be possible to obtain a more rigorous derivation by first appealing to [CGO96]. A more serious problem appears to be that this regime relies on δ being a small parameter (see the more extensive renormalisation examples in [CGO96]) which is likely to take us out of the hexagonal regime, see the phase diagram [EKHG02, Figure 1 a)] or Figure 1.1.

These techniques have already been applied to the Swift-Hohenberg equation in [CGO96, Section V.A]. It is not quite clear how this technique could be applied to Definition 4.2.4 as in this case we would have space and time derivatives of the A_i-coefficients, e.g. $\Delta\partial_t A_1$, which do not appear in any of the current examples.

10.2.2 Evolving Surfaces

Recently, work has been undertaken on formulating a PFC model on an evolving surface. In [SV14] they use the PFC model on a surface to simulate the patterns of distributed particles on a catenoid surface. They claim that defects on surfaces "provide the key to self-assembly into complex hierarchical structures with emergent novel macroscopic properties". In particular [IVC10] suggests that defects on catenoids may allow us to engineer structures with curvature which the PFC model of [SV14] can simulate. It is shown within [SV14] that these PFC simulations can approximate experimental results seen in [IVC10].

In [SV14, Equations (3)-(5)] the PFC equation is formulated as

$$\begin{aligned}\partial_t u &= \Delta_\Gamma \mu \\ \mu &= 2\nu + \Delta_\Gamma \nu + (1-\delta)u + u^3 \\ \nu &= \Delta_\Gamma u\end{aligned}$$

where Δ_Γ is the surface Laplacian. In analogue to Definition 4.2.2 this equation is obtained as the H^{-1}-gradient flow of the Swift-Hohenberg free energy (see also [SV14, Equation (1)]) on the surface Γ

$$\mathcal{F}^\Gamma[u] = \int_\Gamma -|\nabla_\Gamma u|^2 + \frac{1}{2}|\Delta_\Gamma u|^2 + \frac{1}{2}(1-\delta)u^2 + \frac{1}{4}u^4 \mathrm{d}\Gamma \tag{10.7}$$

where ∇_Γ is the surface gradient.

Considering the free energy on the surface (10.7) the analogous minimisation problem to (**P**) (see page 37) is

$$\text{find } u \text{ such that } \mathcal{F}^\Gamma[u] = \min_{\eta \in H^2_\#(\Gamma)} \mathcal{F}^\Gamma[\eta + \bar{u}].$$

The corresponding gradient flow for (10.7) (following (4.1)) is

$$\langle u_t, v\rangle_H = -\delta\mathcal{F}^\Gamma[u, v] \qquad \forall v \in H^2_\#(\Gamma)$$

where the first variation $\delta\mathcal{F}^\Gamma$ is defined analogously to the first variation (3.9). If we define

$$A_\Gamma = (\Delta_\Gamma + I)^2 + \gamma I$$

for constant $\gamma > 0$ then we can choose $H = L^2(\Gamma)$ or $\langle u_t, v\rangle_H = \langle A_\Gamma u_t, v\rangle$ to obtain analogous gradient flows to Definitions 4.2.1 and 4.2.4 where the gradient (∇) and Laplacian are replaced by their corresponding surface operators (∇_Γ and Δ_Γ).

In terms of formulating a numerical algorithm for the gradient flow, the time discretisation should be exactly analogous to the time discretisations of Chapters 6 and 7. However, due to the evolving nature of the surface the spatial discretisation of Chapter 8 will be much more complex. The spatial discretisation used to obtain numerical results in [SV14] is a finite element method. There is extensive literature on methods for finite elements on evolving surfaces, see for example [DE07].

Appendix A

Minimisation of the Hohenberg-Kohn Functional

We follow the method of [DS11, Section II and VI]. Recall that g_N is an arbitrary N-body distribution with permutation invariance, i.e. (2.8), which satisfies (2.9).

We define the functional F by

$$F[g_N] = \int_{\Omega^N} g_N(X_N) H_N(X_N, U_1) + \beta^{-1} g_N(X_N) \ln[N! g_N(X_N)] \mathrm{d}X_N. \tag{A.1}$$

Remark A.0.1. *Recalling the definition of entropy from [Ada06, Theorem 4.7]* (A.1) *can be seen to be analogous to the average of the energy (with respect to g_N) minus the temperature multiplying the entropy.*

Recalling the formula for the equilibrium N-particle density (2.1), we define

$$\hat{g}_N(X_N) = \hat{\rho}_N(X_N) = \frac{\exp[-\beta H_N(X_N, U_1)]}{N! Z_N(U_1, \Omega)}.$$

Inserting this into (A.1) we have

$$\begin{aligned}
F[\hat{g}_N] &= \int_{\Omega^N} \hat{g}_N(X_N) H_N(X_N, U_1) + \beta^{-1} \hat{g}_N(X_N) \ln[N! \hat{g}_N(X_N)] \mathrm{d}X_N \\
&= \int_{\Omega^N} \hat{g}_N(X_N) H_N(X_N, U_1) - \beta^{-1} \hat{g}_N(X_N) \ln[Z_N(U_1, \Omega)] \mathrm{d}X_N \\
&\quad - \int_{\Omega^N} \hat{g}_N(X_N) H_N(X_N, U_1) \mathrm{d}X_N \\
&= \int_{\Omega^N} -\beta^{-1} \hat{g}_N(X_N) \ln[Z_N(U_1, \Omega)] \mathrm{d}X_N \\
&= -\beta^{-1} \ln[Z_N(U_1, \Omega)]
\end{aligned}$$

where the last line follows from the normalisation of $\hat{g}_N$. Thus we have shown that the free

energy is given by

$$\mathcal{F}_N[U_1, \Omega] = F[\hat{g}_N].$$

The functional (A.1) is minimised at the equilibrium density

$$\mathcal{F}_N[U_1, \Omega] = \min_{g_N} F[g_N]. \tag{A.2}$$

Next, we demonstrate this.

Proof. of (A.2).
We consider the functional (A.1) at the equilibrium density and show that it can be manipulated into a form where it only differs from the functional evaluated at a general g_N in the entropy term. To begin we compute

$$\begin{aligned}
&F[\hat{g}_N] - \beta^{-1} \int_{\Omega^N} g_N(X_N) \ln[N! \hat{g}_N(X_N)] \mathrm{d}X_N \\
&= \int_{\Omega^N} \hat{g}_N(X_N) H_N(X_N, U_1) \mathrm{d}X_N + \int \beta^{-1} (\hat{g}_N(X_N) - g_N(X_N)) \ln[N! \hat{g}_N(X_N)] \mathrm{d}X_N \\
&= \int_{\Omega^N} \hat{g}_N(X_N) H_N(X_N, U_1) \mathrm{d}X_N \\
&\quad + \int_{\Omega^N} \beta^{-1} \hat{g}_N(X_N) [-\beta H_N(X_N, U_1) - \ln[Z_N(U_1, \Omega)]] \mathrm{d}X_N \\
&\quad - \int_{\Omega^N} \beta^{-1} g_N(X_N) [-\beta H_N(X_N, U_1) - \ln[Z_N(U_1, \Omega)]] \mathrm{d}X_N \\
&= \int_{\Omega^N} g_N(X_N) H_N(X_N, U_1) \mathrm{d}X_N + \beta^{-1} \ln[Z_N(U_1, \Omega)] \int_{\Omega^N} (g_N(X_N) - \hat{g}_N(X_N)) \mathrm{d}X_N \\
&= \int_{\Omega^N} g_N(X_N) H_N(X_N, U_1) \mathrm{d}X_N
\end{aligned}$$

where the final line follows by the normalisation of g_N and $\hat{g}_N$.

Using this we can write $F[g_N]$ as

$$F[g_N] = F[\hat{g}_N] + \beta^{-1} \int_{\Omega^N} g_N(X_N) \ln \left[\frac{g_N(X_N)}{\hat{g}_N(X_N)} \right] \mathrm{d}X_N. \tag{A.3}$$

The second term on the right-hand side is known as the relative entropy or Kullback-Leibler information [Ada06, Definition 7.1]. We now show that it is non-negative. We know that $\ln[x] \leq x - 1$ for $x \geq 0$ with equality only if $x = 1$. If we define

$$g_N \ln \left[\frac{\hat{g}_N}{g_N} \right] = 0 \quad \text{at} \quad g_N = 0$$

then, since $g_N \geq 0$, we have

$$g_N \ln \left[\frac{\hat{g}_N}{g_N} \right] \leq g_N \left(\frac{\hat{g}_N}{g_N} - 1 \right).$$

Since $\hat{g}_N \geq 0$ we have equality if and only if $g_N = \hat{g}_N$.

Hence we have a bound for the logarithmic term

$$\int_{\Omega^N} g_N \ln\left[\frac{g_N}{\hat{g}_N}\right] \mathrm{d}X_N \geq \int_{\Omega^N} (g_N - \hat{g}_N)\mathrm{d}X_N = 0.$$

The last line follows from the normalisation of g_N and $\hat{g}_N$. This inequality is known as Gibbs' inequality, see [HM06, Appendix B].

Therefore, from (A.3) we have the lower bound for the functional

$$F[g_N] \geq F[\hat{g}_N]$$

with equality if and only if $g_N = \hat{g}_N$. □

Let the one-particle density $\tilde{\rho}$ be defined from g_N via (2.10). Recalling our definition of the Hamiltonian we can now write

$$\mathcal{F}_N[U_1, \Omega] = \min_{\tilde{\rho}} \min_{g_N \to \tilde{\rho}} \left[\int_{\Omega^N} g_N(X_N) \left(\sum_{1 \leq i < j \leq N} U_2(|x_i - x_j|) + \sum_{i=1}^{N} U_1(x_i) + \beta^{-1} \ln[N! g_N(X_N)] \right) \mathrm{d}X_N \right] \tag{A.4}$$

where the relation $g_N \to \tilde{\rho}$ is defined through (2.10), i.e. we choose the minimum g_N that corresponds to $\tilde{\rho}$ through this relation. Recalling Subsection 2.2.2 we can re-write the density

$$\tilde{\rho}(x) = N \int_{\Omega^{N-1}} g_N(x, x_2, .., x_N) \mathrm{d}x_2 \ldots \mathrm{d}x_N$$

which follows from the fact that particles are indistinguishable and hence g_N is invariant under permutation of the x_i. We can now see that the term in (A.4) associated with the external potential U_1 can be re-written as

$$\begin{aligned} \int_{\Omega^N} g_N(x_N) \sum_{i=1}^{N} U_1(x_i) \mathrm{d}X_N &= N \int_{\Omega^N} g_N(x_N) U_1(x_1) \mathrm{d}X_N \\ &= \int_{\Omega} U_1(x) \tilde{\rho}(x) \mathrm{d}x. \end{aligned}$$

Then the minimisation (A.4) can now be written as

$$\mathcal{F}_N[U_1, \Omega] = \min_{\tilde{\rho}} \left[\int_{\Omega} U_1(x) \tilde{\rho}(x) \mathrm{d}x + \mathcal{F}_{HK}[\tilde{\rho}(x)] \right],$$

where the Hohenberg-Kohn functional is given by

$$\mathcal{F}_{\mathrm{HK}}[\tilde{\rho}] = \min_{g_N \to \tilde{\rho}} \left[\int_{\Omega^N} g_N(X_N) \left(\sum_{1 \leq i < j \leq N} U_2(|x_i - x_j|) + \beta^{-1} \ln[N! g_N(X_N)] \right) \mathrm{d}X_N \right].$$

This completes the proof of (2.11) given (2.12) in Section 2.3.

Appendix B

Correlation Function

B.1 $c^{(1)}$ is constant

Consider the first-order contribution

$$\mathcal{F}^1_{\text{exc}}[\rho_N(x)] = -\rho_{\text{ref}} \int_\Omega c^{(1)}(x_1)\psi(x_1)\mathrm{d}x_1.$$

Since the density is invariant under translation t we have

$$\begin{aligned}\mathcal{F}^1_{\text{exc}}[\rho_N(x)] &= -\rho_{\text{ref}} \int_\Omega c^{(1)}(x_1)\psi(x_1+t)\mathrm{d}x_1 \\ &= -\rho_{\text{ref}} \int_\Omega c^{(1)}(x_1-t)\psi(x_1)\mathrm{d}x_1\end{aligned}$$

where the second line follows by a change of variables.

Hence we have

$$\int_\Omega c^{(1)}(x_1-t)\psi(x_1)\mathrm{d}x_1 = \int_\Omega c^{(1)}(x_1)\psi(x_1)\mathrm{d}x_1$$

which holds for all ψ and t.

Therefore for all t

$$c^{(1)}(x_1) = c^{(1)}(x_1-t).$$

Therefore choosing $t = x_1$ we have that $c^{(1)}(x_1) = c^{(1)}(0)$ and thus $c^{(1)}$ is constant.

B.2 $c^{(2)}$ is radial

Consider the second-order contribution

$$\mathcal{F}^2_{\text{exc}}[\rho_N(x)] = -\rho^2_{\text{ref}} \int_\Omega \int_\Omega c^{(2)}(x_1,x_2)\psi(x_1)\psi(x_2)\mathrm{d}x_1\mathrm{d}x_2.$$

Since the density is invariant under translation t we have

$$\begin{aligned}\mathcal{F}^2_{\text{exc}}[\rho_N(x)] &= -\rho^2_{\text{ref}} \int_\Omega \int_\Omega c^{(2)}(x_1, x_2)\psi(x_1 + t)\psi(x_2 + t)\mathrm{d}x_1\mathrm{d}x_2 \\ &= -\rho^2_{\text{ref}} \int_\Omega \int_\Omega c^{(2)}(x_1 - t, x_2 - t)\psi(x_1)\psi(x_2)\mathrm{d}x_1\mathrm{d}x_2\end{aligned}$$

where the second line follows by a change of variables.

Hence we have

$$\int_\Omega \int_\Omega c^{(2)}(x_1 - t, x_2 - t)\psi(x_1)\psi(x_2)\mathrm{d}x_1\mathrm{d}x_2 = \int_\Omega \int_\Omega c^{(2)}(x_1, x_2)\psi(x_1)\psi(x_2)\mathrm{d}x_1\mathrm{d}x_2$$

which holds for all ψ and t.

Therefore for all t

$$c^{(2)}(x_1, x_2) = c^{(2)}(x_1 - t, x_2 - t).$$

Therefore choosing $t = x_2$ we have that $c^{(2)}$ depends only on the distance between particles, i.e.

$$c^{(2)}(x_1, x_2) = c^{(2)}(x_1 - x_2, 0). \tag{B.1}$$

Since the density is rotationally invariant, for a rotation R we have

$$\begin{aligned}\mathcal{F}^2_{\text{exc}}[\rho_N(x)] &= -\rho^2_{\text{ref}} \int_\Omega \int_\Omega c^{(2)}(x_1, x_2)\psi(x_1)\psi(x_2)\mathrm{d}x_1\mathrm{d}x_2 \\ &= -\rho^2_{\text{ref}} \int_\Omega \int_\Omega c^{(2)}(x_1, x_2)\psi(Rx_1)\psi(Rx_2)\mathrm{d}x_1\mathrm{d}x_2 \\ &= -\rho^2_{\text{ref}} \int_\Omega \int_\Omega c^{(2)}(R^T x_1, R^T x_2)\psi(x_1)\psi(x_2)\mathrm{d}x_1\mathrm{d}x_2\end{aligned}$$

where the third line follows from a change of variables and the fact that det$R$=1 for any rotation R.

Since the above equality follows for all ψ we have

$$\begin{aligned}c^{(2)}(x_1, x_2) &= c^{(2)}(R^T x_1, R^T x_2) \\ &= c^{(2)}(R^T(x_1 - x_2))\end{aligned}$$

where the second line follows from the fact that $c^{(2)}(x_1, x_2) = c^{(2)}(x_1 - x_2)$ derived in (B.1).

Hence $c^{(2)}$ is radial.

B.3 $\hat{c}(k)$ is radial

$\hat{c}(k)$ is the Fourier transform of $c^{(2)}$, i.e.

$$\begin{aligned}\hat{c}(k) &= \mathfrak{F}[c^{(2)}] \\ &= \int e^{-ik\cdot x} c^{(2)}(x)\mathrm{d}x.\end{aligned}$$

Since $c^{(2)}$ is rotationally invariant, for any rotation R

$$\begin{aligned}\hat{c}(k) &= \int e^{-ik\cdot x} c^{(2)}(Rx)\mathrm{d}x \\ &= \int e^{-ik\cdot R^T x} c^{(2)}(x)\mathrm{d}x \\ &= \int e^{-iRk\cdot x} c^{(2)}(x)\mathrm{d}x \\ &= \hat{c}(Rk)\end{aligned}$$

where the third and fourth lines follow from a change of variable and the fact that $\det R$=1 for any rotation R.

Since $\hat{c}(k) = \hat{c}(Rk)$, for any rotation R, $\hat{c}(k)$ is radial.

Appendix C

Function Space Results

In this appendix we collect together several important results. The aim is to compile definitions and lemmas which are not specific to the case of the PFC functional. Most of these results are already known, therefore we recall them here for the sake of convenience.

The function spaces $H^k(\Omega)$ are defined in generality in [Eva10, Subsection 5.2.2]:

Definition C.0.1. *Let $k \in \mathbb{N}$. If $\eta \in H^k(\Omega)$, the H^k-norm for η is defined by*

$$\|\eta\|^2_{H^k(\Omega)} := \sum_{i=0}^{k} \|\nabla^i \eta\|^2_{L^2(\Omega)}.$$

C.1 Subspaces of H^2

In this section we give the definitions of some common subspaces of $H^2(\Omega)$ which will be useful in formulating the minimisation problem **(P)** (see page 37).

The first space we introduce is the function space of periodic H^2-functions (see [GP15, Section 2.1] or [CHQZ88, Section A.11 (d)] for an equivalent definition).

Definition C.1.1. *The function space of periodic H^2-functions is defined by*

$$H^2_{\text{per}}(\Omega) := \left\{ \eta \in H^2_{\text{loc}}(\mathbb{R}^d) \;\middle|\; \eta \text{ periodic with respect to } \Omega \right\}.$$

To obtain the correct function space for minimisation we need the space of periodic H^2-functions with average zero. In total, we will introduce three spaces of mean zero functions corresponding to the spaces $H^2(\Omega)$, $L^2(\Omega)$ and $H^{-1}(\Omega)$. All of these spaces are examples of a more general type of Sobolev space denoted by $\dot{H}^m_{\text{per}}$ in [GP15, Section 2.1].

.

Definition C.1.2. *The function space of periodic H^2-functions with zero average is defined*

by

$$H^2_{\#}(\Omega) := \left\{ w \in H^2_{\text{per}}(\Omega) \;\middle|\; \int_\Omega w\,dx = 0 \right\}.$$

We will also need an analogous version of the space $L^2(\Omega)$.

Definition C.1.3. *The function space of periodic L^2-functions with zero average is defined by*

$$L^2_{\#}(\Omega) := \left\{ w \in L^2_{\text{per}}(\Omega) \;\middle|\; \int_\Omega w\,dx = 0 \right\}.$$

In addition, we will need the dual spaces of certain Hilbert spaces therefore we define the general dual space of a Hilbert space $H^k(\Omega)$ (following [Eva10, Section 5.9] and [WW10, Equation (2.4)]).

Definition C.1.4. *The general dual space to $H^m_{\text{per}}(\Omega)$ is denoted by $H^{-m}_{\text{per}}(\Omega)$.*

If $f \in H^{-m}_{\text{per}}(\Omega)$, we define the norm on $H^{-m}_{\text{per}}(\Omega)$ by

$$\|f\|_{H^{-m}_{\text{per}}(\Omega)} := \sup_{\substack{\|\phi\|_{H^m(\Omega)}=1 \\ \phi \in H^m_{\text{per}}(\Omega)}} |\langle \phi, f \rangle|,$$

where $\langle , \rangle$ denotes the pairing between $H^m(\Omega)$ and its dual $H^{-m}(\Omega)$.

As with the spaces $L^2(\Omega)$ and $H^2(\Omega)$, we are interested in the space corresponding to H^{-1} with $⨍ \eta \mathrm{d}x = 0$ for all $\eta \in H^{-1}_{\text{per}}(\Omega)$. The definition for this space is now stated.

Definition C.1.5. *The function space of periodic H^{-1}-functions with zero average is defined by*

$$H^{-1}_{\#}(\Omega) := \left\{ w \in H^{-1}_{\text{per}}(\Omega) \;\middle|\; \int_\Omega w\,dx = 0 \right\}.$$

C.2 Relations between Function Spaces

In this section we state seven lemmas which relate the different function spaces associated with the PFC functional (3.1) and the problem **(P)** (see page 37).

First we recall Ladyzhenskaya's inequality in d-dimensions (see [CDRS09, Equation (5.7)] for $v : \mathbb{T}^2 \to \mathbb{R}$, and [Nir66, Theorem 1] for $v : \Omega \to \mathbb{R}$ where $\Omega \subset \mathbb{R}^d$ has the cone property).

Lemma C.2.1. *Ladyzhenskaya's inequality states that*

$$\|v\|_{L^4(\Omega)} \leq \|v\|^{1-\frac{d}{4}}_{L^2(\Omega)} \|v\|^{\frac{d}{4}}_{H^1(\Omega)}$$

for all $v \in H^1(\Omega)$.

We also recall the generalised Hölder inequality [Che01, Theorem 2.1].

Lemma C.2.2 (The generalised Hölder inequality)**.** *Let $m > 0$ and let $p_1, ..., p_m > 0$ be real numbers such that*

$$\sum_{\alpha=1}^{m} \frac{1}{p_\alpha} = 1.$$

Let $f_\alpha \in L^{p_\alpha}(\Omega)$ with $\alpha = 1, .., m$. Then $\prod_{\alpha=1}^{m} f_\alpha \in L^1(\Omega)$ and

$$\left\| \prod_{\alpha=1}^{m} |f_\alpha| \right\|_{L^1(\Omega)} \leq \prod_{\alpha=1}^{m} \|f_\alpha\|_{L^{p_\alpha}(\Omega)}.$$

We now give a lemma that allows us to simplify the upper bound of the H^k-norm.

Lemma C.2.3. *For $p > 0$ the H^{p+2}-norm can be bounded by the H^{p+2}-semi-norm and the $H^{-\chi}$-norm where $\chi = 0$ or 1. That is, there exists constant $C_1, c_2 > 0$ such that, $\forall v \in H^{p+2}(\Omega)$*

$$\|v\|^2_{H^{p+2}(\Omega)} \leq C_1 \|v\|^2_{H^{-\chi}(\Omega)} + c_2 \|\Delta \nabla^p v\|^2_{L^2(\Omega)}.$$

In particular

$$\|v\|^2_{H^2(\Omega)} \leq C_1 \|v\|^2_{H^{-\chi}(\Omega)} + c_2 \|\Delta \nabla^p v\|^2_{L^2(\Omega)}.$$

Proof. We can see that

$$\begin{aligned}(1 + |k|^2)^{\frac{p+2}{2}} &\leq \begin{cases} 2^{\frac{p+2}{2}} |k|^{p+2} & |k| > 1 \\ 2^{\frac{p+2}{2}} |k|^{-\chi} & |k| \leq 1 \end{cases} \\ &\leq 2^{\frac{p+2}{2}} \left(|k|^{p+2} + |k|^{-\chi} \right). \end{aligned} \tag{C.1}$$

Then using a rescaled version of [BO12, Equation (1.1)] we have from (C.1) that

$$\begin{aligned}\|v\|_{H^2(\Omega)} &\leq \|v\|_{H^{2+p}(\Omega)} \\ &\leq \left\| (1 + |k|^2)^{\frac{p+2}{2}} \hat{v} \right\|_{L^2(\Omega)} \\ &\leq 2^{\frac{p+2}{2}} \left(\| |k|^{p+2} \hat{v} \|_{L^2(\Omega)} + \| |k|^{-\chi} \hat{v} \|_{L^2(\Omega)} \right) \\ &\leq 2^{\frac{p+2}{2}} \left(\|\Delta \nabla^p v\|_{L^2(\Omega)} + \|v\|_{H^{-\chi}(\Omega)} \right), \end{aligned} \tag{C.2}$$

where we use the triangle inequality in the second inequality and the last line follows from [Gra08, Proposition 3.1.2 (10)] and [BO12, Equation (1.1)]. Using Young's inequality on (C.2) we have

$$\|v\|^2_{H^2(\Omega)} \leq 2^{p+3} \left(\|\Delta \nabla^p v\|^2_{L^2(\Omega)} + \|v\|^2_{H^{-\chi}(\Omega)} \right). \qquad \square$$

We now state two lemmas that allow us to bound norms in higher order H^k-spaces in terms of norms related to the operator A_1 (5.4).

Lemma C.2.4. *Let $\eta \in H^2_{\text{per}}(\Omega)$ and $(\Delta + I)^2 \eta \in L^2(\Omega)$, then we have the following bound on the H^4-norm,*

$$\|\eta\|^2_{H^4(\Omega)} \leq C_4 \left(\|(\Delta + I)^2 \eta\|^2_{L^2(\Omega)} + \|\eta\|^2_{H^2(\Omega)} \right)$$

for some $C_4 > 0$.

Proof. Expanding $\|(\Delta + I)^2\eta\|_{L^2(\Omega)}$ and using that η is periodic we have

$$\begin{aligned}\|(\Delta + I)^2\eta\|^2_{L^2(\Omega)} &= \|\Delta^2\eta\|^2_{L^2(\Omega)} + 4\int_\Omega \Delta\eta\Delta^2\eta \mathrm{d}x + 4\|\Delta\eta\|^2_{L^2(\Omega)} + 4\int_\Omega \eta\Delta\eta \mathrm{d}x + \|\eta\|^2_{L^2(\Omega)} \\ &\quad + 2\int_\Omega \eta\Delta^2\eta \mathrm{d}x, \\ &\geq \frac{1}{2}\|\Delta^2\eta\|^2_{L^2(\Omega)} + \frac{1}{2}\|\eta\|^2_{L^2(\Omega)} - 10\|\Delta\eta\|^2_{L^2(\Omega)}, \end{aligned} \tag{C.3}$$

where the final line follows from using Young's inequality with $\epsilon = 1/4$ on the first two inner products and using the periodicity of η to rewrite the final inner product as the H^2-semi-norm.

Using the fact that η is periodic, Young's inequality and that $\|\Delta\eta\|_{L^2(\Omega)} = \|\nabla^2\eta\|_{L^2(\Omega)}$ we have bounds on the H^1- and H^3-semi-norms, that is

$$\begin{aligned}\|\nabla\eta\|^2_{L^2(\Omega)} &= -\int_\Omega \eta\nabla^2\eta \mathrm{d}x \leq \frac{\epsilon}{2}\|\eta\|^2_{L^2(\Omega)} + \frac{1}{2\epsilon}\|\Delta\eta\|^2_{L^2(\Omega)}, \\ \|\nabla^3\eta\|^2_{L^2(\Omega)} &= -\int_\Omega \nabla^4\eta\nabla^2\eta \mathrm{d}x \leq \frac{\epsilon'}{2}\|\Delta^2\eta\|^2_{L^2(\Omega)} + \frac{1}{2\epsilon'}\|\Delta\eta\|^2_{L^2(\Omega)}. \end{aligned}$$

Using these inequalities, that $\|\Delta\eta\|_{L^2(\Omega)} = \|\nabla^2\eta\|_{L^2(\Omega)}$ and the definition of the H^k-norm, Definition C.0.1, we have

$$\begin{aligned}\|u\|^2_{H^4(\Omega)} &= \|\eta\|^2_{L^2(\Omega)} + \|\nabla\eta\|^2_{L^2(\Omega)} + \|\nabla^2\eta\|^2_{L^2(\Omega)} + \|\nabla^3\eta\|^2_{L^2(\Omega)} + \|\nabla^4\eta\|^2_{L^2(\Omega)} \\ &\leq \left(1 + \frac{\epsilon}{2}\right)\|\eta\|^2_{L^2(\Omega)} + \left(1 + \frac{1}{2\epsilon} + \frac{1}{2\epsilon'}\right)\|\nabla^2\eta\|^2_{L^2(\Omega)} + \left(1 + \frac{\epsilon'}{2}\right)\|\nabla^4\eta\|^2_{L^2(\Omega)} \\ &\leq \frac{2+\sqrt{2}}{2}\left(\|\eta\|^2_{L^2(\Omega)} + \|\nabla^2\eta\|^2_{L^2(\Omega)} + \|\nabla^4\eta\|^2_{L^2(\Omega)}\right), \end{aligned}$$

where we have used $\epsilon = \epsilon' = \sqrt{2}$ in the last line. Hence we have the following bound on the H^4-norm

$$\begin{aligned}\|\eta\|^2_{H^4(\Omega)} &\leq \frac{2+\sqrt{2}}{2}\left(\|\eta\|^2_{L^2(\Omega)} + \|\nabla^2\eta\|^2_{L^2(\Omega)} + \|\nabla^4\eta\|^2_{L^2(\Omega)}\right) \\ &\leq (2+\sqrt{2})\left(\|(\Delta + I)^2\eta\|^2_{L^2(\Omega)} + \frac{21}{2}\|\nabla^2\eta\|^2_{L^2(\Omega)}\right) \\ &\leq (2+\sqrt{2})\left(\|(\Delta + I)^2\eta\|^2_{L^2(\Omega)} + \frac{21}{2}\|\eta\|^2_{H^2(\Omega)}\right), \end{aligned}$$

where the second line follows from (C.3) and the final line follows from Definition C.0.1. Setting

$$C_4 = \frac{21(2+\sqrt{2})}{2}$$

completes the proof. □

An interpolation of Hölder's inequality allows us to approximate L^3-terms in terms of L^2- and L^4-norms.

Lemma C.2.5. *For all $\eta \in L^2(\Omega) \cap L^4(\Omega)$ we have*

$$\|\eta\|_{L^3(\Omega)}^3 \leq \|\eta\|_{L^2(\Omega)} \|\eta\|_{L^4(\Omega)}^2.$$

We now state a lemma that follows from the Ladyzhenskaya inequality and allows us to bound the L^4-norm by a combination of the L^2- and H^2-norms.

Lemma C.2.6. *We now show that for all $\eta \in H^2_{\text{per}}(\Omega)$ we have a bound for the L^4-norm in terms of the H^2- and L^2-norms that is independent of dimension. That is for $d = 2$ or $d = 3$ we have*

$$\|\eta\|_{L^4(\Omega)} \leq \sqrt[8]{2} \|\eta\|_{H^2(\Omega)}^{\frac{1}{2}} \|\eta\|_{L^2(\Omega)}^{\frac{1}{2}}. \tag{C.4}$$

Proof. From Ladyzhenskaya inequality (Lemma C.2.1) we have

$$\|\eta\|_{L^4(\Omega)} \leq \|\eta\|_{H^1(\Omega)}^{\frac{d}{4}} \|\eta\|_{L^2(\Omega)}^{1-\frac{d}{4}},$$

so for $d = 2$ the result follows immediately by the embedding $H^2(\Omega) \subset H^1(\Omega)$. For $d = 3$ we have

$$\|\eta\|_{L^4(\Omega)} \leq \|\eta\|_{H^1(\Omega)}^{\frac{3}{4}} \|\eta\|_{L^2(\Omega)}^{\frac{1}{4}}. \tag{C.5}$$

Given this, the bound we require for the H^1-norm is

$$\|\eta\|_{H^1(\Omega)}^{\frac{1}{2}} \leq C \|\eta\|_{H^2(\Omega)}^{\frac{1}{4}} \|\eta\|_{L^2(\Omega)}^{\frac{1}{4}} \tag{C.6}$$

for some $C > 0$.

Using the definition of the H^1-norm, Definition C.0.1, and the fact that η is periodic we have

$$\begin{aligned} \|\eta\|_{H^1(\Omega)}^2 &= \|\eta\|_{L^2(\Omega)}^2 + \|\nabla \eta\|_{L^2(\Omega)}^2 \\ &= \|\eta\|_{L^2(\Omega)}^2 - \int_\Omega \eta \Delta \eta \mathrm{d}x. \end{aligned}$$

Using Cauchy-Schwartz on the right-hand term we have

$$\begin{aligned} \|\eta\|_{H^1(\Omega)}^2 &\leq \|\eta\|_{L^2(\Omega)}^2 + \|\eta\|_{L^2(\Omega)} \|\Delta \eta\|_{L^2(\Omega)} \\ &\leq \|\eta\|_{L^2(\Omega)} \left(\|\eta\|_{L^2(\Omega)} + \|\Delta \eta\|_{L^2(\Omega)} \right). \end{aligned} \tag{C.7}$$

Consider the term on the right side

$$\begin{aligned}\left(\|\eta\|_{L^2(\Omega)} + \|\Delta\eta\|_{L^2(\Omega)}\right)^2 &= \|\eta\|^2_{L^2(\Omega)} + 2\|\eta\|_{L^2(\Omega)}\|\Delta\eta\|_{L^2(\Omega)} + \|\Delta\eta\|^2_{L^2(\Omega)} \\ &\leq 2\left[\|\eta\|^2_{L^2(\Omega)} + \|\Delta\eta\|^2_{L^2(\Omega)}\right] \\ &\leq 2\|\eta\|^2_{H^2(\Omega)} \end{aligned} \tag{C.8}$$

where the second line follows by Young's inequality and the last line follows from the definition of the H^2-norm, Definition C.0.1.

Inserting (C.8) into (C.7) we have

$$\|\eta\|^2_{H^1(\Omega)} \leq \sqrt{2}\|\eta\|_{L^2(\Omega)}\|\eta\|_{H^2(\Omega)}. \tag{C.9}$$

Therefore (C.6) is satisfied with $C = \sqrt[8]{2}$.

Inserting (C.6) into (C.5) and using that $1 \leq \sqrt[8]{2}$ (C.4) is satisfied for $d = 2$ and $d = 3$.

□

Finally we state a lemma that allows us to bound the L^3-norm by a combination of the L^2- and H^2-norms.

Lemma C.2.7. *We now show that for all $\eta \in H^2_{\text{per}}(\Omega)$ we have a bound for the L^3-norm in terms of the H^2- and L^2-norms that is independent of dimension. That is for $d = 2$ or $d = 3$ we have*

$$\|\eta\|_{L^3(\Omega)} \leq \sqrt[4]{2}\|\eta\|^{\frac{1}{2}}_{H^2(\Omega)}\|\eta\|^{\frac{1}{2}}_{L^2(\Omega)}.$$

Proof. Recall the L^4-bound (Lemma C.2.6) and the interpolation of the L^3-norm (Lemma C.2.5), that is

$$\begin{aligned}\|\eta\|_{L^4(\Omega)} &\leq \sqrt[8]{2}\|\eta\|^{\frac{1}{2}}_{H^2(\Omega)}\|\eta\|^{\frac{1}{2}}_{L^2(\Omega)}, \\ \|\eta\|^3_{L^3(\Omega)} &\leq \|\eta\|_{L^2(\Omega)}\|\eta\|^2_{L^4(\Omega)}.\end{aligned}$$

Combining these we have

$$\|\eta\|^3_{L^3(\Omega)} \leq \sqrt[4]{2}\|\eta\|^2_{L^2(\Omega)}\|\eta\|_{H^2(\Omega)} \tag{C.10}$$

Using that $H^2(\Omega) \subset L^2(\Omega)$, that is

$$\|\eta\|^{\frac{1}{2}}_{L^2(\Omega)} \leq \|\eta\|^{\frac{1}{2}}_{H^2(\Omega)}. \tag{C.11}$$

Combining (C.10) and (C.11) gives the result.

□

Appendix D

Proof of Theorem 5.2.1

Theorem ([HJ15, Theorem 11.2.7])**.** .

Assume that $\hat{A} = \delta^2\mathcal{E}[0]$ *is a semi-Fredholm operator and that* $N = ker\hat{A} \subset Z$.

Assume that:

• *(H2)* $\mathcal{E} : U \to \mathbb{R}$ *is analytic in the sense of Definition 5.2.3 where* $U \subset W$ *is an open neighbourhood of* 0*, such that* $\delta\mathcal{E}(U) \subset Z$ *and* $\delta\mathcal{E} : U \to Z$ *is analytic.*

Then there exists $\theta \in \left(0, \frac{1}{2}\right]$, $\sigma > 0$ *and* $c > 0$ *such that*

$$\|u\|_V < \sigma \Rightarrow \|\delta\mathcal{E}[u]\|_{V^*} \geq c|\mathcal{E}[u]|^{1-\theta}.$$

First we need a C^1 map from V to V^* in a neighbourhood of the origin this follows from the following proposition.

Proposition D.0.1 (Proposition 11.2.3 of [HJ15])**.** *Assume that* $\hat{A} = \delta^2\mathcal{E}[0]$ *is a semi-Fredholm operator and let*

$$\begin{aligned} \mathcal{N} : V &\to V^* \\ u &\mapsto \Pi u + \delta\mathcal{E}[u]. \end{aligned}$$

Then there exists a neighbourhood of 0*,* $W_1(0)$ *in* V*, a neighbourhood of* 0*,* $W_2(0)$ *in* V^* *and a* C^1 *map* $\Psi : W_2(0) \to W_1(0)$ *which satisfies*

$$\begin{aligned} \mathcal{N}(\Psi(f)) &= f, && \forall f \in W_2(0), \\ \Psi(\mathcal{N}(u)) &= u, && \forall u \in W_1(0), \\ \|\Psi(f) - \Psi(g)\|_V &\leq C_1\|f - g\|_{V^*}, && \forall (f, g) \in W_2(0). \end{aligned}$$

where $C_1 > 0$.

Proof. The function $\mathcal{N}$ is C^1 and $D\mathcal{N}(0) = \Pi + \hat{A}$ is an isomorphism. Therefore classical local inversion theorem applies to give us Ψ. □

We can now establish that in a neighbourhood of 0 this C^1-map corresponds to an analytic map $\Psi_1 : Z \to W$.

Lemma D.0.8 (Lemma 11.2.8 of [HJ15]). *There exists a neighbourhood of* 0, $V_1(0)$ *in* W, *a neighbourhood of* 0, $V_2(0)$ *in* Z *and an analytic map* $\Psi_1 : V_2(0) \to V_1(0)$ *which satisfies*

$$\begin{aligned} \mathcal{N}(\Psi_1(f)) &= f, && \forall f \in V_2(0), \\ \Psi_1(\mathcal{N}(u)) &= u, && \forall u \in V_1(0), \\ \Psi_1 &= \Psi, && \in V_2(0) \cap W_2(0) \\ \|\Psi(f) - \Psi(g)\|_W &\leq C_1 \|f - g\|_Z, && \forall (f, g) \in V_2(0) \cap W_2(0). \end{aligned}$$

Proof. We first establish that

$$\begin{aligned} \mathcal{N} : W &\to Z, \\ u &\mapsto \Pi u + \delta\mathcal{E}[u], \end{aligned}$$

is a C^1-diffeomorphism near 0, because $D\mathcal{N}(0) = \Pi + \hat{A} = \mathcal{L} \in L(W, Z)$ is an isomorphism and the classical local inversion theorem applies. Therefore we can find a neighbourhood $V_1(0)$ of 0 in W and a neighbourhood $V_2(0)$ of 0 in Z such that $\mathcal{N} : V_1(0) \to V_2(0)$ is a C^1-diffeomorphism. Finally it is clear that $\Psi_1 = \mathcal{N}^{-1}$ in $V_2(0) \cap W_2(0)$. By [HJ15, Theorem 2.3.7] we have Ψ_1 is analytic in $V_2(0)$. □

We now split our energy bound into two parts, one where the classical Łojasiewicz inequality for analytic functions can be applied and one which is the difference between the energy and its analytic approximation. We can then use the properties of Ψ and $\delta\mathcal{E}$ to bound the norm of the discrete first variation by $\|\delta\mathcal{E}\|_{V^*}$. Finally, we use the properties of Ψ and $\delta\mathcal{E}$ to bound the difference between the energy and its analytic approximation by $\|\delta\mathcal{E}\|_{V^*}^2$.

We first give our analytic approximation of the energy near the origin.

Let $(\varphi_1, \varphi_2, ..., \varphi_d)$ denote an orthonormal basis of $\ker(\hat{A})$ relative to the inner-product of H. For $\xi \in \mathbb{R}^d$ small enough to achieve $\Pi(u) = \sum_{j=1}^d \xi_j \varphi_j \in W_2(0)$ we define

$$\Gamma(\xi) = \mathcal{E}\left[\Psi\left(\sum_{j=1}^d \xi_j \varphi_j\right)\right].$$

By the chain rule (see [HJ15, Theorem 2.3.5]) since $\mathcal{E} : U \to \mathbb{R}$, $\delta\mathcal{E} : U \to Z$ and $\Psi : V_2(0) \cap W_2(0) \to V_1(0)$ are analytic, the function Γ is real analytic in some neighbourhood of 0 in $\mathbb{R}^d$. We now have by sub-additivity

$$|\mathcal{E}[u]|^{1-\theta} \leq |\Gamma(\xi)|^{1-\theta} + |\Gamma(\xi) - \mathcal{E}[u]|^{1-\theta}.$$

Applying the classical Łojasiewicz inequality (see [HJ15, Theorem 10.1.3] and [Loj62] or

[ŁZ99] for a proof) to the scalar analytic function Γ defined above we obtain (since $1-\theta \in (0,1)$).

$$|\mathcal{E}[u]|^{1-\theta} \leq \frac{1}{C_0}\|\nabla\Gamma(\xi)\|_{\mathbb{R}^d} + |\Gamma(\xi) - \mathcal{E}[u]|^{1-\theta}. \tag{D.1}$$

We first consider the gradient term. We want to bound this by $\|\delta\mathcal{E}\|_{V^*}$.

Lemma D.0.9 (see [HJ15, Proposition 11.2.4])**.** *We can bound the discrete gradient by $\|\delta\mathcal{E}\|_{V^*}$, that is*

$$\|\nabla\Gamma(\xi)\|_{\mathbb{R}^d} \leq C\|\delta\mathcal{E}[u]\|_{V^*} \tag{D.2}$$

where $C > 0$.

Proof. Consider the norm of $\nabla\Gamma$

$$\begin{aligned}\|\nabla\Gamma(\xi)\|_{\mathbb{R}^d} &= \left\|\frac{\partial\Gamma}{\partial\xi_k}(\xi)\varphi_k\right\|_{V^*}, \\ &\leq \left\|\frac{\partial\Gamma}{\partial\xi_k}(\xi)\varphi_k - \delta\mathcal{E}\left[\Psi\left(\sum_{j=1}^d \xi_j\varphi_j\right)\right]\right\|_{V^*} + \left\|\delta\mathcal{E}\left[\Psi\left(\sum_{j=1}^d \xi_j\varphi_j\right)\right]\right\|_{V^*}. \end{aligned} \tag{D.3}$$

We want to approximate the first term of the left-hand side. First differentiate Γ

$$\begin{aligned}\frac{\partial\Gamma}{\partial\xi_k} &= \frac{\mathrm{d}}{\mathrm{d}s}\,\mathcal{E}\left[\Psi\left(\sum_{j\neq k}\xi_j\varphi_j + (\xi_k+s)\varphi_k\right)\right]\Bigg|_{s=0}, \\ &= \left\langle \delta\mathcal{E}\left[\Psi\left(\sum_{j=1}^d \xi_j\varphi_j\right)\right], D\Psi\left(\sum_{j=1}^d \xi_j\varphi_j\right)\varphi_k\right\rangle.\end{aligned}$$

Using this we have

$$\begin{aligned}&\left\|\frac{\partial\Gamma}{\partial\xi_k}(\xi)\varphi_k - \delta\mathcal{E}\left[\Psi\left(\sum_{j=1}^d \xi_j\varphi_j\right)\right]\right\|_{V^*} \\ &= \left\|\sum_{k=1}^d \left\langle \delta\mathcal{E}\left[\Psi\left(\sum_{j=1}^d \xi_j\varphi_j\right)\right], D\Psi\left(\sum_{j=1}^d \xi_j\varphi_j\right)\varphi_k - \varphi_k\right\rangle\varphi_k\right\|_{V^*}.\end{aligned}$$

Therefore we have

$$\begin{aligned}&\left\|\frac{\partial\Gamma}{\partial\xi_k}(\xi)\varphi_k - \delta\mathcal{E}\left[\Psi\left(\sum_{j=1}^d \xi_j\varphi_j\right)\right]\right\|_{V^*} \\ &\leq \sum_{k=1}^d \left\|\delta\mathcal{E}\left[\Psi\left(\sum_{j=1}^d \xi_j\varphi_j\right)\right]\right\|_{V^*}\left\|D\Psi\left(\sum_{j=1}^d \xi_j\varphi_j\right)\varphi_k - \varphi_k\right\|_{V^*}\end{aligned}$$

using that $D\Psi$ is continuous and $D\Psi(0)u = u$ we have

$$\left\| \frac{\partial \Gamma}{\partial \xi_k}(\xi)\varphi_k - \delta\mathcal{E}\left[\Psi\left(\sum_{j=1}^{d}\xi_j\varphi_j\right)\right]\right\|_{V^*} \leq |\xi| \left\| \delta\mathcal{E}\left[\Psi\left(\sum_{j=1}^{d}\xi_j\varphi_j\right)\right]\right\|_{V^*}.$$

Hence using this equation in (D.3) we have

$$\begin{aligned}\|\nabla\Gamma(\xi)\|_{\mathbb{R}^d} &\leq C_4\|\delta\mathcal{E}[\Psi(\Pi(u))]\|_{V^*},\\ &= C_4\|\delta\mathcal{E}[\Psi(\Pi(u))] - \delta\mathcal{E}[u] + \delta\mathcal{E}[u]\|_{V^*},\end{aligned}$$

since $\mathcal{E}$ is C^1 we have

$$\begin{aligned}\|\nabla\Gamma(\xi)\|_{\mathbb{R}^d} &\leq C_4\|\delta\mathcal{E}[u]\|_{V^*} + C_3C_4\|\Psi(\Pi(u)) - u\|_V,\\ &\leq C_4\|\delta\mathcal{E}[u]\|_{V^*} + C_3C_4\|\Psi(\Pi(u)) - \Psi(\Pi(u) + \delta\mathcal{E}[u])\|_V,\end{aligned}$$

where we have used the definition of Ψ in the last line. Using the continuity of Ψ we have (D.2). □

Consider the energy difference term of (D.1).

Lemma D.0.10 (see [HJ15, Proposition 11.2.4])**.** *We can bound the difference between the energy and its analytic approximation by the square of $\|\delta\mathcal{E}[u]\|_{V^*}$, That is,*

$$|\mathcal{E}[u] - \Gamma(\xi)| \leq K\|\delta\mathcal{E}[u]\|_{V^*}^2. \tag{D.4}$$

Proof.

$$\begin{aligned}|\mathcal{E}[u] - \Gamma(\xi)| &= |\mathcal{E}[u] - \mathcal{E}[\Psi(\Pi(u)]|,\\ &= \left|\int_0^1 \frac{\mathrm{d}}{\mathrm{d}t}[\mathcal{E}[u + t(\Psi(\Pi(u)) - u)]]\mathrm{d}t\right|,\\ &= \left|\int_0^1 \langle\delta\mathcal{E}[u + t(\Psi(\Pi(u)) - u)], \Psi(\Pi(u)) - u\rangle\mathrm{d}t\right|,\\ &\leq \|\Psi(\Pi(u)) - u\|_V \int_0^1 \|\delta\mathcal{E}[u + t(\Psi(\Pi(u)) - u)]\|_{V^*}\mathrm{d}t,\\ &= \|\Psi(\Pi(u)) - u\|_V \int_0^1 \|\delta\mathcal{E}[u] - \delta\mathcal{E}[u] + \delta\mathcal{E}[u + t(\Psi(\Pi(u)) - u)]\|_{V^*}\mathrm{d}t,\\ &\leq \|\Psi(\Pi(u)) - u\|_V \int_0^1 \|\delta\mathcal{E}[u]\|_{V^*} + \|\delta\mathcal{E}[u + t(\Psi(\Pi(u)) - u)] - \delta\mathcal{E}[u]\|_{V^*}\mathrm{d}t,\\ &\leq \|\Psi(\Pi(u)) - u\|_V \int_0^1 (\|\delta\mathcal{E}[u]\|_{V^*} + tC_3\|\Psi(\Pi(u)) - u\|_{V^*})\mathrm{d}t,\end{aligned} \tag{D.5}$$

where the last line follows by the continuity of $\delta\mathcal{E}$. The definition of Ψ and its continuity

give us

$$\begin{aligned}\|\Psi(\Pi(u)) - u\|_V &= \|\Psi(\Pi(u)) - \Psi(\Pi(u) + \delta\mathcal{E}[u])\|_V, \\ &\leq C_7\|\delta\mathcal{E}[u]\|_{V^*}.\end{aligned}$$

Therefore, using this bound in (D.5), we have (D.4). □

Inserting the bound for the energy difference (D.4) and the bound for the derivative (D.2) into the bound for the power of the energy (D.1) we have

$$|\mathcal{E}[u]|^{1-\theta} \leq \frac{C}{C_0}\|\delta\mathcal{E}[u]\|_{V^*} + K^{1-\theta}\|\delta\mathcal{E}[u]\|_{V^*}^{2(1-\theta)}. \tag{D.6}$$

Since $\mathcal{E}$ is C^1 we have

$$\|\delta\mathcal{E}[u] - \delta\mathcal{E}[v]\|_{V^*} \leq C_3\|u - v\|_V.$$

There exists a constant $\hat{C} > 0$ such that $\|\delta\mathcal{E}[0]\|_{V^*} \leq \hat{C}$. Therefore

$$\|\delta\mathcal{E}[u]\|_{V^*} \leq \|\delta\mathcal{E}[u] - \delta\mathcal{E}[0] + \delta\mathcal{E}[0]\|_{V^*} \leq C_3\|u\|_V + \hat{C}.$$

Hence $\|\delta\mathcal{E}[u]\|_{V^*} \leq C_3\sigma + \hat{C}$ and from (D.6) we have

$$\begin{aligned}|\mathcal{E}[u]|^{1-\theta} &\leq \|\delta\mathcal{E}[u]\|_{V^*}\left(\frac{C}{C_0} + K^{1-\theta}\right)\left(1 + \|\delta\mathcal{E}[u]\|_{V^*}^{1-2\theta}\right), \\ &\leq \|\delta\mathcal{E}[u]\|_{V^*}\left(\frac{C}{C_0} + K^{1-\theta}\right)\left(1 + (C_3\sigma + \hat{C})^{1-2\theta}\right).\end{aligned}$$

Therefore, there exists $\sigma > 0, c > 0$ such that

$$\|\delta\mathcal{E}[u]\|_{V^*} \geq c|\mathcal{E}[u]|^{1-\theta}, \qquad \forall u \in V \text{ such that } \|u\|_V < \sigma.$$

Hence [HJ15, Theorem 11.2.7] is proved.

Appendix E

Trust Region Method

Another method for solving problem **(P)** (see page 37), which is similar to the H^2-gradient flow method used in Chapter 6, is based on the trust region method (see [NW06, Chapter 4] for a general trust method). This is a method that is widely used in optimisation (see [CGT00, Section 1.3] for a wide range of references on applications of trust region methods) and hence provides a good comparison method for the methods of Algorithms 6.1.1 and 7.1.1. A trust region method that automatically enforces the constraint that the average is preserved is the constrained trust region method of [BSS87]; however, this method does not include a pre-conditioner and therefore the computational cost grows with the number of grid points.

We follow a pre-conditioned trust-region method based on the Steihaug method of [Ste83]. We introduce a minor modification from the Steihaug method in that the average is conserved by each update. This specific pre-conditioned constrained trust region approach is a novel method; however, the convergence and stability theory is very similar to that of the Steihaug method of [Ste83].

At each step, if the energy decease is large enough, we update out iterate as $u_{n+1} = u_n + \Pi d_n$, where Π is defined by (8.9) and Πd_n is the minima of

$$q_n(d) := \langle \delta\mathcal{F}[u_n], \Pi d\rangle + \frac{1}{2}\langle \delta^2\mathcal{F}[u_n]\Pi d, \Pi d\rangle,$$

subject to $\|\Pi d\|_{A^{(n)}} \leq \Delta$, where the norm is the one introduced by the averaged second variation operator, Definition 6.1.1. Therefore at each step we solve a sub-problem, which we now define.

Definition E.0.1 (Trust-region Sub-problem)**.**

$$\begin{aligned} \text{minimize}: &\ \langle \delta\mathcal{F}[u_n], \Pi d\rangle + \frac{1}{2}\langle \delta^2\mathcal{F}[u_n]\Pi d, \Pi d\rangle, \\ \text{subject to}: &\ \|\Pi d\|_{A^{(n)}} \leq \Delta. \end{aligned}$$

Remark E.0.1. *In principle the $A^{(n)}$-norm could be replaced by the A-norm with $\gamma = \gamma_{\text{om}}$ where γ_{om} is defined through* (8.10) *and* (8.11)*. As shown in Figure E.1 this choice of norm does not seriously affect the speed of convergence.*

The PFC functional's second variation (3.10) is not positive definite; therefore the sub-problem is solved using the method of [Ste83, Section 2] which is capable of dealing with non-positive second variations. As in [Ste83, Section 2] we have three different termination criteria for the sub-problem. First, we terminate when we have a sufficiently good approximation for the quasi-Newton step, i.e. the solution to the sub-problem without the constraint. Second, we terminate if the norm of the projection of the approximation is too large. Our final termination criterion is that if we encounter a direction of negative curvature we move from the current iterate along the proposed direction to the boundary.

At each step of the trust-region algorithm we update the size of the trust region using the method of [NW06, Algorithm 4.1]. We evaluate the ratio

$$\rho_n = \frac{\mathcal{F}[u_n] - \mathcal{F}[u_n + \Pi d_n]}{-q_n(d_n)},$$

then the size of the trust region at the $n+1$th step becomes

$$\Delta_{n+1} = \begin{cases} \frac{1}{4}\Delta_n & \text{if } \rho_n < \frac{1}{4}, \\ \min(2\Delta_n, \hat{\Delta}) & \text{if } \rho_n > \frac{3}{4} \text{ and } \|\Pi d_n\|_{A^{(n)}} = \Delta_n, \\ \Delta_n & \text{otherwise,} \end{cases} \tag{E.1}$$

where $\hat{\Delta} > 0$ is the maximum size allowed for the trust region and we define an initial trust region size $\Delta_0 > 0$. For $\eta \in [0, 1/4]$ we update u_n by

$$u_{n+1} = \begin{cases} u_n + \Pi d_n & \text{for } \rho_n > \eta, \\ u_n & \text{otherwise.} \end{cases}$$

We can see that in unconstrained optimisation (i.e. Δ arbitrarily large) the minimisation problem, Definition E.0.1, is equivalent to the Newton method (4.3) and hence is broadly similar to the H^2-gradient flow approach of Chapter 6. In theory the trust-region approach would involve inverting a dense operator, the second variation (3.10); however, using the method of [Ste83, Section 2] (which is similar to a conjugate gradient method) we never actively invert the dense second variation.

Energy stability follows from the update step, [Ste83, Equation (3.1)-(3.2)], i.e. we update only if

$$\rho_k = \frac{\mathcal{F}[u_k] - \mathcal{F}[u_k + \Pi d_k]}{-q_n(d_k)} \geq \eta,$$

where $\eta > 0$. We note by definition that $q_n(0) = 0$ therefore for energy stability we only need to prove that, in the sub-problem Definition E.0.1, $\|\Pi d_k\|_{A^{(n)}}$ is strictly increasing and q_n is strictly decreasing which is the analogue of [Ste83, Theorem 2.1].

Convergence follows by analogy with [Ste83, Theorem 3.1].

E.1 Algorithm

Using this notation we can now formulate the discrete trust region algorithm. This algorithm is very similar to [NW06, Algorithm 4.1], however we state it here for convenience. Again $\bar{u}$ and δ are fixed constants.

Algorithm E.1.1.

(0) INPUT $U_0, \eta \in [0, 1/4], \hat{\Delta} > 0, \Delta \in (0, \hat{\Delta})$

(1) FOR $n = 0, 1, 2, \ldots$

(2) $\gamma_n = \max\left(\gamma_{\min}, 3\overline{U_n^2} - \delta\right)$

(3) SOLVE Definition E.0.1 with the termination criteria of [Ste83, Section 2]

(4) CALCULATE $q_n(d_n) := \langle \delta \mathcal{F}_N[U_n], \Pi d_n \rangle + 0.5 \langle \delta^2 \mathcal{F}_N[U_n] \Pi d_n, \Pi d_n \rangle$,

(5) CALCULATE $\rho_n = (\mathcal{F}_N[U_n] - \mathcal{F}_N[U_n + \Pi d_n])/(-q_n(d_n))$

(6) UPDATE Δ_{n+1} using (E.1)

(7) UPDATE $U_{n+1} = \begin{cases} U_n + \Pi d_n & \text{for } \rho_n > \eta, \\ U_n & \text{otherwise} \end{cases}$

E.2 Choice of Pre-conditioner

We wish to prove that for the trust region algorithm, Algorithm E.1.1, the choice of an adaptive γ in line (2) is justified. To show this we will compare Algorithm E.1.1 to an adaptation of this algorithm where line (2) is replaced by $\gamma_n = \gamma_{\text{om}}$ for all n. We plot the number of FFTs needed for convergence against the number of grid points for these two trust region algorithms. To negate the divergence issue discussed in Subsection 8.2.5 we also choose the minimum number of grid points to be $N = 12$.

We can see from Figure E.1 that, as suggested in Remark E.0.1, Algorithm E.1.1 performs marginally better than its analogue with $\gamma = \gamma_{\text{om}}$ for all n. By comparison with the adaptive and fixed line search simulations of Section 9.2, we expect that this improvement will be more dramatic, though still small, for simulations on larger domains. Therefore from this point onwards when considering the trust method we will use Algorithm E.1.1 only.

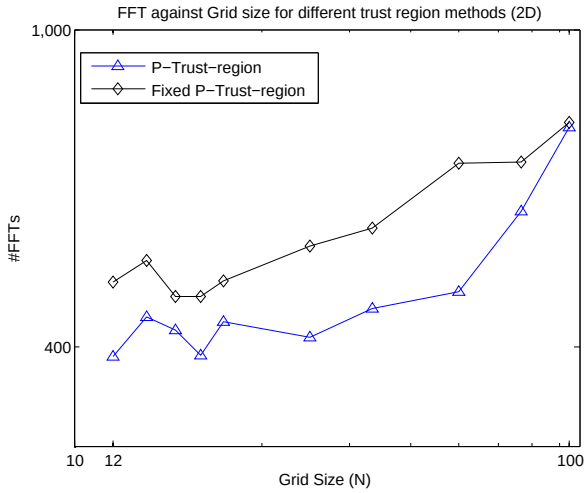

Figure E.1: Number of FFTs required for convergence of the solution against grid size, from random initial conditions, using the trust region method, Algorithm E.1.1, and its analogue with $\gamma = \gamma_{\text{om}}$. For fixed residual tolerence 10^{-7}.

Bibliography

[Ada75] R.A. Adams. *Sobolev Spaces*. Pure and Applied Mathematics. Academic Press Inc, 1975.

[Ada06] S. Adams. Lectures on mathematical statistical mechanics. *Communications of the Dublin Institute for Advanced Studies, Series A, No. 30*, 2006.

[AGD+07] B.P. Athreya, N. Goldenfeld, J.A. Dantzig, M. Greenwood, and N. Provatas. Adaptive mesh computation of polycrystalline pattern formation using a renormalisation-group reduction of the phase-field crystal model. *Physical Review E*, 76:056706, 2007.

[AM00] N. Argaman and G. Makov. Density functional theory-an introduction. *American Journal of Physics*, 68:69–79, 2000.

[AZ15] E. Asadi and M.A. Zaeem. A review of the quantitative phase-field crystal modeling of solid-liquid structures. *Journal of The Minerals, Metals & Materials Society*, 67(1), 2015.

[AZB14] E. Asadi, M.A. Zaeem, and M.I. Baskes. Phase-field crystal model for fe connected to meam molecular dynamics simulations. *Journal of The Minerals, Metals & Materials Society*, 66(3), 2014.

[Ban11] G.S. Bansel. *Advanced Operator Splitting Based Semi-Implicit Spectral Methods to Solve the Binary and Single Component Phase-Field Crystal Model*. PhD thesis, Brunel Centre for Advance Solidification Technology, Brunel University, 2011.

[Bar15] S. Bartels. *Numerical Methods for Non-Linear Partial Differential Equations*, volume 47 of *Springer Series in Computational Mathematics*. Springer, 2015.

[BN08] D. Behmardi and E.D. Nayeri. Introduction of fréchet and gâteaux derivative. *Applied Mathematical Sciences*, 2(20):975–980, 2008.

[BO12] Á. Bényi and T. Oh. The sobolev inequality on the torus revisited. *Publicationes Mathematicae Debrecen*, 83(3):359–374, 2012.

[BPRS12] J. Berry, N. Provatas, J. Rottler, and C.W. Sinclair. Defect stability in phase-field crystal models: Stacking faults and partial dislocations. *Physical Review B*, 86:224112, 2012.

[Bre11] H. Brezis. *Functional Analysis, Sobolev Spaces and Partial Diffferential Equations*. Springer, 2011.

[BSS87] R.H. Byrd, R.B. Schnabel, and G.A. Shultz. A trust region algorithm for nonlinearly constrained optimization. *SIAM Journal of Numerical Analysis*, 24(5):1152–1170, 1987.

[CDRS09] S.L. Cottar, M. Dashti, J.C. Robinson, and A.M. Stuart. Bayesian inverse problems for functions and applications to fluid mechanics. *Inverse Problems*, 25:115008, 2009.

[CE94] X. Chen and C.M. Elliott. Asymptotics for a parabolic double obstacle problem. *Proceedings of the Royal Society of London, Series A*, 444:429–445, 1994.

[CF10] R. Chill and E. Fašangová. Gradient systems. *Lecture Notes of the 13th International Internet Seminar, MatFyzPress, Prague*, 2010.

[CGO96] L.Y. Chen, N. Goldenfeld, and Y. Oono. Renormalization group and singular perturbations: Multiple-scales, boundary layers and reductive perturbation theory. *Physical Review E*, 54(1):376–394, 1996.

[CGT00] A.R. Conn, N.I.M. Gould, and P.L. Toint. *Trust Region Methods*. MOS-SIAM Series on Optimization, 2000.

[Che01] W.S. Cheung. Generalizations of hölder's inequlaity. *International Journal Of Mathematics and Mathematical Sciences*, 26(1):7–10, 2001.

[Chi06] C. Chicone. *Ordinary Differential Equations with Applications*. Texts in Applied Mathematics, Springer Science+Business Media, Inc, 2nd edition, 2006.

[CHQZ88] C. Canuto, M.Y. Hussaini, A. Quarteroni, and T.A. Zang. *Spectral Methods in Fluid Dynamics*. Springer Series in Computational Physics. Springer-Verlag, 1988.

[CW08] M. Cheng and J.A. Warren. An efficient algorithm for solving the phase field crystal model. *Journal of Computational Physics*, 227:6241–6248, 2008.

[DE07] G. Dziuk and C.M. Elliott. Finite elements on evolving surfaces. *Journal of Numerical Analysis*, 27:262–292, 2007.

[DS11] W.S.B. Dwandaru and M. Schmidt. Variational principle of classical density functional theory via levy's constrained search method. *Physical Review E*, 83:061133, 2011.

[EG04] K.R. Elder and M. Grant. Modeling elastic and plastic deformation in nonequilibrium processing using phase field crystals. *Physical Review E*, 70:051605, 2004.

[EKHG02] K.R. Elder, M. Katakowski, M. Haataja, and M. Grant. Modeling elasticity in crystal growth. *Physical Review Letters*, 88(24):245701, 2002.

[EP10] K.R. Elder and N. Provatas. *Phase Field Methods in Materials Science and Engineering*. Wiley-VCH, 2010.

[EPB+07] K.R. Elder, N. Provatas, J. Berry, P. Stefanovic, and M. Grant. Phase field crystal modeling and classical density functional theory. *Physical Review B*, 75:064107, 2007.

[ES86] C. Elliott and Z. Songmu. On the cahn-hilliard equation. *Archive for Rational Mechanics and Analysis*, 96(4):339–357, 1986.

[Eva79] R. Evans. The nature of the liquid-vapour interface and other topics in the statistical mechanics of non-uniform classical fluids. *Advances in Physics*, 28(2):143–200, 1979.

[Eva10] L. Evans. *Partial Differential Equations*, volume 19 of *Graduate Studies in Mathematics*. American Mathematical Society, 2010.

[EW13] M. Elsey and B. Wirth. A simple and efficient scheme for phase field crystal simulation. *ESAIM: Mathematical Modelling and Numerical Analysis*, 47:1413–1432, 2013.

[Eyr98] D. Eyre. Unconditionally gradient stable time marching the cahn-hilliard equation. *MRS Proceedings*, 529, 1998.

[Fre06] G.H. Fredrickson. *The Equilibrium Theory of Inhomogeneous Polymers*, volume 134 of *International Series of Monographs on Physics*. Oxford Science Publications, 2006.

[GAD05] N. Goldenfeld, B.P. Athreya, and J.A. Dantzig. Renormalization group approach to multiscale simulation of polycrystalline materials using the phase field crystal model. *Physical Review E*, 72:020601, 2005.

[GAD06a] N. Goldenfeld, B.P. Athreya, and J.A. Dantzig. Renormalisation group approach to multiscale modelling in materials science. *Journal of Statistical Physics*, 125(5/6):1019–1027, 2006.

[GAD06b] N. Goldenfeld, B.P. Athreya, and J.A. Dantzig. Renormalisation-group theory for the phase-field crystal equation. *Physical Review E*, 74:011601, 2006.

[GP15] M. Grasselli and M. Pierre. *Energy Stable and Convergent Finite Element Schemes for the Modified Phase Field Crystal Equation*. hal-01118961, 2015.

[Gra08] L. Grafakos. *Classical Fourier Analysis.* Graduate Texts in Mathematics. Springer New York, 2nd edition, 2008.

[GTTP11] L. Gránásy, G. Tegze, G.I. Tóth, and T. Puztai. Phase-field crystal modelling of crystal nucleation, heteroepitaxy and patterning. *Philosophical Magazine*, 91(1):123–149, 2011.

[GW14] M. Grasselli and H. Wu. Well-posedness and longtime behaviour for the modified phase field crystal equation. *Mathematical Models and Methods in Applied Sciences*, 24(14), 2014.

[HE08] Z-F. Huang and K.R. Elder. Mesoscopic and microscopic modeling of island formation in strained film epitaxy. *Physical Review Letters*, 101:158701, 2008.

[HJ15] A. Haraux and M.A. Jendoubi. *The Convergence Problem for Dissipative Autonomous Systems: Classical Methods and Recent Advances.* SpringerBriefs in Mathematics. Springer, 2015.

[HM06] JP. Hansen and I.R McDonald. *Theory of Simple Liquids.* Academic Press, Elsevier, 3rd edition, 2006.

[HP57] E. Hille and R.S. Phillips. *Functional Analysis and Semi-Groups*, volume 31 of *Colloquim Publications.* American Mathematical Society, 1957.

[HWWL09] Z. Hu, S.M. Wise, C. Wang, and J.S. Lowengrub. Stable and efficient finite-difference nonlinear-multigrid schemes for the phase field crystal equation. *Journal of Computational Physics*, 228:5323–5339, 2009.

[Isl97] S. Islam. Fixed point technique in differential equations. diploma thesis, International Centre for Theoretical Physics, Trieste, 1997.

[IVC10] W.T.M. Irvine, V. Vitelli, and P.M. Chaikin. Pleats in crystals on curved surfaces. *nature*, 468:947–951, 2010.

[JAEAN09] A. Jaatinen, C.V. Achim, K.R. Elder, and T. Ala-Nissila. Thermodynamcs of bcc metals in phase-field-crystal models. *Physical Review E*, 80:031602, 2009.

[KN14] G. Karali and Y. Nagase. On the existence of solution for a cahn-hilliard/allen-cahn equation. *Discrete and Continuous Dynamical Systems-Series S*, 7(1):127–137, 2014.

[KZ05] A.J. Kurdila and M. Zabarankin. *Convex Functional Analysis, Systems & Control: Foundations & Applications.* Birkhäuser Verlag, 2005.

[Lar14] Ø. Larsen. A phase field crystal study of grain growth in one and two dimensions. Master's thesis, Faculty of Mathematics and Natural Sciences, University of Oslo, 2014.

[Lev12] A. Levitt. Convergence of gradient-based algorithms for the hartree-fock equations. *ESIAM: Mathematical Modelling and Numerical Analysis*, 46(06), 2012.

[Łoj62] S. Łojasiewicz. Une propriété topologique des sous-ensembles analytiques réels. In *Les Équations aux Dérivées Partielles*, volume 117, pages 87–89, Paris, 1962. Colloques Internationaux du Centre National de La Recherche Scientifique.

[LSL15] H.G. Lee, J. Shin, and J-Y. Lee. First and second order operator splitting methods for the phase field crystal equation. *Journal of Computational Physics*, 299:82–91, 2015.

[ŁZ99] S. Łojasiewicz and M.A. Zurro. On the gradient inequality. *Bulletin of the Polish Academy of Sciences*, 47(2), 1999.

[Mel01] J. Meller. *Encyclopedia of Life Sciences*. John Wiley & Sons,Ltd, 2001.

[MNRR96] J. Málek, J Nečas, M. Rokyta, and M. Růžička. *Weak and Measure-Valued Solutions to Evolutionary PDEs*, volume 13 of *Applied Mathematics and Mathematical Computation*. Chapman Hall, 1996.

[Mur12] A.I. Murdoch. *Physical Foundations of Continuum Mechanics*. Cambridge University Press, 2012.

[Nir66] L. Nirnberg. An extended interpolation inequality. *Annali della Scuola Normale Superiore di Pisa Classe di Scienze*, 20(4):733–737, 1966.

[NW06] J. Nocedal and S.J. Wright. *Numerical Optimization*. Springer Series in Operations Research. Springer Science+Business Media, LLC, 2nd edition, 2006.

[PDA+07] N. Provastas, J.A. Dantzing, B. Athreya, P. Chan, P. Stefanovic, N. Goldenfeld, and K.R. Elder. Using the phase-field crystal method in the multi-scale modeling of microstructure evolution. *The Journal of The Minerals, Metals & Materials Society*, 59(7):83–90, 2007.

[Pel11] D.E. Pelinovsky. *Localization in Periodic Potentials From Schrödinger Operators to the Gross–Pitaevskii Equation*, volume 390 of *London Mathematical Society Lecture Note Series*. Cambridge University Press, 2011.

[Pen13] J-P. Penot. *Calculus Without Derivatives*, volume 266 of *Graduate Texts in Mathematics*. Springer, 2013.

[Rin07] W. Ring. A newton-type total variation diminishing flow. In T.F. Chan X.C. Tai, K.A. Lie and S. Osher, editors, *Image Processing Based on Partial Differential Equations*, Mathematics and Visualization, pages 123–148. Springer Berlin Heidelberg, 2007.

[Rob55] H. Robbins. A remark on stirling's formula. *The American Mathematical Monthly*, 62(1):26–29, 1955.

[RS50] W.T. Read and W. Shockley. Dislocation models of crystal grain boundaries. *Physical Review*, 78(3):275–289, 1950.

[SHP06] P. Stefanovic, M. Haataja, and N. Provatas. Phase field crystals with elastic interactions. *Physical Review Letters*, 96:225504, 2006.

[Sim83] L. Simon. Asymptotics for a class of non-linear evolution equations, with applications to geometric problems. *Annals of Mathematics, Second Series*, 118(3):525–571, 1983.

[Sim87] J. Simon. Compact sets in the space $l^p(0,t;b)$. *Annali di Mathematica pura ed applicata (4)*, 146:65–96, 1987.

[Ste83] T. Steihaug. The conjugate gradient method and trust regions in large scale optimization. *SIAM Journal of Numerical Analysis*, 20(3):626–637, 1983.

[SV14] V. Schmid and A. Voigt. Crystalline order and topological charges on capillary bridges. *Soft Matter*, 10:4694–4699, 2014.

[Tre00] L.N. Trefethen. *Spectral Methods in Matlab*. SIAM, 2000.

[WG02] J.A. White and A. González. The extended variable space approach to density functional theory in the canonical ensemble. *Journal of Physics: Condensed Matter*, 14:11907–11919, 2002.

[WGT+12] R. Wittkowski, T. Gruhn, G.I. Tóth, G. Tegze, L. Gránásy, H. Emmerich, and H Löwen. Phase-field-crystal models for condensed matter dynamics on atomic length and diffusive time scales; an overview. *Advances in Physics*, 61(6):665–743, 2012.

[WK07] K.A. Wu and A. Karma. Phase-field crystal modeling of equilibrium bcc-liquid interfaces. *Physical Review B*, 76:184107, 2007.

[WV12] K.A. Wu and P.W. Voorhees. Phase-field crystal simulations of nanocrystalline grain growth in two dimensions. *Acta Materialia*, 60:407–419, 2012.

[WW10] C. Wang and S.M. Wise. Global smooth solutions of the three-dimensional modified phase field crystal equation. *Methods and Applications of Analysis*, 17(2):191–212, 2010.

[WWL09] S.M. Wise, C. Wang, and J.S. Lowengrub. An energy-stable and convergent finite-difference scheme for the phase field crystal equation. *SIAM Journal of Numerical Analysis*, 47(3):2269–2288, 2009.

[YR79] M. Yussouff and T.V. Ramakrishnan. First-principles order-parameter theory of freezing. *Physical Review B*, 19(5):2775–2794, 1979.

[ZMQ13] Z. Zhang, Y. Ma, and Z. Qiao. An adaptive time-stepping strategy for solving the phase field crystal model. *Journal of Computational Physics*, 249:204–215, 2013.